Investigation of Heating Systems Based on Solar Assisted Air Source Heat Pumps

A thesis submitted by
Liwei Yang

in part fulfilment of the requirements for the degree of
Doctor of Philosophy
in the
School of Engineering and Materials Science
Queen Mary, University of London
Mile End Road
London, E1 4NS, UK
2022

Declaration

I declare that the contents of this dissertation are original and it has not been submitted in whole or in part for consideration for any other degree or qualification in this, except for those with specific reference made to the work of others. This dissertation is based on my own work and includes nothing which is the outcome of work done in collaboration, except where specific indications have been made in the text.

Name: Liwei Yang

Signature:

August 24th, 2022

Abstract

Solar assisted air source heat pump (SAASHP), combining solar thermal energy and heat pump, shows great potential as a promising energy-saving heating technology. It is widely considered for supplying hot water (HW), space heating (SH) and/or space cooling in the domestic sector. The performance of SAASHPs can be affected by many factors such as system configuration, component size, weather conditions and working conditions. This project is aimed to find an efficient and cost-effective heating system based on SAASHP in UK weather conditions as a green heating method for the domestic sector.

The serial, parallel and dual-source indirect expansion solar assisted air source heat pumps are modelled and simulated under the weather conditions in London using TRNSYS to investigate the operation performance over a typical year. These three heat pumps are applied to provide space heating and hot water of 300 L per day for a typical single-family house. The simulation results show comparisons of the three systems. The serial type heat pump shows the highest seasonal performance factor of 5.5, but requires a solar collector of 45 m^2 and a thermal energy storage tank of 3000 L. The dual-source and parallel type heat pumps show slightly lower seasonal performance factors of 4.4 and 4.5, respectively, requiring a solar collector of 18 m^2 and a thermal energy storage tank of 500 L. Furthermore, the results show that the air source part contributes to an important proportion of the heat provision and stable operation of the systems. The yearly seasonal performance factor higher than 4.4 achievable by the three heat pumps suggests that they are potentially applied in the regions with relatively lower solar irradiance. The economic analyses indicate that the parallel and dual-source type heat pumps provide cost effective alternatives to replacing the gas-boiler heating system.

The set hot-water-supply temperature of the heating system affects both the system operation performance and the thermal comfort condition of the house. The effect of low temperature heating on the system operation performance is investigated to figure out the way to significantly save electricity. A single-family house is chosen as the reference building and the heating system is modelled and simulated under the weather conditions in London, Aughton and Aberdeen in the UK over a year. The set hot-water-supply temperatures are taken to be 40 ^oC, 45 ^oC, 50 ^oC and 55 ^oC. For the heating systems, with the decrease in set hot-water-supply temperature from 55 ^oC to 50 ^oC, 45 ^oC and 40 ^oC, the yearly seasonal performance factor increases and the yearly total

electricity consumption decreases. The results show that low temperature heating enables a significant reduction in electricity consumption of such heating systems.

To achieve high thermal performance and low cost, solar assisted air source heat pump heating systems are numerically simulated by integrating compound parabolic concentrator-capillary tube solar collectors. The heating system is used to provide both space heating and hot water for a single-family house in London, UK. The operation of the heating system is simulated by TRNSYS. The results are compared with those of the heating systems using flat plate solar collectors of the same area. The concentrated solar collectors increase the utilisation of solar energy by 6.5%, reduce the electricity consumption by 6.1% and thus increase the seasonal performance factor by 6.8%. Particularly, for almost the same seasonal performance factor, the area required for the concentrated solar collector is 12 m^2 while the area required for the flat plate solar collector is 18 m^2, leading to one third collector size reduction and hence significant cost reduction and convenient installation. According to both system performance and economic analysis, CPC-CSC with an area of around 9 m^2 is recommended. Considering further improvements in system design and operation, the heating system using smaller size CPC-CSC e.g. 6 m^2 can potentially achieve a higher SPF_{sys}. Since solar collectors with a smaller size can be much more easily adopted for domestic use, using CPC-CSC benefits the wide rollout of SAASHP heating systems for domestic heating.

Keywords: Solar assisted air source heat pump, Domestic heating, Compound parabolic concentrator capillary tube solar collector, Low-temperature heating, Seasonal performance factor, Numerical simulation, Economic analysis

Acknowledgements

I would like to acknowledge all the technical and emotional support over the past four years. First of all, I do appreciate my supervisor, Prof. Huasheng Wang for his kind decision on accepting me as a PhD student and for his supervision of my project. Following the guidance from Prof. Wang, my knowledge, skills and abilities are greatly improved. I grew from a learner to a researcher with a good understanding of sustainable thermal energy systems.

My appreciation also goes to our co-operators, Dr. Tong Yang, Dr. Rongji Xu and Dr. Yerzhan Belyayev. Dr. Yang provides the basic criteria for building design and the newly updated information to me. She taught me to make a reasonable design for practical application. Dr. Xu generously shares the modelling of his novel collector with me, which contributes a lot to enhance my system design. Dr. Belyayev gives me directions for the research trend and helps me to select my research focus. With their assistance, I have the chance to conduct my project efficiently and effectively.

I wish to express my thanks to my software trainer, Mr. Shaogang Yang, and my colleagues, Dr. Nan Hua, Dr. Jionghui Liu, Dr Qiang Sheng, Dr. Xinyu You, Dr. Jinhuan Pu and Mr. Yu Xia. Their introductions to software and research skills ease my way of PhD study. I also appreciate my new colleagues, Miss Dilara Suulker and Mr Burak Alpargu for the good atmosphere in our group which encourage me to face the tough periods of Covid-19.

I sincerely appreciate my friends, Miss Yiqing Yang and Miss Jinran Liu for their accompany during each stressful time. I warmly thank my friends Miss Yu Yuan, Mr Yu Cao and Mr Shiming Liu for their support in my daily life. My appreciations go to my aunt, Miss Xiaoxia Yang, my cousin, Mr Tong Jin, and their cat, Miss Xiaowu Jin for the joys with them.

Finally, and most importantly, I do appreciate the China Scholarship Council-Queen Mary University of London joint PhD scholarship for the financial support on my study and life. I wish to say “thanks” to my parents and my parents-in-law for their love and encouragement. I also appreciate my beloved husband Dr. Wenbin Zhou for his love and efforts in my study and life.

Liwei Yang

Contents

List of figures

List of tables

Nomenclature

A	area, m^2
A_{val}	aperture temperature of expansion valve, m^2
C_i	initial cost difference, GBP
C_{i0}	initial cost of the studied system, GBP
C_{ieh}	initial cost of the electrical water heater, GBP
C_{o0}	operation cost of the studied system, GBP
C_{oeh}	operation cost of the electrical water heater, GBP
COP	coefficient of performance
C_{spy}	cost saving per year, GBP
c_p	specific heat capacity, J/(kg K)
E_{sc}	average amount of energy received per square meter of a solar collector, W/m^2
HC	heating capacity, W
L	average monthly value of atmosphere lucidity
P	power of water pump, kW
P_{pb}	payback period, year
Q_{ce}	clean energy used in the system, kWh
$Q_{HP,con}$	thermal energy obtained at the condenser of a heat pump, kWh
Q_{HW}	thermal energy for hot water, kWh
$Q_{loss,\ SC}$	heat loss from solar collector, kWh
Q_{SC}	thermal energy obtained by a solar collector, kWh
Q_{SH}	thermal energy for space heating, kWh
Q_{su}	solar energy used, kWh
Q_{sup}	thermal energy supply, kWh
Q_{TES}	thermal energy storage, kWh
Q_{loss}	heat loss from CPC-CSC per meter, kWh/m
Q_{max}	maximum thermal energy storage capacity, kWh
I	local solar irradiance for the tilted surface, W/m^2
SF	solar fraction (solar heating ability)
SPF	seasonal performance factor
t	time, s

T_{amb}	ambient air temperature, ^{o}C
T_{evp}	evaporating temperature, ^{o}C
T_{room}	room air temperature, ^{o}C
T_{SC}	temperature of solar collector, ^{o}C
T_{HWS}	outlet temperature of a hot water tank, ^{o}C
T_{HWS}*	set hot-water-supply temperature, ^{o}C
T_{con}	condensing temperature, ^{o}C
T_{max}	temperature of storage tank fully-charged, ^{o}C
T_{min}	temperature of storage tank fully-discharged, ^{o}C
$T_{sc,in}$	temperature at the inlet of solar collector, ^{o}C
T_{wt}	water temperature in the storage tank, ^{o}C
V	volume, m^3
v_a	wind speed, m/s
W_{cp}	work done by compressor, kWh
W_{fan}	work done by fan, kWh
W_{pump}	work done by pump, kWh
W_{tot}	total work done by compressor, fans, pumps, kWh
W_{HP}	electricity consumed by a heat pump, kWh

Greek Letters:

σ	Stefan-Boltzmann constant
η	efficiency
η_{sc}	efficiency of solar collector
η_v	volumetric efficiency of compressor
ρ	density, kg/m^3

Abbreviation:

ASHP	air source heat pump
CPC	compound parabolic concentrator
CSC	capillary tube solar collector
DX-SAASHP	direct expansion solar-assisted air source heat pump
ETC	evacuated tube collector
FPC	flat plate collector
GHG	greenhouse gases

GSHP	ground source heat pump
GWP	global warming potential
HP	heat pump
HW	hot water
HWS	hot water storage
IEA	International Energy Agency
IX-SAASHP	indirect expansion solar-assisted air source heat pump
LFL	lower flame limit
ODP	ozone depletion potential
PCM	phase change material
PV	photovoltaic
PV/T	photovoltaic/thermal
SAASHP	solar-assisted air source heat pump
SAGSHP	solar-assisted ground source heat pump
SAHP	solar-assisted heat pump
SC	space cooling
SFH	single family house
SH	space heating
SHW	solar hot water
SWHP	heat pump used hot water from a solar collector as heat source
SWH	solar water heater
TES	thermal energy storage
TRNSYS	TRaNsient SYstem Simulation program
WSHP	water source heat pump

Journal publications related to this thesis

1. **Yang L.W.**, Xu R.J., Hua N., Xia Y., Zhou W.B., Yang T., Belyayev Ye., Wang H.S., Review of the advances in solar-assisted air source heat pumps for the domestic sector, **Energy Conversion and Management** 247(2021)114710
2. **Yang L.W.**, Hua N., Pu J.H., Xia Y., Zhou W.B., Xu R.J., Yang T., Belyayev Ye., Wang H.S., Analysis of operation performance of three indirect expansion solar assisted air source heat pumps for domestic heating, **Energy Conversion and Management** 252(2022)115061
3. **Yang L.W.**, Li Y., Yang T., Wang H.S., Low temperature heating operation performance of a domestic heating system based on indirect expansion solar assisted air source heat pump, **Solar Energy** 244(2022)134-154
4. **Yang L.W.**, Xu R.J., Zhou W.B., Li Y., Yang T., Wang H.S., Investigation of solar assisted air source heat pump heating system using compound parabolic concentrator-capillary tube solar collectors, **Energy Conversion and Management**, Revised
5. Xu R., Zhao Y., Chen H., Wu Q., **Yang L.,** Wang H., Numerical and experimental investigation of a compound parabolic concentrator-capillary tube solar collector, **Energy Conversion and Management** 204 (2020) 112218
6. Xu R., He Z., **Yang L.,** Xu S., Wang R., Wang H., Study on concentration performance of compound parabolic concentrator-microchannel solar collector with tracking system, **Renewable Energy** 200(2022)809-820

1. Introduction

1.1 Background

To meet the UK's goal of Net Zero emissions of greenhouse gases by 2050, the sales of gas boilers will be phased out by 2033 [1]. Currently, according to EDF company, gas takes 78% of total energy consumption for heating in the UK [2]. In the UK, heating took up 48% of the total energy consumption in 2013, and the domestic sector accounted for 57% of the entire heating demand [3]. In 2017, domestic heating took up 80% of the total domestic energy consumption [4]. It is important to find an alternative to the gas boiler to achieve clean heating in the domestic sector.

Heat pumps (HPs) can be considered as a both energy efficient and renewable energy technology. The use of this technology to increase buildings' energy efficiency by utilizing low-grade thermal energy from existing heating supply systems is of significant interest today. By 2030, HP should provide 22.1% of domestic heating compared with 5% in 2019 [5]. The coefficient of performance (*COP*) and seasonal performance factor (*SPF*) are parameters to evaluate the performance of HPs [6]. HPs can be divided into air source heat pumps (ASHP), ground source heat pumps (GSHP), water source heat pumps (WSHP) and solar assisted heat pumps (SAHP). Depending on the purpose of the application, climate conditions, and technical and economic parameters, each of them has its own advantages and disadvantages. To significantly reduce energy consumption and improve the performance of HPs, many studies have been devoted to increasing the share of renewable energy.

In the past two decades, many studies of solar assisted air source heat pumps (SAASHPs) for the domestic sector have been conducted. Two approaches to solar boosting that have been reported are direct expansion SAASHP (DX-SAASHP) and indirect expansion SAASHP (IX-SAASHP). In the DX-SAASHPs, refrigerant is circulated directly through the solar collectors which serve as the HP evaporator. Investigations on DX-SAASHPs were devoted to exergy analyses [7], performance evaluation of the entire system and individual components [8], refrigerants [9], various applications such as hot water (HW) provision [10], space heating (SH), drying and desalination [11].

DX-SAASHPs have not been widely used compared with IX-SAASHPs. In IX-SAASHPs, an intermediate heat transfer fluid is circulated through the solar collectors and the installation is simplified but requires an additional heat exchanger. An IX-

SAASHP performs better than either ASHP [12] or solar heating [13]. For example, the application of serial IX-SAASHP in the Canadian domestic sector reduced green house gas (GHG) emissions by 19% [14]. The use of an air source evaporator in addition to a solar collector allows for extracting heat from the ambient air when solar radiation is not available, which expands the capability of the system. However, there is an issue of frost formation on the outdoor unit when the ambient air temperature is below zero, especially in humid regions. The *COP* and *SPF* of the system can be improved by integrating thermal energy storage (TES) [15, 16]. Current studies on IX-SAASHPs are focused on types of solar collectors including photovoltaic/thermal [17], energy and exergy analyses [18], components modelling [19], environment-friendly refrigerants [20], system performance and efficiency parameters [21], hydraulics and control [22], mathematical modelling approaches (artificial neural networks, life cycle assessment, TRNSYS, etc.) [23], different applications (SH, drying, desalination, etc.) [24], and market and economic analyses [25-27] and influences of ambient conditions [28].

Many theoretical, numerical simulations and experimental studies on SAASHP have been conducted in recent years. The utilization of SAASHP for HW and/or SH as well as space cooling (SC) has shown great achievements in the decarbonization of heating and cooling. However, previous studies on SAASHPs were focused on areas with latitudes below 50^{o} where ambient temperature and solar irradiation intensity are relatively high. Applications of SAASHPs in regions at higher latitudes, such as the UK, are rarely considered. In addition, international environmental protocols have imposed restrictions on the use of refrigerants according to ODP and GWP parameters. This limits the utilisation of the commonly used refrigerants while current studies on the operation performances of SAASHPs using environment-friendly refrigerants are insufficient.

1.2 Aims and objectives

This study aims to find a renewable, reliable and reasonable heating system for domestic heating in UK weather conditions.

The objectives of the project include:

- to use TRNBuild software to establish the standard reference buildings;
- to use TRNSYS software to simulate serial, parallel and dual-source IX-SAASHPs for space heating and hot water in London;
- to investigate the low-temperature heating performance of dual-source IX-SAASHP heating system in UK weather conditions;

- to use a compound parabolic concentrator-capillary tube solar collector (CPC-CSC) to improve the heating system.

1.3 Contribution to the knowledge

Currently, most existing studies of SAASHP are in mid-latitude regions. Higher latitude regions such as the UK (above 50^{o}) are rarely considered. Solar collector adopted for SAASHP mainly follows the design for solar hot water (SHW) systems. Some specific solar collectors for SAASHP have been proposed but the performances using these collectors are not efficient. Most of them lead to a *COP* below 4.0. Solar collector matching TES methods is hardly considered. Details for the literature review will be discussed in Chapter 2.

This study is focused on applications of heating systems based on SAASHP in UK weather conditions. The results suggest that parallel and dual-source SAASHP are feasible for domestic heating in higher latitude regions. CPC-CSC is used which has high collector efficiency at high temperatures, benefitting working with sensible TES methods. The system using CPC-CSC achieves an *SPF* of 4.7 in London weather conditions.

In addition, operation performances of low temperature heating and ultra-low temperature heating are investigated. Different from district heating, this study is focused on individual domestic heating, which can give a reference for distributed heating. The results suggest that, using ultra-low temperature heating, electricity consumption can be reduced by 19% per year. This provides valuable inspiration for approaches to Net Zero.

1.4 Thesis layout

This work is aimed to study the application of IX-SAASHP for domestic heating in weather conditions in the UK. In Chapter 2, existing papers for the investigations of SAASHP have been reviewed in terms of system configuration, component innovation and defrosting methods. The current research status of SAASHP is concluded to find the potential to utilise SAASHP in the UK.

In Chapter 3, three reference buildings under International Energy Agency (IEA) standards, single-family house (SFH) 15, SFH 45 and SFH 100 are modelled in TRNBuild to describe a general scope of different building types in the UK. The SFH 45 building is selected to represent a moderate space heating demand over a typical meteorological year in the following chapters.

In Chapter 4, based on the model of the SFH 45 building, serial, parallel and dual-source IX-SAASHPs are modelled in TRNSYS under weather conditions in London. The systems work for SH at 18-22 ^{o}C in heating periods and HW of 300 L/day over a year.

Corresponding economic analyses are conducted to understand the three kinds of IX-SAASHP systems in the view of markets.

In Chapter 5, the operation performances of dual-source IX-SAASHP with different hot water supply temperatures are simulated. The systems operate to provide SH and HW for the weather conditions in London, Aughton and Aberdeen. Corresponding economic analyses are conducted to understand the influence of hot water supply temperatures on costs and savings.

In Chapter 6, to further improve the system performances, a compound parabolic concentrator - capillary tube solar collector (CPC-CSC) designed and modelled by our co-operators from Beijing University of Civil Engineering and Architecture is used for the dual-source IX-SAASHP systems. The CPC-CSC is modelled in TRNSYS based on the results of numerical simulations covering the weather conditions in the UK. Then the self-written CPC-CSC module is used in the model of dual-source IX-SAASHP for SH and HW in London. The system using the CPC-CSC is compared with that using a flat plate collector. Comparison analyses for systems using different areas of CPC-CSC are also conducted, as well as economic analysis.

In Chapter 7, conclusions obtained from the simulation results and analyses are summarised. The research focus for future work is proposed.

2. Literature Review

Solar assisted air source heat pumps (SAASHPs) include direct expansion (DX-) SAASHP, indirect expansion (IX-) SAASHP and hybrid systems. In the DX-SAASHPs, the solar collector serves as an evaporator whereas in the IX-SAASHPs, a heat exchanger connects the refrigerant and water loops. The DX-SAASHPs mainly include basic and dual-source DX-SAASHPs. Compared with basic DX-SAASHP, the dual-source DX-SAASHP has an extra air source heat exchanger [29]. The IX-SAASHPs mainly include serial and dual-source systems. In the IX-SAASHPs, a heat exchanger is used to transfer heat from the solar collector to the refrigerant. In the hybrid system, an ASHP is parallel to the solar HW loop. Some special SAASHPs have been studied, such as two-stage DX-SAASHP, vapour ejector-enhanced DX-SAASHP, auto-cascade IX-SAASHP, composite IX-SAASHP and trans-critical hybrid system.

The performance of SAASHP is evaluated by the coefficient of performance (*COP*), seasonal performance factor (*SPF*) and solar fraction (*SF*). *COP* is defined by Eq. (2-1) [30]

$$COP = Q_{\text{HP, con}} / W_{\text{tot}} \tag{2-1}$$

where $Q_{\text{HP, con}}$ is the heating capacity and W_{tot} is the total electricity consumed by the compressor, fans and pumps given by Eq. (2-2)

$$W_{\text{tot}} = W_{\text{fan}} + W_{\text{cp}} + W_{\text{pump}} \tag{2-2}$$

where W_{fan} is the electricity consumed by fans, W_{cp} is the electricity consumed by the compressor, and W_{pump} is the electricity consumed by pumps.

SPF is the seasonal performance factor that evaluates the efficiency over the whole heating season. It is the ratio of the total thermal energy delivered by the SAASHP to the total electric energy consumed by the compressor, pump and fan, given by Eq. (2-3).

$$SPF = \int Q_{\text{HP,con}}\, dt \,/ \int W_{\text{tot}}\, dt \tag{2-3}$$

where *t* is time.

The *SF* is the solar fraction defined by Eq. (2-4) [31]

$$SF = (Q_{sc} - Q_{loss}) / Q_{sup} \quad (2\text{-}4)$$

where Q_{sc} is the average amount of thermal energy collected by a solar collector, Q_{loss} is the heat loss of the system and Q_{sup} is the thermal energy supply to the building.

The investigation methods on various SAASHPs available in the literature are briefly summarised in Table 2-1 It is apparent that basic DX-SAASHP and serial IX-SAASHP draw the most attention. Experiments and theoretical analyses are two of the most common research methods. Simulation methods, especially using TRNSYS software, are mainly employed to study IX-SAASHP.

Table 2-1: Research methods of SAASHP systems

		DX-SAASHP					IX-SAASHP				Hybrid SAASHP		
		Basic	Dual-source	Two-stage	Vapour ejector enhanced	Trans-critical	Serial	Dual-source	Cascade	Compo-site	Basic	Cascade	Trans-critical
Experiment	Practice	[65], [70], [72], [73], [74], [76], [77], [127], [134], [135], [138], [139], [140], [141], [142], [143], [144], [145], [146], [147], [154], [193], [194], [195], [196], [197], [198], [199], [200], [230], [234]	[33], [37], [162], [163], [164], [201], [202], [216], [243]	-	-	[218], [232], [246]	[41], [42], [47], [48], [49], [64], [66], [67], [75], [80], [81], [96], [101], [104], [165], [166], [167], [168], [204], [205], [209], [229], [236], [244]	[81], [222]	-	[211]	[64], [47], [48], [66], [96], [180], [181], [182], [205], [233], [238]	-	[56], [11]
	Lab	[35], [60], [61], [126], [135], [148], [149], [150], [192], [213], [217]	[29], [215]	-	[228]	-	[78], [169], [170], [171], [172], [204], [206], [219], [220], [221]	[44], [94], [95], [186], [187], [214]		[50]	[79], [183]	[51]	[55]
Simulation	CARNOT Blockset	-	-	-	-	-	[62], [173]	-	-	-	-	-	-
	TRNSYS	[207]	[243]	-	-	-	[46], [54], [63], [82], [90], [97], [165], [169], [174], [175], [176], [205], [219], [220], [221], [245], [249]	[46], [63], [231], [241]	-	[211]	[46], [63], [182], [184], [185], [205], [208], [233], [240], [249]	-	[55], [57], [58], [212]
	SOLSIM	-	-	-	-	-	[224]	-	-	-	[224]	-	-
	Artificial neural network	[139], [145], [147], [234]	-	-	-	-	-	-	-	-	-	-	-

Analy-sis	First law	[5], [32], [60], [61], [65], [70], [71], [73], [74], [76], [77], [126], [127], [135], [136], [142], [143], [144], [151], [152], [153], [154], [155], [156], [157], [158], [192], [193], [194], [195], [213], [223], [230], [237], [242], [248]	[29], [33], [34], [207], [215], [216], [243]	[36], [210]	[38], [39], [40], [226], [227], [228], [235]	[232]	[31], [47], [66], [68], [69], [75], [78], [96], [101], [109], [165], [166], [168], [170], [176], [177], [178], [179], [203], [204], [209], [225], [229]	[44], [109], [214], [231], [239]	[52], [210]	[211]	[31], [47], [43], [79], [66], [96], [179], [180], [183], [208]	[51]	[56], [212]
	Second law	[5], [74], [77], [155], [156], [158], [159], [223]	[29], [162], [163], [164], [202]	-	[39], [40], [227], [235]	-	[49], [66], [75], [179]	[214], [222]	-	-	[66], [179]	-	-
	Economic	[153], [160], [161], [217], [242]	[201], [202], [207], [215]	[36]	-	-	[41], [54], [78], [80], [104], [161], [165], [169], [175], [176], [179], [204], [240], [249]	[222], [231]	-	-	[161], [182], [185], [179], [208], [247], [249]	-	[57], [212]

2.1 Direct expansion system

The DX-SAASHPs (see Figs. 2-1 and 2-2) use solar collectors as their evaporators to achieve higher *COP* due to higher evaporation temperatures. Simulation results by Chow et al. showed a year-average *COP* of 6.46 [32]. Bare solar collectors (roll-bond evaporators) are preferably used in DX-SAASHPs to reduce solar radiation loss by glass reflection and to extract thermal energy from ambient air.

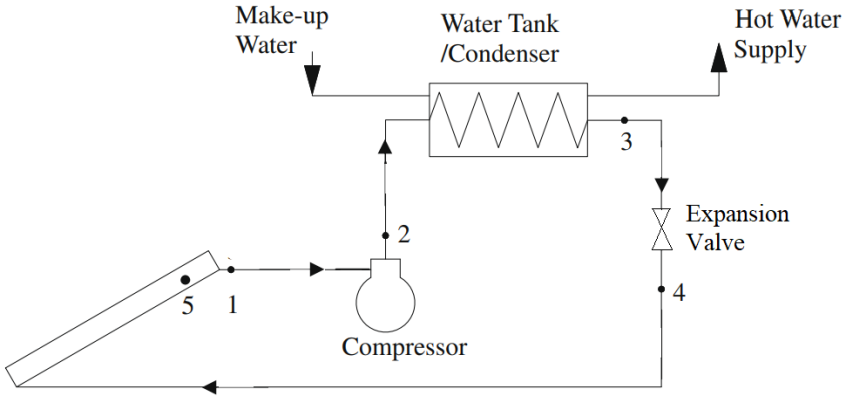

Fig. 2-1: Schematic of a DX-SAASHP (heating) (reproduced from [32]).

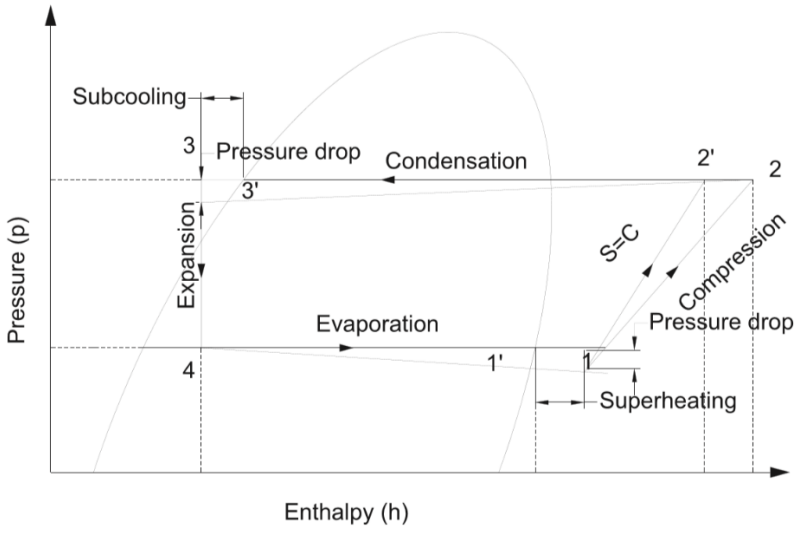

Fig. 2-2: *P-h* diagram of the DX-SAASHP [20].

Fig. 2-2 shows the ideal thermodynamic cycle on the *P-h* diagram of the DX-SAASHP system. The superheating at the inlet of the compressor and the subcooling at the outlet of the condenser are indicated. In the actual cycle, the flow resistance results in a significant pressure drop at the outlets of the evaporator and the condenser.

The evaporator can be arranged in series or parallel to the solar collector in DX-SAASHPs. Fig. 2-3 shows a serial evaporator-collector system for HW [29]. This system has *COP*s ranging from 3.5 to 2.5 as water temperature increases from 30 ºC to 50 ºC. Fig. 2-4 shows a parallel dual-source DX-

SAASHP [34]. This system exhibits better *COP* than the DX-SAASHP shown in Fig. 2-3, especially at low solar irradiance [33, 34, 35]. The heat transfer rates in the solar collector and evaporator affect the distribution of refrigerant flows and hence determine the *COP*. Experimental results showed the *COP* of a DX-SAASHP in solar-source solely mode 30%-50% higher than that in ASHP mode [33]. Numerical simulation results showed that the averaged *COP* of a DX-SAASHP in the dual-source mode was 14.1% higher than that in the solar-source-only mode in low solar irradiance of 100 W/m^2 [34].

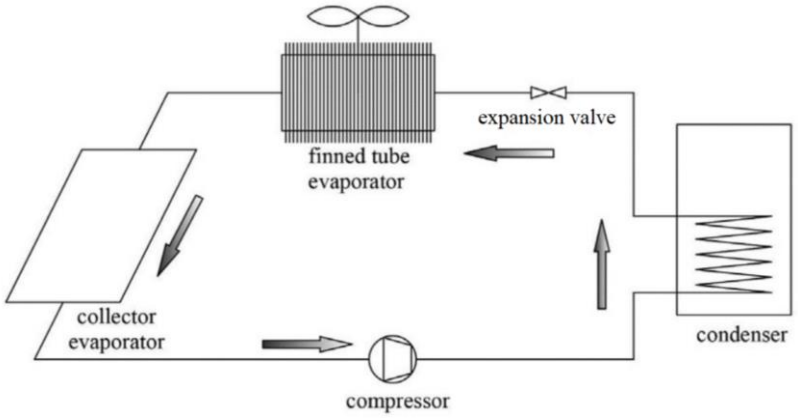

Fig. 2-3: Schematic of a DX-SAASHP for SC and HW (reproduced from [29]).

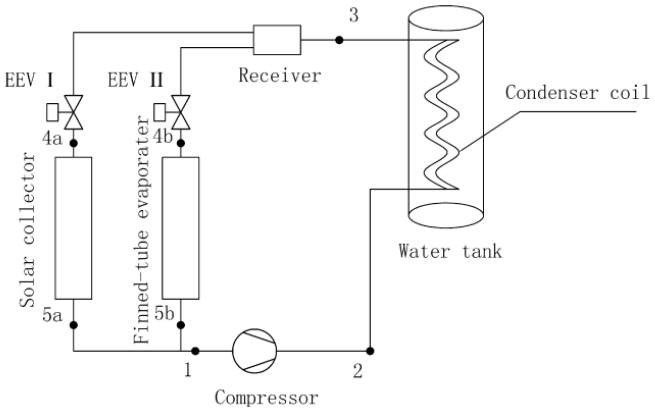

Fig. 2-4: Schematic of a parallel dual-source DX-SAASHP [34].

The DX-SAASHP of two-stage vapour-compression cycles has been developed for high temperature (60-90 ºC) application (see Fig. 2-5) [36]. Fig. 2-6 shows the two-stage vapour-compression cycles on the *T-s* diagram. The refrigerant evaporates in the solar collector to a saturation state (8-1) and is compressed by the low-pressure compressor (1-2). The superheating vapour (2) is cooled in the flash tank by saturated liquid (7) up to saturated vapour (3). In the low-pressure cycle, the refrigerant is throttled in the expansion valve (7-8) and feeds the evaporator in state 8. For the high-pressure cycle, the saturated vapour is compressed by the high-pressure compressor (3-4) and then condensed in the condenser (4-5), and finally expands at the expansion valve (5-6).

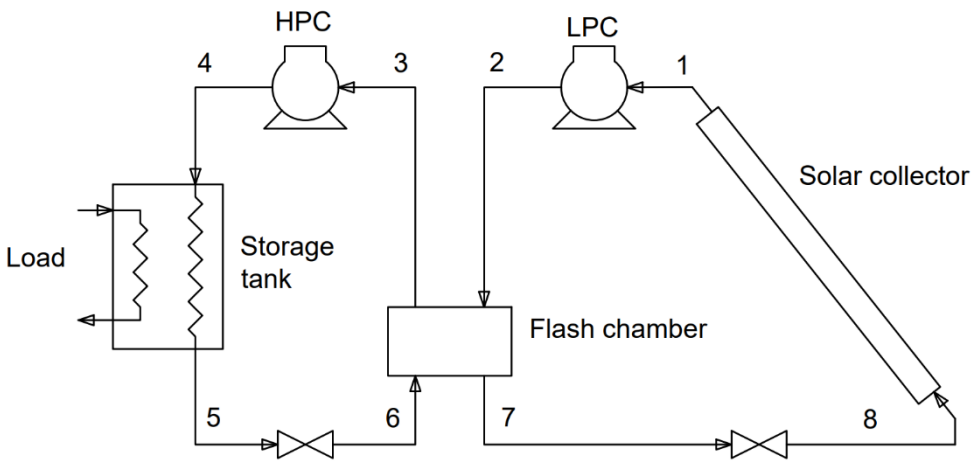

Fig. 2-5: DX-SAASHP with two-stage vapour-compression cycles (reproduced from [36]).

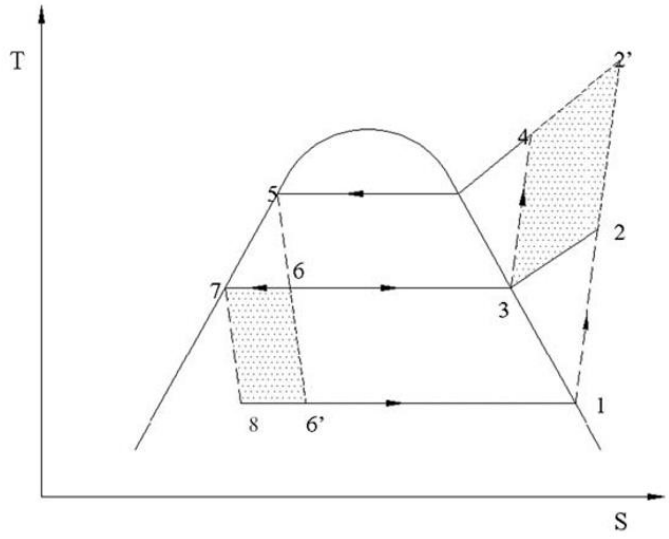

Fig. 2-6: *T-s* diagram of the two-stage DX-SAASHP [36].

Kuang and Wang designed a multi-functional DX-SAASHP for SH, SC and HW provision, with a radiant floor, a fan and a water tank [37]. The experiment expresses a *COP* of 2.1-2.7 for SH-only mode. In SC-only mode, this system adopts a storage tank to balance the night cold thermal energy storage and the daytime demand, but the cold energy storage efficiency (30%) and *COP* (2.9) are not satisfactory. In HW-only mode, the cycle provides 200-1000 litre HW with a temperature of 50 °C daily. It should be noticed that this system is only studied in single-function modes. In multi-function mode, the interaction among components may result in heat losses and require more energy input. The system in the multi-function mode needs to be further studied.

Vapour ejection can reduce the pressure ratio of compressors and thus improve system efficiency. Zhu et al. proposed a dual-nozzle vapour-ejector to assist the compressor and reduce energy consumption [38]. The arrangement of the vapour-ejector enhanced DX-SAASHP, as well as its *p-h*

diagram and vapour ejector construction are shown in Fig. 2-7 (a), (b) and (c). The dual-nozzle vapour ejector connects the low-temperature (air source) and the high-temperature (solar source) evaporators. The simulation results of this system show that the *COP* and heating capacity are 4.6%-34% and 7.8%-52%, respectively, higher than those of the conventional vapour ejector-compression cycle. The ratio of pressures can be further reduced for a larger temperature difference between the two evaporators.

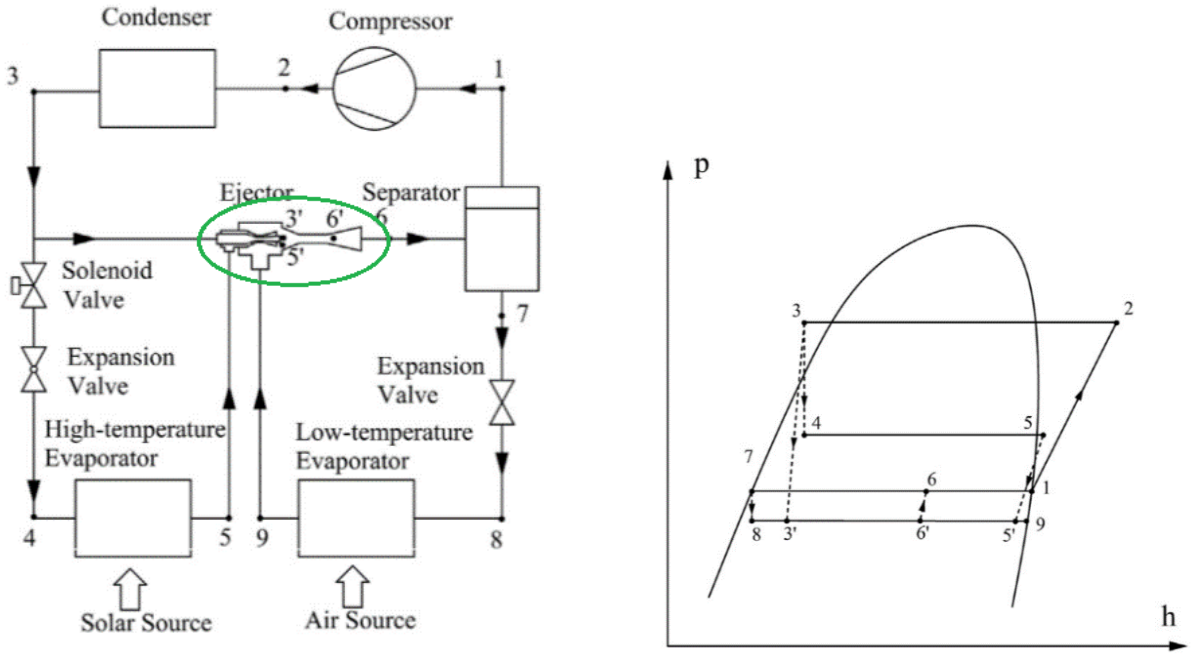

(a) Schematic of the system (b) *p-h* diagram

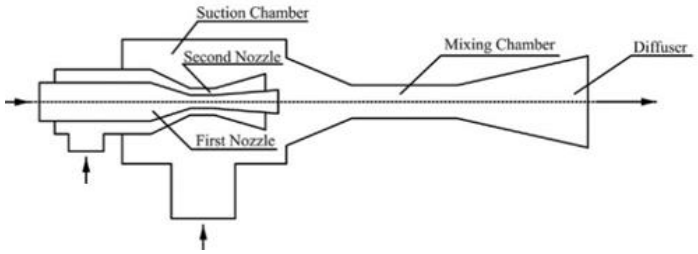

(c) Dual-nozzle vapour ejector

Fig. 2-7: Dual-nozzle vapour ejector SAASHP system [38].

The vapour ejector enhanced DX-SAASHPs have been further developed in [39] and [40] (see Figs. 2-8 & 2-9). In [39], the superheated vapour discharged by the compressor condenses (2-3) and then flows into the throttle valve (3-4) and the liquid pump (3-6), respectively. The low-pressure stream absorbs heat from the air source (4-5). The high-pressure stream evaporates to the superheated vapour in the solar collector (6-7). The superheated vapour works as the primary flow of the vapour ejector and expands to a two-phase flow with little liquid (7-7') to entrain the vapour from the evaporator (5-5'). The two streams are mixed in the mixing chamber (8) and are then compressed in

the diffuser (8-1) and the compressor (1-2). Theoretical analysis suggests that, compared with the conventional HP, this system can lead to increases of 15.3%, 38.1% and 52.8% in the *COP*, heating capacity and heating exergy output, respectively.

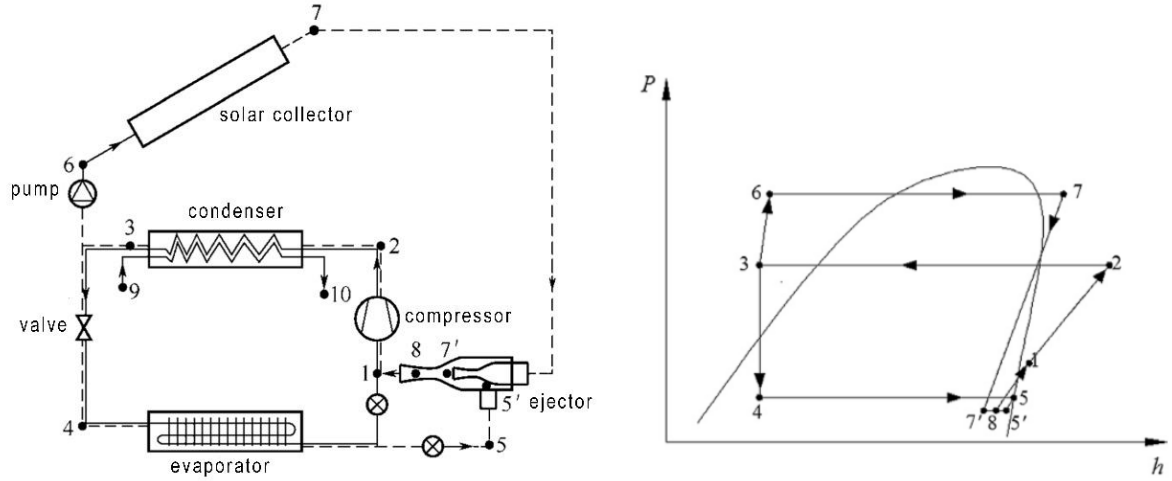

(a) Schematic of the system (b) *p-h* diagram

Fig. 2-8: Vapour ejector enhanced SAASHP system and the corresponding *p-h* diagram [39].

An adjustable DX-SAASHP system with a solenoid valve between the condenser and the vapour ejector was analysed theoretically [40]. It has a pure vapour ejector-compression mode and a pure solar-assisted vapour ejector-compression mode. The superheated refrigerant vapour condenses to saturated or subcooled states (2-3). In mode A, the liquid works as the primary flow of the vapour ejector directly. In mode B, the liquid evaporates (3-4) in the solar collector and then works as the primary flow. The two-phase fluid is separated into saturated liquid (5-6) and saturated vapour (5-1) in the phase separator. The liquid part expands to two-phase fluid (6-7) and then evaporates to saturated or superheated states (7-8). This is the secondary flow of the vapour ejector. The vapour part is then compressed (1-2). The simulation results suggest that the *COP* and heating capacity are 13.8% and 20.4% higher than those of the conventional vapour-ejector enhanced vapour-compression HP. On average, this cycle outperforms the vapour-compression HP in *COP* by 25.1%. However, these concepts lack validation from practical experiments.

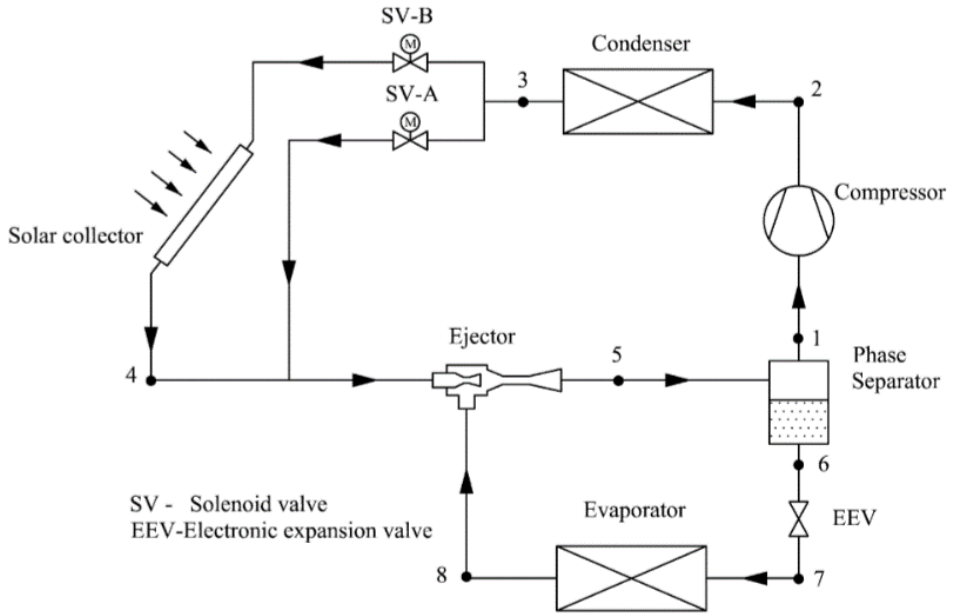

(a) Schematic of the system.

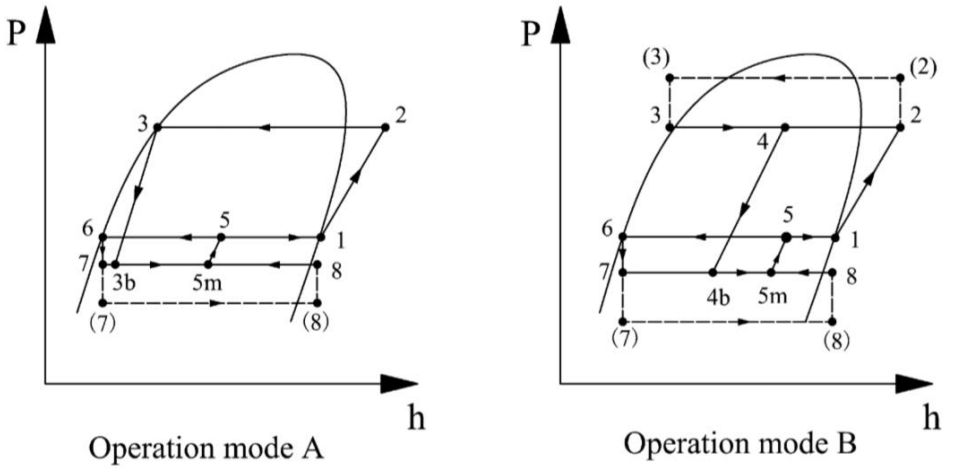

(b) *p-h* diagram of two operation modes

Fig. 2-9: Adjustable vapour ejector enhanced SAASHP system [40].

2.2 Indirect expansion system

IX-SAASHPs include serial and dual source systems. In serial IX-SAASHPs, the thermal energy collected by the solar collector heats the water in the water loop and the hot water is circulated to the evaporator of the HP. Dual-source IX-SAASHP enables both ambient air and solar energy as heat sources. Generally, the systems of IX-SAASHPs are more complicated than DX-SAASHPs.

Serial IX-SAASHPs use the thermal energy collected by the solar collector as the heat source. To balance the heat demand and supply, TES connects either to the solar collector and the evaporator (see Fig. 2-10(a)) or to the condenser and the end use (see Fig. 2-10(b)). The TES also works as a buffer to reduce the noise and voltage shocks caused by the frequent start-up and shutdown of HP. In

Fig. 2-10(a) SH by air is achieved by condensers placed in rooms. In Fig. 2-10(b) SH by water is achieved by circulating hot water to radiators. Although the utilisation of solar thermal energy increases the HP performance, the system *COP* is lower than that of the HP due to the power consumed by the additional components. Experimental results of a serial IX-SAASHP showed an HP *COP* of 3.8 and its system *COP* of 2.9 [41]. Experimental results of a similar serial IX-SAASHP showed the HP *COP* ranging from 2.5 to 3.5, and the system *COP* is around 20% lower [42]. Fig. 2-11 illustrates a serial IX-SAASHP with dual TES tanks [43]. Compared with IX-SAASHPs in Fig. 2-11 (b), this system can reduce the frequency of HP start-up and shutdown.

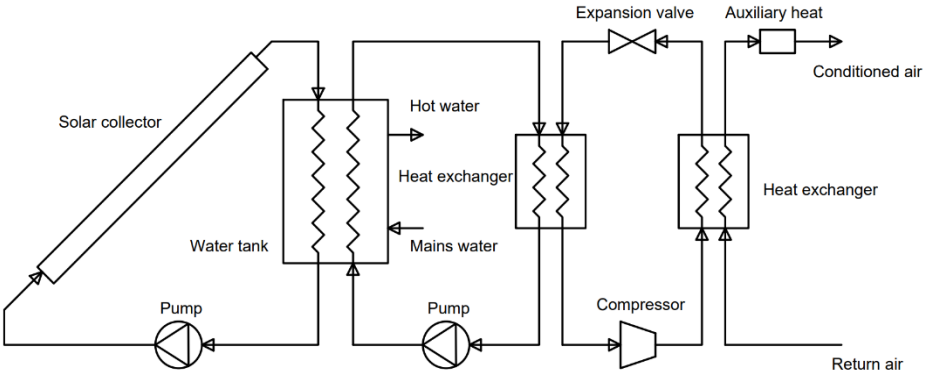

(a) Space heating by air (reproduced from [63]).

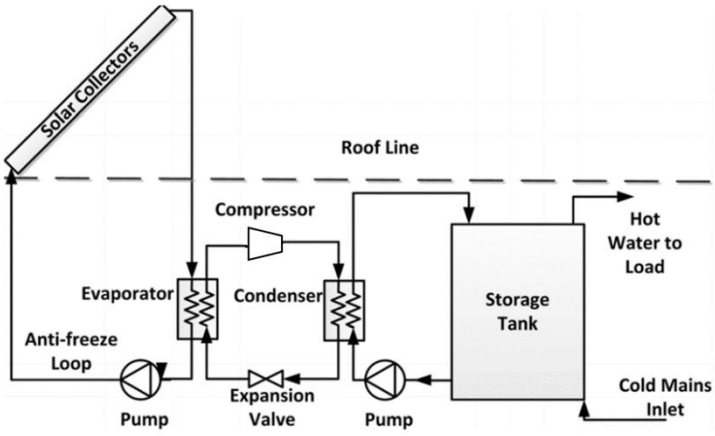

(b) Space heating by water (reproduced from [15]).

Fig. 2-10: Serial IX-SAASHP.

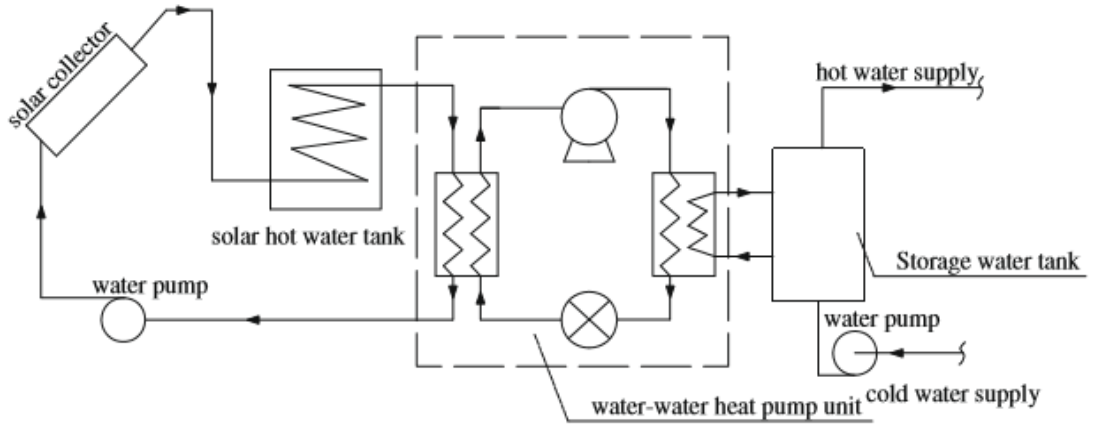

Fig. 2-11: Serial IX-SAASHP using dual water tanks [43].

Fig. 2-12 shows a dual source IX-SAASHP which utilises both solar thermal energy and ambient air as the heat sources. Two evaporators are separately connected to an air-water heat exchanger and solar collector loop. A TES tank is in the solar collector loop. The HP provides HW and SH by air. Cai et al. conducted numerical and experimental studies of a multi-functional dual-source IX-SAASHP [44]. In HW mode, when the solar water temperature increases from 20 ºC to 35 ºC, the electricity consumption increases by 16.5% and the *COP* increases by 15.9%. The *COP* increases from 2.35 to 2.57 with the solar irradiance increasing from 0 to 800 W/m^2. In SH mode, when the solar water temperature increases from 20 ºC to 40 ºC, the *COP* increases by 20.2%, and the heating capacity increases by 42.6%. While the *COP* decreased by 26.3% and heating capacity decreased by 7.5% with the increase in indoor air temperature from 16 ºC to 28 ºC.

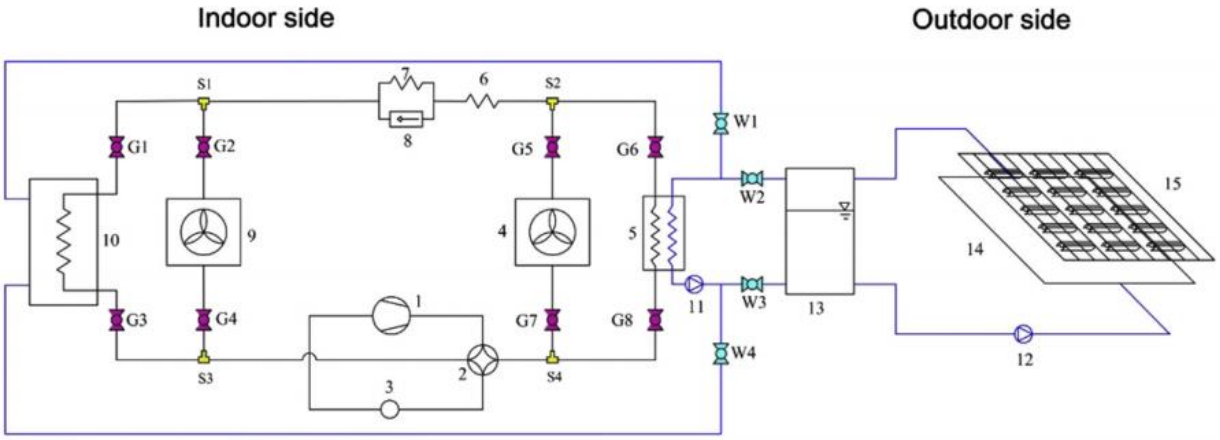

Fig. 2-12: Dual source IX-SAASHP. 1 - compressor, 4 – air source evaporator, 5 – heat exchanger, 9 - condenser, 10 – water tank, 13 – water TES tank, 14 and 15 – two solar collectors [44].

Numerical simulations were performed to compare the performance amongst the serial and dual-source IX-SAASHPs and hybrid SAASHP [46]. The results show that a hybrid SAASHP using a solar collector of 14 m^2 achieves an *SPF* of 3.65 and consumes 2317 kWh of electricity, while a serial IX-

SAASHP using a solar collector of 30 m^2 achieves an *SPF* of 3.53 and consumes 2401 kWh of electricity. A dual-source IX-SAASHP using a solar collector of 14 m^2 achieves an *SPF* of 3.70 and consumes 2289 kWh of electricity. It is seen that the performance of the dual-source IX-SAASHP and hybrid SAASHP are almost the same. Due to the system's simplicity, the hybrid SAASHP is more attractive. However, some experimental studies draw opposite conclusions. Experimental studies in [47,48] show a *COP* of 4.0 of a serial IX-SAASHP and a *COP* of 3.0 of a hybrid SAASHP, respectively. Experiments in [49] found that a serial IX-SAASHP can reach a *COP* of 2.95, and a dual-source IX-SAASHP can reach a *COP* of 2.90.

Fig. 2-13 shows a novel component and system configuration proposed based on conventional IX-SAASHP [50]. The composite heat exchanger is used to replace the conventional water-to-water heat exchanger in serial IX-SAASHPs to absorb solar thermal energy and thermal energy from ambient air. A composite heat exchanger is designed by inserting a tube into a finned tube. Hot water from the solar loop flows inside the inner tube and refrigerant flows in the annulus. This system has three working modes i.e. solar-only, air-only and dual-source modes. Experimental results show that, compared with the air-only mode, in the dual-source mode, the *COP* increases by 59% and the heating capacity increases by 62% at the ambient temperature of -15 °C. When the temperature difference between solar water and ambient air is 5 °C, the *COP* and heating capacity in the dual-source mode are 49% and 51% higher than those in the air-only mode.

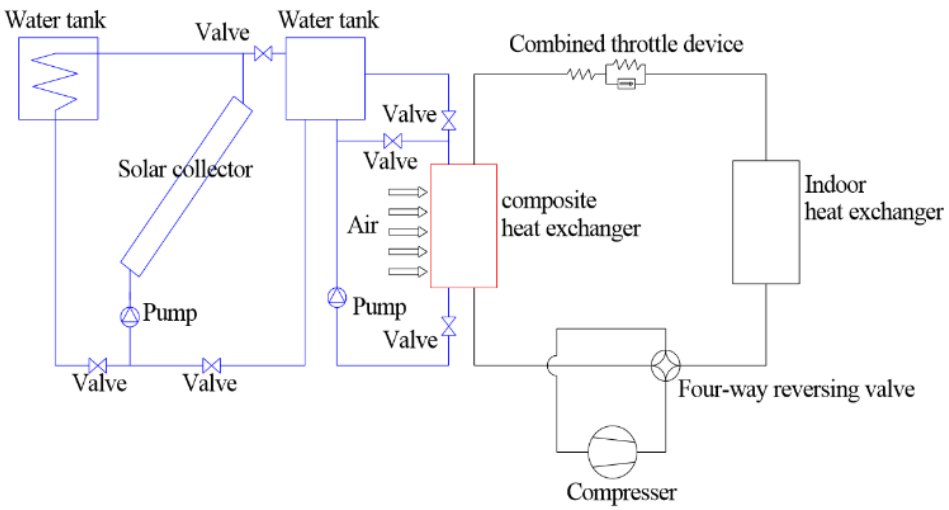

(a) Schematic of the system

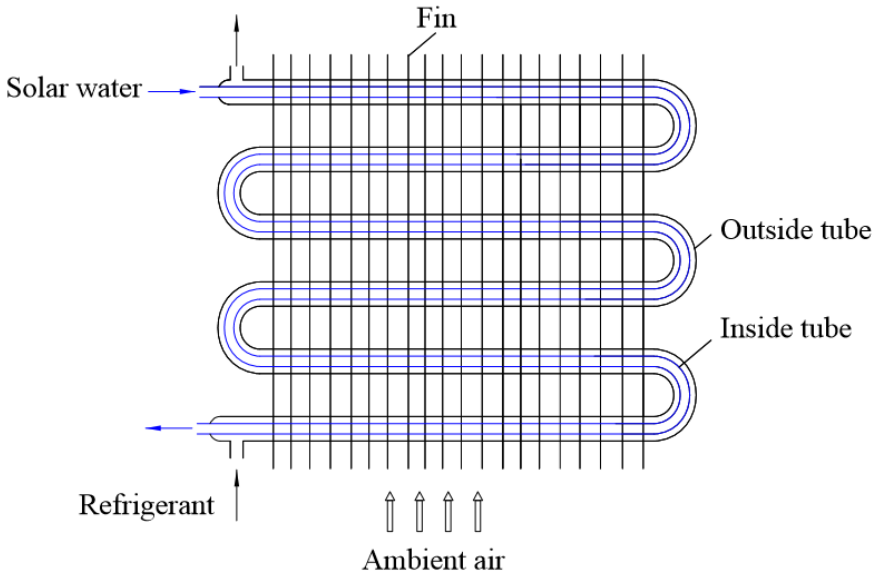

(b) Composite heat exchanger

Fig. 2-13: Dual-source IX-SAASHP with a composite heat exchanger [50].

The use of two coupled compression cycles may incur high capital costs and electricity consumption. To reduce energy costs, a solar-assisted auto-cascade HP using a single compressor with zeotropic mixture R32/R290 has been proposed to maintain a wide range of outdoor air and heating circuit temperatures (see Fig. 2-14) [52]. To achieve an auto-cascade cycle, a phase separator is used with the cascade heat exchanger. The compressed superheated vapour (1-2) condenses to saturated or subcooled liquid (2-3). Then the liquid flows through the sub-cooler I (3-4) and expansion valve I (4-5) into the flash tank, where the two-phase fluid absorbs heat from the solar heating loop (5-6). The refrigerant is separated into the R290 dominant liquid (6-6l) and the R32 dominant vapour (6-6v). The R290 dominant liquid is passed through expansion valve II (6v-7) to the cascade heat exchanger and vaporised completely (7-8). The R32 dominant vapour is transferred to the cascade heat exchanger (6v-9) and thoroughly condensed via the sub-cooler II (9-10). Then the condensed fluid goes to the low-temperature evaporator through expansion valve III (10-11), absorbing heat from ambient air (11-12). Fluids from the low-temperature evaporator flow back through the sub-cooler II (12-13). Then it (13-14) is mixed with the vapour from the cascade heat exchanger (8-14) and returned to the compressor through the sub-cooler (14-1). Simulation results suggest that, compared with conventional ASHP, this novel system increases *COP* and volumetric heating capacity by 4.2%-9.9% and 4.4%-9.7%, respectively. These improvements greatly rely on the heat absorption ratio and the composition of the zeotropic mixture.

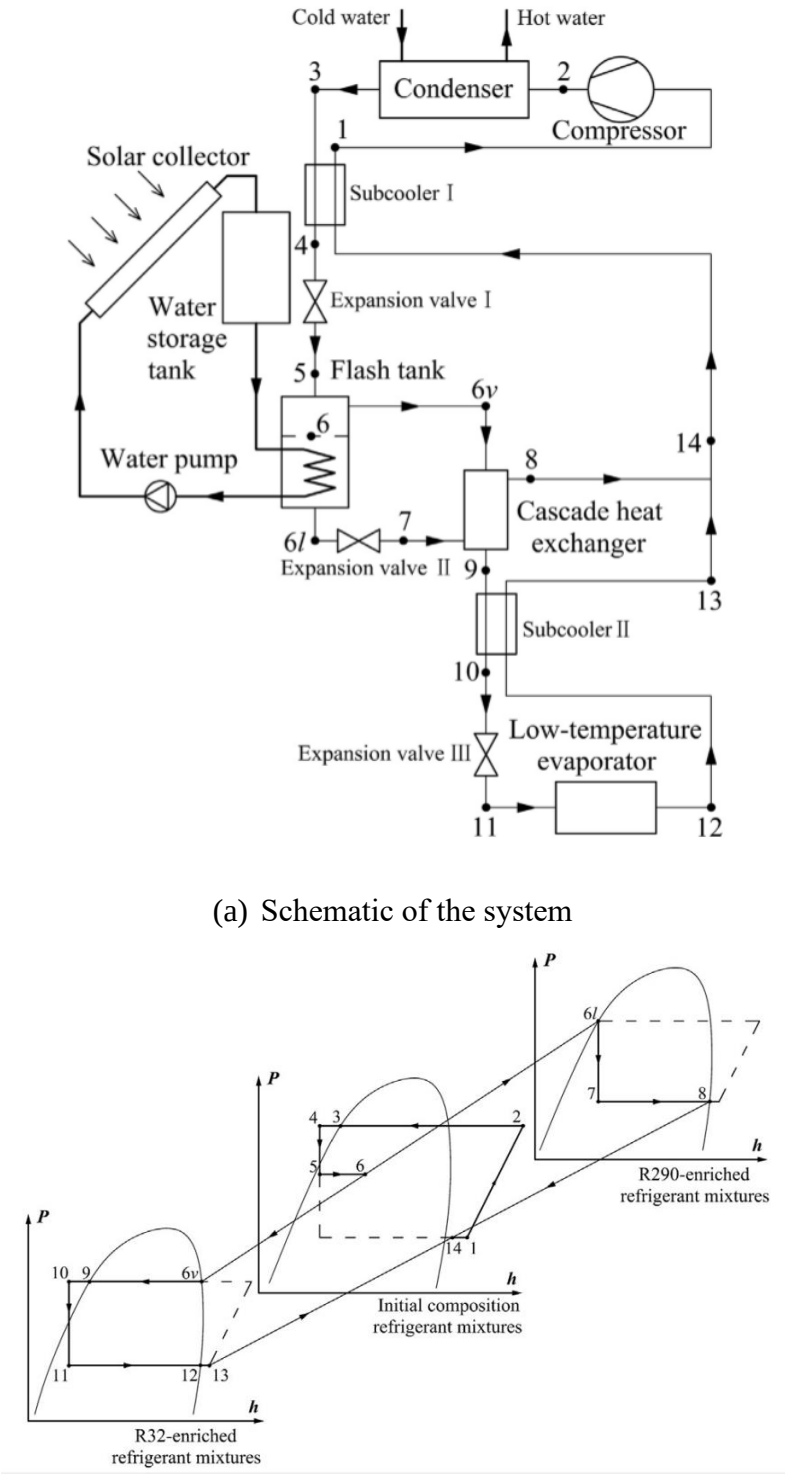

(a) Schematic of the system

(b) *p-h* diagrams of the cycles

Fig. 2-14: Solar-assisted auto-cascade ASHP [52].

Fig. 2-15 illustrates a composite IX-SAASHP with an HP parallel to the solar collectors in cold weather conditions in Canada [53, 54]. The hot water leaving the solar collectors is further heated up in the condenser of the HP and then heat the water in the TES tank. The HP absorbs residual heat after the heat exchange and cools the water entering the solar collectors. The reduced collector inlet

temperature improves the collector efficiency and thus the *COP*. It requires a lower capacity HP and consumes less electricity.

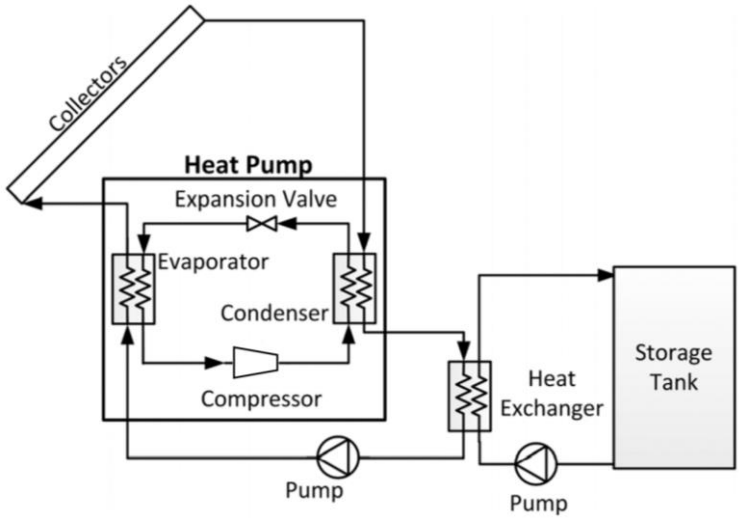

Fig. 2-15: A composite IX-SAASHP (reproduced from [15]).

2.3 Hybrid system

In hybrid SAASHPs (see Fig. 2-16), ASHP and solar collector water loops work independently. In Fig. 2-16 (a) HW and SH by air are achieved by an ASHP and solar heating with a TES tank. In summer, the ASHP can provide SC. In Fig. 2-16 (b) an ASHP and a solar collector loop provide hot water to a TES tank to achieve SH by water. Compared with serial systems, hybrid SAASHPs are more widely used [10].

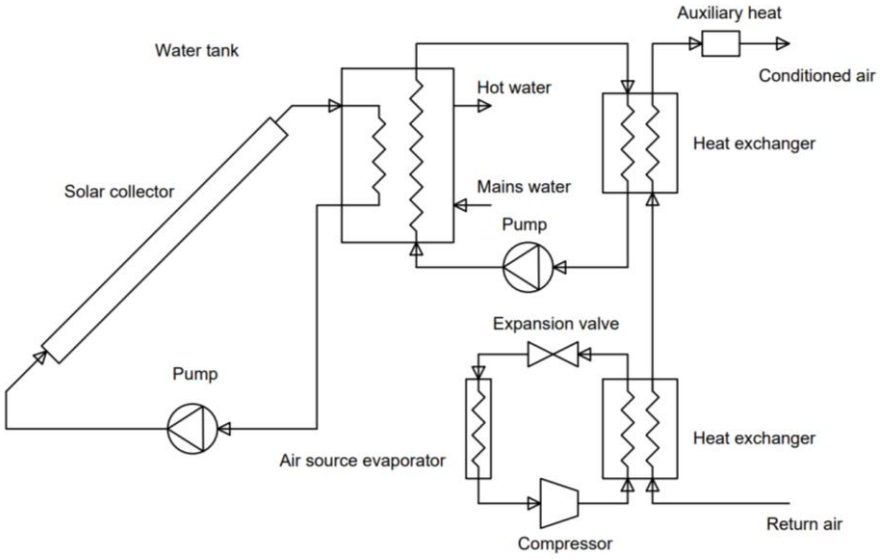

(a) Hot water and space heating by air (reproduced from [63]).

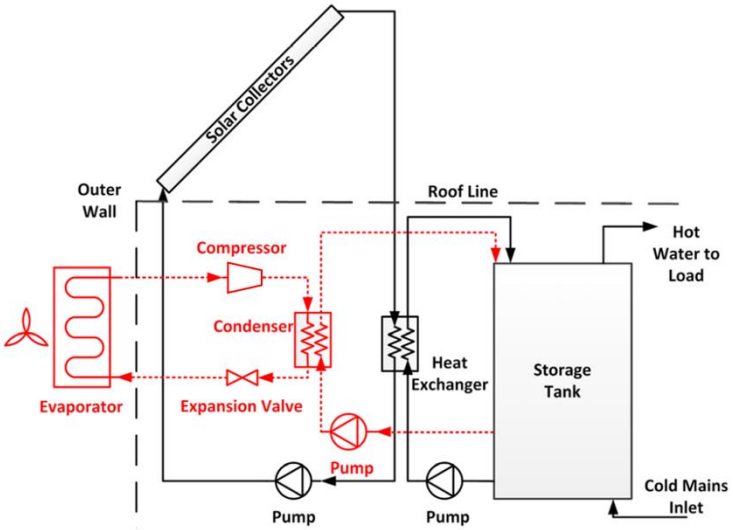

(b) Space heating by water (reproduced from [15]).

Fig. 2-16: Hybrid SAASHP.

A single-stage vapour-compression HP cannot deliver heat above 50 ºC at low ambient temperatures. To increase the temperature range between the outdoor air and the heating circuit, two-stage cascade HPs are used in cold climate regions or to ensure the demand for a higher temperature lift. A solar-assisted two-stage cascade HP is proposed by Yerdesh et al. [51] where solar thermal collectors and a cascade ASHP simultaneously heat the hot water in the TES tank (see Fig. 2-17). It was shown that combining a cascade ASHP with solar collectors increases energy efficiency by 30% compared with a conventional two-stage cascade HP. The cascade HP includes two single-stage cycles that operate separately with two different refrigerants, the low temperature cycle (LTC) and the high temperature cycle (HTC). Using the R32/R290 refrigerant pair, this system can have the maximum *COP* of 2.4 when the condensing temperature is 50 ºC and evaporating temperature is -10 ºC.

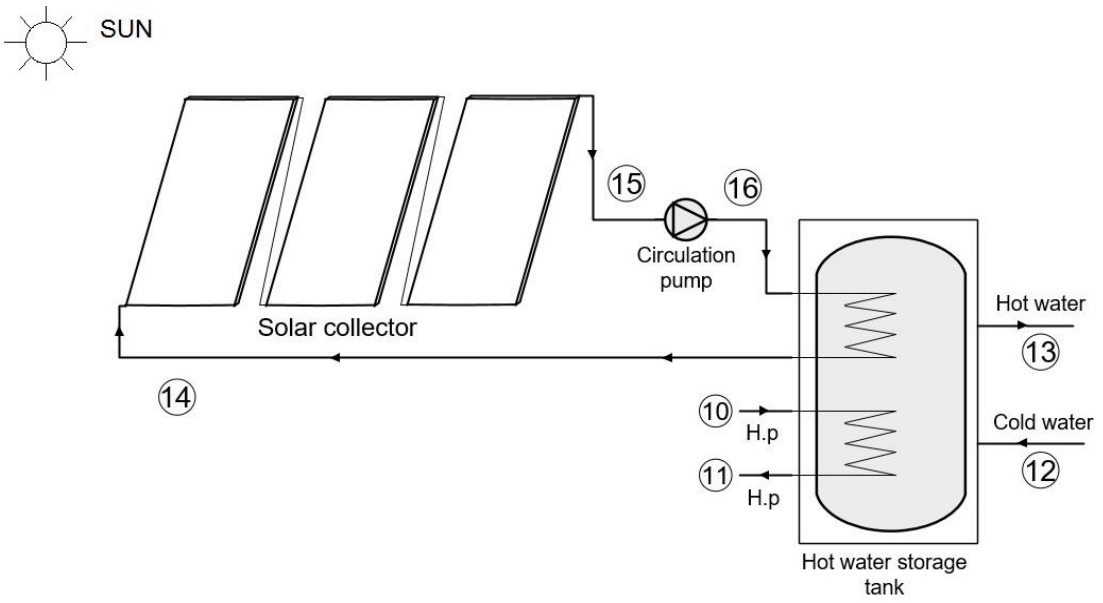

(a) Solar collector loop

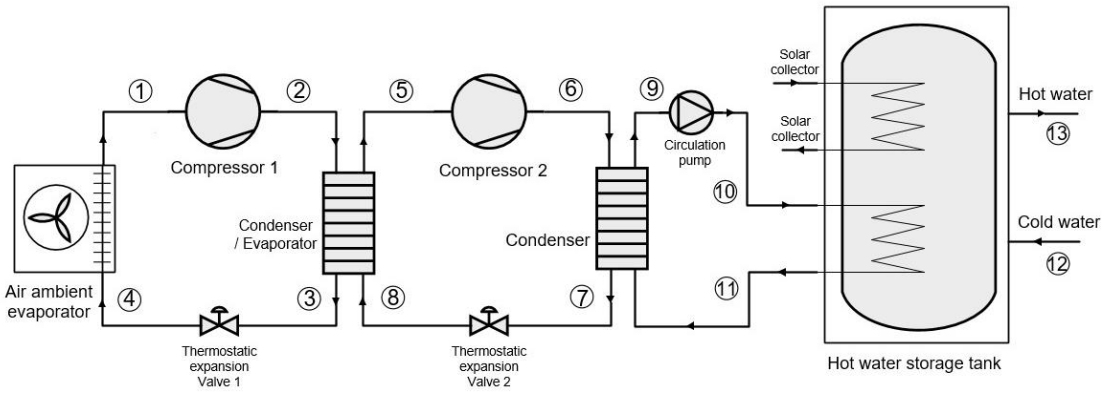

(b) Cascade HP loop

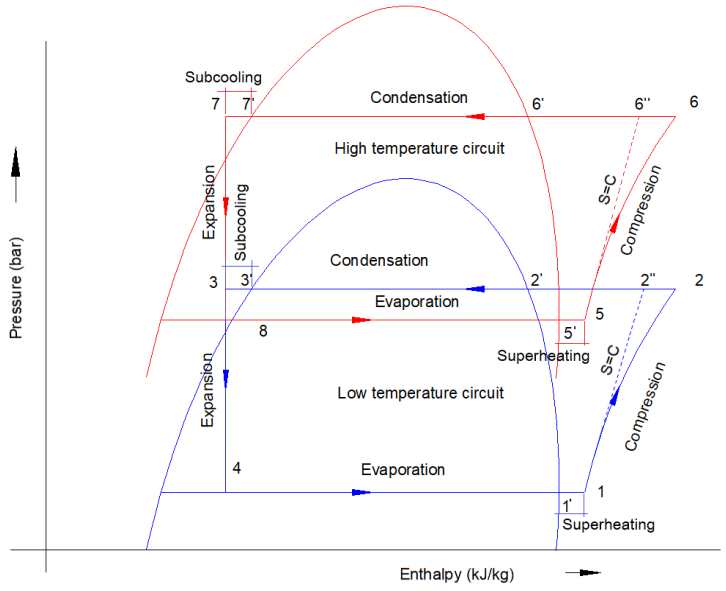

(c) *p-h* diagram.

Fig. 2-17: Solar-assisted cascade ASHP [51].

A solar thermal collector can be integrated with a hybrid trans-critical carbon dioxide (CO_2) HPs for SH, SC and HW (see Fig. 2-18) [55, 56, 57, 58]. In SH and HW mode, the *COP* and heating capacity are about 2.3 and 6 kW [57, 58], while in SC mode the *COP* and heating capacity are 4 and 8 kW, respectively [55].

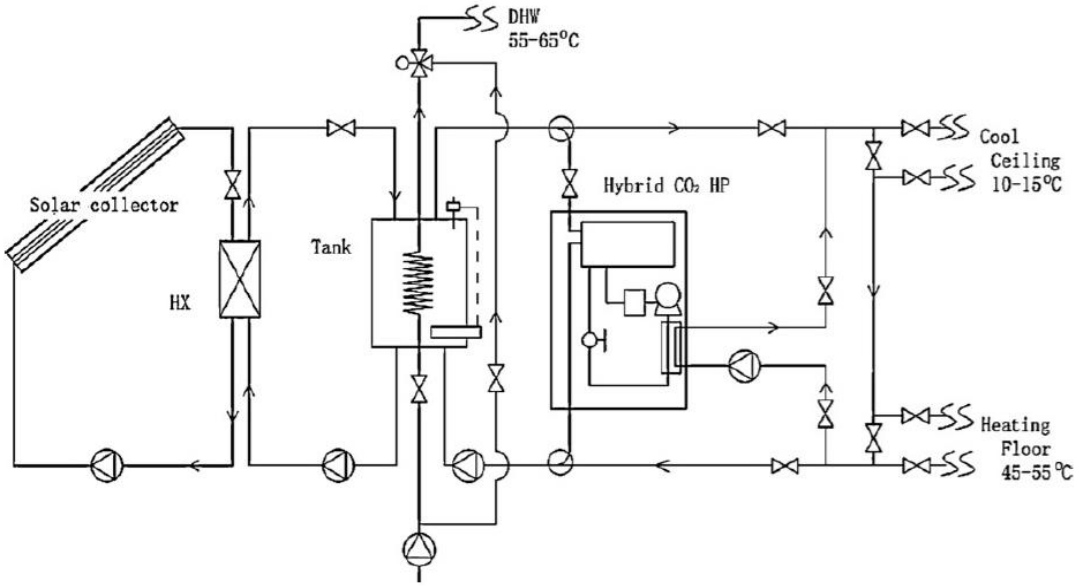

Fig. 2-18: Trans-critical SAASHP [55].

2.4 Solar collector

The solar collector is an important component for the thermal energy input of SAASHPs. A flat plate collector is commonly selected in recent studies. To absorb more thermal energy from ambient air, the collector/evaporator is designed by coating solar selective materials on the surface of an evaporator. Collector/evaporator is mainly used in DX-SAASHPs. In IX-SAASHP, evacuated tube solar collectors draw more attention. Fig. 2-19 introduces the matching relation between solar collectors and system configurations. Table 2-2 lists some open literature where collector/evaporator and evacuated tube collectors have been employed in SAASHPs. It can be noticed that systems using advanced solar collectors can achieve a *COP* of 3-5. Especially, those for SH can work at ambient temperature below 0 °C.

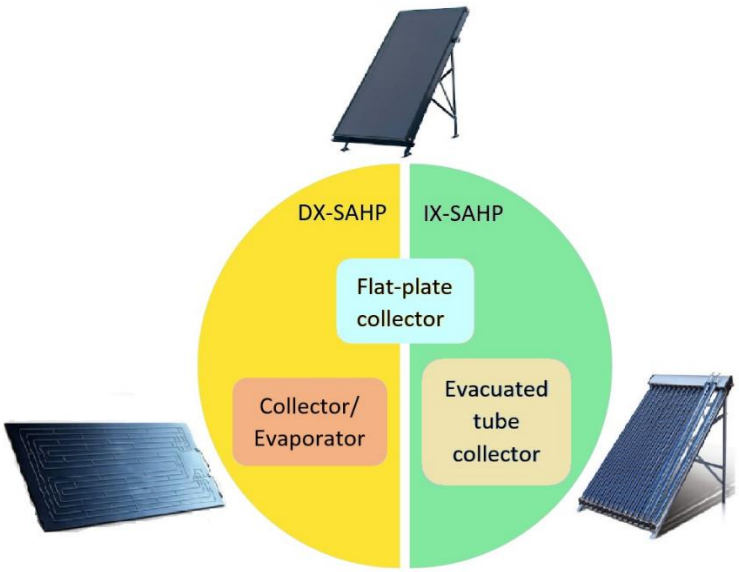

Fig. 2-19: Matching relation between solar collectors and system configurations.

The thermal energy collected by a solar collector, Q_{sc}, is determined by Eq. (2-5) [59]

$$Q_{sc} = AE_{sc}\eta_{sc}\{1\text{-}a[(T_{sc,in}\text{-}T_{amb})/L]+b[(T_{sc,in}\text{-}T_{amb})/L]^2\} \quad (2\text{-}5)$$

where A, E_{sc}, and η_{sc} are the area, the average amount of energy received per square meter and collector efficiency, respectively, a and b are coefficients determined by experiments, $T_{sc,in}$ is the water/refrigerant temperature at the inlet of solar collector, T_{amb} is the temperature of ambient air, and L is the average monthly value of atmosphere lucidity.

2.4.1 Flat plate solar collector

Flat plate collectors are commonly adopted in SAASHPs. Bare (uncovered) flat plate collectors enable to use of thermal energy from solar radiation and ambient air. The experiment of Sun et al. [60] suggests that, at the outdoor temperature of 0 -10 ºC, the collector efficiency of a bare solar collector ranges from 40% to 70%, where water vapour condensation occurs on the solar collector. The experiment study of Scarpa and Tagliafico [61] suggests that, due to water vapour condensation on the solar collector, a DX-SAASHP using a bare collector achieves a *COP* of 5.8 at weak solar radiation.

There is a noticeable influence of collector area on system performance. Increasing the collector area can enhance the *SF* of a SAASHP [30], almost in a linear relation [62]. A larger collector area can improve *COP* since it brings more solar energy input [63]. Both system configuration and collector area affect collector efficiency. With the same collector area of 30 m^2, the collector in a serial IX-SAASHP shows higher collector efficiency (62%-70%) than that in a hybrid SAASHP (with a η_{sc} of 54%-60%) [47, 48]. With a smaller collector area of 20 m^2 in a serial IX-SAASHP, the collector efficiency ranges from 33% to 47% [41].

Table 2-2: Utilisation of collector/evaporator and evacuated tube collector

Authors	Location	Function of HP	Refrigerant	Solar collector		TES		T_{amb} (°C)	*HC* (kW)	*COP*	Comments	Related work
				type	area (m^2)	type	Vol. (m^3)					
Kuang et al., 2003 [67]	Qingdao, China 36°N	SH, HW	-	coated, covered	11	water	2.1	-10-4	4.99	2.19	-	
Huang et al., 2005 [35]	Taiwan, China 23°N	HW	R134a	bare, collector/ evaporator	1.98 sunny, 1.8 dark	water	0.24	34.9	-	3.32	-	
Liang et al., 2011 [79]	-	SH	R22	evacuated tube	0 10 20 30	water	-	-1.2-9.5	10	3.3-4 3.3-4.3 3.3-4.6 3.3-5	-	
Caglar and Yamali, 2012 [78]	-	SH	R407C	evacuated tube	-	water	0.12	-	5.87	5.56	-	
Deng et al., 2013 [57]	Shanghai, China 31.17°N	HW, SH	CO_2	evacuated tube with compound parabolic concentrator	30	water	0.5	-5-5	-	2.38	A transcritical hybrid SAASHP	[55], [58]
He et al., 2014 [177]	-	HW	R134a, R600a, R22	covered, heat pipe	-	water	-	10-30	-	3.69-5.27	-	
Chaturvedi et al., 2014 [153]	-	HW	R134a	collector/ evaporator	3	-	-	-	0.366-0.603	1.7-5.61	-	
He et al., 2015 [170]	London, UK 51°N	HW	R134a	covered, heat pipe	2.4	water	0.03, 0.2	25	2.253	4.93	-	
Wang et al., 2015 [171]	-	SC, SH, HW	R407C	evacuated tube	-	water	0.15	7, 12, 20	2.56-4.24 (SH)	3.75-4.72 (SH)	-	[172]
Shan et al., 2016 [181]	Beijing, China 40°N	SH	-	evacuated tube	-	water	0.72, 0.8	-13.3-4.5	3.9	2.5-3.0	-	
Dong et al., 2017 [77]	Taiyuan, China 38°N	SH	R407C	coated, collector/evaporator	0.4	Na_2SO_4	0.8	-15-7	0.186	2.94	-	

Youssef et al., 2017 [81]	London, UK 51°N	HW	R134a	evacuated tube	3.021	water paraffin	0.3 30 kg	-	0.54-0.81	4.21-4.99	A serial/dual-source IX-SAASHP	
Buker and Riffat, 2017 [204]	-	SH, HW	R134a	solar thermal roof	1.92	water	0.055	27	-	2.29		
Liu et al., 2017 [206]	-	HW	-	evacuated tube	-	water	-	-5 7	42-55 53-65	1.8-2.7 2.6-3.2	Using a composite heat exchanger	
Youssef et al., 2017 [244]	London, UK 51.5 °N	HW	-	evacuated tube	3.021	water PCM	0.3 30 kg	-	9.632	4.7		
Li et al., 2018 [235]	-	SH	R134a, R1234yf, R141b	evacuated tube	33	water	-	20	20.9	4.2	An ejector enhanced DX-SAASHP	
Lee et al., 2018 [236]	Seoul Korea, 37 °N	HW	R1233zd(E), R134a	air-based flexible solar collector	35.2	water	0.6	2.08-10.92	0.83-3.29	1.12-3.99		
Kim et al., 2018 [209]	-	HW	R134a	collector/evaporator	24	water	-	21	7.21	3.4		
Han et al., 2018 [239]	-	SH, HW	-	evacuated tube	10	PCM water	510 kg 1	-23.4-20	0-45	0-8.3		
Huan et al., 2019 [205]	Xi'an, China 34 °N	HW	-	evacuated tube	860	water	55	24-37	$2.8x10^6$ - $3.2x10^6$	4.87	Serial IX-SAASHP	
					860	-	-		$2.7x10^6$	10-20	Hybrid SAASHP	
Aktas et al., 2019 [223]	-	HW	R410A	double pass collector	-	Paraffin RT42	-	-	-	3.3-3.8		
Stritih et al., 2019 [225]	-	SH	R407C	evacuated tube	25	paraffin RT 31 water	- 3	-	-	4.3-5.7		
Kong et al., 2020 [195]	Qingdao, China 36 °N	HW	R134a	microchannel solar collector	2.09	water	0.2	-3.4-10.7	0.6-1.1	1.65-3.43	A DX-SAASHP using a microchannel condenser	[197]
			R290					-3-14.8	0.5-1.4	1.26-4.61		
Xian et al., 2020 [201]	Guangzhou, China, 23 °N	HW	R134a	PCM microchan	1.11	water	0.04	8-15	0.35-0.55	1-4		[202]

				nel solar regenerator							
Kutlu et al., 2020 [203]	-	HW	R134a	evacuated tube	4	PCM	0.15	9-25	-	3.4-4.6	
Ran et al., 2020 [207]	-	SH	R410a	flat plate collector with fan	2	-	-	7	0.58-0.82	3.12-3.89	
Vega and Cuevas, 2020 [241]	-	SH	-	evacuated tube	22.5	water	0.3	10.2	-	SPF 3.8-4.7	
				uncovered	22.5					SPF 3.7-3.8	
		HW	-	evacuated tube	225	water	22.7	10.2	-	SPF 3.3-4	
				uncovered	225					SPF 2.8-2.9	
Liu et al., 2020 [208]	Xining, China 36.6 ^{o}N	SH	-	evacuated tube	10	water	0.8	-18.2-29.88	-	2.3-4.2	[247]
Ji et al., 2020 [217]	-	SH	-	collector/evaporator	-	-	-	5-15	1.3-1.8	2.2-2.6	
Li et al., 2020 [222]	Suqian, China 34 ^{o}N	SH, HW	R134a	air-type PCM evacuated tube	16	water	0.2	-3.1-11.9	2.6-3.6	2.5-6.5	
Treichel and Cruickshank, 2021 [219]	-	HW	R134a	air-type solar collector	1.26	water	0.189	-	-	1.9-2.4	[220], [221]

To improve collector efficiency, collector plate can be coated with black paintings [31, 43, 46, 47, 48, 64, 65, 66, 67, 68, 69]. Some collectors use serpentine tubes or other special tubes between the plates [35, 65, 70]. The simulation results of a DX-SAASHP using an uncovered and coated collector with a serpentine tube over a year showed daily *COP*s varying from 1.7 (in summer) to 2.5 (in autumn) with an average value higher than 2.0. [65]. The simulation results of a DX-SAASHP using a flat plate collector with a spiral tube showed monthly *COP*s between 4.0 (in summer) and 6.0 (in winter) [70]. The "contradictory" *COP*s in summer and winter are due to the high water temperature in summer which leads to high condensation temperature and low system efficiency. In terms of the effect of weather conditions, the simulation results of a DX-SAASHP using a flat plate collector with a serpentine tube showed *COP*s from 3.83 to 4.69 on sunny days [71]. Especially, in rainy winter, the average *COP* can still achieve 3.3, with the lowest *COP* of 2.51. Similar conclusions can be drawn from experiments where the average *COP*s vary from 5.21 to 6.61 [72, 73]. On a rainy night, *COP* can still reach 3.11 [74].

A novel flat plate collector whose absorber plate is a dimpled and spot-welded steel radiator is shown in Fig. 2-20 [67]. With an area of 11m^2, this novel collector achieves an average collector efficiency of 67.2% at low operating temperature in a serial IX-SAASHP. The system *COP* is 2.19 and the *COP* of HP is 2.55. As a comparison, another serial IX-SAASHP using a conventional flat plate collector obtains a collector efficiency of 60.1% but a system *COP* of 3.08 [75].

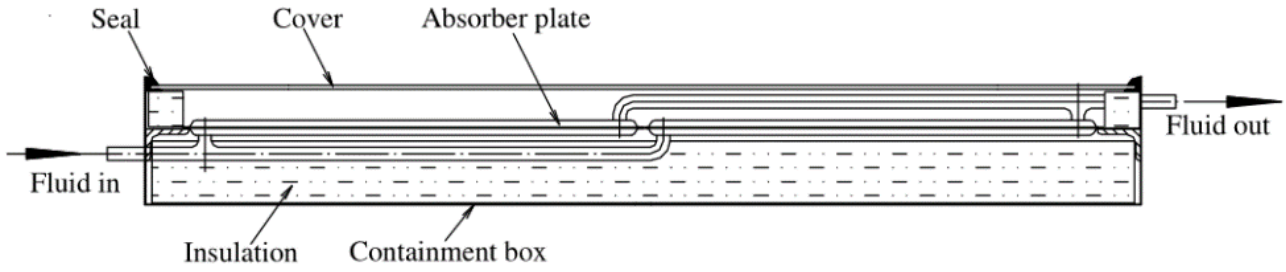

Fig. 2-20: A novel flat plate collector [67].

2.4.2 Solar collector/evaporator

The heating reliability of DX-SAASHP is better than that of direct solar heating since DX-SAASHP can consume more electricity to maintain supply temperature at lower solar availability, but still worse than that of ASHP. To further improve the reliability of DX-SAASHP, both solar and ambient thermal energies can be used by adding an air evaporator or using an uncovered flat plate collector. For example, a collector area of 3.24 m^2 is considered ideal for an uncovered flat plate collector in a DX-SAASHP [76].

To earn a higher year-average *COP*, a larger flat plate collector can be used but it is not economical [32]. Kaygusuz suggests that, when the number of collectors is doubled, *COP* is increased

by 37% while the cost is increased by 65% [31]. Thus, to improve *COP* at a low cost, a collector/evaporator, designed by coating the evaporator surface with solar selective materials, is a good alternative to extract more thermal energy. The average *COP* of a system using a finned tube collector/evaporator is 2.94, 8.1% more than that of conventional ASHP [77]. The average heating efficiency and exergy efficiency are raised by 20% and 8%, respectively.

2.4.3 Evacuated tube solar collector

IX-SAASHPs and hybrid SAASHP for SH require a large collector area of flat plate collector. For a serial-hybrid SAASHP, a simulation study reveals a reasonable collector area of 35 m^2 for a covered flat plate collector [66]. To obtain a smaller system, the evacuated tube collector is an alternative. Simulation and experimental results of a serial IX-SAASHP using evacuated tubes show the maximum *COP*s of 6.33 and 6.38, respectively [78]. For a hybrid SAASHP using evacuated tube collectors, the *COP* can be around 5 at the highest daily solar irradiance [79]. The evacuated tube collector can be integrated with latent TES to further improve thermal performance. For example, an experiment of a serial IX-SAASHP using both an evacuated tube collector and latent TES shows a *COP* of 10.03 [80]. This high *COP* may result from the improvements in both solar collector and TES methods.

2.5 Thermal energy storage

TES is used to balance energy demand and supply. SAASHPs need to mitigate solar energy discontinuity since an overcast for more than 20 minutes can lead to an apparent decrease in the outlet temperature of the collector [83]. Both sensible and latent heat TESs are used in SAASHPs. The seasonal TES is suitable for regions with larger seasonal variations of solar energy availability and heating demand. Table 2-3 summarizes the studies involving latent heat and seasonal TESs. The studies on the sensible heat TES are summarized in Tables 2-4 and 2-5. On average, with improvements in storage methods, systems can perform better with an *SPF* of around 4-5.

Table 2-3: Studies of SAASHPs using latent heat and seasonal TESs

Authors	Location	Function of HP	Refrigerant	Solar collector		TES		T_{amb} (°C)	T_{con} (°C)	*HC* (kW)	*COP*	*SPF*	Comments	Related work
				type	area (m^2)	type	volume (m^3)							
Esen, 2000 [101]	Trabzon, Turkey 41°N	SH	-	flat plate	30	$CaCl_2$	1090 kg	4.5-16.4	-	-	-		-	
Kaygusuz, 2000 [47]	Trabzon, Turkey 41°N	SH	R22	coated, flat plate	30	$CaCl_2$	1500 kg	-3-16	40-55	0.04	4 for serial, 3 for hybrid systems		A serial-hybrid SAASHP	[31], [48], [64], [66], [96], [224]
Yumrutas et al., 2003 [69]	Isparta, Turkey 37.8°N	SH	-	coated, covered, flat plate	30	water (and soil)	300	-9	-	10	4-8		Seasonal TES	[68]
Reuss et al., 2006 [104]	Attenkirchen, Germany 51°N	SH, HW	-	flat plate	764	water soil	500 6800 water equal	-	-	-	3.2-4.4		Seasonal TES	
Qi et al., 2008 [109]	Beijing, China 40 °N	SH	-	flat plate	30, 40, 50, 60	$CaCl_2$	228, 456	-14.8	-	3.025	4.2		A serial/dual-source IX-SAASHP with seasonal latent TES	
Trinkl et al., 2009 [62]	Wuerzburg, Germany 50°N	HW, SH	-	covered, flat plate	30	water/ ice water	12.5 0.3-1	5	-	0.59 for SH and 0.23 for HW	-	4.6	-	
					34.38	water/ ice water	11 0.5				-	4.7		
					24.83	water/ ice water	15 0.5				-	4.3		
Winteler et al., 2014 [173]	Wuerzburg, Germany 50°N	HW, SH	-	bare	10	water/ice	10	-	-	1.09	-	4.25	-	
					13					1.74	-	4.47		
					20					2.26	-	4.12		
					30		20			3.59	-	3.73		
					10		10			0.6	-	3.73		
					10					1.11	-	4.23		

	Strasbourg, France 48°N				20					2.31	-	4.02		
Cabonell et a. 2014 [90]	Strasbourg, France 48°N	SH, HW	-	bare and covered, coated	10-30	waste water	0.13	-	-	0.005 /m²	-	2-7	-	
						water/ice	10-30							
					20-40	waste water	0.13			0.0114 /m²	-	2-4.5		
						water/ice	20-50							
Carbonell et al., 2014 [82]	Strasbourg, France 48°N	SH, HW	-	covered (including 5 m² uncovered collector)	15	ice	25	-	-	0.973	-	5.01	-	[98],
					20		20				-	5.53		[99],
					30		20				-	5.90		[100]
							40			1.147	-	4.78		
					45		30				-	5.1		
Li et al., 2014 [175]	Beijing, China 40 °N	SH, HW	-	flat plate	150	water	105	-6.5	-	-	6.2		Seasonal TES	
Qv et al, 2015 [95]	Shanghai, China 31.17°N	SC	R22	-	-	RT5HC	10.5 kg	30-43	-	7.242	2.3-3	-	Using a novel triple-sleeve energy storage exchanger	[93], [94], [187]
		SH						-17		3.58	2.8	-		
Tamasauskas et al., 2015 [97]	Montreal, Canada 45°N	SC, SH, HW	R507a	covered, flat plate	11.9, 26.8	4% (by mass) propylene glycol/ water	5	-	-	0.935	-	2.53	-	[174]
	Toronto, Canada 43.5°N							-	-	0.863	-	2.55		
	Vancouver, Canada 49°N							-	-	0.767	-	2.43		
Lerch et al., 2015 [46]	Graz, Austria 47°N	SH, HW	-	-	-	water	0.3	-12	-	5.36	-	2.55	ASHP	[191]
				covered, coated, flat plate	14	water	1				-	3.65	Hybrid SAASHP	
				bare, coated	30	water	1				-	3.53	Serial IX-SAASHP systems	
				bare, coated	30	water	1				-	3.56		
						water/ice	0.6							
				covered, coated	14	water	1				-	3.68	A hybrid SAASHP using air	

													preheated by solar as a heat source
				covered, coated	14	water	1				-	3.7	A dual-source IX-SAASHP
Qu et al., 2015 [80]	Beijing, China 40°N	SH	-	vacuum tube	16.2	water Na_2SO_4	0.85 0.8	-	-	-	10.03		-
Youssef et al., 2017 [81]	London, UK 51°N	HW	R134a	evacuated tube	3.021	water paraffin	0.3 30 kg	-	-	0.54-0.81	4.21-4.99		A serial/dual-source IX-SAASHP
Youssef et al., 2017 [244]	London, UK 51.5 °N	HW	-	evacuated tube	3.021	water PCM	0.3 30 kg	-	-	9.632	4.7		
Han et al., 2018 [239]	-	SH, HW	-	evacuated tube	10	PCM water	510 kg 1	-23.4-20	-	0-45	0-8.3		
Aktas et al., 2019 [223]	-	HW	R410A	double pass collector	-	paraffin RT42	-	-	60	-	3.3-3.8		
Stritih et al., 2019, [225]	-	SH	R407C	evacuated tube	25	paraffin RT 31 water	- 3	-	-	-	4.3-5.7		
Kutlu et al., 2020 [203]	-	HW	R134a	evacuated tube	4	PCM	0.15	9-25	-	-	3.4-4.6		
Lu et al., 2020 [249]	-	SH	-	-	40	water	40 2	-5-37	-	-	3.95 3.5	- -	Seasonal TES Normal TES

2.5.1 Sensible heat thermal energy storage

Typical air, geothermal and water source HPs make use of sensible heat as heat sources. Sensible heat can also be used to store thermal energy. Water and soil are widely used as mediums for sensible heat TES. The maximum capacity for sensible heat TES, Q_{max}, is determined by Eq. (2-6) [30]

$$Q_{max}=\rho V c_p(T_{max} - T_{min}) \quad (2\text{-}6)$$

where ρ, V and c_p are the density, volume and specific heat capacity of the TES medium. T_{max} is the temperature of the TES tank fully-charged and T_{min} is the temperature of the TES tank fully-discharged.

Geothermal TES can be integrated into a serial IX-SAHP using boreholes as the TES container (see Fig. 2-21) [84]. A numerical simulation of a solar-geothermal hybrid HP showed that the system can save energy by 2.08 TJ per year, equivalent to 70-ton standard coal and corresponding to 234-ton carbon dioxide emission [85]. An experiment demonstrated that the utilisation of ground TES helps to improve the *COP* from 2.95 to 3.36 compared with SAASHP [49]. However, since a deep borehole is required for sufficient heat exchange with the ground, the excavation increases the installation cost of geothermal heat exchangers. Moreover, the heat stored in summer may not equal the heat extracted in winter, influencing underground temperature balance [85].

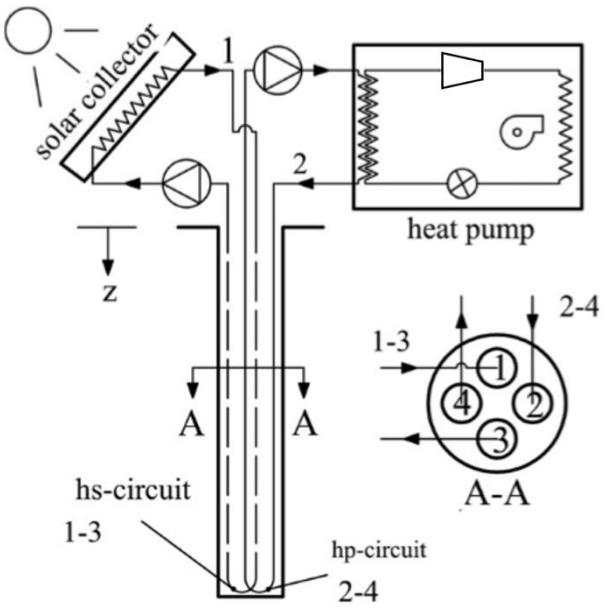

Fig. 2-21: Solar-geothermal hybrid source HP (reproduced from [84]).

Water TES is more popular than geothermal TES since water has a higher thermal capacity and the manufacturing of water tanks requires much less capital cost. Water tank with a high degree of thermal stratification shows 5.3% energy saving over one year than fully-mixed water tank [86] because the uniform distribution of water temperature reduces exergy [87]. Diffusers can be used to

enhance thermal stratification. This increases the energy efficiency of the system by 15%-20% compared with that using a fully-mixed water tank [88]. A low water flow rate contributes to a high degree of thermal stratification. Therefore, the water flow rate can be optimized considering the heating capacity and *COP* [44]. Water TES can be integrated with other components for heat recovery. An early study of a DX-SAASHP nested the evaporator/collector into a solar pond (TES) [89]. It achieved a *COP* higher than 3.0 in winter and a maximum *COP* of 8.4 in summer. A numerical simulation showed that recovering heat from waste-water stored can enhance the *SPF* of a SAASHP from 4% to 20% and recovering heat from drain water can improve the *SPF* by 2% [90].

2.5.2 Latent heat thermal energy storage

Latent thermal energy is embodied in the phase change material (PCM) at a constant temperature and is greatly larger than sensible thermal energy. A study on a serial/dual-source IX-SAASHP suggests that latent heat TES can increase the *COP* by 6.1% and 14% on sunny and cloudy days [81]. Another study designs a multi-function system which uses solar energy, latent TES and ground source [91]. In the latent TES mode, this SAHP achieves an average *COP* of 4.86, almost twice of that the GSHP mode. When the latent heat TES is used as a heat source, a *COP* of 4.67 has been achieved.

PCMs are commonly stored in tanks and their storage efficiency is hardly influenced by system configurations. For example, for both serial IX-SAASHPs and hybrid systems, the storage efficiencies of PCM-filled tanks are equal to 63% [47, 48]. Due to some characteristics of PCM, such as the volume change during the phase change process, tank selection for latent heat TES differs from that for sensible heat TES. Using a rectangular tank can decrease the melting time by 50% compared with using a cylindrical tank with the same volume and heat transfer area [92].

A novel triple-sleeve heat exchanger has been proposed as shown in Fig. 2-22 [93]. The refrigerant flows in the inner tube and PCM is filled between the inner and the middle tubes. Heat transfer fluid absorbs thermal energy in the solar collector and flows inside the outer tube. The effect of the temperature of the heat transfer fluid on TES is higher than that of its flow rate. Ni et al. investigated a SAASHP with this triple-sleeve heat exchanger [94]. Compared with an ASHP, at an ambient temperature above 38 ^{o}C, the cooling *COP* of the SAASHP using the novel heat exchanger is 17% higher; at an ambient temperature below -10 ^{o}C, the heating *COP* of this system is enhanced by 65% [95].

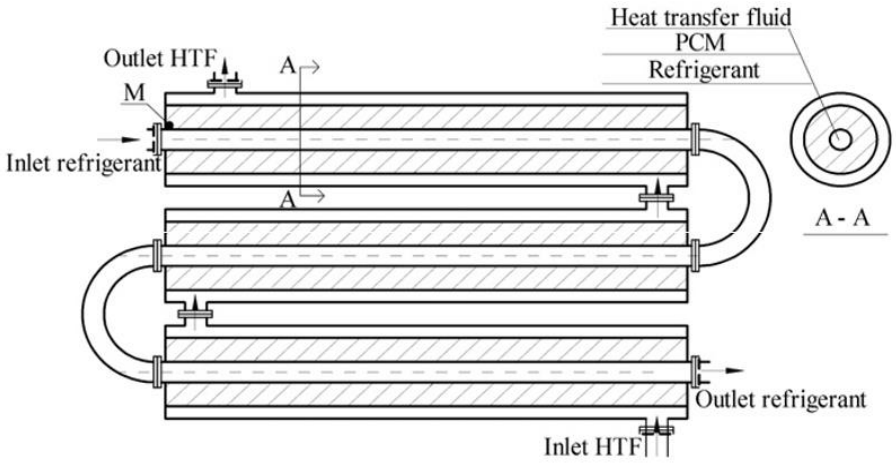

Fig. 2-22: Triple-sleeve heat exchanger [93].

Commonly used PCMs include paraffin, calcium chloride ($CaCl_2$), sodium sulphate (Na_2SO_4) and ice slurry. A novel serial/dual-source IX-SAASHP with paraffin for latent heat TES shows improvement in *COP*, especially on cloudy days [119]. A serial-hybrid SAASHP using $CaCl_2$ as the TES medium reaches a seasonal *COP* of 4.5 with a storage efficiency of 0.62 [96]. Generally, PCMs have poor thermal conductivity, which leads to higher thermal resistance and lower heat transfer. It also increases the time of charging and discharging processes, and thus impacts the overall system efficiency. However, studies involving both sensible and latent heat TESs suggest that latent heat TES is superior to sensible heat TES. A dual-tank serial IX-SAASHP using Na_2SO_4 shows a *COP* of 10.03, about 3.5 times higher than that of a system only using sensible heat TES [80]. The collection efficiency (the ratio of thermal energy stored in water or PCM to the collected solar thermal energy) increases by 50% when the latent heat TES is used, while the influence of the sensible heat TES is negligible. Another dual-tank serial IX-SAASHP using ice slurry as the PCM reaches an *SPF* of 4.6, where solar energy meets 78% of the heat demand [62].

Water/ice is the most available and eco-friendly PCM. Compared with an electrical resistance heating system, a serial IX-SAASHP using ice slurry as the PCM saves energy consumption by 86% [54, 97]. However, a SAASHP using sensible heat TES can also save 81% of energy consumption. A model of a reversible ice storage tank, which uses three plate heat exchangers: two attached to the tank wall and one inserted in ice, was proposed and validated for solar heating [98, 99]. Based on the model, the *SPF* of a SAASHP using ice storage is predicted to be around 5.0 [82]. For the ice storage buried in a borehole, energy extraction can be influenced by ground properties [100]. Under two extreme ground conditions, the energy injection of the two heat exchangers on the wall fluctuates by 6%, and the energy injection of the heat exchanger in ice significantly fluctuates by 20%.

It should be noticed that increasing collector area or latent heat TES volume can improve system performance. Taking economic factors into account, to achieve the same performance, an increase in collector area is more beneficial [46, 62, 82].

2.5.3 Seasonal thermal energy storage

Solar TES includes daily and seasonal storage. The daily storage stores solar thermal energy collected during the daytime and releases it at night. The seasonal TES stores the solar thermal energy collected in summer for heating in winter and/or in winter for cooling in summer. The seasonal TES is suitable for high latitude regions where seasonal solar energy and heating demand are dramatically mismatched [101]. Seasonal TES allows solar energy to provide more than 50% of the annual heating demand [102]. Compared with daily TES, seasonal TES requires a large storage volume and collector area, consequently high cost [30].

Commonly used mediums for seasonal TES include water, gravel-water, ground and aquifer. Different mediums require different start-up time to pre-heat surrounding soil up to normal operating conditions [102]. Tanks using water and gravel-water need to be buried (partly) in the ground. The ground and aquifer are directly employed as underground TES mediums. The buried water tank can be independent of ground properties due to its good insulation [102]. This additional insulation cost can be partly compensated by lower excavation costs. The results of a serial IX-SAASHP using an underground hemispherical surface tank for seasonal TES suggest that a small burial depth is capable of achieving desired annual *COP* and temperature of the storage tank [68, 69]. The aquifer and ground TESs have better economic efficiencies than burial tanks [103]. Combining cost effective methods with high thermal capacity methods may improve the system performance. For example, a system combining hot water and ground storage achieves an *SF* of 74% and a system *COP* of 4.4 [104]. It is worth noting that the change in ground temperature may bring disadvantages to the environment [30].

Water has a higher specific heat capacity while solid mediums allow a higher temperature range for higher TES capacity [105]. In the cold climate regions, since the heat loss increases with the increase in temperature difference between storage mediums and surroundings, low-temperature seasonal TES is suitable [106] and benefits storage stratification and thus storage efficiency [107]. The lower temperature of the fluid entering the solar collector also improves collector efficiency [108]. PCM is a promising medium for low-temperature seasonal TES. The size of the latent heat TES is much smaller than that of a sensible heat TES. Numerical simulations were conducted to examine the annual periodic performance of a dual-source IX-SAASHP using a seasonal latent heat TES [109]. This system achieves an *SPF* of about 4.2.

2.6 Defrosting

The frosting is an issue influencing the reliable operation and efficiency of ASHPs in winter, especially in humid regions. Frost build-up on the surface of the evaporator deteriorates heat transfer and efficiency and eventually shutdown of ASHPs [110,111]. The mechanisms of frosting and

defrosting on the surface of the evaporator are reviewed in [112, 113, 114]. Song et al. [114] comprehensively reviewed the defrosting methods including cycle reversing [115], hot gas bypass [116], electric heater [117], dehumidification [118] and polymer coatings [119]. The principle of the cycle reversing, hot gas bypass and electric heater is to melt the frost layer. The periodic defrosting required not only consumes electricity but also causes mismatching in the heating demand. The cycle reversing requires a well-designed control strategy to balance the SH demand and effective defrosting [115]. The dehumidification requires replacing or regenerating desiccant periodically as the moisture absorption capacity drops [118]. The polymer coating enables the reduction of the surface free energy and ice adherence force and hence delays frosting [119], where the challenge is to sustain the performance of the coating surface.

TES can assist the conventional defrosting methods [114, 120]. As shown in Fig. 2-23, a PCM storage is parallel to the condenser [121]. During the period of reverse-cycle defrosting, no thermal energy is provided for indoor SH. The stored heat assists to shorten the defrosting period by 38% [122]. The PCM storage is placed around the compressor to use the waste heat [123]. During the reverse-cycle defrosting, ASHP continues to provide SH because the stored waste heat is delivered to both indoor and outdoor heat exchangers. The defrosting time and total energy consumption are 65% and 27.9%, respectively, lower than conventional reverse-cycle defrosting. Over the whole test period, the *COP* and total heating capacity increased by 1.4% and 14.2% with the power input increasing by 12.6%.

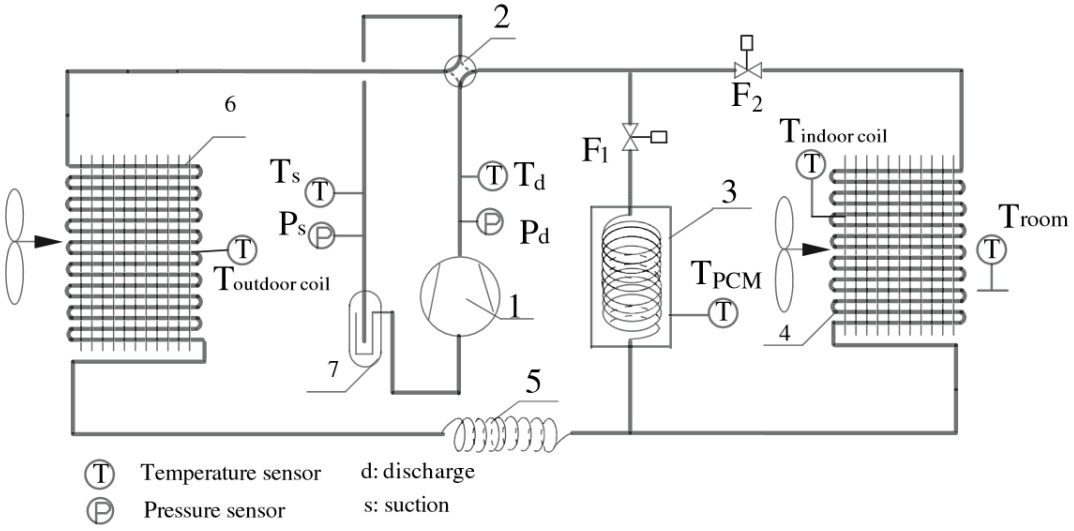

Fig. 2-23: Reverse-cycle defrosting ASHP system with energy storage [121, 122].

Fig. 2-24 shows an ASHP using a PCM-filled tank and an additional evaporator coated with desiccant in series [124]. This system enables continuous heat provision in both heating and regeneration modes. In the heating mode, the air is dehumidified as it flows through the desiccant-coated evaporator (9) and then flows through the evaporator (12). The refrigerant is condensed in a

condenser embedded in the water TES tank (4) and then releases the residual heat in the PCM TES tank (6). The refrigerant absorbs the latent heat released during the air dehumidifying process in the desiccant-coated evaporator (9). This increases the evaporation temperature of the evaporator (12) to avoid frosting. In the regeneration mode, refrigerant is condensed in a condenser embedded in a water TES tank (4) and releases the residual heat for desiccant regeneration as it flows in two evaporators (9 and 12). The refrigerant vaporises as it flows through the PCM TES tank (6) and absorbs the stored thermal energy. Experimental results of this ASHP show a *COP* of 2.81, 7.3% and 46.3% higher than those of hot-gas bypass defrosting and electric heaters [124]. The heating performance of ASHP is also superior to that of ASHP using reverse-cycle defrosting, especially in cold weather conditions [125].

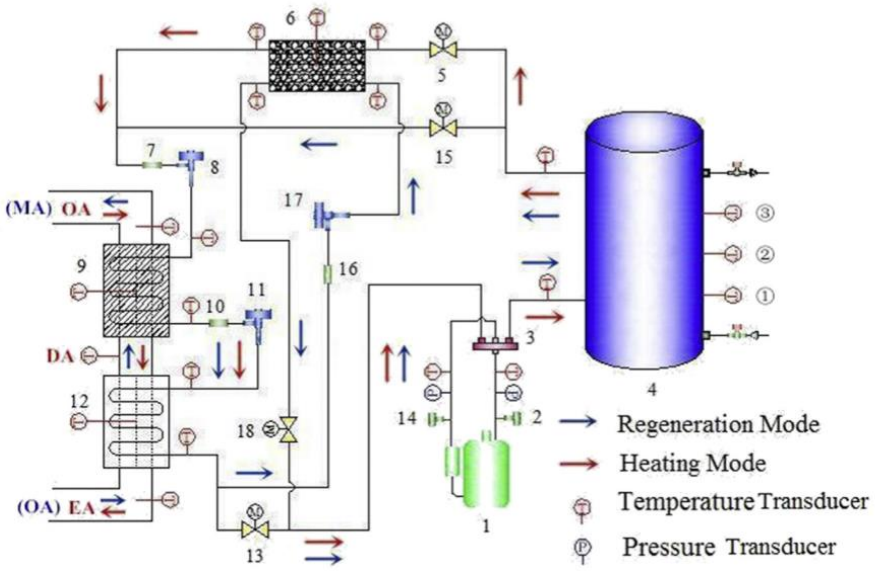

Fig. 2-24: ASHP with energy storage and dehumidification [124, 125]. 1 - compressor, 4 - water TES tank, 6 - PCM TES tank, 9 - desiccant-coated evaporator, 12 – evaporator.

For SAASHP, defrosting is only a concern for outdoor evaporators. Solar thermal energy helps to reduce frost on solar collectors [126]. Kong et al. [127] numerically and experimentally studied a DX-SAASHP under frosting conditions. The results showed that frosting on solar collectors can be significantly delayed. Experiments [128] show that the frosting on a solar collector is much slower than that on an evaporator and after a 6-hour experiment, frost is merely seen on the solar collector. At a lower solar irradiance of 100 W/m^2 and higher relative humidity of 70%, no frost is observed when the ambient temperature is higher than -3 ^{o}C.

2.7 Observations and outlook

Current studies on SAASHP focus on the match and improvements of system configuration. However, there is a lack of improvements in each component and its matching application in SAASHP.

This section summarises recent research status in terms of system configuration, solar collector, TES, working conditions, refrigerants and their influences on system performance. In addition to Table 2-2 summarizing the details regarding the utilisation of collector/evaporator and evacuated tube solar collector and Table 2-3 summarizing the details about the studies of SAASHPs using latent heat and seasonal TESs, Tables 2-4 and 2-5 give the details of the typical studies of DX-SAASHP and IX-SAASHP. The statistic summaries given in these tables provide an overall view of the studies on this topic and sufficient information for the further analysis below.

Table 2-4: Research on DX-SAASHP using flat plate collectors and water tank

Authors	Location	Function of HP	Refrigerant	Solar collector		Volume of TES (m^3)	T_a (°C)	T_{con} (°C)	*HC* (kW)	*COP*	Related work
				type	area (m^2)						
Chaturvedi and Shen, 1984 [33]	-	HW	R12	bare	3.39	-	-4-22	40-50	-	2-3	
Chaturvedi et al., 1998 [134]	Virginia, USA 37.8°N	HW	R12	bare	3.48	-	10-27	40	1-1.5	2.5-4.0	[152], [159]
Axaopoulos et al., 1998 [140]	Athens, Greece 38°N	HW	R12	bare	2	0.158	5-40	-	0.14 /m^2	3.42	
Ito et al., 1999 [76]	Kanagawa, Japan 36°N	HW	R12	bare	3.24	-	8	-	-	5.3	
Huang and Chyng, 1999 [148]	-	HW	R134a	bare	1.57	0.12	31.3	45.6	-	3.83	
Huang and Chyng, 2001 [137]	Taiwan, China 23°N	HW	R134a	bare	1.44	0.105	27-37	45-68	0.678-0.926	2.5-3.7	[141]
Hawlader et al., 2001 [192]	-	HW	R134a	bare	3	0.25	26-36	-	-	4-9	
Torres-Reyes and Cervantes, 2001 [162]	Mexico 23°N	SH	R22	-	4.5	-	20-32	-	2.8-5.37	2.56-3.46	[163], [164]
Chyng et al., 2003 [65]	Taiwan, China 23°N	HW	R134a	bare, coated	1.86	0.105	-	-	-	1.7-2.5	
Kuang et al., 2003 [70]	Shanghai, China 31.17°N	HW	R22	bare	2	0.15	3-12	-	-	4-6	
Ito et al., 2005 [146]	-	-	R22	-	1.91	-	-	-	-	4.5-6.5	
Chata et al., 2005 [151]	-	-	R12, R22, R134a, R404A, R407C, R410A	bare covered	15.6 17.2	-	5	60	7	3.8	

Kuang and Wang, 2006 [37]	Shanghai, China 31.17°N	SC, SH, HW	R22	bare	10.5	0.2, 1	7.9-12.1	-	5.8-7.6	2.1-2.7 (SH)	
Xu et al., 2006 [71]	Nanjing, China 32°N	HW	R22	bare	2.2	0.15	5	-	-	2.51-4.69	
Anderson and Morrison, 2007 [138]	Sydney, Australia 34°S	HW	R22	bare	4	0.27	25 20	-	-	5-7 3-5	
Huang and Lee, 2007 [142]	-	HW	R134a	coated none	-	0.115 0.24 0.13 0.2	-	-	-	2.12-2.72 2.24-3.57 1.85-2.53 2.48-2.78	
Kara et al., 2008 [5]	Izmir, Turkey 38°N	SH	R22	bare	4	-	2	55	1.75	-	
Mohanraj et al., 2008 [139]	Calicut, India 11°N	SH	R22	covered, coated	2	-	29-33.3	60	-	1.98-2.57	[145], [147]
Chow et al. 2010 [32]	Hong Kong, China 22°N	HW	R134a	bare	12	2.5	30-32.8 13-15.8	58.1-63.5 51.65-55.85	4.82-6.3 3.52-5.33	6.57-10.7 4.31-9.14	
Kong et al. 2011 [73]	Shanghai, China 31.17°N	HW or SH	R22	bare	4.2	0.15	20.6-28.9	-	0.208-0.27	5.21-6.61	[72], [74], [87]
Fernández-Seara et al., 2012 [150]	-	HW	R134a	bare	-	0.3	7-22	21.2-57.9	-	3.23	
Moreno-Rodríguez et al., 2012 [143]	Madrid, Spain 40°N	HW	R134a	-	5.6	0.3	11-19	57	0.275-0.3125	1.7-2.9	
Moreno-Rodríguez et al., 2013 [144]	Madrid, Spain 40°N	SH	R134a	-	5.6	-	0-20	32-40	2.375-2.917	1.9-2.7	
Molinaroli et al., 2014 [136]	-	SH	R407C	bare	40.32 29.12 22.40 16.80	-	-5, 0, 5, 10, 15	50	7.5	2.2-4.3	
Sun et al. 2014 [149]	Shanghai, China 31.17°N	HW	R134a	coated	1.92	0.15	26	-	-	4.5-8.5	[60]

Scarpa and Tagliafico, 2016 [61]	-	HW	R134a, R600a	bare	1	0.025	5.3, 16.5, 33.2	45	0.216, 0.295, 0.392	5.8	[155], [156], [158]
Deng and Yu, 2016, [34]	-	HW	R134a	-	2	0.15	-	55.1-57.6	-	4.46-4.74	
Paradeshi et al., 2016 [135]	Calicut, India 11.15ºN	SH	R22	-	2	-	-	-	2.0-3.6	1.8-2.8	
Kong et al., 2017 [157]	-	HW	R410A	bare	4.2	0.15	25.7	-	3.14-4.27	3.62-8.6	[154]
Mohamed et al., 2017 [126]	-	SH, HW	R407C	bare	4.22	0.2	6.5-8.5	86	3.3-4.2	2.7-3.9	
Paradeshi et al., 2018 [234]	Calicut, India 11.15 ºN	SH	R22, R433A	covered	2	-	-	-	1.9-3.5	-	
Cai et al., 2019 [29]	-	HW	-	bare	4.2	0.15	5-15	31-50	1.5-2.5	2.5-3.5	
Huang et al., 2019 [213]	-	SH	-	bare, coated	4	-	-5-5	-	0.75-1.1	1.5-2	
Duarte et al., 2019 [230]	Pampulha, Brazil	HW	R134a, R290, R600a, R744, R1234yf	coated	1.65	0.2	25-33	-	-	2.25-2.91	
Rabelo et al., 2019 [242]	-	HW	R134a, R290	uncovered	1.65	0.2	25	60, 65, 70	1.37	2.5	
Cao et al., 2020 [237]	-	HW	R134a	covered	4.2	0.15	25.7	-	-	4-6	
Cai et al., 2020 [215]	-	SH	-	bare, coated	4	-	2-15	-	2.4-2.7 parallel; 2.35-2.6 serial	4.5-4.58 parallel; 4.33-4.5 serial	
Liu et al., 2020 [243]	Qinghai, China 36 ºN	SH	R22	-	6	1.8	-3.1	45	-	2-4	
Zhang et al., 2020 [216]	Hefei, China 32 ºN	SH, SC	-	bare, coated	-	0.3	5.9-14	-	-	2.87-3.8	

Table 2-5: Research on IX-SAASHP and hybrid SAASHP using flat plate collector and water tank

Authors	Location	Function of HP	Refrigerant	Solar collector		Volume of TES (m^3)	T_a (^oC)	*HC* (kW)	*COP*	*SPF*	Related work
				type	area (m^2)						
Freeman et al., 1979 [63]	Madison, USA 43°N Albuquerque, USA 35°N Charleston, USA 38°N	SH, HW	-	-	10, 20, 30, 40, 50, 60	0.075 per m^2 solar collector	-	1.95 (SH), 0.68 (HW) 0.94 (SH), 0.68 (HW) 0.485 (SH), 0.68 (HW)	2 (hybrid) 2.5 (dual-source) 2.8 (serial)	-	
Yumrutas and Kaska, 2004 [42]	Gaziantep, Turkey 37.18°N	SH	R22	covered	7.4	0.65	7.8-16.1	-	2.5-3.5	-	
Dikici and Akbulut, 2008 [75]	Elazig, Turkey 38.41°N	SH	R22	-	11.1	0.18	3.9	3.844	3.08	-	[49]
Li and Yang, 2009 [161]	-	HW	R22	-	6	0.4	15-30	11	4 (DX-SAASHP), 4 (serial), 3 (hybrid)	-	
Chaichana et al., 2010 [166]	Chiang Mai, Thailand 18.8°N	HW	R22:R124:R152a (20%: 57%: 23%)	bare	4, 8, 12, 16, 20	0.3, 0.6, 0.9, 1.2	13.7-36.2	-	4.1-4.6	-	[168]
Li and Yang, 2010 [43]	Hong Kong, China 22°N	HW	R22	covered	390	32	15 25	-	3.5 3.86	-	
Bakirci and Yuksel, 2011 [41]	Erzurum, Turkey 41°N	SH	R134a	coated, covered	1.64	2	-10.86	3.801	2.86	-	
Sterling and Collins, 2012 [54]	Ottawa, Canada 45°N	HW	-	-	4	0.5	-	0.634	2.5-5	-	[53]
Tagliafico et al., 2012 [178]	-	HW	-	bare	1.78	-	0-15	150	-	-	
Chow et al., 2012 [165]	Hong Kong, China 22°N	SH, HW	R22	-	1400	-	10-23	-	4.48-4.56	-	
Panaras et al., 2014 [183]	Athens, Greece 23.5°N	HW	-	coated	2.58	0.28	18.5	0.643	2.12	-	[180]

Banister and Collins, 2015 [169]	-	HW	-	-	2.5, 5, 7.5, 10	0.3, 0.45	-	-	2.3-6.3	-	
Fraga et al., 2015 [167]	Geneva, Switzerland 46°N	SH, HW	-	bare	116	6 + 0.3*8	-2.4-20.5	2.13 (SH), 5.28 (HW)	-	2.9	[229]
Ji et al., 2015 [186]	Lab based	HW, SH, SC	-	-	3.2	0.2	7	1.2-2.4 (HW) 1.4-2.2 (SH)	1.75-3 (HW) 2.35-2.75 (SH)	-	
Cai et al., 2016 [44]	Lab based	SH, SC, HW	-	-	3.2	0.3	7	1.9-2.4 (HW) 1.3-1.5 (SH)	2-3.25 (HW) 2.25-2.5 (SH)	-	[214]
Poppi et al., 2016 [185]	Zurich, Switzerland, 47°N	SH, HW	R410A	-	9.28	0.763	-10	0.347 (HW), 0.944 (SH)	-	3.16	[184]
								0.347 (HW), 1.966 (SH)	-	2.43	
	Carcassonne, France 43°N						-5	0.307 (HW), 0.419 (SH)	-	3.85	
								0.307 (HW), 1.047 (SH)	-	2.93	
Liu et al., 2016 [50]	Zhengzhou, China 34°N	HW, SH	-	-	-	-	-15, -10, -7, -5, 2, 7	1.2-2.9	2-3.1	-	
Li and Kao, 2017 [182]	Taipei, China 25°N	HW	R410A	-	3.84	0.46	-	-	-	3.92	
						0.92			-	4.36	
	Kaohsiung, China 22.5°N					0.46			-	4.31	
						0.92			-	4.83	
Bellos and Tzivanidis, 2017 [176]	-	SH	-	-	5-80	1	-1.4-14	5-15	4	-	

Li and Kao, 2018 [240]	-	HW	-	-	5	0.4+0.2, 0.5+0.25, 0.6+0.3	4-30	-	-	-
Ran et al., 2020 [231]	Lhasa, China	SH, HW	-	-	300	10	-	120	-	6.92
	Chengdu, China							90	-	3.61
	Beijing, China							180	-	3.27
	Shenyang China							270	-	2.45
Liu et al., 2020 [238]	Chongqing, China 29 °N	HW	R410a	-	5.5	0.25	5-40	-	2-5.2	-
Wang et al., 2020 [233]	Changsha, China 28.5 °N	HW	R134a	covered	150	10	20-30	-	1.5-3.5	-
Long et al., 2021 [211]	-	HW	-	-	12	0.3	26-32	3-11	1.5-5.5	-

Working fluid determines the selection of the compressor and therefore the corresponding components. Fig. 2-25 summarises the number of open literature per year for SAASHPs using different refrigerants. It can be seen that, generally, the number of studies on SAASHPs shows an apparent increase in the past 10 years. Currently, refrigerants such as R22, R134a, R32, R410A and R407C are normally used in HPs due to their good thermodynamic and thermophysical properties [20]. Due to the composition shift and temperature glide, the currently used mixed refrigerants have technical limitations [129]. The parameters that determine the environmental impacts of refrigerants are the ozone depletion potential (ODP) and global warming potential (GWP). These parameters are high for the specified refrigerants. International environmental protocols [130, 131, 132] have imposed restrictions on the use of refrigerants according to ODP and GWP parameters. According to the Kigali Agreement [131], natural refrigerants such as hydrocarbon refrigerants and carbon dioxide (R744) were found to be long-term sustainable options for HPs [20]. For example, the performances of R1270 and R290 are closer to that of R22 but their flammability requires more safety considerations while retrofitting [83]. Current studies on environment-friendly refrigerants with low GWP, such as R32 and R290, are insufficient and need to be further investigated. R32 is a more environment-friendly alternative refrigerant to R410A in HPs and it is most commonly used in Japan for supplying HW. However, due to flammability (A2L) issues some countries are researching other retrofits, such as R454B. R290 is the most popular refrigerant for HPs in Europe not only for HW but also for SH applications. The recent increase in refrigerant inventory limit (IEC 60335-2-89 [133]) enables greener refrigerants such as R32 and R290 in these applications.

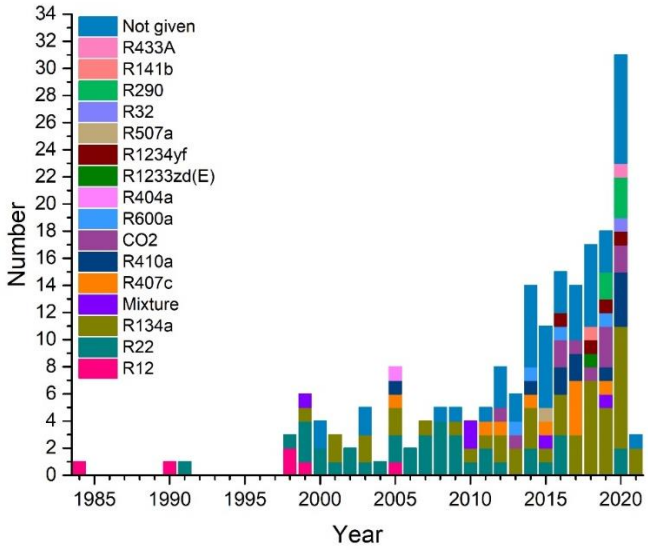

Fig. 2-25: Number of papers published in journals per year for SAASHPs using different refrigerants.

The geographic location affects solar availability and thus the research interests on SAASHP. Fig. 2-26 shows the number of investigations on SAASHPs in different countries. It can be noticed that the majority of studies have been located in China (48%), Turkey (10%), the USA and Canada (5%). The studies in the UK are only 3%. SAASHPs for the domestic sector are mainly investigated by researchers from mid-latitude (20^o - 50^o) countries where SH is required in winter and HW is required throughout the year under the medium solar energy availability and temperate climate conditions (-15 °C - 30 °C). SAASHPs for high-latitude areas need to be further investigated.

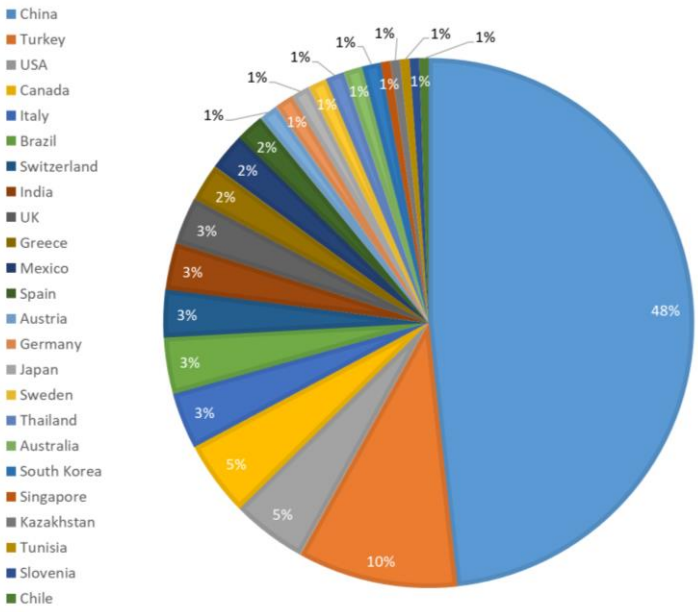

Fig. 2-26: Distribution of investigations in countries.

Generally, the higher solar irradiance leads to the higher *COP* of SAASHP [33, 71, 73, 77, 134, 135, 136, 192]. For example, a numerical simulation of DX-SAASHP for HW has tested the effects of various parameters (see Figs. 2-27 and 2-28) [73]. As solar irradiance increases from 300 to 1000 W/m^2, *COP* increases from 4.2 to 6. In this process, solar collector efficiency decreases from 1.5 to 0.85. It should be noticed that an uncovered collector is used in the study which absorbs thermal energy from both solar irradiation and ambient air. At lower solar irradiance, the collector mainly absorbs thermal energy from ambient air and achieves an efficiency over 1; at higher solar irradiance, the collector mainly absorbs thermal energy from solar energy and the efficiency is lower than 1 because of heat loss. For a covered collector, the trend is the same but less apparent [108].

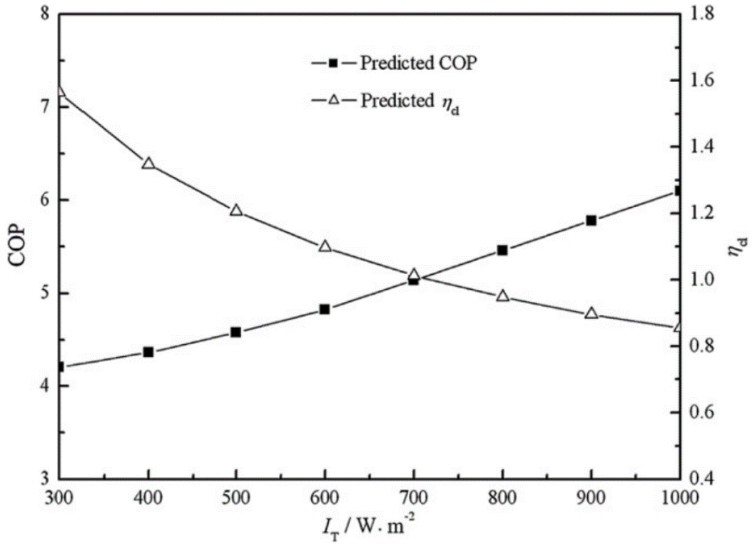

Fig. 2-27: Effects of solar irradiance I_T on *COP* of the SAASHP and the collector efficiency η_{cl} [73].

In terms of ambient temperature, as Fig. 2-28 shows, high ambient temperature leads to higher *COP* and collector efficiency [73]. With the increase of ambient temperature from 5 ºC to 35 ºC, *COP* increases from 4.5 to 5.7, and collector efficiency increases from 0.75 to 1.07 since as ambient temperature increases, a collector can earn more thermal energy from the air and thus increase efficiency.

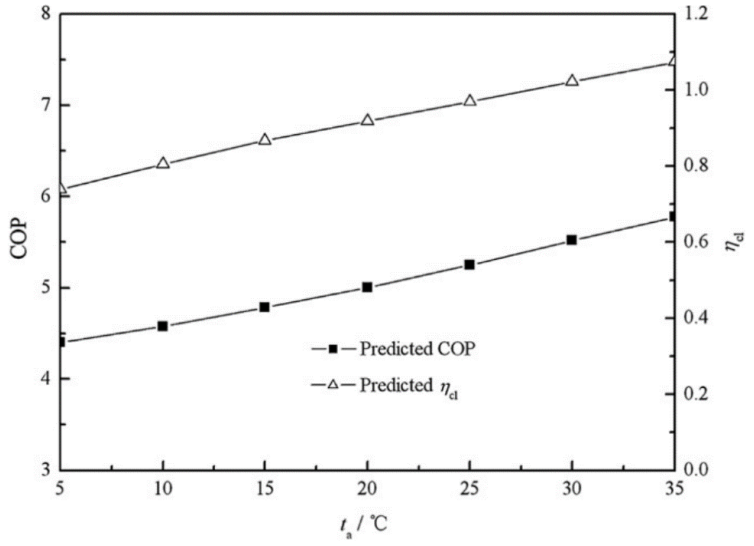

Fig. 2-28: Effects of ambient temperature t_a on *COP* and collector efficiency η_{cl} [73].

The required output temperature has a negative linear influence on *COP*. As Fig. 2-29 shows, a study of a DX-SAASHP for HW concluded that the higher the output water temperature was, the lower the system *COP* would be [35, 65, 70, 137]. As the output water temperature increases from 25 ºC to 60 ºC, the *COP* drops from 3.7 to 2.7 linearly. An

experiment of a DX-SAASHP for HW shows that, with a rise of the temperature difference between output water and the ambient environment from 5 °C to 40 °C, *COP* drops from 5 to 2 (see Fig. 2-30) [138]. This is, as output water temperature increases, compressor discharge pressure increases, and therefore energy consumption increases [44]. In turn, as the inlet source temperature decreases, compressor suction pressure decreases. The increase in pressure ratio brings lower *COP*.

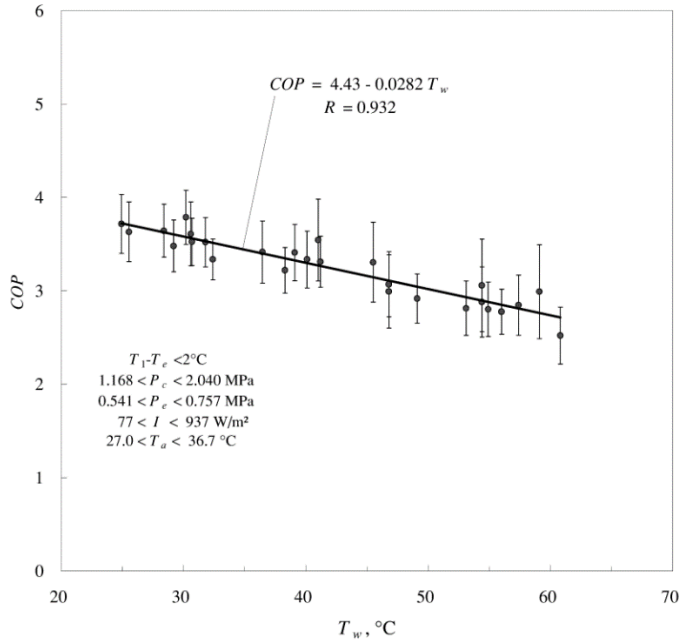

Fig. 2-29: Effect of output water temperature T_w on *COP* [137].

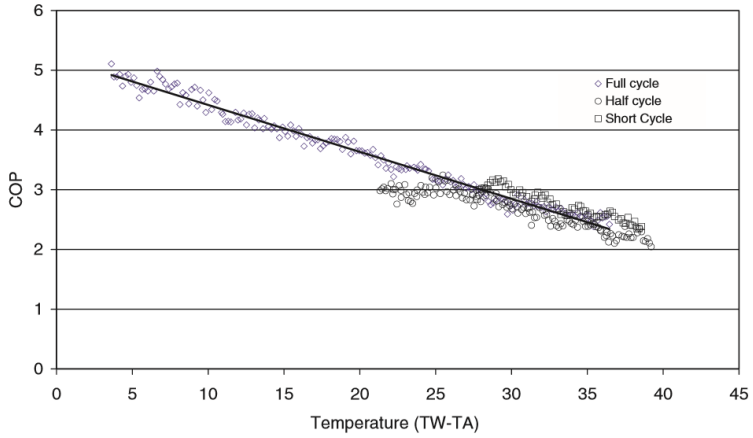

Fig. 2-30: *COP* as a function of the temperature difference between average water temperature in water tank to ambient air, T_w-T_a [138].

Fig. 2-31 summarises the effect of ambient temperature on *COP* of the SAASHPs for different end use in published papers. The advanced systems refer to the SAASHPs involving innovations in the aspects of solar collector, TES and system configuration. In this figure, the *COP* values are taken as the average values and the ambient temperatures are taken as the

lowest values of the working conditions. The ambient temperature ranges from -15 ºC to 30 ºC and *COP* ranges from 2 to 8.5. The majority of the *COP*s obtained range from 2 to 6. Especially, an IX-SAASHP for SH using seasonal latent heat TES earned a *COP* of ca. 4.2 at -15 ºC [109]. Similarly, another IX-SAASHP with seasonal TES for SH achieved a higher *COP* of ca. 8.5 with a collector area of 40 m^2 and a storage volume of 1960 m^3 [68]. Interestingly, the *COP* values of two DX-SAASHPs shown in [32] and [139] vary significantly. This concerns many reasons. The DX-SAASHP in [32] uses R134a as the working fluid and uses an uncovered collector of 12 m^2; the DX-SAASHP in [139] uses R22 as the working fluid and uses a covered collector of 2 m^2. Overall, advanced IX-SAASHP is ideal for SH as well as HW, and DX-SAASHP is more suitable for HW. For multi-functional SAASHP, advanced IX-SAASHP is the best choice.

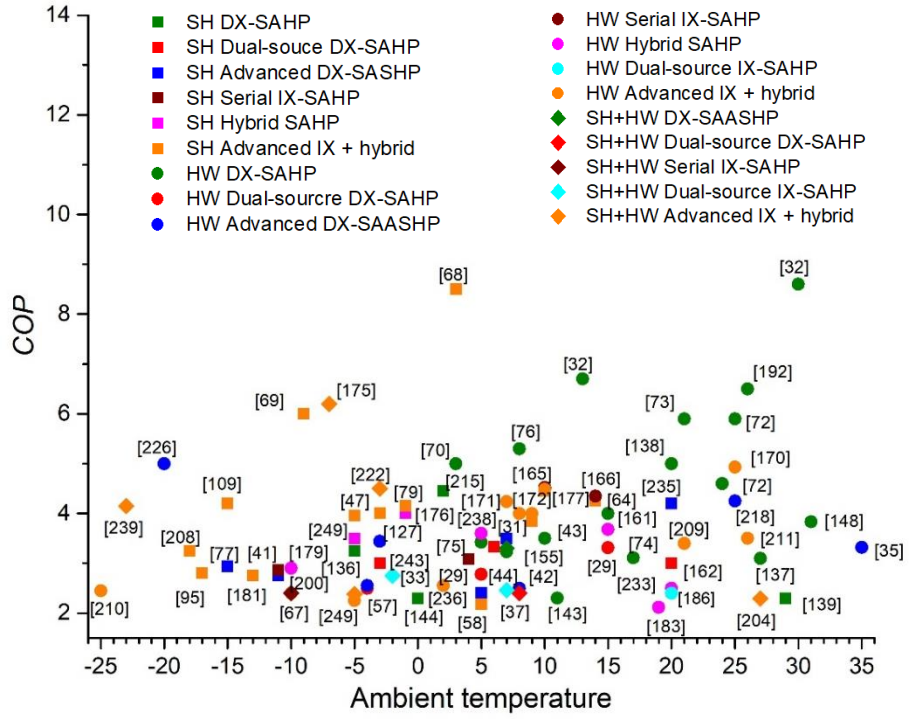

Fig. 2-31: *COP* vs ambient temperature of the SAASHPs for SH and HW.

Fig. 2-32 summarises the number of open literature having different *COP* where *COP* values take the average of values given in the studies. It can be observed that the *COP* values of most of these SAASHPs are located in the range of 2.0 to 6.0. The dual-source IX-SAASHP achieves *COP* lower than 3.5. The hybrid SAASHP, serial IX-SAASHP, advanced DX-SAASHP and dual-source DX-SAASHP can achieve *COP* less than 6. Both the DX-SAASHP and advanced IX-SAASHP can achieve *COP* higher than 6, promisingly up to 10.5. Considering the economic aspect, DX-SAASHP and hybrid SAASHP shares a similar payback

period of around 4.5 years, while the payback period of serial IX-SAASHP is around 7 years [161].

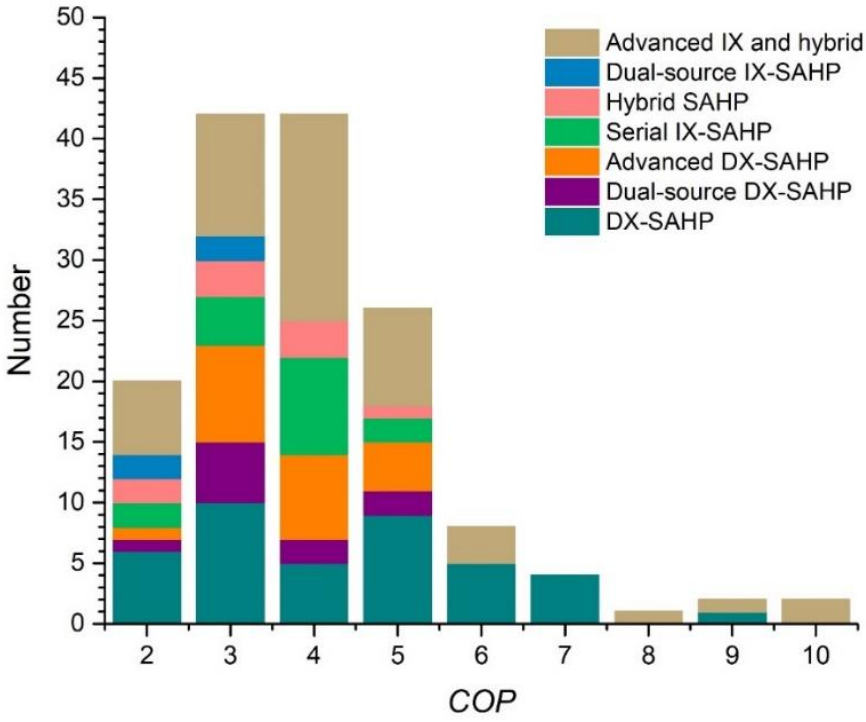

Fig. 2-32: Number of journal papers vs *COP*.

It can be concluded from the above that solar collectors and thermal energy storage have a significant influence on the system performance. The influences are displayed in Fig. 2-33, where the solid line represents the *SPF* and the dashed line represents the yearly electricity consumption, that larger collector area and storage volume lead to a higher *SPF* and lower electricity consumption [76, 96, 135, 192]. According to Ito et al.'s [76] and Carbonell et al.'s [90] simulations, uncovered collectors are superior to covered collectors with a collector area lower than 15 m^2. This situation results from that, at a larger collector area, more solar thermal energy can be collected, and collector temperature can be higher, leading to a larger possibility of heat loss which can be reduced by glass cover; at a smaller collector area, the thermal energy obtained from solar energy is not that high where ambient air can work as a heat source without cover.

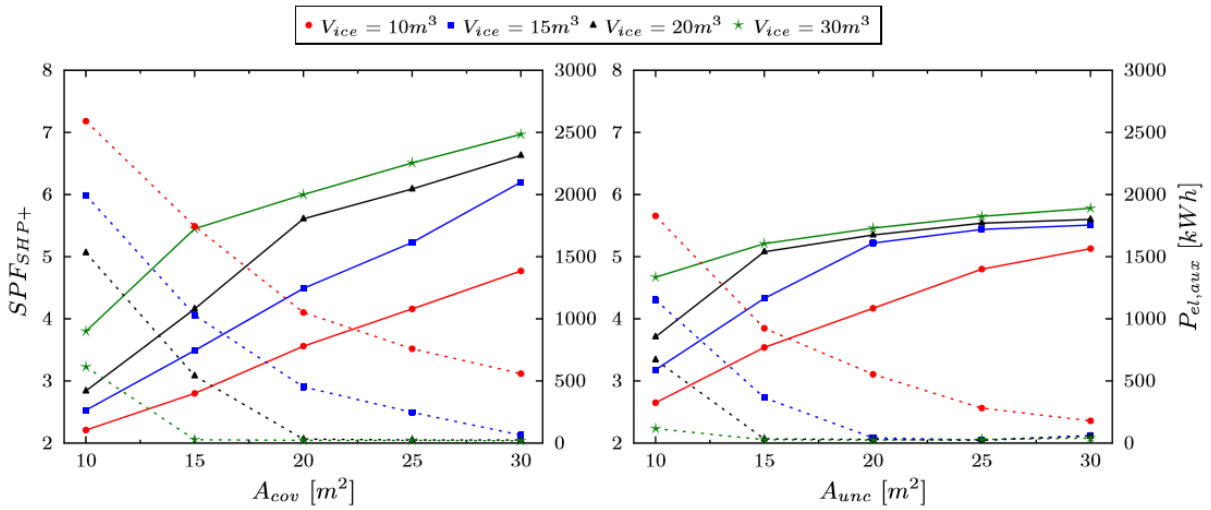

(a) Covered solar collector (b) Uncovered solar collector

Fig. 2-33: *SPF* and yearly auxiliary energy as function of ice storage volume and solar collector area for building SFH 45 [90].

For larger collector areas, a covered collector with proper storage volume can help to achieve an *SPF* over 6. Small-scale SAASHPs for the domestic sector require high-efficient solar collectors to reduce collector area at the same *SF* and working conditions. This may be achieved by auxiliary components, such as a compound parabolic concentrator [55, 57, 58, 108]. Xu et al.'s [108] simulation revealed that a collector using a compound parabolic concentrator and capillary tube absorber can achieve higher collecting temperature and higher collector efficiency than that of a flat plate collector of the same size. According to Ito et al. [76], collector plate thickness and tube pitch can affect system *SPF* according to plate material and ambient temperature. Larger plate thickness and lower tube pitch result in higher *SPF*. Simulation of an uncovered collector suggested that the influence of plate thickness is apparent at the smaller thickness and tends to be less at the larger thickness. Other parameters such as the inclination angle of solar collectors hardly affect *SPF* and collector efficiency [41, 108]. This situation may result from that, at sufficient solar availability, the collector temperature arrives the equilibrium status due to thermal energy collection and heat loss. Thus, collector efficiency is not that sensitive to inclination angles where the collection performance is more influenced by factors such as the specific heat of working fluid and pump speed.

Current studies on solar collectors mainly adopt the collectors designed for solar domestic HW. The specific collectors for SAASHP are needed to be developed, which should match the development of TES methods and the requirements of the SAASHP. Currently, for most systems using sensible heat TES, a solar collector is expected to achieve a higher outlet

temperature to store more thermal energy in the same storage volume. In the future, as PCM is adopted to improve TES efficiency and combined with defrosting for the smooth operation of systems with the evaporator, e.g., hybrid SAASHP, the required collector outlet temperature can be lower, just above the phase change temperature. A novel control strategy proposed by Xu et al. can be used to control the fluid flow rate and outlet temperature of solar collectors based on working conditions, enabling the optimization of SAASHPs [188].

Increasing investigations of SAASHPs are seen in the most recent years. Great efforts have been put to develop highly efficient and compact components to match the working conditions of SAASHPs and hence to improve the system performance. Particularly, eco-friendly refrigerants such as R1234yf, R1233zd(E), R433A, R32 and R290 are used to deal with global warming.

3. Working conditions of the heating system

This chapter introduces the working conditions of the studied heating system in terms of the heating demand of space heating and weather conditions. This gives the references for the component selections in the later simulations. This project is aimed to analyse the applications of SAASHP for space heating and hot water in the UK. To calculate and investigate the performance of the SAASHP, the heating demands should be first determined. Three reference buildings, SFH 15, SFH 45 and SFH 100 are modelled referring to the models of IEA standards as presented in [250]. The weather conditions consider three typical cities in the UK from south to north. According to data availability, London (51.5^o N), Aughton (53.5^o N) and Aberdeen (57.5^o N) are selected for case studies.

3.1 Building parameters

The reference buildings adopted in this study share the same general building geometry fixed by inside measures. The different buildings are then derived by applying the different wall thicknesses and windows. The common, independent geometry and the different insulation thicknesses are summarized in Tables 3-1 and 3-2. Fig. 3-1 displays the building structure and naming convention. Fig. 3-2 shows the view of the envelope parts with naming conventions for the areas. The corresponding inside and outside areas of the building envelope are listed in Table 3-3. The buildings are simplified as one common thermal zone in the TRNBuild model. Internal walls and floors are only depicted for the sake of completeness and are only considered as thermal mass in the simulation.

Table 3-1: Building type independent geometry [250]

Parameter	a (m)	b (m)	f (m)	g (m)	h (m)	m (m)	r (m)	α	β
Measure	5.46	2.64	7	10	2.6	0.4	1.87	45^o	20^o

Table 3-2: Building type specific geometry [250]

Parameter	c (m)	d (m)	e (m)	j (m)	k (m)	s (m)
SFH 15	7.856	10.856	6.505	0.428	0.445	0.255
SFH 45	7.696	10.696	6.445	0.348	0.385	0.215
SHF 100	7.536	10.536	6.365	0.268	0.305	0.095

Table 3-3: Inside and outside areas of the building envelope [250]

Building		A=da	B=bd	C=c(e+r/2)	D=de	E=dc
Net (inside) area (m^2)	all	54.6	26.4	45.7	56	70
Gross (outside) area (m^2)	SFH 15	59.7	28.9	55.9	66.8	86.8
	SFH 45	58.8	28.4	54.3	65.1	83.8
	SFH 100	57.5	27.8	52	62.8	79.4

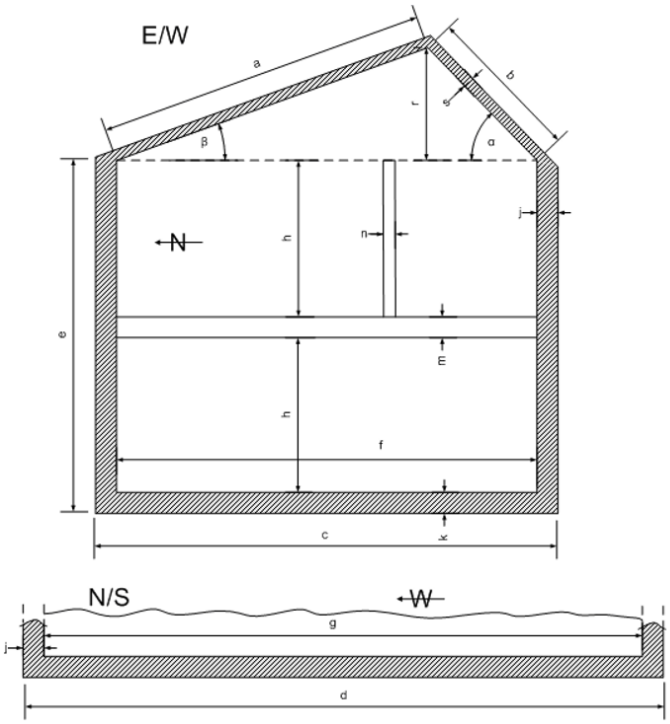

Fig. 3-1: View of the E/W section of the building with naming convention (top), cropped view of the N/S section (bottom). [250].

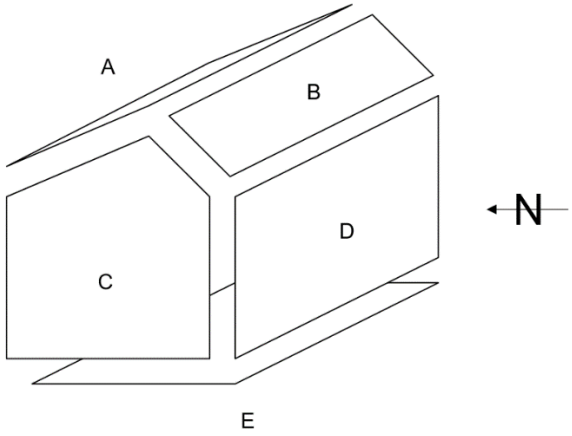

Fig. 3-2: View of the envelope parts with naming convention for the areas [250]

In the simulation, sky view factors are set at 0.5 for all walls, 0.75 for the south facing roof and 0.89 for the north facing roof (in agreement with the physical shape of the object and an open horizon). For both sides of the walls, the solar absorption is set at 0.65. The long-wave emission of the outside (back) is 0.97 and that of the inside (front) is 0.96. Both the ceiling emission and the floor emission are set at 0.65.

The construction of opaque building elements is listed in Table 3-4. The properties of the windows are listed in Table 3-5. Since some window models are not contained in the TRNBuild library and cannot be self-established, similar models are selected as alternatives. All the windows have inner shadings with a factor of 0.25. The shadings open when the horizontal global irradiation reaches 300 W/m^2, and close when the global irradiation drops to 200 W/m^2. The total heat transfer coefficients for the walls are set to be 7.69 W/(m^{2}K) to the inside and 25 W/(m^{2}K) to the outside (ambient) [250].

A minimal, passive, constant air change rate of 0.4 per hour is used for ventilation. Heat gains caused by inhabitants are set at 72 kJ/h and 144 kJ/h for convective and radiative gains per person with a moisture emission of 0.059 kg/h. The schedules of occupancies and electrical equipment are displayed in Figs. 3-3 and 3-4, and listed in Tables 3-6 and 3-7.

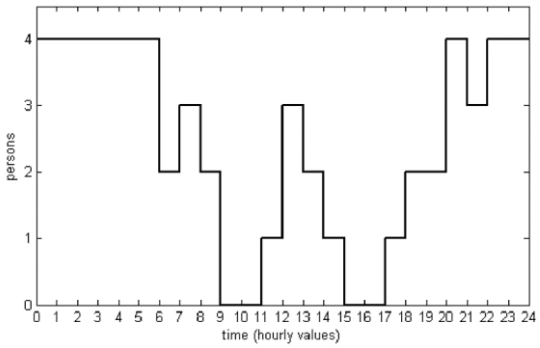

Fig. 3-3: Occupation profile of a day, fraction of present persons [250]

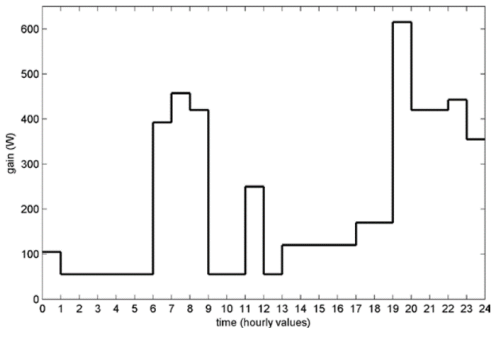

Fig. 3-4: Electrical gain profile for one day [250]

Table 3-4: Construction of opaque building elements [250]

	Layer (from inner to outer surfaces)	Layer thickness (m)			Density (kg/m^3)	Conductivity (W/mK)	Capacity (kJ/kg·K)	U-value construction (W/m^2K)			Convective heat transfer coefficient (W/m^2K)	
		SFH 15	SFH 45	SFH 100				SFH 15	SFH 45	SFH 100	inner	outer
External wall	Plaster inside	0.015	0.015	0.015	1200	0.6	1	0.182	0.286	0.667	3.06	17.78
	brick	0.21	0.21	0.21	1380	0.7	1					
	EPS	0.2	0.12	0.04	17	0.04	0.7					
	Plaster outside	0.003	0.003	0.003	1800	0.7	1					
Ground	Wood	0.015	0.015	0.015	600	0.15	2.5	0.136	0.175	0.281	Floor	0.000028
	Plaster floor	0.08	0.08	0.08	2000	1.4	1					
	Sound insulation	0.04	0.04	0.04	80	0.04	1.5					
	Concrete	0.15	0.15	0.15	2000	1.33	1.08					
	XPS	0.22	0.16	0.08	38	0.037	1.45					
Roof (s)	Gypsum board	0.025	0.025	0.025	900	0.211	1	0.161	0.196	0.565	Ceiling	17.78
	Plywood	0.015	0.015	0.015	300	0.081	2.5					
	Rockwool	0.2	0.16	0.04	60	0.036	1.03					
	Plywood	0.015	0.015	0.015	300	0.081	2.5					

Table 3-5: Window arrangements

	Window area (m^2)	Glass area (m^2)	Frame / window	g-value			U-glass (W/m^2K)			u-frame (W/m^2K)		
				SFH 15	SFH 45	SFH 100	SFH 15	SFH 45	SFH 100	SFH 15	SFH 45	SFH 100
North	3	2.6	0.15	0.408	0.632	0.755	0.4	1.1	2.8	1.6	1.8	2.3
South	12	10.2										
East	4	3.4										
West	4	3.4										

Table 3-6: Occupation profile

Time	0-6	6-7	7-8	8-9	9-11	11-12	12-13	13-14	14-15	15-17	17-18	18-20	20-21	21-22	22-24
Person	4	2	3	2	0	1	3	2	1	0	1	2	4	3	4

Table 3-7: Electrical gain profile

Time	0-1	1-6	6-7	7-8	8-9	9-11	11-12	12-13	13-17	17-19	19-20	20-22	22-23	23-24
Gain (W)	105	55	392.5	457.5	420	55	250	55	120	170	615	420	442.5	355

Table 3-8: Weather conditions in London, Aughton and Aberdeen

	London			Aughton			Aberdeen		
	Min	Max	Average	Min	Max	Average	Min	Max	Average
Ambient temperature, ^{o}C	-3	18.3	6.61	-3.95	16	7.42	-6.7	16.8	5.64
Solar radiation intensity on the titled surface, W/m^2	0.96	1115.73	199.3	0.94	1101.98	229.2	0.93	1113.9	233.8
Wind speed, m/s	0.1	14.1	4.23	0.15	23.51	5.82	3.35	16.1	4.99

The radiant floor is used for all three types of buildings. The radiant floor is modelled as an active layer with a thickness of 0.08 m at 0.04 m depth in the floor, as shown in Fig. 3-5. Water is used as the working fluid inside the radiant floor. The distance between the neighbour pipes is 0.1 m. The pipes have an outside diameter of 0.016 m and a wall thickness of 0.002 m. The conductivity of the pipes is set at 5.04 kJ/h-mK.

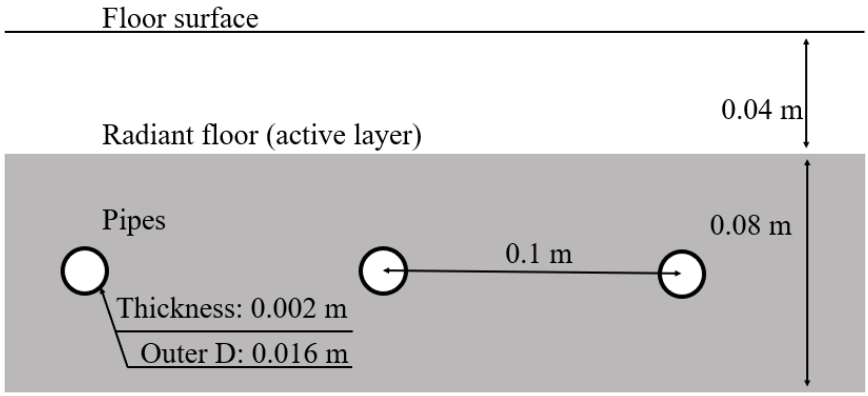

Fig. 3-5: Schematic of the radiant floor (active layer)

3.2 Weather conditions

Weather conditions in London, Aughton and Aberdeen during the heating season are summarised in Table 3-8. Fig. 3-6 introduces the annual ambient temperatures of three selected locations over a typical metrological year. It can be seen that the ambient temperature in Aberdeen is generally lower than those in London and Aughton. In winter, the temperature in London is almost the same, sometimes lower than, that in Aughton; in summer, the temperature in London is higher than that in Aughton.

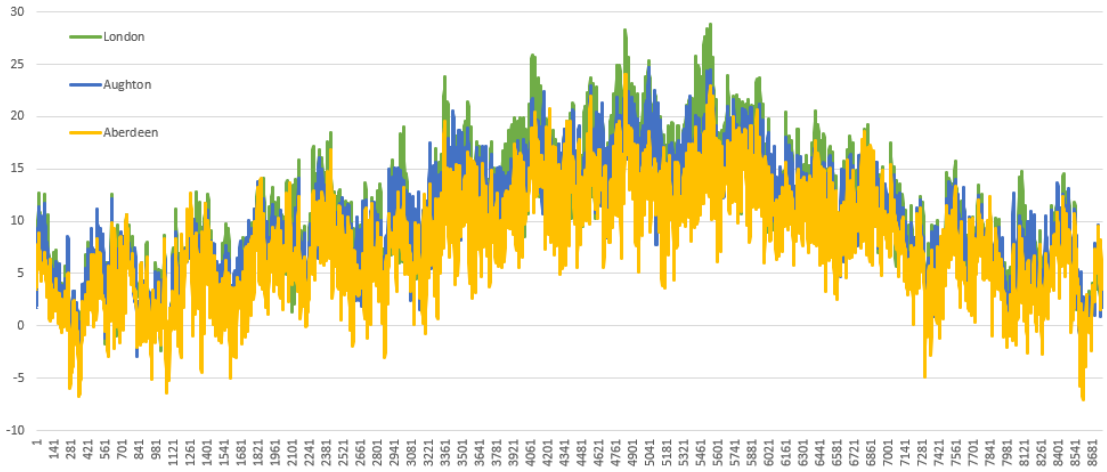

Fig. 3-6: Annual ambient temperature

The ground temperature for a given point is calculated according to the mean surface temperature (equal to the yearly average air temperature), the amplitude of surface temperature (the maximum air temperature of the year minus mean surface temperature), and the time shift (the day the minimum air temperature occurs at). Table 3-9 lists the parameters used to determine the hourly ground temperature at the three selected locations.

Table 3-9: Ground Temperature

Location	London	Aughton	Aberdeen
Mean surface Temperature (^oC)	10.78	10.04	7.84
The amplitude of surface temperature (^oC)	18.04	14.61	16.17
Time shift	12	359	359

Fig. 3-7 shows the variations of ground temperature against depth under weather conditions in London. For three reference buildings, the depths take the thicknesses of the ground.

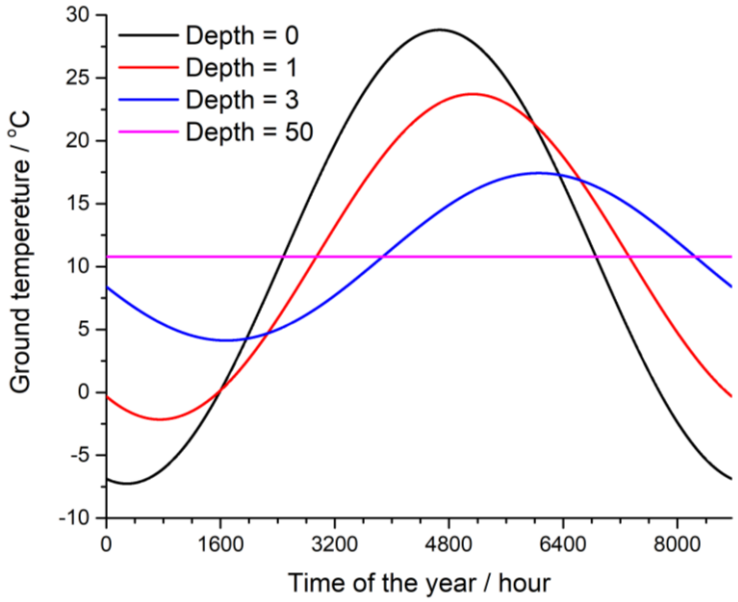

Fig. 3-7: Ground temperature at different depth under weather conditions in London

The key parameters to describe the weather conditions in three selected cities during the heating season are listed in Table 3-10. The average daily tilted surface radiation in December, kJ/ (d·m^2), is an important parameter to evaluate solar availability. It can be seen that Aughton has the largest solar irradiance in December though it has medium latitude. As Fig. 3-8 shows, in 2019, e.g. Aughton has the largest average sunshine duration in December while the average sunshine duration in London is influenced by the Thames River [251].

Table 3-10: Weather conditions in London, Aughton and Aberdeen during the heating season

		London	Aughton	Aberdeen
Latitude		51.5º N	53.5º N	57.5º N
Average sky cover rate (Daytime)		81.32%	77.32%	75.83%
Ambient temperature (ºC)	Min	-3	-3.95	-6.7
	Max	18.3	16	16.8
	Average	6.61	7.42	5.64
Solar radiation intensity (W/m^2)	Min (Daytime)	0.96	0.94	0.93
	Max	1115.73	1101.98	1113.9
	Average (Daytime)	199.3	229.2	233.8
Wind speed (m/s)	Min	0.1	0.15	0.1
	Max	14.1	23.51	16.1
	Average	4.23	5.82	4.99
Titled surface radiations in December, kJ/ ($d \cdot m^2$)		2876.88	3837.38	2667.05

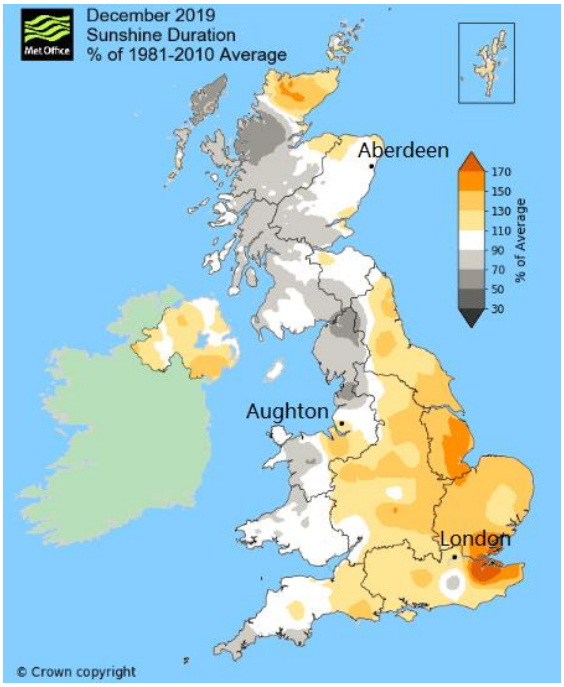

Fig. 3-8: UK maps of sunshine duration in December 2019 [251]

3.3 Building Model

Fig. 3-9 shows the building model in TRNSYS. Two calculators to define the orientation of the building and the radiation in each area. The building parameters introduced above are set in the building module by TRNBuild. The weather data module reads the weather data of the selected locations. A ground temperature module, Type 501, is used to simulate the ground temperature. A calendar, Type 14h, is used to control the heating periods. A calculator is added

to convert the unit of the transient heating load from kJ/h to kW. A quantity integrator, Type 24, is used to calculate the yearly heating demand. Printers and online plotters are used to put out the data and figures.

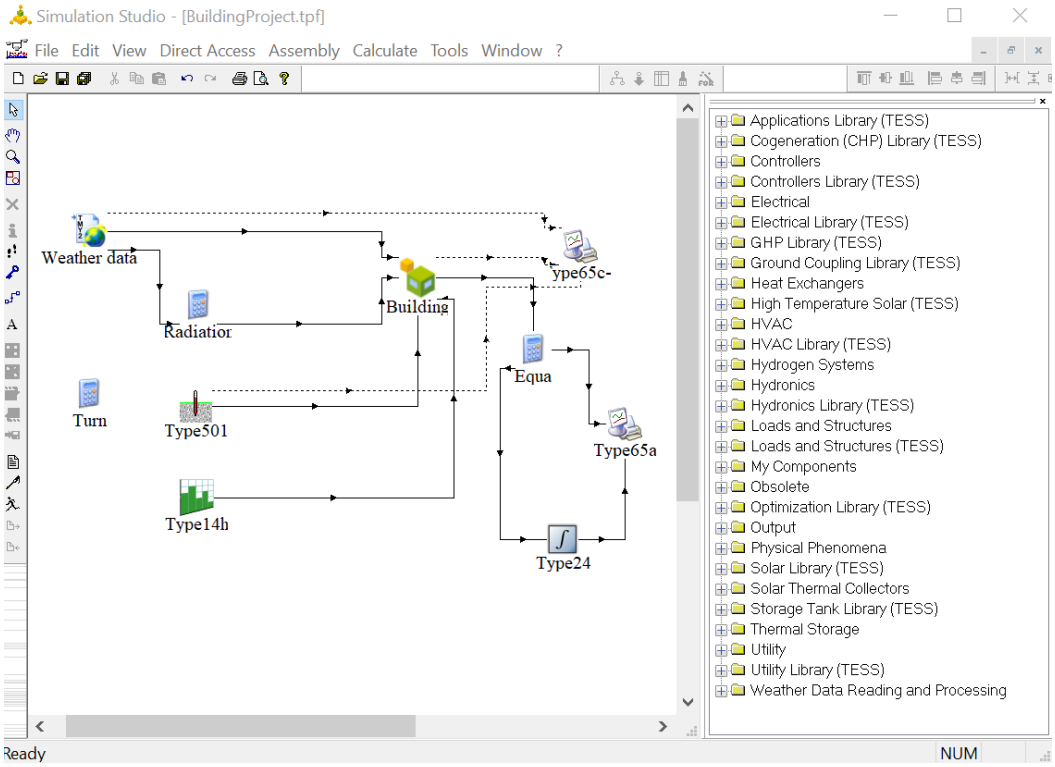

Fig. 3-9: Building model in TRNSYS

The heating temperature in the heating periods is set at 20 ^{o}C. To calculate the heating load, room temperatures at 0 hour are also set at 20 ^{o}C. The heating periods are set to be when ambient air temperatures are below 12 ^{o}C, 14 ^{o}C and 15 ^{o}C for the SFH 15, SFH 45, and SFH 100, respectively, as listed in Table 3-11. Since the house is almost occupied all day, space heating is designed for the whole day during the heating periods. For convenience, the heating season is set to be 1st October to 30th April in the further comparisons. The rest period in the year is the non-heating season.

Table 3-11: Heating periods for reference building in selected locations

	London			Aughton			Aberdeen		
	SFH 15	SFH 45	SFH 100	SFH 15	SFH 45	SFH 100	SFH 15	SFH 45	SFH 100
Heating periods (hour)	0-2736, 7224-8760	0-2736, 7224-8760	0-3192, 6600-8760	0-2808, 7152-8760	0-2808, 7104-8760	0-3168, 6576-8760	0-3048, 7056-8760	0-3072, 7056-8760	0-3768, 6072-8760

3.4 Calculated results

The total heating loads (kWh) and heating loads (kW) for the SFH 15 (black), SFH 45 (red) and SFH 100 (blue) in the three selected locations are simulated over a year (8760 hours) as shown in Figs. 3-10 3-11 and 3-12.

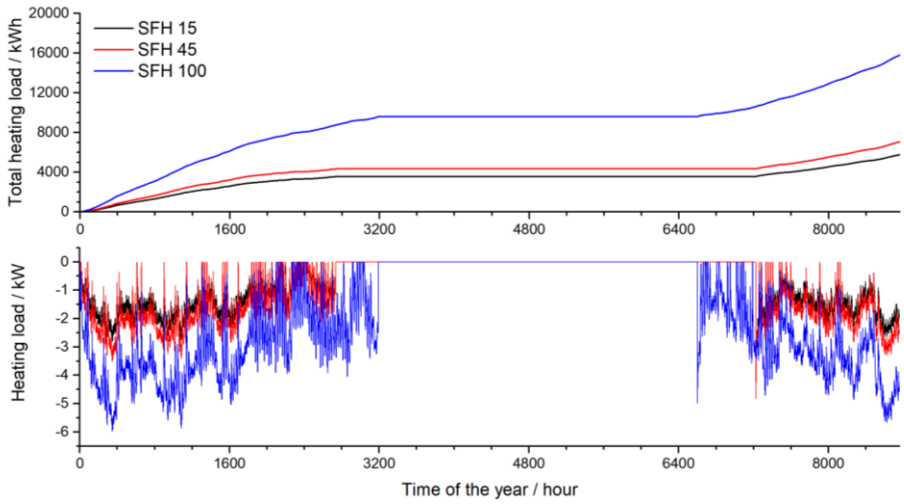

Fig. 3-10: Heating loads in London

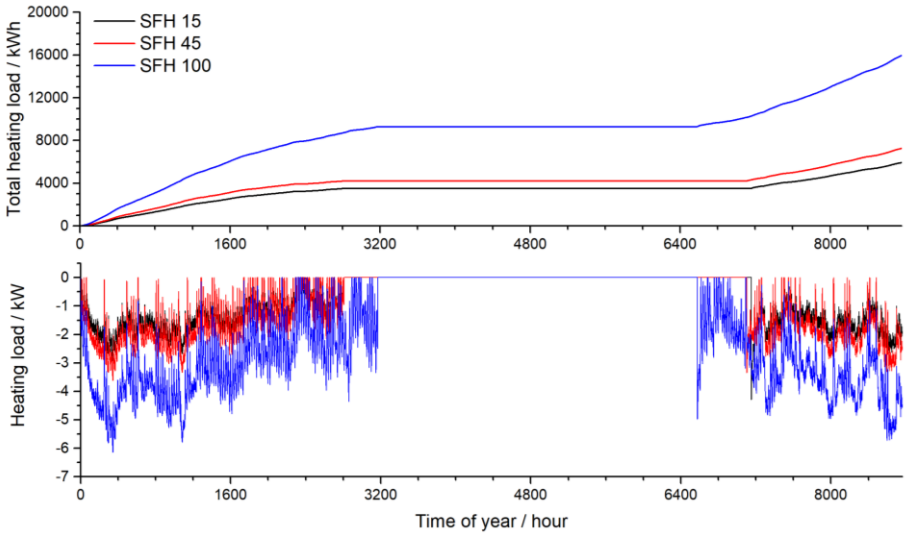

Fig. 3-11: Heating loads in Aughton

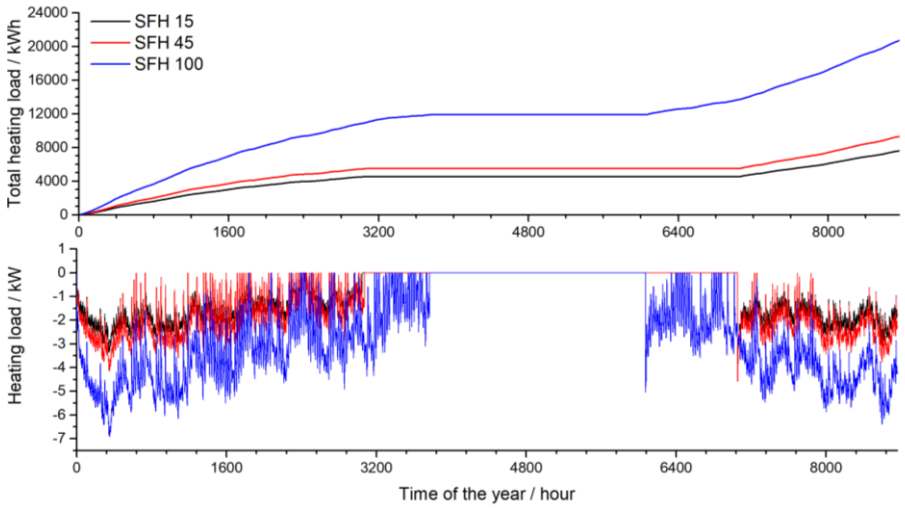

Fig. 3-12: Heating loads in Aberdeen

It can be seen that for the reference buildings in the selected locations, at the beginning of the heating periods, a ‘pin’ load occurs, greatly higher than normal heating loads on those days. The key parameters for the heating loads and demands are summarised in Table 3-12. The peak load and the average load are calculated ignoring the sudden ‘pin’ load at the beginning of the heating periods.

Table 3-12: Summary for heating loads and demands

	London			Aughton			Aberdeen		
	SFH 15	SFH 45	SFH 100	SFH 15	SFH 45	SFH 100	SFH 15	SFH 45	SFH 100
Peak load (kW)	2.84	3.53	5.99	2.94	3.63	6.15	3.36	4.15	6.93
Average load (kW)	1.39	1.76	3.05	1.38	1.73	3.05	1.62	2.03	3.34
Total demands (MWh)	5.75	7.05	15.79	5.93	7.26	15.96	7.60	9.32	20.73

4. Comparative analysis for three types of Indirect expansion solar assisted air source heat pumps

This chapter investigates serial, parallel and dual-source indirect expansion solar assisted air source heat pumps using TRNSYS to investigate the operation performance over a typical year. The operation modes are specifically designed for the weather conditions in London. These three heat pumps are applied to provide space heating and hot water of 300 L per day for a typical single-family house. The simulation results show the operation performance of the three systems is more efficient than previous studies in the literature that they achieve yearly seasonal performance factors higher than 4.4. Considering both operation performance and economic efficiency, this study displays the possibility to use parallel and dual-source SAASHP in regions with relatively lower solar irradiance and replace the gas-boiler heating system.

4.1 Description of the heating systems

In this work, serial, parallel and dual-source IX-SAASHPs are modelled and simulated using TRNSYS 17. The operation modes of the systems are specifically designed for UK weather conditions. Water is used as the medium to transport heat and to store thermal energy. Refrigerants R134a and R410A are used as the working fluids of SWHP and ASHP, respectively. In each HP system, two water tanks are employed for TES. One tank stores thermal energy collected by the solar collector and the other serves as TES for the end use i.e. providing HW and/or SH. Details about the systems are described below.

4.1.1 Serial system

Fig. 4-1(a) shows a serial IX-SAASHP system, which consists of a solar collection loop (in black), an SWHP unit (in green), an HW loop (in blue) and an SH loop (in red). The solar collector converts solar energy into thermal energy and the heat is transferred to water being circulated by pump 1 (3). The thermal energy is normally stored in the TES tank 1 (valve 2 open) but the hot water can also be circulated to either SWHP (valves 2 and 14 closed, valve 6 open) or to the TES tank 2 (valves 2 and 6 closed, valve 14 open). The SWHP consists of a water-to-refrigerant evaporator (8), a compressor (9), a condenser (10), and an expansion valve (11). When the SWHP is in operation, TES tank 1 (4) serves as the low-temperature heat source and TES tank 2 (15) serves as the high-temperature heat source. When the system provides hot

water, the mains cold water flows into the TES tank 2. When the system is in operation for heating, pump 4 (16) circulates the hot water in TES tank 2 through the radiant floor (17).

Fig. 4-1(b) shows the flow chart for control of the serial system operation. The room air temperature (T_{room}), ambient air temperature (T_{amb}), local solar irradiance (I) as well as water temperatures at several locations such as the temperatures at the inlet and outlet of the solar collector (T_1, T_2), the temperature at the outlet of TES tank 1 to load (T_3), hot water storage (HWS) temperature (T_{HWS}) are measured/monitored for control of the serial system operation. The water temperature at the outlet of the evaporator (T_4), the water temperatures at the inlet and outlet of the condenser (T_5 and T_6) and the temperature of the mains cold water supply (T_7) are measured/monitored for analysis of energy conservation of the heating system. Table 4-1 gives the rule-based look-up table for control of the serial system operation.

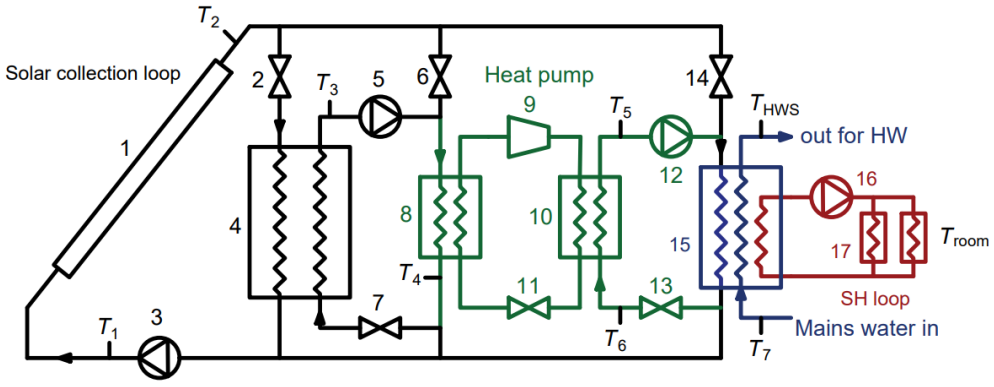

1: Solar collector 2, 6, 7, 13, 14: Valves 3: Pump 1 4: TES tank 1 5: Pump 2
8: Water-to-refrigerant evaporator 9: Compressor 10: Condenser
11: Expansion valve 12: Pump 3 15: TES tank 2 16: Pump 4 17: Radiant floor

a) Schematic of the serial system

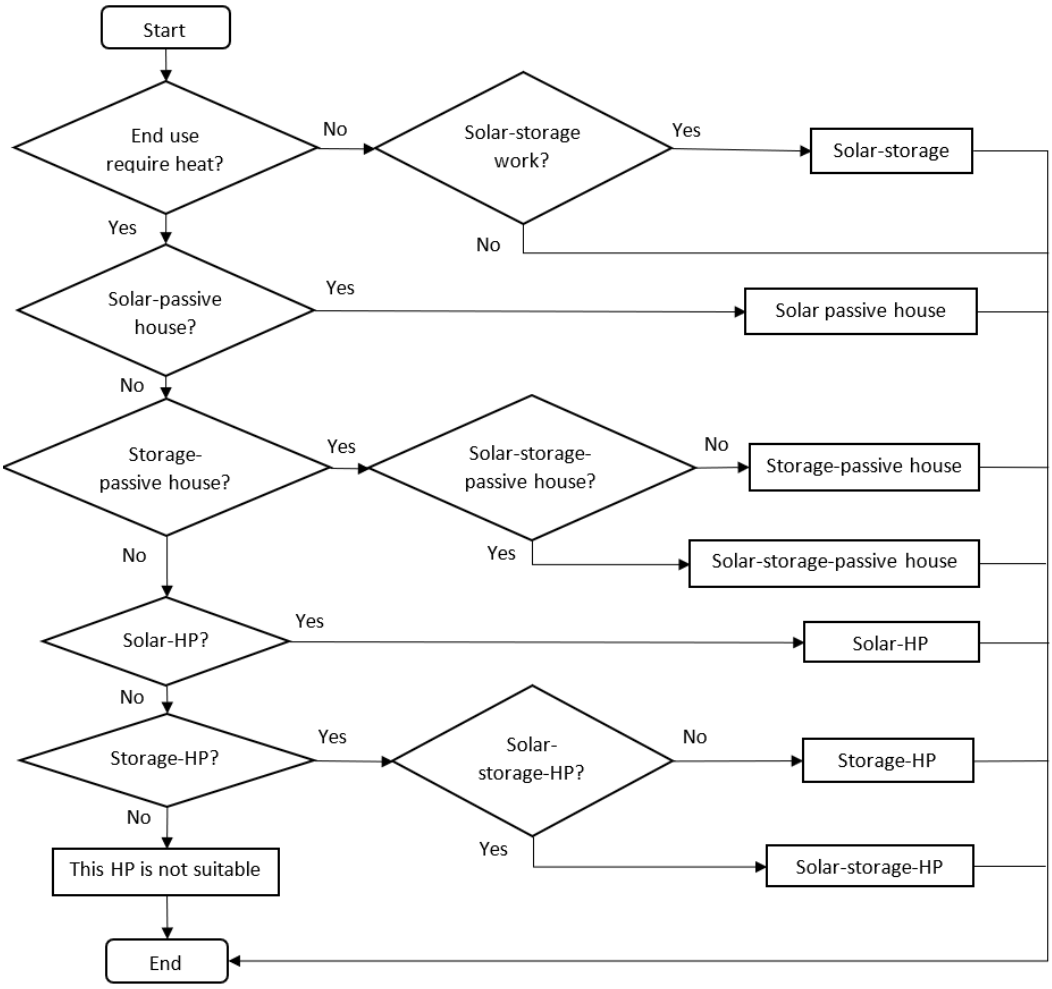

b) Flow chart for system operation control

Fig. 4-1: System and operation control of the serial IX-SAASHP

Table 4-1: The rule-based look-up table for control of the serial system operation

Operation mode	**Temperature range (ºC)**	**Pumps**				**Valves**					**SWHP**
		3	5	12	16	2	6	7	13	14	
Collector–TES 1	$T_2 > T_3$, $T_{HWS} > 50$	O	X	X	X	O	X	X	X	X	X
Collector–TES 1–TES 2	$T_2 > T_3 > 50 > T_{HWS}$	O	O	X	X	O	O	O	X	O	X
Collector-TES 1–SWHP-TES 2	$T_2 > T_3$, $-5 < T_3 < 50$, $T_{HWS} < 50$	O	O	O	X	O	X	O	O	X	O
Collector–SWHP-TES 2	$T_2 < T_3$, $50 > T_2 > -5$, $T_{HWS} < 50$	O	X	O	X	X	O	X	O	X	O
Collector-TES 2	$T_{HWS} < 50 < T_2 < T_3$	O	X	X	X	X	X	X	X	O	X
TES 1–TES 2	$T_3 > 50 > T_{HWS}$	X	O	X	X	X	O	O	X	O	X
TES 1–SWHP-TES 2	$-5 < T_3 < 50$, $T_{HWS} < 50$	X	O	O	X	X	X	O	O	X	O
SH: TES 2	$T_{room} < 18$	X	X	X	O	X	X	X	X	X	X
SH: Collector–TES 1	$T_2 > T_3$, $T_{HWS} > 50$, $T_{room} < 18$	O	X	X	O	O	X	X	X	X	X
SH: Collector–TES 1–TES 2	$T_2 > T_3$, $T_{HWS} < 50$, $T_{room} < 18$	O	O	X	O	O	O	O	X	O	X
SH: Collector–TES 1–SWHP–TES 2	$T_2 > T_3$, $-5 < T_3 < 50$, $T_{HWS} < 50$, $T_{room} < 18$	O	O	O	O	O	X	O	O	X	O
SH: Collector–SWHP–TES 2	$T_2 < T_3$, $50 > T_2 > -5$, $T_{HWS} < 50$, $T_{room} < 18$	O	X	O	O	X	O	X	O	X	O
SH: Collector-TES 2	$T_{HWS} < 50 < T_2 < T_3$, $T_{room} < 18$	O	X	X	O	X	X	X	X	O	X
SH: TES 1-TES 2	$T_3 > 50 > T_{HWS}$, $T_{room} < 18$	X	O	X	O	X	O	O	X	O	X
SH: TES 1–SWHP -TES 2	$-5 < T_3 < 50$, $T_{HWS} < 50$, $T_{room} < 18$	X	O	O	O	X	X	O	O	X	O

Note: Collector: Solar collector. TES 1: Water TES tank1. TES 2: Water TES tank 2.

O: Pumps and SWHP are in operation; Valves are open. X: Pumps and SWHP are not in operation; Valves are closed.

4.1.2 Parallel system

Fig. 4-2 shows a parallel IX-SAASHP, which consists of a solar collection loop (in black), an ASHP unit (in green), an HW loop (in blue) and an SH loop (in red). The thermal energy is stored in TES tank 1 (valve 2 open) and circulated to TES tank 2 by pump 2 (valve 12 open). The ASHP consists of an air-to-refrigerant evaporator (6), an expansion valve (7), a compressor (8) and a condenser (9). When the ASHP is in operation, the ambient air serves as the low-temperature heat source.

Fig. 4-2(b) shows the flow chart for control of the parallel system operation. Compared with the serial system, the same temperatures are measured/monitored for control of the parallel system operation. The air temperature at the outlet of the evaporator (T_4), the water temperatures at the inlet and outlet of the condenser (T_5 and T_6) and the temperature of the mains cold water supply (T_7) are measured/monitored for analysis of energy conservation of the heating system. Table 4-2 gives the rule-based look-up table for control of the parallel system operation.

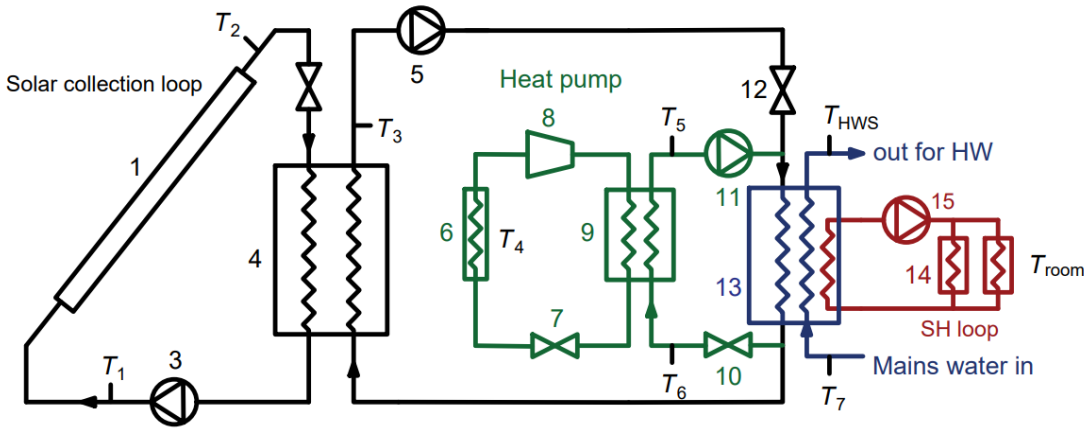

1: Solar collector 2, 10, 12: Valves 3: Pump 1 4: TES tank 1 5: Pump 2
6: Air-to-refrigerant evaporator 7: Expansion valve 8: Compressor
9: Condenser 11: Pump 3 13: TES tank 2 14: Radiant floor 15: Pump 4

a) Schematic of parallel system

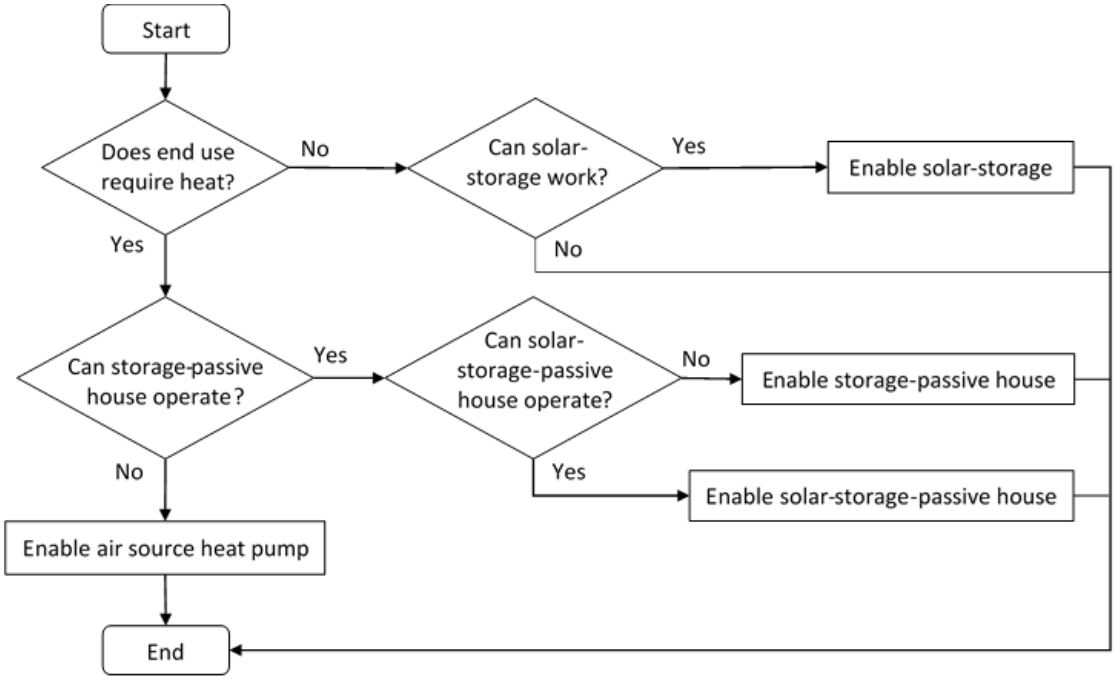

b) Flow chart for system operation control

Fig. 4-2: System and operation control of the parallel IX-SAASHP

Table 4-2: The rule-based look-up table for control of the parallel system operation

Operation mode	**Temperature range (°C)**	**Pumps**				**Valves**			**ASHP**
		3	5	11	15	2	10	12	
Collector-TES 1	$T_2 > T_3$, $T_{HWS} > 50$	O	X	X	X	O	X	X	X
Collector–TES 1-TES 2	$T_2 > T_3 > 50 > T_{HWS}$	O	O	X	X	X	X	O	X
ASHP-TES 2	$T_3 < 50$, $T_{HWS} < 50$	X	X	O	X	X	O	X	O
TES 1–TES 2	$T_3 > 50 > T_{HWS}$	X	O	X	X	X	X	O	X
SH: TES 2	$T_{room} < 18$	X	X	X	O	X	X	X	X
SH: Collector-TES 1	$T_2 > T_3$, $T_{HWS} > 50$, $T_{room} < 18$	O	X	X	O	O	X	X	X
SH: Collector–TES 1–TES 2	$T_2 > T_3 > 50 > T_{HWS}$, $T_{room} < 18$	O	O	X	O	X	X	O	X
SH: ASHP–TES 2	$T_3 < 50$, $T_{HWS} < 50$, $T_{room} < 18$	X	X	O	O	X	O	X	O
SH: TES1–TES 2	$T_3 > 50 > T_{HWS}$, $T_{room} < 18$	X	O	X	O	X	X	O	X

Note: Collector: Solar collector. TES 1: Water TES tank1. TES 2: Water TES tank 2.

O: Pumps and ASHP are in operation; Valves are open. X: Pumps and ASHP are not in operation; Valves are closed.

4.1.3 Dual-source system

Fig. 4-3 shows a dual-source IX-SAASHP, which consists of a solar collection loop (in black), an SW-ASHP unit (in green), an HW loop (in blue) and an SH loop (in red). The SW-ASHP consists of a water-to-refrigerant evaporator (7), an air-to-refrigerant evaporator (8), a condenser (11), a compressor (12), and an expansion valve (13). When the SWHP is in operation, the TES tank 1 (4) serves as the low-temperature heat source. When the ASHP is in operation, the ambient air serves as the low-temperature heat source.

Fig. 4-3(b) shows the flow chart for control of the dual-source system operation. Compared with the serial and parallel systems, the same temperatures are measured/monitored for control of the dual-source system operation. The water and air temperatures at the outlet of the evaporator (T_4 and T_5), the water temperatures at the inlet and outlet of the condenser (T_6 and T_7) and the temperature of the mains cold water supply (T_8) are measured/monitored for analysis of energy conservation of the heating system. Table 5 gives the rule-based look-up table for control of the dual-source system operation.

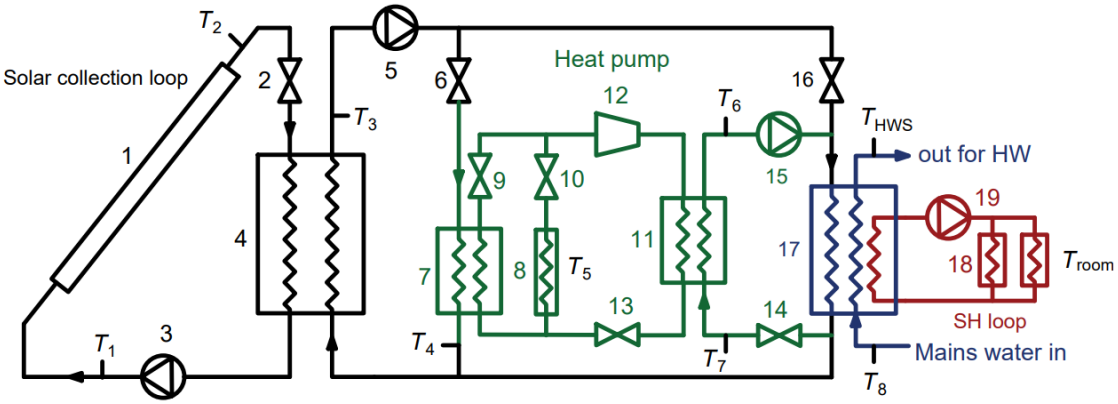

1: Solar collector 2, 6, 9, 10, 14, 16: Valves 3: Pump 1 4: TES tank 1 5: Pump 2
7: Water-to-refrigerant evaporator 8: Air-to-refrigerant evaporator
11: Condenser 12: Compressor 13: Expansion valve 15: Pump 3
17: TES tank 2 18: Radiant floor 19: Pump 4

a) Schematic of dual-source system

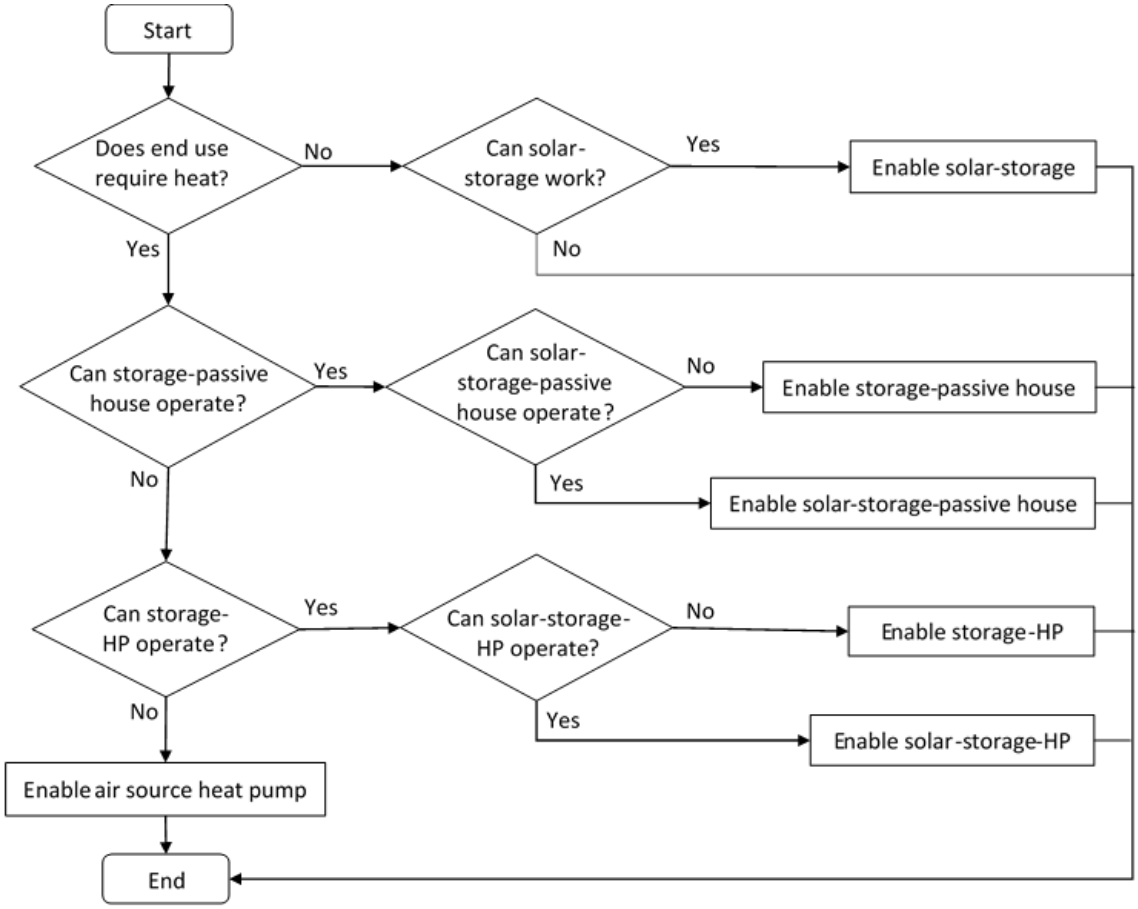

b) Flow chart for system operation control

Fig. 4-3: System and operation control of the dual-source IX-SAASHP

Table 4-3: The rule-based look-up table for control of the dual-source system operation

Operation mode	Temperature range (ºC)	Pumps				Valves						ASHP	SWHP
		3	5	15	19	2	6	9	10	14	16		
Collector-TES 1	$T_2 > T_3$, $T_{HWS} > 50$	O	X	X	X	O	X	X	X	X	X	X	X
Collector-TES 1-TES 2	$T_2 > T_3 > 50 > T_{HWS}$	O	O	X	X	O	X	X	X	X	O	X	X
Collector-TES 1–SWHP-TES 2	$T_2 > T_3$, $T_{amb} < T_3 < 50$, $T_{HWS} < 50$	O	O	O	X	O	O	O	X	O	X	X	O
ASHP-TES 2	$T_{amb} > T_3$, $T_{HWS} < 50$	X	X	O	X	X	X	X	O	O	X	O	X
TES 1-TES 2	$T_3 > 50 > T_{HWS}$	X	O	X	X	X	X	X	X	X	O	X	X
TES 1–SWHP-TES 2	$T_{amb} < T_3 < 50$, $T_{HWS} < 50$	X	O	O	X	X	O	O	X	O	X	X	O
SH: TES 2	$T_{room} < 18$	X	X	X	O	X	X	X	X	X	X	X	X
SH: Collector-TES 1	$T_2 > T_3$, $T_{HWS} > 50$, $T_{room} < 18$	O	X	X	O	O	X	X	X	X	X	X	X
SH: Collector-TES 1–TES 2	$T_2 > T_3 > 50 > T_{HWS}$, $T_{room} < 18$	O	O	X	O	O	X	X	X	X	O	X	X
SH: Collector-TES 1-SWHP–TES 2	$T_2 > T_3$, $T_{amb} < T_3 < 50$, $T_{HWS} < 50$, $T_{room} < 18$	O	O	O	O	O	O	O	X	O	X	X	O
SH: ASHP–TES 2	$T_{amb} > T_3$, $T_{HWS} < 50$, $T_{room} < 18$	X	X	O	O	X	X	X	O	O	X	O	X
SH: TES 1-TES 2	$T_3 > 50 > T_{HWS}$, $T_{room} < 18$	X	O	X	O	X	X	X	X	X	O	X	X
SH: TES 1–SWHP–TES 2	$T_{amb} < T_3 < 50$, $T_{HWS} < 50$, $T_{room} < 18$	X	O	O	O	X	O	O	X	O	X	X	O

Note: Collector: Solar collector. TES 1: Water TES tank1. TES 2: Water TES tank 2.

O: Pumps, SWHP and ASHP are in operation; Valves are open. X: Pumps, SWHP and ASHP are not in operation; Valves are closed.

4.2 Modelling and simulation methods

TRNSYS 17 is used for the simulations. The working conditions of the systems, selection of TRNSYS modules and simulation schemes are described below.

4.2.1 Working conditions

The systems are designed to provide SH and HW for the building over a year. The T_{room} for thermal comfort is set to be 18 ^{o}C – 22 ^{o}C in the heating season. In the HP heating mode, the water temperature in the TES tank 2 is controlled to be not lower than 50 ^{o}C [252]. Four fifteen-minute water draws per day at a rate of 300 kg/h are used to represent typical low flow showers at 6 a.m., 8 a.m., 8 p.m., and 10 p.m. every day. To avoid scalding, the hot water supply temperature is set at 40 ^{o}C [253], which is supplied by mixing the stored hot water and mains water at the outlet of the hot water tank. For safe operation of the system, in the SHW operation mode, the maximum HWS temperature is controlled to be 80 ^{o}C.

4.2.2 Selection of TRNSYS modules

Since flat plate solar collectors occupy about half of the current market share [26], the flat plate solar collector is selected as the solar collector. Solar collector module of Type 1b in TRNSYS is chosen to model this type of solar collector. To investigate the performances of the configurations of the three systems, the auxiliary heater is not used, and the demanded thermal energy is fully provided by the HPs and SHW. If the heat provided by the heating system is insufficient, the HWS temperature will be lower than the temperature set, and the room air temperature will fall below the temperature set for thermal comfort.

The sizing of the system is based on the demands of SH and HW. To meet the demands, different systems have different sizes of components. Since the serial system uses thermal energy collected by a solar collector as the sole heat source, the required solar collector area is large to be 45 m^2 and the required size of the water TES tank is large to 3 m^3. Since the parallel and dual-source systems have ASHP for compensation at low solar energy availability, the required sizes of solar collector and water TES tank are much smaller, 18 m^2 and 500 L, respectively, to ensure SHW temperature to be higher than 40 ^{o}C in non-heating seasons. When the SHW temperature is below 50 ^{o}C in non-heating seasons, the HP operates to ensure the HWS temperature in the safe range to inhibit bacteria.

The rated flow rates (m) of the pumps are determined by Eq. (4-1) and the rated power (P) is calculated by Eq. (4-2):

$$m=Q/(c\cdot\Delta T) \quad (4\text{-}1)$$

$$P=m\cdot H/(360\eta) \quad (4\text{-}2)$$

where Q is the peak load, c is the specific heat of working fluid, ΔT is the designed temperature difference, H is the head of the pump and η is the efficiency of the pump.

All the HPs are set at a heating capacity of 8 kW. In the models of serial and dual-source IX-SAASHPs, the SWHP module (Type 668) is modified based on a sample file of 30HXC-HP2 from Carrier United Technologies. In the models of the parallel and dual-source IX-SAASHPs, the ASHP module (Type 941) is modified based on the sample file of YVAS012, York, Jonson Control. Note that the ASHP module (Type 941) available in TRNSYS does not consider the frosting and defrosting and their effects on the ASHP performance. It is anticipated that the results provide a deep understanding of the application potential of SAASHPs in high latitude regions. In the model of dual-source IX-SAASHP, the dual-source HP is simulated by combining an SWHP (Type 668) and an ASHP (Type 941). TRNSYS modules selected for modelling the components of the three systems and relevant parameters are listed in Table 4-4. Fig. 4-4 shows the TRNSYS models and control functions for serial, parallel and dual-source IX-SAASHPs [254]. The solid lines stand for the pipe connections, and the dot lines stand for the control connections. The parameters that define the models of the components are obtained from the experimental data of the component products available in the market.

Table 4-4: TRNSYS modules selected for modelling the components of the three systems and relevant parameters

Component	Module	System	Parameter	Value
Solar collector	Type 1b	Serial system	Area	45 m^2
		Parallel and dual-source systems	Area	18 m^2
			Inclination angle	51.5^o
			Tested flow rate	30 kg/hm^2
		All systems	Intercept efficiency	0.8
			Efficiency slope	13 kJ/hm^2k
			Efficiency curvature	0 kJ/hm^2k^2
			1st order IAM	0.2
			2nd order IAM	0
TES tank 1	Type 4a	All systems	Heat loss coefficient	0.2 W/(m^2 K)
		Serial system	Volume	3000 L
			Height	2.15 m
		Parallel and dual-source systems	Volume	500 L
			Height	1.175 m
TES tank 2	Type 4a	All systems	Heat loss coefficient	0.2 W/(m^2 K)
			Volume	300 L
			height	1 m
ASHP	Type 941	Parallel and dual-source systems	Blower power	0.15 kW
			Total air flow rate	1500 l/s
			User defined file	YVAS012, York, Jonson Control
SWHP	Type 668	Serial and dual-source systems	User defined file	30HXC-HP2, Carrier United Technologies
Pump 1	Type 110	All systems	Rated flow rate	500 kg/h
			Rated power	30 W
Pump 2	Type 110	All systems	Rated flow rate	800 kg/h
			Rated power	50 W
Pump 4	Type 110	All systems	Rated flow rate	800 kg/h
			Rated power	50 W
Pump in SWHP loop	Type 110	Serial and dual-source systems	Rated flow rate	870 kg/h
			Rated power	50 W
Pump in ASHP loop	Type 110	Parallel and dual-source systems	Rated flow rate	870 kg/h
			Rated power	50 W

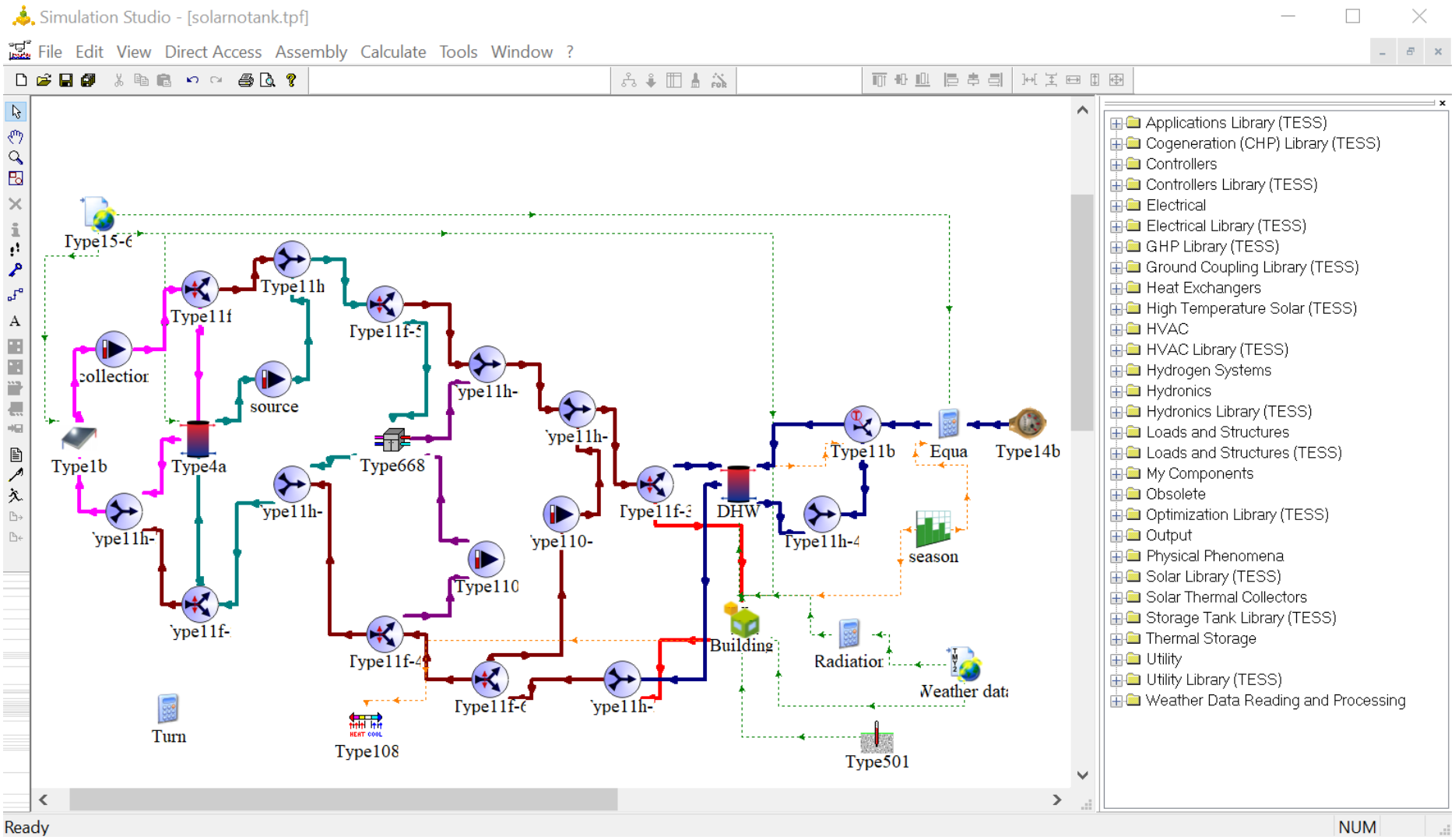

a) Serial IX-SAASHP

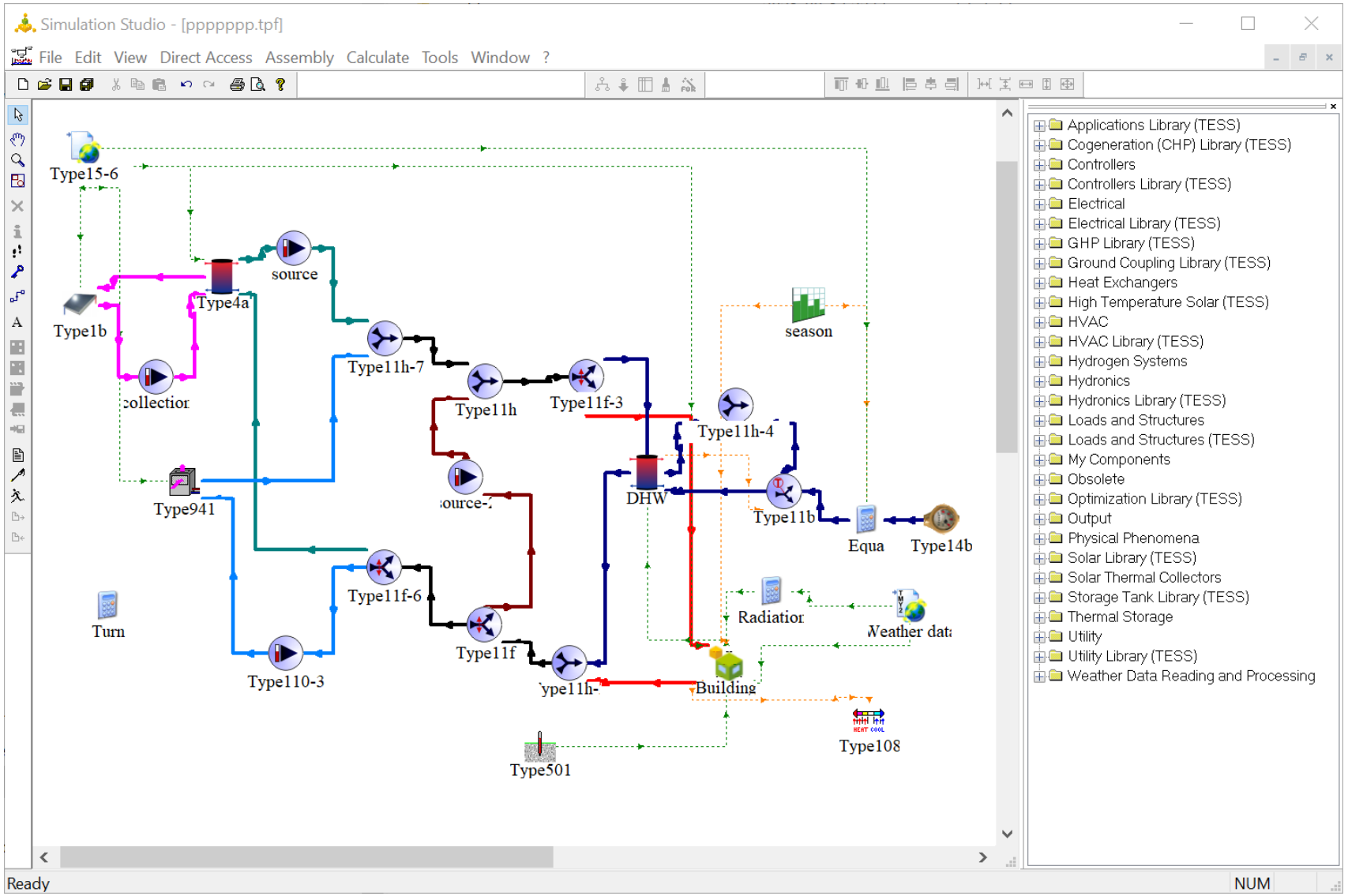

b) Parallel IX-SAASHP

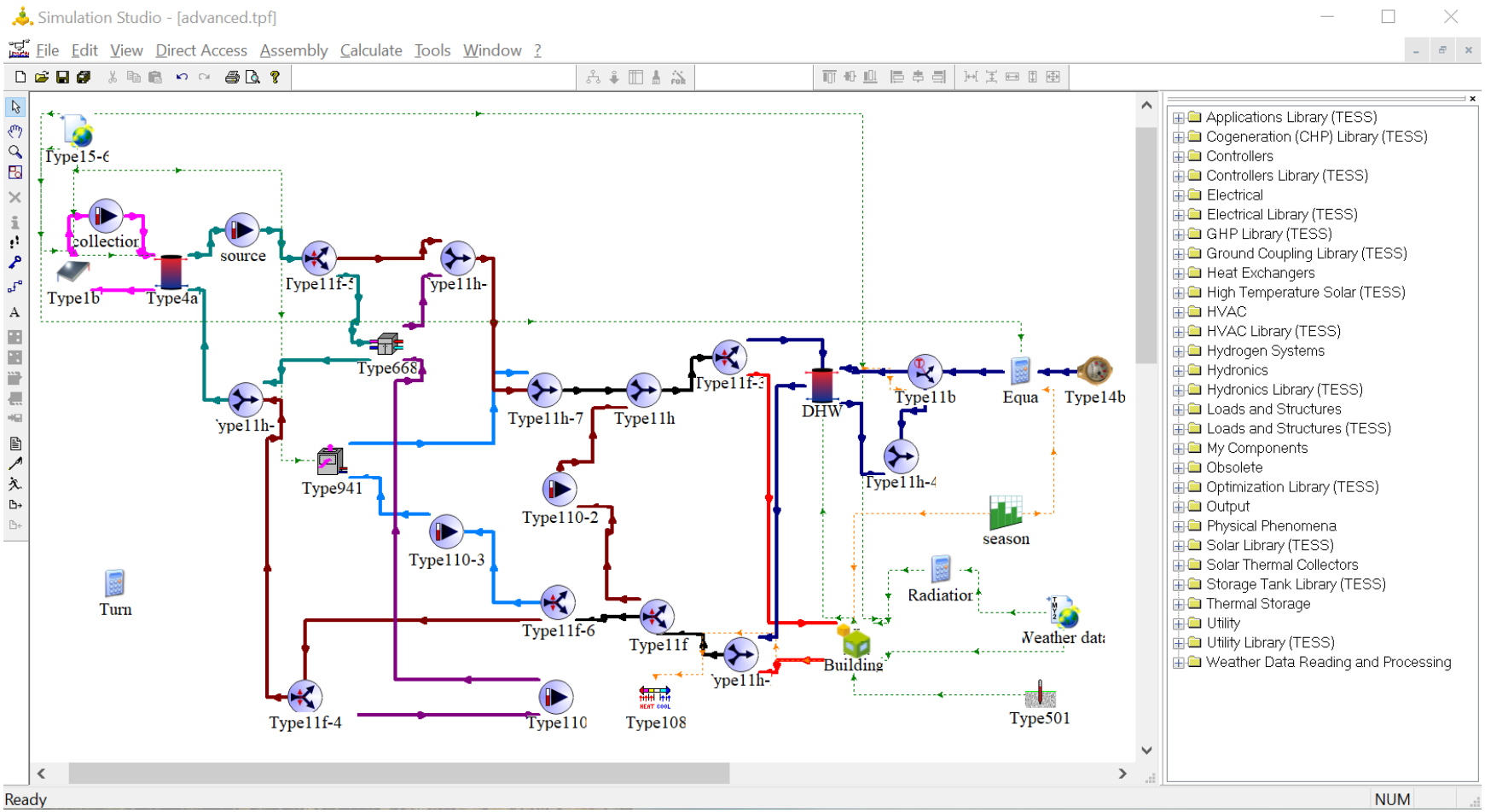

c) Dual-source IX-SAASHP

Fig. 4-4: TRNSYS models and control functions for serial, parallel and dual-source IX-SAASHPs.
(Solid lines: pink - solar collector-TES tank 1 loop; dark red - bypass; green - TES tank 1-SWHP loop; purple - SWHP loop; light blue - ASHP loop; black - user side loop; brown - TES tank 2-radiant floor loop; red - SH loop; dark blue - HW loop). (Dot lines: orange - monitored parameters; dark green - weather parameters).

4.2.3 Simulation scheme

The operation period is set at one year with a time step of 1 minute considering time efficiency and accuracy. The systems start to operate from the middle of the year (4380 h) with an initial water temperature of 13.4 ^{o}C in the TES tanks, which is the water temperature of the mains water supply.

4.3 Evaluation of performance

The three IX-SAASHPs have different system configurations. They all include a vapour-compression cycle HP. Their performance can be evaluated by the performance indicators.

4.3.1 Thermodynamics cycle of the heat pumps

Fig. 4-5 shows the ideal vapour-compression cycles of the ASHP (1-2-3-4-1) and SWHP (5-6-7-4-5) on the *P-h* diagram. The degree of superheat of the refrigerant vapour entering the compressor is taken to be the same for both HPs. The flow resistance on the refrigerant side in both the evaporator and condenser is neglected. Compared with the ASHP, the SWHP has a higher evaporating temperature. According to Fig. 4-5, SWHP can have more thermal energy absorbed in the expansion process and require less work done by the compressor at the same condensing temperature.

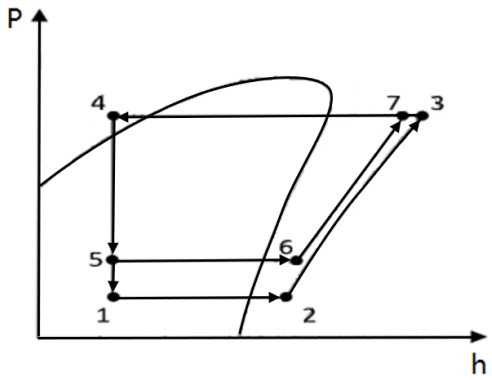

Fig. 4-5: *P-h* diagram of ideal vapour-compression cycle HPs

4.3.2 System performance indicators

The performance of the heating systems is evaluated by a variety of indicators including the room air temperature, HWS temperature, *SPF* of the system (SPF_{sys}), *SPF* of the HP (SPF_{HP}), *COP* of the HP module, and the solar fraction (*SF*). The room air temperature is an indication of whether the heat provision by the heating system meets the heat demand of the building. The measured room air temperature is also the quantity that determines the on/off operation of the heating system. The HWS temperature indicates the amount of thermal energy stored in the TES tanks and also determines the on/off operation of the SWHP. The SPF_{sys}

describes the overall performance of the whole heating system over the heating season of the year and is defined by Eq. (4-3):

$$SPF_{sys}=\frac{\int(Q_{SH}+Q_{HW})dt}{\int W_{tot}dt} \quad (4\text{-}3)$$

where Q_{SH} and Q_{HW} are the thermal energies supplied by the system for SH and HW, respectively, and W_{tot} is the total electricity consumed by the HP and all water pumps given by Eq. (4-4):

$$W_{tot}=W_{HP}+W_{pumps} \quad (4\text{-}4)$$

where W_{HP} is the electricity consumed by the HP calculated by Eq. (4-5):

$$W_{HP}=j_{ASHP}W_{ASHP}+j_{SWHP}W_{SWHP} \quad (4\text{-}5)$$

where W_{ASHP} and W_{SWHP} are the electricity consumed by the ASHP and SWHP, respectively, j_{ASHP} and j_{SWHP} have values of either 1 or 0 representing the on or off operation status of ASHP and SWHP. For serial system, j_{ASHP} = 0 and j_{SWHP} = 1. For parallel system, j_{ASHP} = 1 and j_{SWHP} = 0. For dual-source systems, j_{ASHP} and j_{SWHP} can be 1 or 0, depending on their on/off operation status.

The SPF_{HP} describes the overall performance of an HP over the heating season and is defined by Eq. (4-6):

$$SPF_{HP}=\frac{\int Q_{HP,con}dt}{\int W_{HP}dt} \quad (4\text{-}6)$$

where $Q_{HP,con}$ is the heat transferred from the condenser of the HP to water circulating to TES tank 2, given by Eq. (4-7):

$$Q_{HP,\,con}=j_{ASHP}Q_{ASHP,\,con}+j_{SWHP}Q_{SWHP,\,con} \quad (4\text{-}7)$$

where $Q_{ASHP,\,con}$ and $Q_{SWHP,\,con}$ are the heat transferred from the condenser of ASHP and SWHP to water circulating to TES tank 2, respectively.

The *COP* of the HP is defined by Eq. (4-8):

$$COP=Q_{HP,\,con}/W_{HP} \quad (4\text{-}8)$$

The *SF* of the heating system, the contribution ratio of the solar thermal energy collected to the system heat provision over the heating season, is defined by Eq. (4-9):

$$SF=1-\frac{\int(Q_{ASHP,con}+W_{SWHP})dt}{\int(Q_{HW}+Q_{SH})dt} \quad (4\text{-}9)$$

4.4 Results and discussions

Based on the three IX-SAASHPs, the models in TRNSYS are established. Simulations are performed and the system performances are then obtained.

4.4.1 Seasonally heating performance

Fig. 4-6 shows the variations of the room air temperature (T_{room}, the black line) and the HWS temperature (T_{HWS}, the red line) over the heating season for serial, parallel and dual-source IX-SAASHPs. It is seen that the HWS temperature may suddenly drop to below 50 °C because after water draws, feedwater enters the hot water tank. However, the IX-SAASHPs respond quickly to lift the HWS temperature to above 50 °C. From Fig.7(a), it is seen that, the serial IX-SAASHP cannot meet the heat demand in winter; in some cases the room air temperature is below 18 °C. The lowest room air temperature is 13.4 °C and the lowest HWS temperature of 11.3 °C. The lowest water temperature at the outlet of the evaporator is -7.1 °C. This is still within the safe operation range of the system according to the operation introduction of the 30HXC-HP2 of Carrier United Technologies.

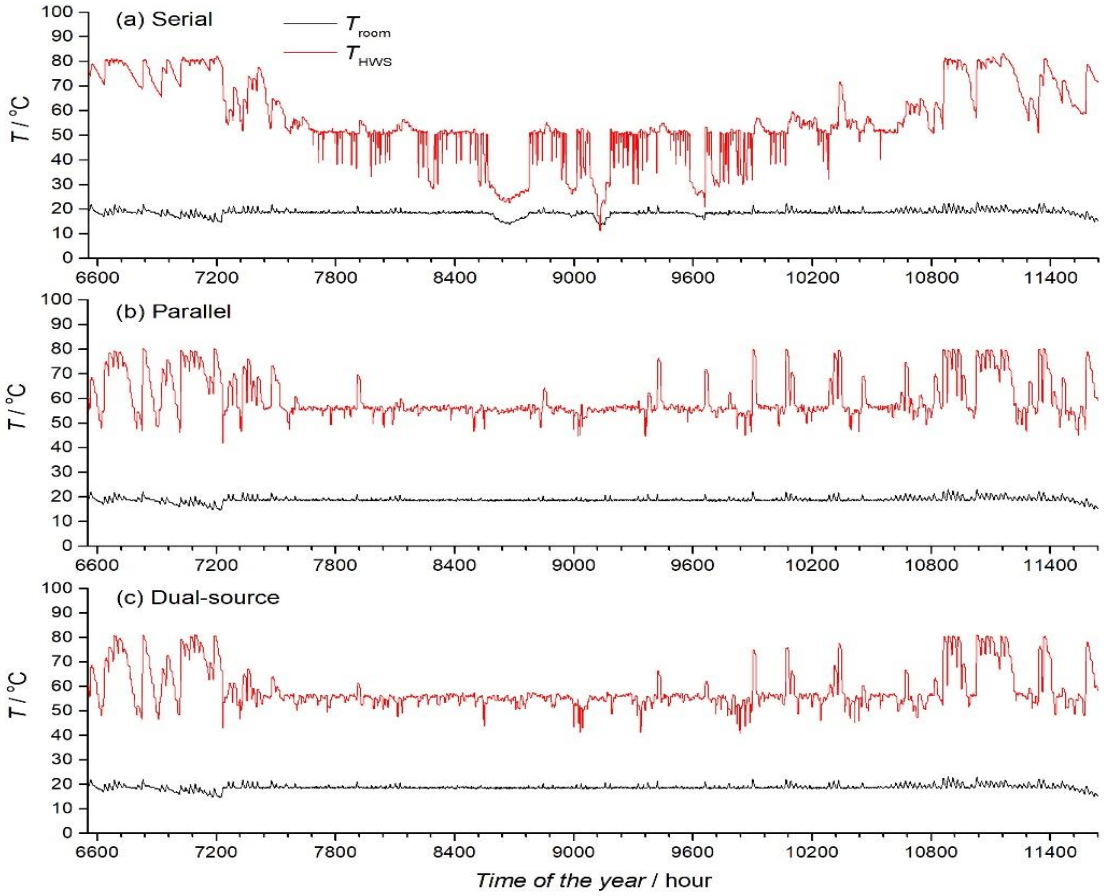

Fig. 4-6: Variations of room air temperature and HW temperature at the outlet of TES tank 2 for three systems over a heating season

During the simulation of serial IX-SAASHP, to improve the heating capacity in winter, larger collector areas, collectors with better efficiencies and larger storage tanks have been tried.

It was found that heating capacity is mainly limited by solar irradiation intensity, rather than component parameters. Improving collector area and efficiency can hardly enhance system performance. For example, when a solar collector of 48 m^2 is used, the lowest room temperature and HWS temperatures are almost the same, 13.5 ^oC and 11.5 ^oC, respectively. When a solar collector with an intercept efficiency of 0.85 is used, the lowest room temperature and HWS temperatures are almost the same, 13.7 ^oC and 11.5 ^oC, respectively. The use of a larger TES tank 1 increases the capacity of TES, but may reduce its water temperature i.e. the heat source temperature for SWHP, resulting in lower heat provision of the system. When a TES tank 1 of 3.5 m^3 is used, the lowest HWS temperature is almost the same at 11.4 ^oC, but the lowest HWS temperature occurs 4 times in winter. In addition, the lowest room air temperature drops even to 11.8 ^oC.

As shown in Fig. 4-6 (b) and (c), the use of ASHP makes the system meet the heat demands well. The lowest water temperature at the outlet of the SWHP evaporator is about -5 ^oC and the air temperatures at the outlet of the ASHP evaporator are also about -5 ^oC. This ensures the safe operation of SWHP and ASHP over the heating season.

4.4.2 Daily heat provision

Fig. 4-7 shows the variations of daily heat provision (kWh) for SH and HW for three systems over a heating season. The blue column represents the daily heat provision for SH and the pink column represents that for HW. The columns are stacked to represent the total heat provision. It can be seen that the heat provision for space heating is mainly required from December to February. The parallel and the dual-source IX-SAASHPs have almost the same daily heat provision, higher than that of the serial IX-SAASHP. The largest daily heat provisions from parallel and dual-source systems are around 100 kWh. On the same day, the serial system only provides thermal energy of 3.2 kWh. Especially, in December, the daily heat provision of the serial system is obviously lower than those of the other systems.

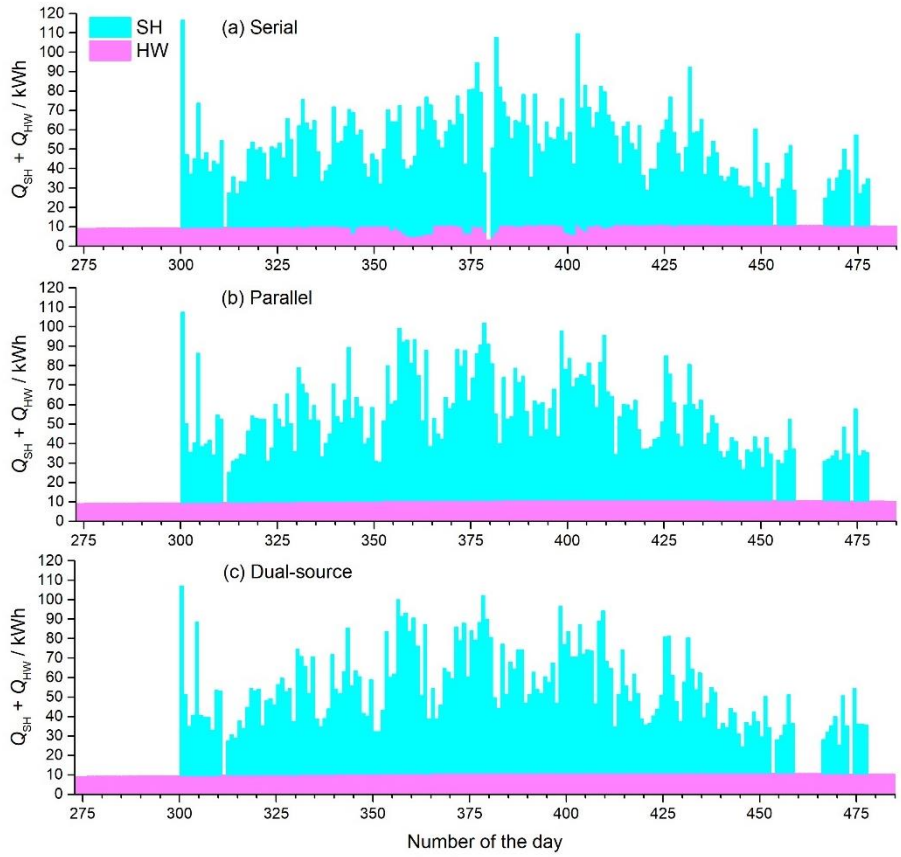

Fig. 4-7: Variations of daily heat provision for SH and HW for three systems over a heating season

Fig. 4-8 shows the variations of daily heat provision (kWh) supplied by direct SHW (green), ASHP (red) and SWHP (orange) for three systems over a heating season. The columns are stacked to represent the total daily heat provision. The black line refers to the daily HW provision as a reference. The thermal energy loss and storage from the hot water tank are included as a part of the daily heat provision. For the serial system, the use of solar energy as the sole heat source providing heat either directly or by the SWHP may result in zero heat provision e.g. on the 14th (379th) day. For the dual-source system, a large proportion of heat is provided by the ASHP. This suggests the importance of employing ASHP in a heating system for stable operation while the SWHP benefits to improve system performance.

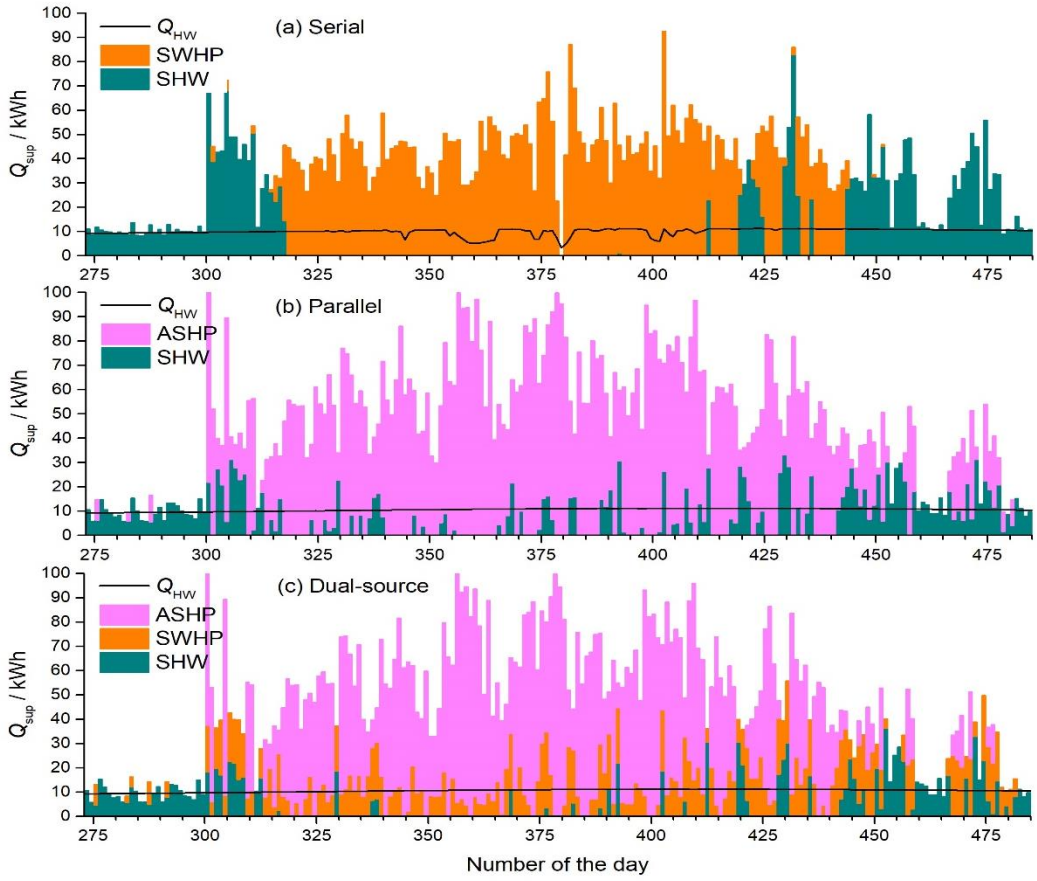

Fig. 4-8: Variations of daily heat provision supplied by direct SHW, ASHP and SWHP for three systems over a heating season

Fig. 4-9 displays the variations of daily electricity consumed (kWh) by the systems over a heating season. The red column is the electricity consumed by the ASHP, the orange column is that by the SWHP and the purple column is that by the pumps. The columns are stacked to represent the total electricity consumed by the system. In all systems, pumps are mainly used to support HPs. The electricity consumed by the pumps in SHW periods is low, only around 0.1 - 0.4 kWh per day. Since parallel and dual-source systems have smaller solar collectors and storage tanks, their solar utilisation is lower than that of serial systems. Their electricity consumption is thereby higher. The largest electricity consumption is around 32 kWh on the 14th day. However, considering the large scale of the serial system, its electricity consumption is still relatively high. The largest electricity consumption is around 25 kWh a day because serial IX-SAASHP requires more pumps during operation. This indicates that it is not feasible to use solar thermal energy as the dominant heat source in London.

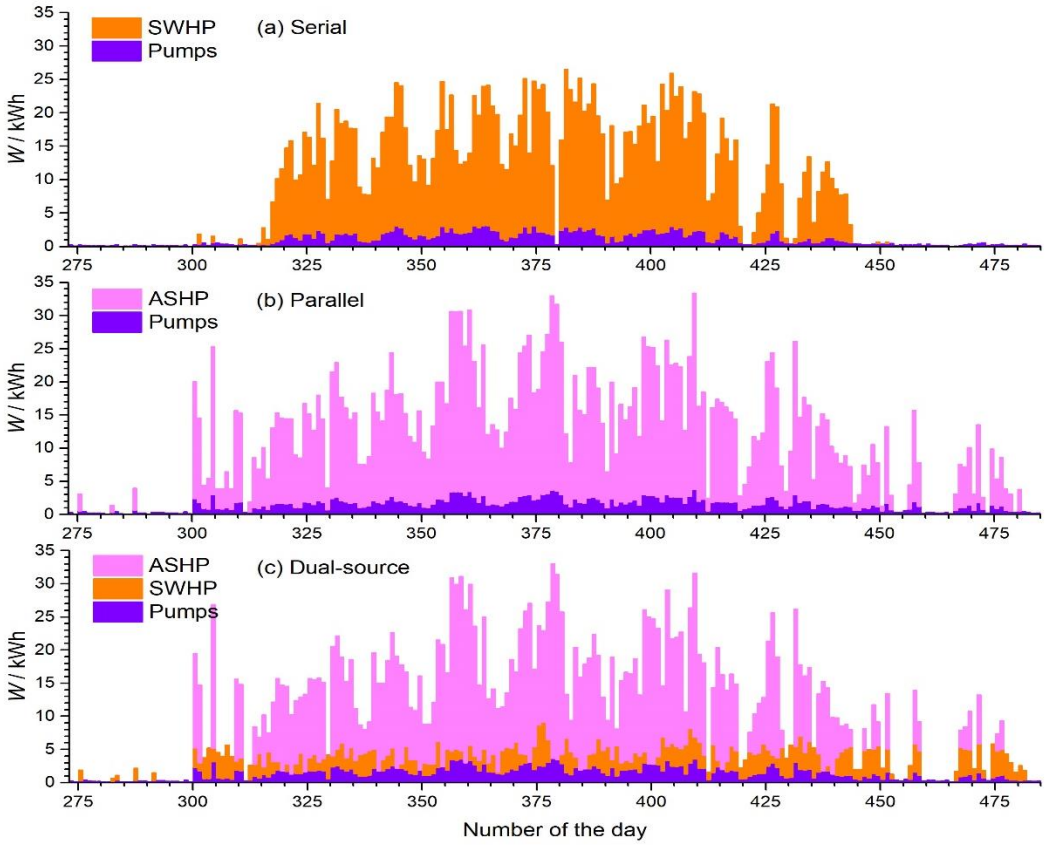

Fig. 4-9: Variations of daily electricity consumed by the systems over a heating season

Fig. 4-10 shows variations of daily solar thermal energy (kWh) used for SH and HW over a heating season. The green column is the solar thermal energy to SHW, and the orange column is that to SWHP. The columns are stacked to represent the total solar thermal energy collected in the system. The black line refers to the average daily HW provision for reference. On most days using SWHP, solar thermal energy mainly works as the heat source to the SWHP and that left for direct SHW is limited. Especially, for the serial system, solar thermal energy is purely used for SWHP in winter.

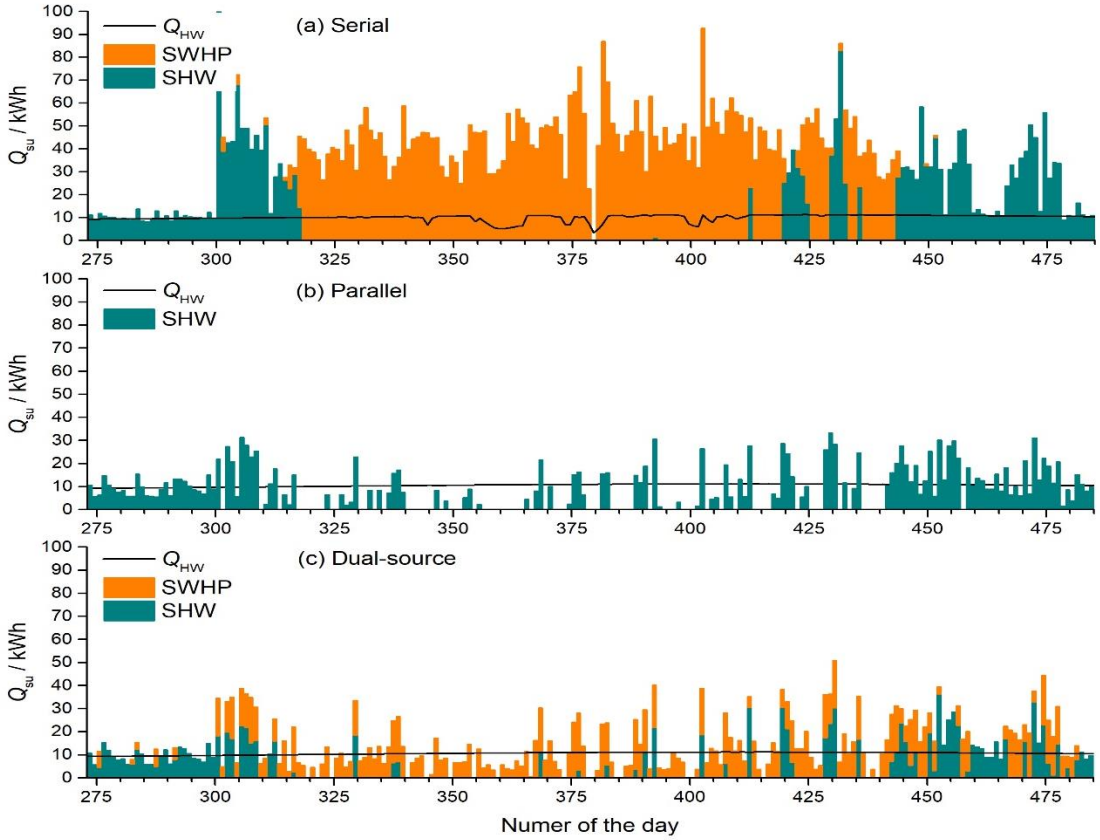

Fig. 4-10: Variations of daily solar thermal energy used for SH and HW over a heating season

Fig. 4-11 shows the variations of daily thermal energy storage (Q_{TES}) in serial (blue), parallel (black) and dual-source (red) IX-SAASHPs over a heating season. Positive value refers to the thermal energy charged and negative value refers to the thermal energy discharged. Comparison between Figs. 11 and 12 indicates that using SWHP increases the utilisation of solar thermal energy and seasonal storage. For example, at the beginning of the heating period, in the serial system, the storage tank discharges around 100 kWh of thermal energy stored in non-heating seasons. On the one hand, employing seasonal thermal storage can balance the seasonal difference between solar irradiance and heat demand, improving the system performance. On the other hand, large requirements on seasonal thermal storage imply insufficient solar availability in winter, impacting the stability of system operation.

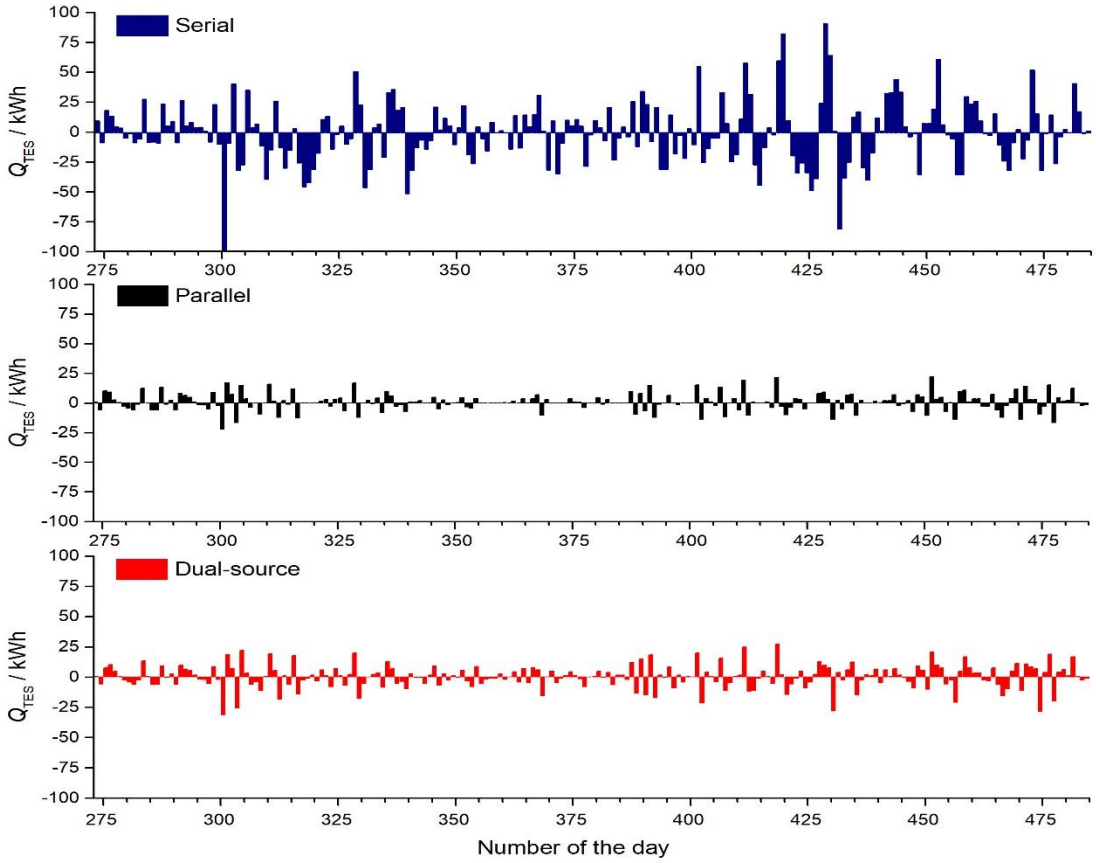

Fig. 4-11: Variations of daily thermal energy storage (Q_{TES}) over a heating season. Positive value refers to the thermal energy charged and negative value refers to the thermal energy discharged.

4.4.3 Efficiencies of the heat pump module(s)

Fig. 4-12 shows the variations of daily averaged *COP* of the HPs in three systems over a heating season. The daily average *COP*s of the SWHP in the serial system and the ASHP in the parallel system are in black and red, and those of the ASHP and SWHP of the dual-source IX-SAASHP are in blue and green. It can be seen that, in the serial IX-SAASHP, the *COP* of the SWHP module ranges from 3 to 7. Wherein, the *COP* ranges from 3 to 5 on most occasions. In the parallel system, the *COP* of the ASHP module ranges from 2.5 to 4.5. Even though the serial IX-SAASHP has a higher *COP* of the HP module, according to the previous analysis, it has low heat provision due to the limits of weather conditions. In the dual-source IX-SAASHP, the *COP* of the SWHP and ASHP modules are the same as those in serial and parallel systems, ranging from 2.5 to 4.5 and from 3 to 7, respectively.

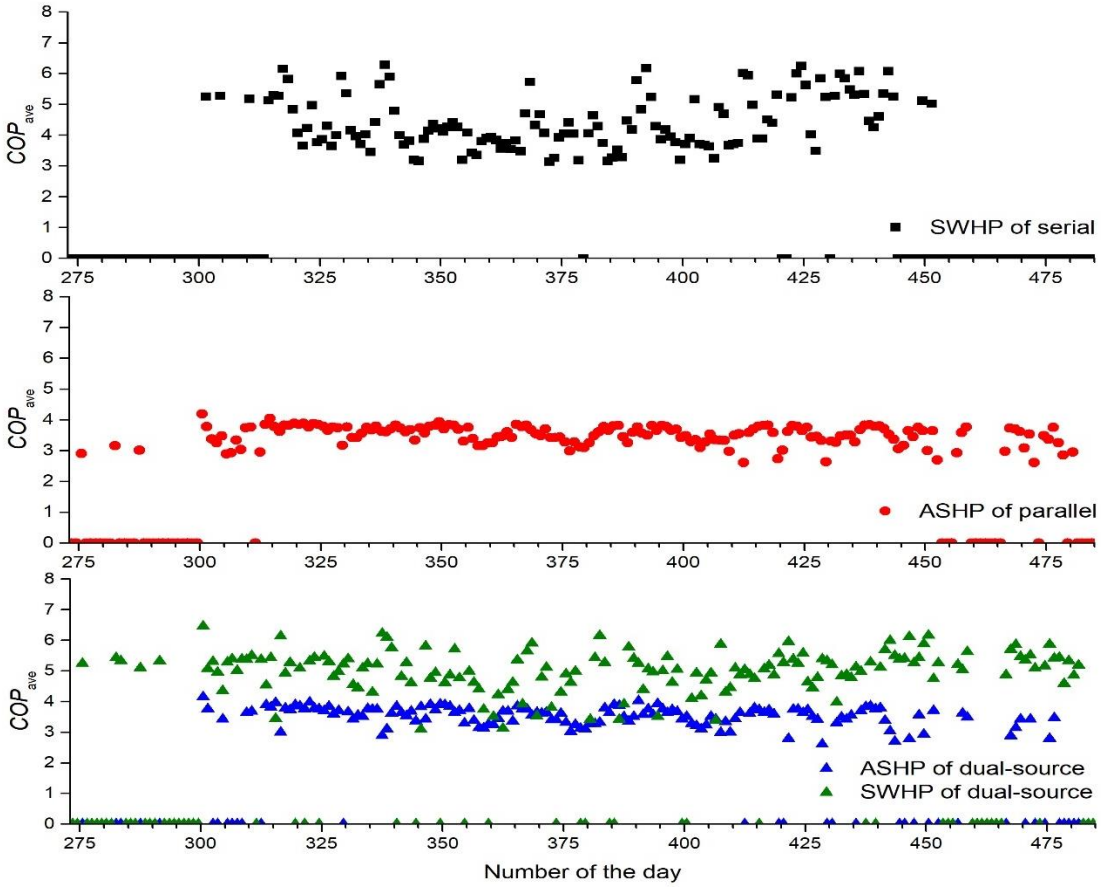

Fig. 4-12: Variations of daily averaged *COP* of the HPs in three systems over a heating season.

Fig. 4-13 shows the SPF_{sys} of the system (blue symbols) and SPF_{HP} of the HPs (black symbol for SWHP and red symbols for ASHP) for three systems. In all three systems, the lowest daily SPF_{HP} is 2.9-3.1. Considering the electricity consumed by pumps, SPF_{sys} is lower than SPF_{HP} in HP dominant periods. The lowest daily SPF_{sys} of the serial and parallel systems is 2.4 and that of the dual-source system is 2.9. All the lowest daily SPF_{sys}s occur in December.

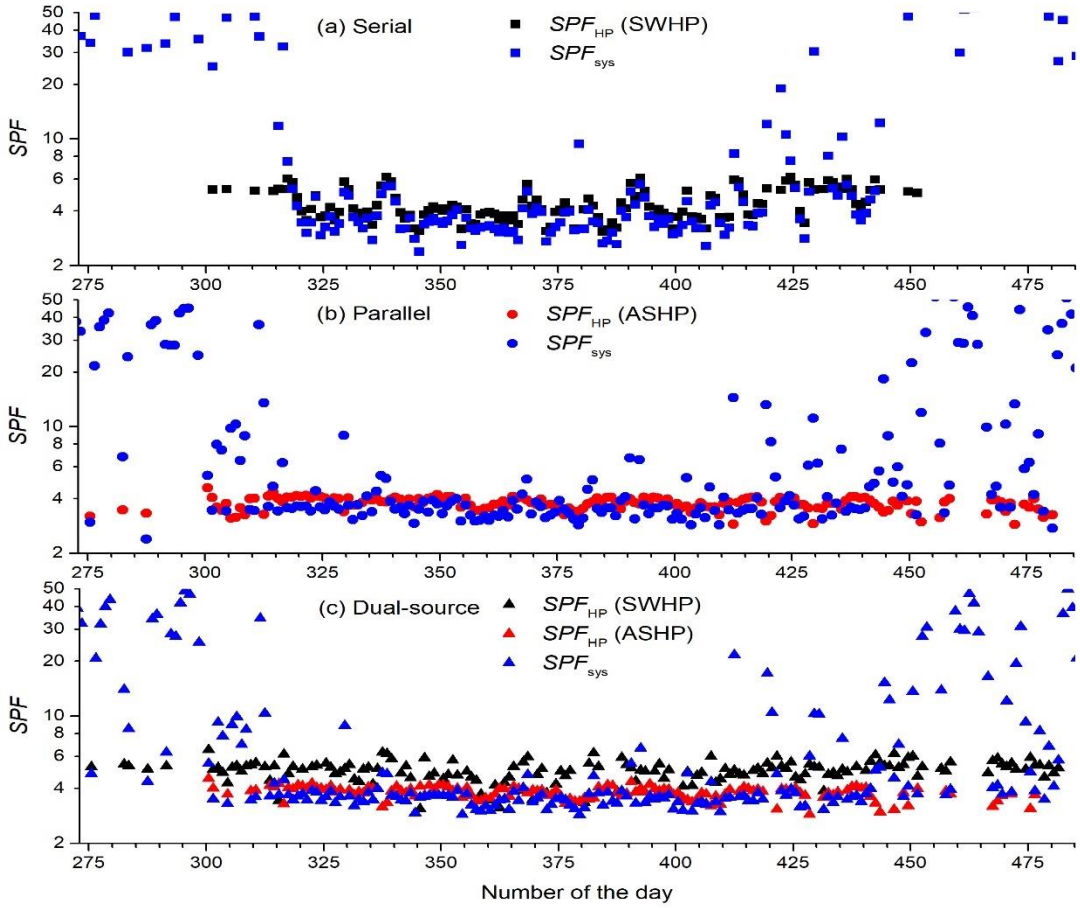

Fig. 4-13: Variations of daily SPF_{sys} and SPF_{HP} over a heating season

4.4.4 Yearly operation performance

The overall operation performances of the IX-SAASHPs are listed in Table 4-5. The system simulation considers heat exchange with the ambient environment and the thermal energy stored in the tanks at the beginning and the ending.

Table 4-5: Overall operation performance of the IX-SAASHPs

System		Period	Serial	Parallel	Dual-source
Heat provision (kWh)	HW	Heating season	2124.8	2235.2	2237.7
		Non-heating season	1427.3	1426.9	1427.5
	SH		7270.5	7523.7	7527.9
	Total		10822.6	11185.8	11193.1
Heat provision (kWh)	SWHP		7008.6	0	2289.1
	ASHP		0	8218.0	6586.6
	Solar	Heating season	2567.1	1802.6	1187.6
		Non-heating season	1528.7	1444.1	1409.4
	SWHP		1705.7	0	449.2
	ASHP		0	2136.9	1737.7

Electricity consumption (kWh)	Water pumps	Heating season	233.2	304.7	295.0
		Non-heating season	27.8	42.7	40.7
	Total		1966.763	2511.3	2522.6
SPF_{HP}	SWHP		4.1	0	5.1
	ASHP		0	3.8	3.8
COP_{ave}	SWHP		4.5	0	5.0
	ASHP		0	3.5	3.5
Solar thermal energy (kWh)	To SWHP		5302.9	0	1839.9
	To end use	Heating season	2567.1	1802.6	1187.6
		Non-heating season	1528.7	1444.2	1409.4
	Total		9980.0	3593.2	4706.7
Thermal energy from ambient air (kWh)			0	6054.1	4848.9
SF	Heating season		83.8%	18.5%	31.0%
	Yearly		86.7%	29.0%	39.6%
SPF_{sys}	Heating season		4.9	4.0	3.9
	Yearly		5.5	4.5	4.4

All the IX-SAASHPs can obtain yearly SPF_{sys} above 4.4. This suggests that, for the weather conditions in London, IX-SAASHPs can be a promising choice for SH and HW. Compared with the systems in Table 2-5, the three systems show good operation performance even in a higher-latitude region. It is interesting to note that, using the same area of solar collector and TES tank volume, the parallel system has a lower yearly *SF* (29%) than the dual-source system (39.6%), but both systems share similar SPF_{sys}, 4.5 and 4.4. This means that in the dual-source system, the electricity consumed by pumps balances the electricity saved by using solar energy. In addition, it should be noticed that, though the dual-source IX-SAASHPs always have a *COP* under 3.5 in previous studies, for the weather conditions in London, the dual-source system can be comparable to the parallel system. This suggests that the dual-source IX-SAASHP is of higher application potential in high altitude regions.

For all three systems, space heating accounts for around 67% of the total heat demand. This suggests that, although SH takes a shorter period, it is more important than HW in the domestic heating sector. To make the domestic heating sector greener, advanced technologies in various aspects helping reduce the heat demand for space heating, such as low *U*-value materials and passive design, need to be developed.

In terms of heat provision, the HPs contribute to the most heat provision (around 83%) and also consume the most of the overall electricity consumption (around 85%). To increase heat provision and reduce operation costs, it is important to improve HP technologies for higher *COP* such as using a highly efficient compressor, suitable refrigerant and heat exchangers with enhanced heat transfer and improved design.

4.4.5 Economic analyses

To evaluate and compare the economic performance of IX-SAASHPs, economic analyses are conducted for IX-SAASHPs, electric water heater and gas boiler, as well as electric heater and gas boiler boosted SHW systems.

For economic analyses, the total energy consumption of the heating systems, Q_{tot}, is calculated by Eq. (4-10):

$$Q_{tot} = (Q_{sh} + Q_{hw} - Q_{ce})/\eta \quad (4\text{-}10)$$

where Q_{ce} is the clean energy (extracted from solar and ambient air sources) used by the heating system and η is the efficiency of the electric water heater and gas boiler.

The payback period, P_{pb}, is defined based on the electric water heater by Eq. (4-11)

$$P_{pb} = C_i / C_{spy} \quad (4\text{-}11)$$

where C_i is the initial cost difference and C_{spy} is the cost saving per year calculated by Eq. (4-12) and Eq. (4-13), respectively.

$$C_i = C_{i0} - C_{ieh} \quad (4\text{-}12)$$

$$C_{spy} = C_{o0} - C_{oeh} \quad (4\text{-}13)$$

where C_{i0} and C_{o0} are the initial and operation costs of the heating system, respectively, C_{ieh} and C_{oeh} are the initial and operation costs of the electric water heater.

The efficiencies of the electric water heater and gas boiler are taken from [161] to be 0.95 and 0.85, respectively. The electric water heater and gas boiler have a TES tank of 300 L. For the SHW systems, the sizes of the solar collector and outdoor TES tank are taken to be the same as those of the dual-source IX-SAASHP and therefore both systems have the same amount of solar thermal energy collected i.e. ca. 4.71 MWh. The heat provisions of the three heating systems for SH and HW over the year is ca. 11.19 MWh. It is noted that, for the serial system, the heat provision of ca. 10.82 MWh is insufficient to meet the requirement of thermal comfort sometimes and the rest heat needed is assumed to be provided by the auxiliary electric heaters with an efficiency of 0.95 for economic analysis of the heating systems.

The current energy prices are taken from E. On Energy (a UK energy supplier) to be £400.2 per MWh for electricity and £ 106.8 per MWh for gas (prices in June 2022) [255]. The prices of the components of the heating systems are obtained from an online market where the flat plate solar collector price is around £30 per m^2, the water tank price is £290 per 100 L, and a pump with a head of 15 m and a capacity of 15 L/min is around £10 [256]. All three heating systems have a capacity of 8 kW. The systems are estimated to be easy to connect to the current space heating and water heater. The installation costs are assumed to be 3 hours for the SHW

system and 6 hours for SAASHPs with a cost of 80 per hour [257]. The shipping fees for international shipping are not included in the current economic analysis.

The results of the economic analysis for 2022 are listed in Table 4-6. Though the gas boiler is the cheapest one today, they are expected to be phased out by 2033. The gas boiler boosted SHW is the second cheapest one and has a similar payback period to the parallel IX-SAASHP. This suggests that the parallel IX-SAASHP can be a good alternative for replacing gas boiler boosted SHW from now on. The payback period of the electric heater boosted SHW is almost 1.7 times that of the parallel IX-SAASHP. The serial IX-SAASHP has the longest payback period due to its high initial cost. In general, IX-SAASHPs can save more operation costs than electric water heaters and electric heater boosted SHW. Considering both operation performance and economic efficiency, this study suggests the feasibility of using SAASHP in UK weather conditions to achieve a clean future.

4.5 Summary

In this chapter, TRNSYS has been used to simulate the operation performances of serial, parallel and dual-source IX-SAASHPs for SH and HW in London. The economic analysis has also been conducted according to the market of the IX-SAASHPs. The following conclusions can be drawn:

1. All three IX-SAASHPs can achieve a yearly SPF_{sys} higher than 4.4, suggesting their potential to be applied for domestic heating under weather conditions in high latitude regions.
2. The heat provision of the serial IX-SAASHP is limited by the availability of solar irradiance. Since solar energy is the sole heat source of the serial system, it requires large sizes of solar collectors and TES tanks, resulting in high installation costs and a longer payback period.
3. The parallel IX-SAASHP has the simplest pipe connection and control function. It shows the highest SPF_{sys} and the most stable operation performance.
4. The dual-source IX-SAASHP shows a much lower cost than the serial system and similar operation performance to the parallel system.
5. The parallel IX-SAASHP has the lowest payback period of 0.72 years and the dual-source IX-SAASHP has a payback period of 0.92 years.

Table 4-6: Results of economic analysis for electric heater, SHW and IX-SAASHP heating systems (2022)

		Electric water heater	**Gas boiler**	**Electric heater boosted SHW**	**Gas boiler boosted SHW**	**Serial IX-SAASHP**	**Dual-source IX-SAASHP**	**Parallel IX-SAASHP**
Heat provision per year, MWh		11.19	11.19	11.19	11.19	10.82 + 0.37	11.19	11.19
Efficiency/performance		0.95	0.85	0.95	0.85	*SPF*=5.5, 0.95	*SPF*=4.4	*SPF*=4.5
Energy consumption per year, MWh		11.8	13.2	7.2	8.0	2.1	2.2	2.2
Initial cost, £	collector	0	0	540	540	1350	540	540
	tanks	870	870	2320	2320	9570	2320	2320
	Heater/HP	60	15	60	15	460+60	1085	330
	pumps	0	0	20	20	30	30	30
	Installation	0	0	240	240	480	480	480
	total	930	885	3180	3135	11950	4455	3700
Operation cost, £		4713.9	1406.0	2881.4	854.4	667.2	897.7	875.1
Cost saving per year, £		-	3307.9	1832.5	3859.5	4046.7	3816.2	3838.8
Payback period, year		-	-	1.23	0.57	2.71	0.92	0.72

5. Investigation of Low temperature heating operation performance of indirect expansion solar assisted air source heat pump

The set hot-water-supply temperature of the heating system affects both the system operation performance and the thermal comfort condition of the house. Operation performances of low temperature heating and ultra-low temperature heating are investigated. Different from district heating, this study is focused on individual domestic heating, which can give a reference for distributed heating. A single-family house is chosen as the reference building and the heating system is modelled and simulated under the weather conditions in the locations of London, Aughton and Aberdeen in the UK over a year. The set hot-water-supply temperatures are taken to be 40 ^{o}C, 45 ^{o}C, 50 ^{o}C and 55 ^{o}C. For the heating systems, with the decrease in set hot-water-supply temperature from 55 ^{o}C to 50 ^{o}C, 45 ^{o}C and 40 ^{o}C, the yearly total electricity consumption decreases by 5.6%, 10.5% and 19.1% in London; 5.6%, 10.4% and 14.9% in Aughton; and 4.4%, 10.3% and 13.3% in Aberdeen, respectively. The results show that low temperature heating enables a significant reduction in electricity consumption of such heating systems. This provides valuable inspiration for approaches to Net Zero.

5.1 Seasonally heating performance for different set hot-water-supply temperatures

Fig. 5-1 displays the variations of the room air temperature (black) and hot water temperature at the outlet of TES tank 2 (T_{HWS}) over a heating season for different T_{HWS}*. When T_{HWS} drops down below T_{HWS}*, the heat pump switches on to increase T_{HWS}. It is seen that the temperature drops in T_{HWS} occur more frequently for lower T_{HWS}* due to the lower capacity of TES at a lower temperature. When T_{HWS}* is set at 40 ^{o}C – 50 ^{o}C, in all these three locations, the heating system can provide sufficient thermal energy and maintain T_{HWS} around 5 K higher than T_{HWS}*. This suggests that though the heating demand in Aberdeen is much higher than those in London and Aughton, the heating system with the same heating capacity can provide sufficient heat to meet the heating demand in Aberdeen. However, when T_{HWS}* is set at 55 ^{o}C, the heating system under weather conditions in London and Aughton works well and achieves a T_{HWS} of around 60 ^{o}C; in Aberdeen, the heating system can only maintain a T_{HWS} of 57 ^{o}C, slightly higher than the set temperature.

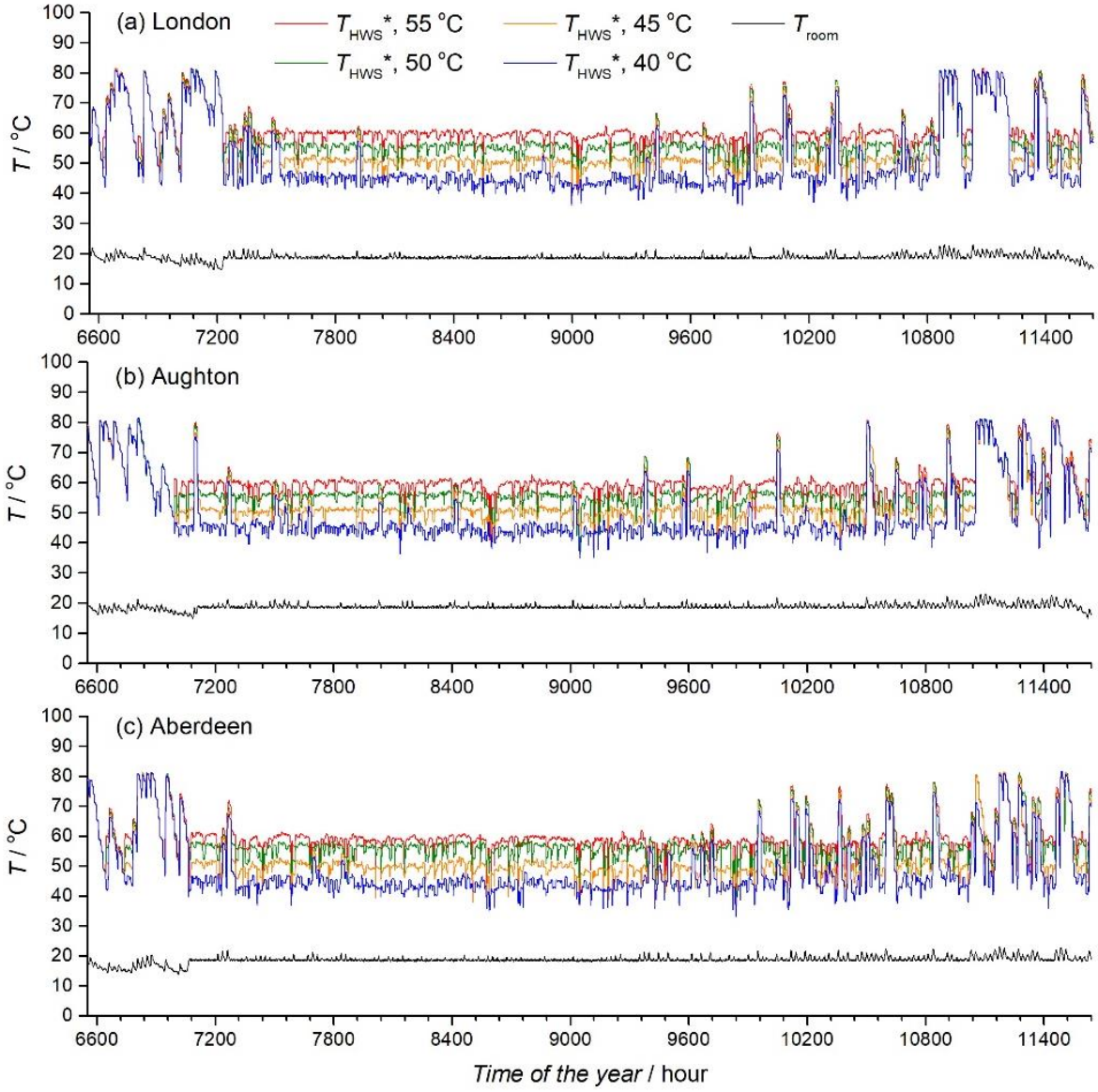

Fig. 5-1: Variations of room air temperature and hot water temperature at the outlet of TES tank 2 over a heating season for different T_{HWS}*.

Taking the operation performance of the heating system in London, for example, Fig. 5-2 shows the daily variations of heat provision for space heating (green) and hot water (yellow) over a heating season for different T_{HWS}*. The stacked instantaneous values show the total heat provision. The variation of the heat provision for space heating is seen as different for different T_{HWS}*. This is attributed to the influence of thermal energy stored in building structures at different temperatures. When T_{HWS}* is set at 40 °C, the heat provision for hot water is slightly lower than the heat demand at the beginning of heating periods (300th day) while at other temperatures of T_{HWS}*, the heat provision meets well with the heat demands. This is because the lower capacity of tank 2 TES at T_{HWS}* of 40 °C is hardly to meet the sudden increase in heat demand.

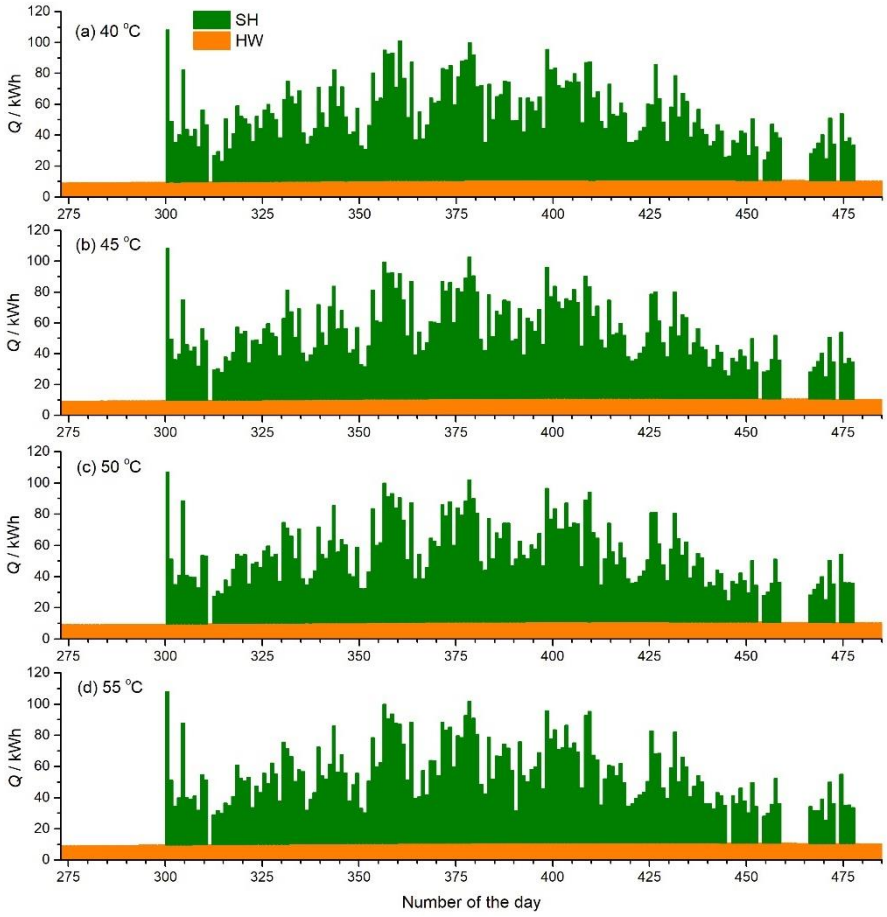

Fig. 5-2: Daily variations of heat for space heating and hot water over a heating season for different T_{HWS}*.

Fig. 5-3 displays the daily variations of heat provision for space heating and hot water by direct SHW, ASHP and SWHP over a heating season for different T_{HWS}*. The red column represents the daily heat provision by ASHP, the yellow column represents that by SWHP, and the purple column represents that by direct SHW. The stacked chart shows the total heat provision. For different T_{HWS}*, the proportions of heat provision contributed by ASHP, SWHP and direct SHW are almost the same and the heat provision by ASHP is dominant. The direct SHW contributes to the main heat provision in the non-heating period. Additionally, in the non-heating period, for example 273th-300th days, the increased contribution of SWHP is observed as T_{HWS}* increases.

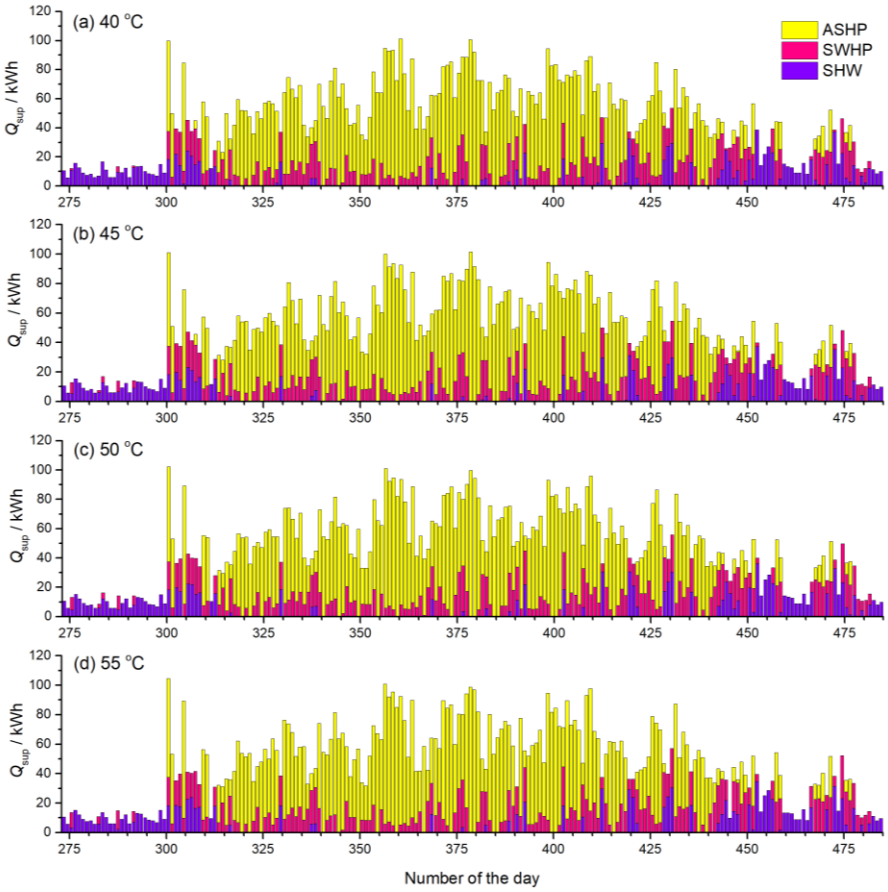

Fig. 5-3: Daily variations of heat for space heating and hot water by direct SHW, ASHP and SWHP over a heating season for different T_{HWS}*.

Fig. 5-4 shows the daily variations of electricity consumed by ASHP (yellow), SWHP (red) and SHW (blue) over a heating season for different T_{HWS}*. Referring to Fig. 7, the electricity is mainly consumed by ASHP. It is also seen that the electricity consumed by SWHP increases as T_{HWS}* increases in the non-heating period. As T_{HWS}* increases, the electricity consumption by ASHP and SWHP increase since the condensing temperature increases. For example, on the 381st (16th) day, the total electricity consumptions are 30.9 kWh and 33.5 kWh for T_{HWS}* of 40 ^{o}C and 55 ^{o}C, respectively.

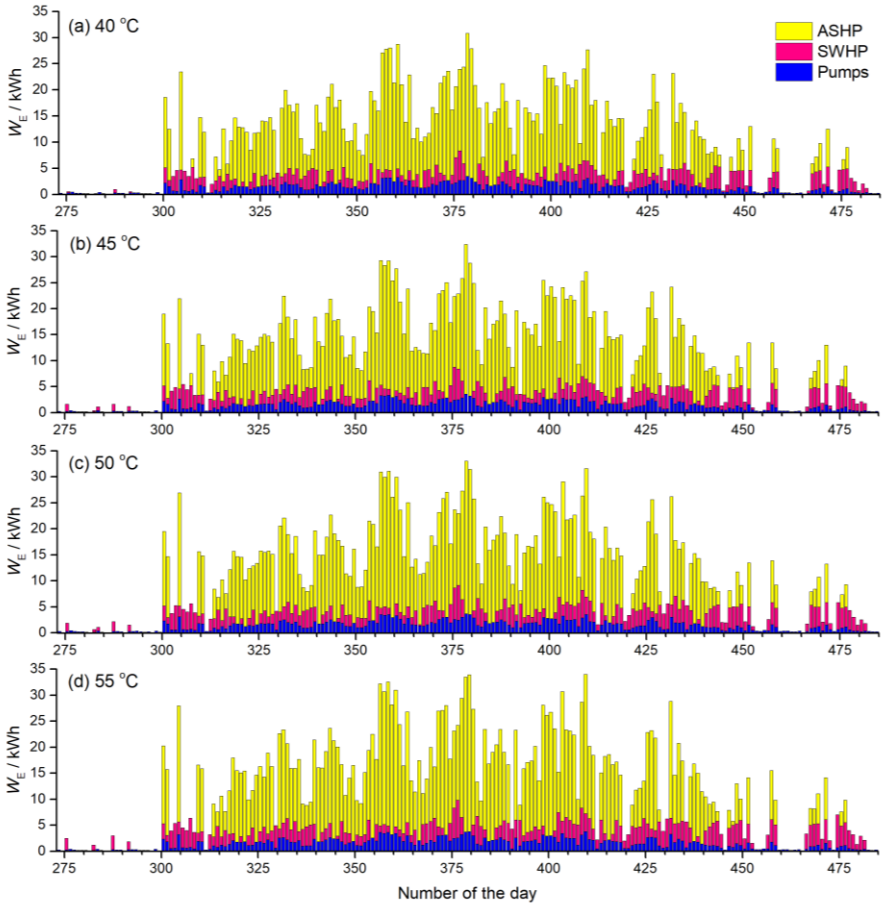

Fig. 5-4: Daily variations of electricity consumed by ASHP, SWHP and SHW over a heating season for different T_{HWS}*.

Fig. 5-5 shows the daily variations of thermal energy extracted from solar energy either used as the heat source for SWHP (pink) or directly for hot water (SHW, blue) over a heating season for different T_{HWS}*. The total solar energies used are almost the same for different T_{HWS}*. As T_{HWS}* increases, the capacity for direct SHW decreases and therefore more solar thermal energy is used by SWHP. For T_{HWS}* of 45 °C and above, SWHP is often operated in non-heating periods while in this temperature range, as T_{HWS}* increases, the total solar energy used by SWHP in non-heating periods remains almost the same.

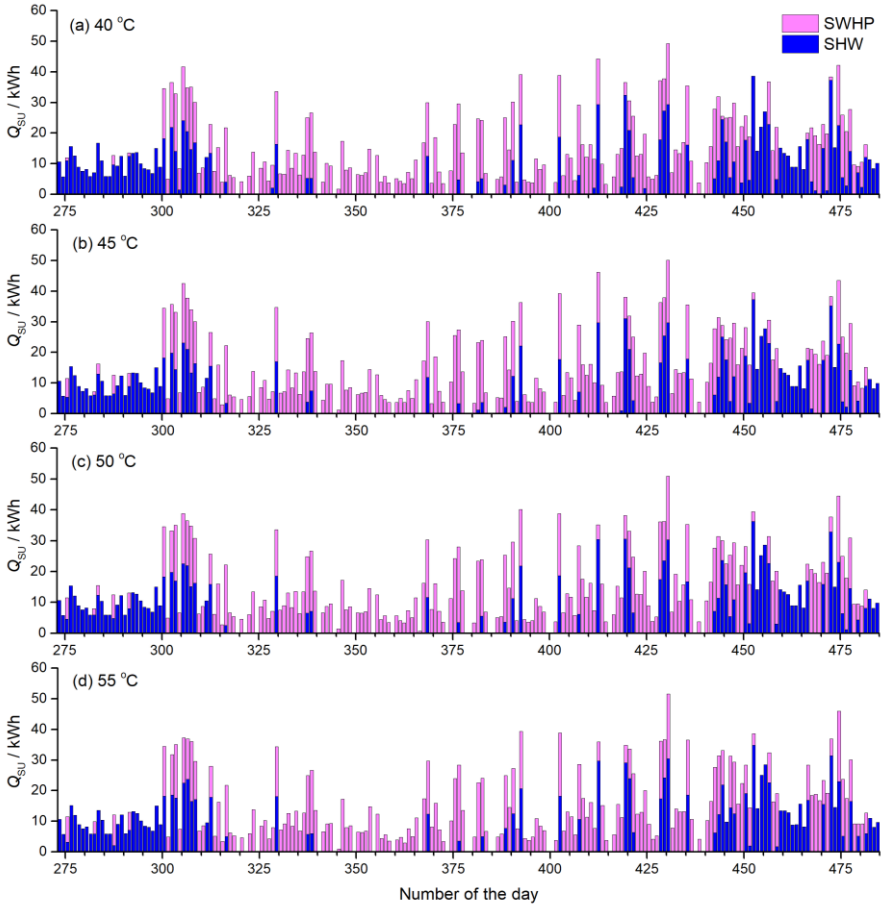

Fig. 5-5: Daily variations of thermal energy extracted from solar energy either used as the heat source for SWHP or directly for hot water (SHW) over a heating season for different T_{HWS}*.

Fig. 5-6 shows the daily variations of Q_{TES} charged (positive) and discharged (negative) of tank 2 over a heating season for different T_{HWS}*. Although T_{HWS}* influences the storage capacity, the daily TES charged and discharged look similar for all different T_{HWS}*.

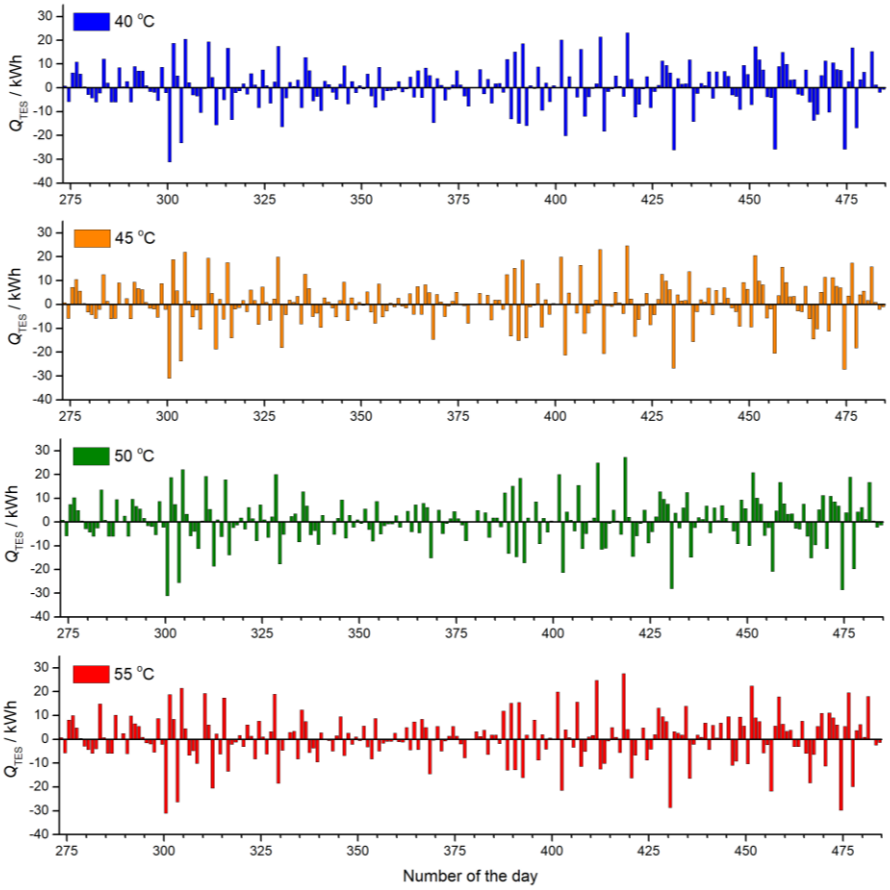

Fig. 5-6: Daily variations of Q_{TES} charged (positive) and discharged (negative) over a heating season for different T_{HWS}*.

Fig. 5-7 shows the variations of daily averaged *COP*s of ASHP and SWHP over a heating season for different T_{HWS}*. For both ASHP and SWHP, *COP* decreases as T_{HWS}* increases. The variation among COP_{ASHP} for different T_{HWS}* is relatively small, around 1.0 while the variation among COP_{SWHP} for different T_{HWS}* is larger, around 2.0. The COP_{ASHP} ranges mainly in 3.0-4.0 while the COP_{SWHP} ranges mainly in 4.0-6.0. On some days such as the 315th day, for both ASHP and SWHP their *COPs* at lower T_{HWS}* are higher than those at higher T_{HWS}*.

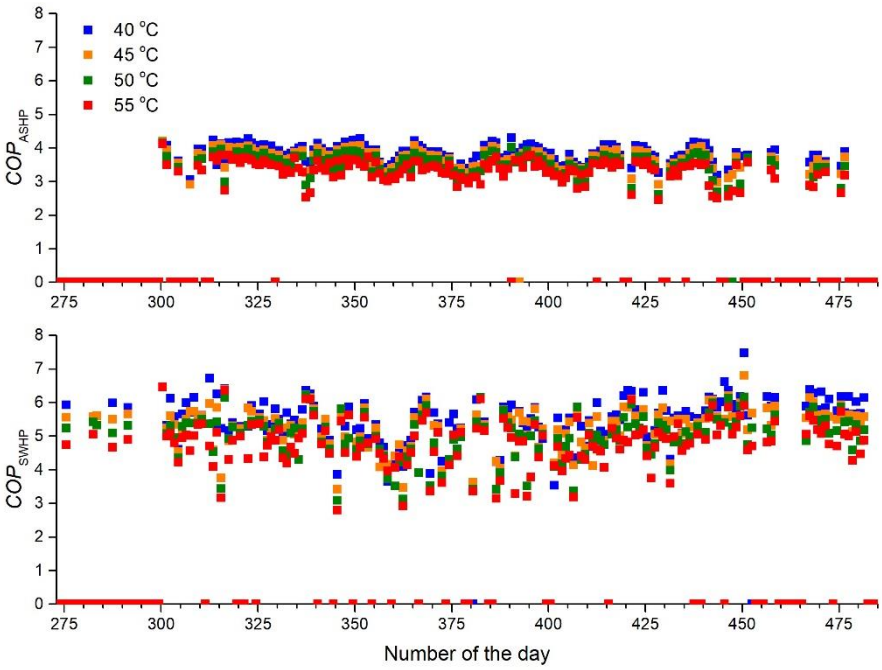

Fig. 5-7: Variations of daily averaged *COP* of the HPs over a heating season for different T_{HWS}*.

Fig. 5-8 shows the daily variations of SPF_{sys} and SPF_{HP} over a heating season for different T_{HWS}*. SPF_{HP} shows the same trend as COP_{HP}. The influence of T_{HWS}* on SPF_{sys} is seen as complicated. On most days, low temperature heating achieves better performance, especially in the non-heating period. However, on some days such as the 312th day, the trend of the performance is inverse. On some days such as the 479th (114th) day, SPF_{sys} is not influenced by T_{HWS}*; SPF_{sys} decreases as T_{HWS}* decreases from 55 ^{o}C but reaches the highest value at T_{HWS}* of 40 ^{o}C.

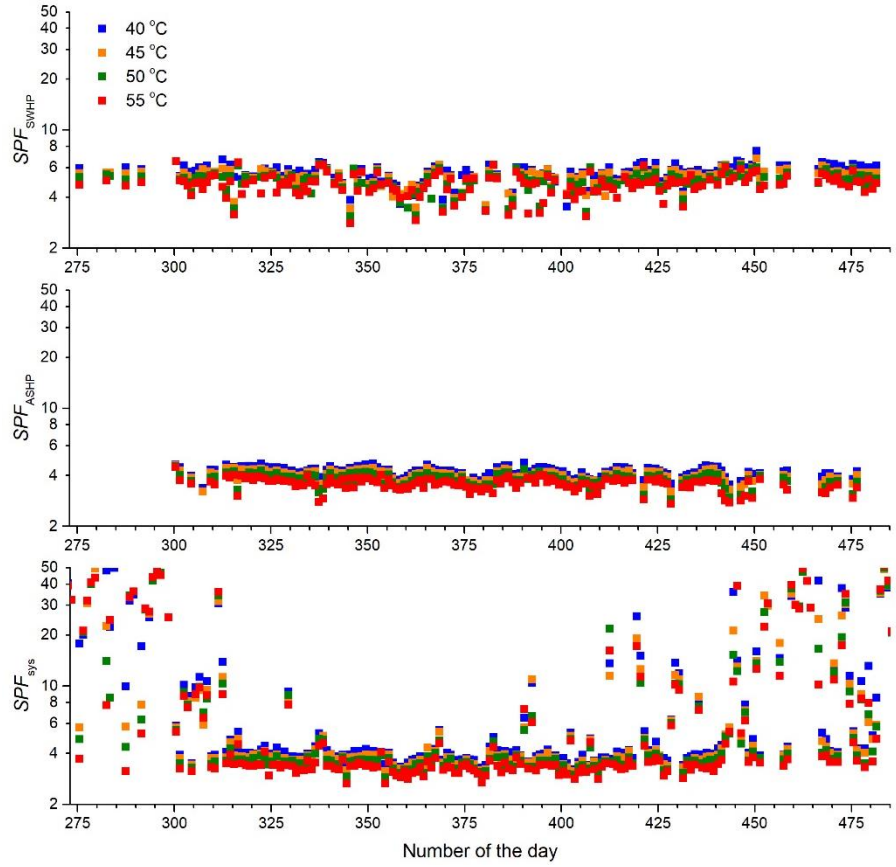

Fig. 5-8: Daily variations of SPF_{sys} and SPF_{HP} over a heating season for different T_{HWS}*.

5.2 Low temperature heating performance for London, Aughton and Aberdeen

The performances of low temperature heating of the heating system under the weather conditions in London, Aughton and Aberdeen are analysed and compared. Fig. 5-9 shows the daily variations of heat provision for space heating (green) and hot water (yellow) over a heating season in London, Aughton and Aberdeen, respectively. The heat provision for hot water in Aberdeen is the highest, followed by Aughton and London. This is due to their mains cold water temperatures. The heat provision for space heating shows the same trend as the heating load shown in Chapter 3. In Aberdeen, the daily heat provision for space heating is the highest with a large variation and a peak value of 108.4 kWh. In London and Aughton, the daily heat provisions for space heating are relatively lower with peak values of 90.5 kWh and 90.8 kWh. The heat provision for space heating in Aughton shows less variation.

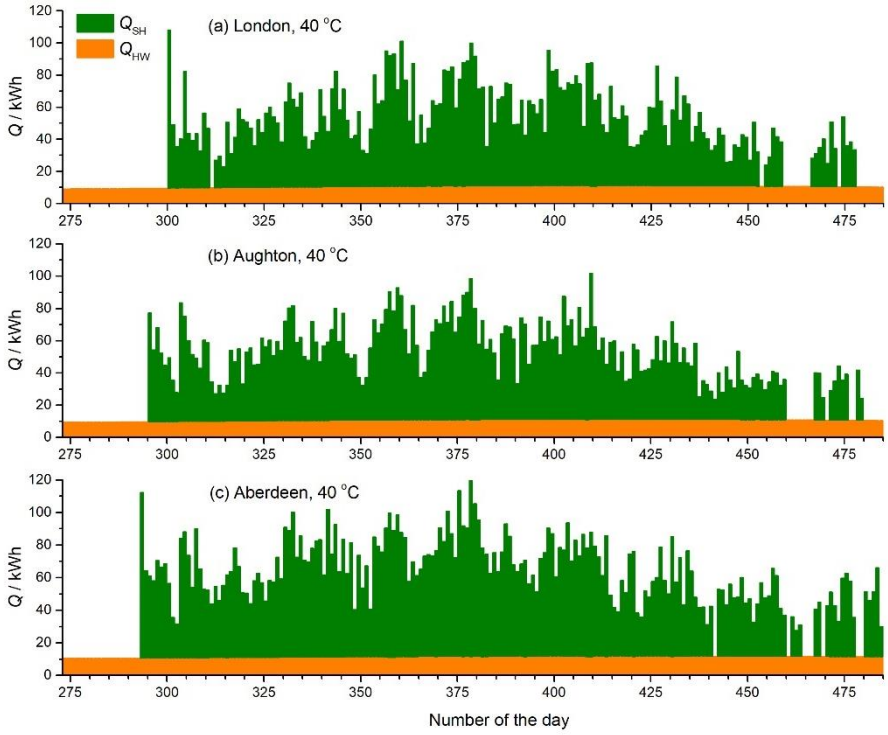

Fig. 5-9: Daily variations of heat for space heating and hot water over a heating season in London, Aughton and Aberdeen

Fig. 5-10 shows the daily variations of heat provision for space heating and hot water by direct SHW (purple), ASHP (yellow) and SWHP (red) over a heating season in London, Aughton and Aberdeen, respectively. In the heating season, ASHP, SWHP and direct SHW contribute to 66.3%, 21.2% and 12.5% of the total heat in London, 63.1%, 24.6% and 12.3% in Aughton and 67.3%, 22.9% and 9.8% in Aberdeen, respectively. It is seen that the heat provided by ASHP is about three times that by SWHP and about six times that by direct SHW in the three locations. It is also noted that on some days e.g. from 329th to 385th, all the heat is solely supplied by HPs (ASHP 87.6% and SWHP 12.4%) in Aberdeen.

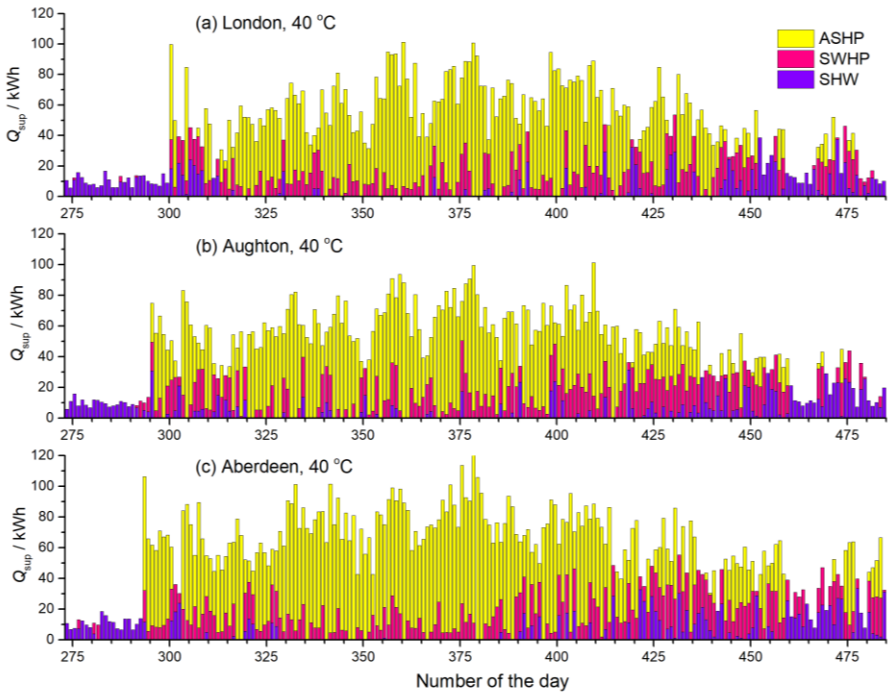

Fig. 5-10: Daily variations of heat for space heating and hot water by direct SHW, ASHP and SWHP over a heating season in London, Aughton and Aberdeen

Fig. 5-11 shows the daily variations of electricity consumed by ASHP (yellow), SWHP (red) and pumps (blue) over a heating season in London, Aughton and Aberdeen, respectively. The electricity consumptions over the heating season in London, Aughton and Aberdeen are 2221.1 kWh, 2246.5 kWh and 3067.0 kWh. In the heating season, the proportions of the electricity consumption by ASHP, SWHP and pumps are 70.9%, 16.7% and 12.4% in London, 68.5%, 19.1% and 12.3% in Aughton and 70.9 %, 17.4% and 11.6% in Aberdeen, respectively. It is seen that the electricity consumed by ASHP is about four times that by SWHP and about five times that by pumps in the three locations. Though heat is not supplied directly by SHW in the period of 329th – 385th day in Aberdeen, the electricity consumption by water pumps is 146.2 kWh to assist the operation of SWHP and to charge the TES tank 1.

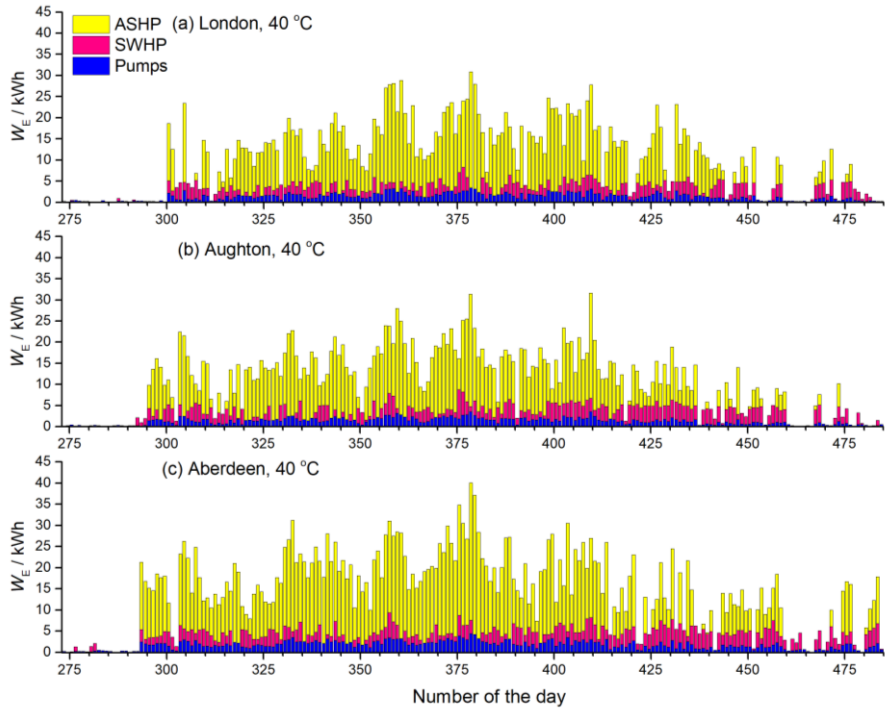

Fig. 5-11: Daily variations of electricity consumed by ASHP, SWHP and pumps over a heating season in London, Aughton and Aberdeen

Fig. 5-12 shows the daily variations of thermal energy extracted from solar energy either used as the heat source for SWHP (pink) or direct solar hot water (SHW, blue) over the heating season in London, Aughton and Aberdeen, respectively. In the heating season, the total solar energies utilized in London, Aughton and Aberdeen are 3.0 MWh, 3.3 MWh and 3.6 MWh, respectively. The proportions of the solar energy utilized by SWHP and direct SHW are 58.2% and 41.8% in London, 62.3% and 37.7% in Aughton and 65.7% and 34.3% in Aberdeen, respectively. It is seen that more solar energy is utilized by SWHP at higher latitudes. On some days, e.g. 426th (61st) day, the solar thermal energy extracted in London is only 5.79 kWh while those in Aughton and Aberdeen are 21.9 kWh and 39.3 kWh. Furthermore, in December, solar thermal energy is seen to provide a large direct SHW of 69.8 kWh in Aughton. This is due to the unpredictable weather conditions in these locations.

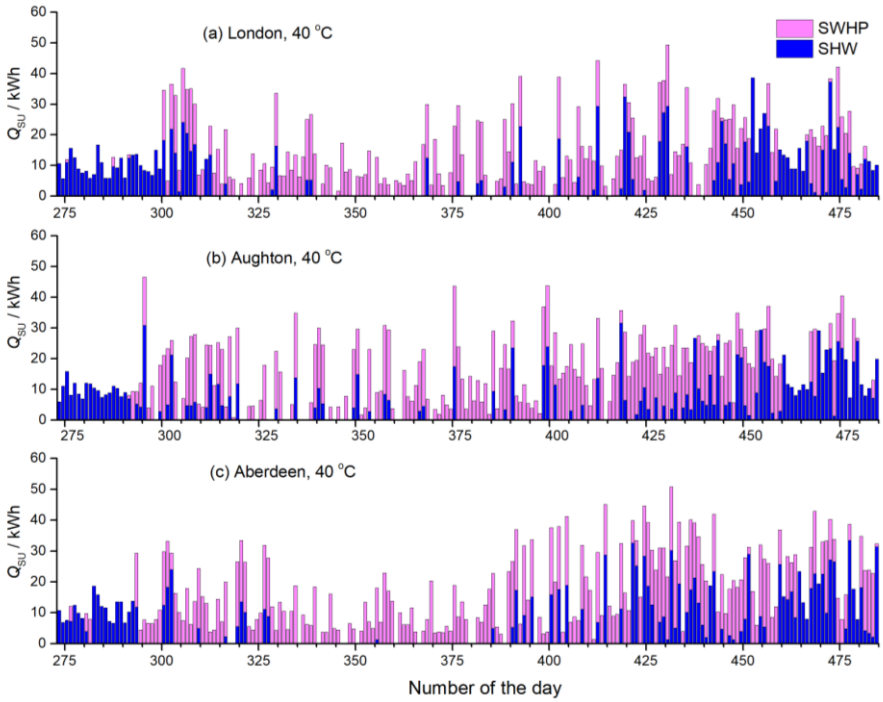

Fig. 5-12: Daily variations of thermal energy extracted from solar energy either used as the heat source for SWHP or directly for hot water (SHW) over a heating season in London, Aughton and Aberdeen

Fig. 5-13 shows the daily variations of averaged *COP* of the HPs over a heating season in London (blue), Aughton (orange) and Aberdeen (green). In all three locations, the values of COP_{ASHP} fall in the range of 3.0-4.0. The COP_{ASHP} in Aberdeen is slightly lower than those in London and Aughton. The averaged values of COP_{ASHP} are 3.8, 3.8 and 3.6 in London, Aughton and Aberdeen, respectively. In contrast, the values of COP_{SWHP} in the three locations vary largely from 3.0 to 7.0 in autumn and winter while in early spring (since the 440th day), the values of COP_{SWHP} for the three locations fall in the range of 5.5-6.5. This is due to the large variations in solar irradiance in autumn and winter and fewer variations in spring. The averaged values of COP_{SWHP} are 5.6, 5.6 and 5.4 in London, Aughton and Aberdeen, respectively. It is seen that the average value of COP_{SWHP} is much higher than that of COP_{ASHP}. This is attributed to the higher evaporation temperature of the refrigerant in the water-to-refrigerant evaporator than that in the air-to-refrigerant evaporator.

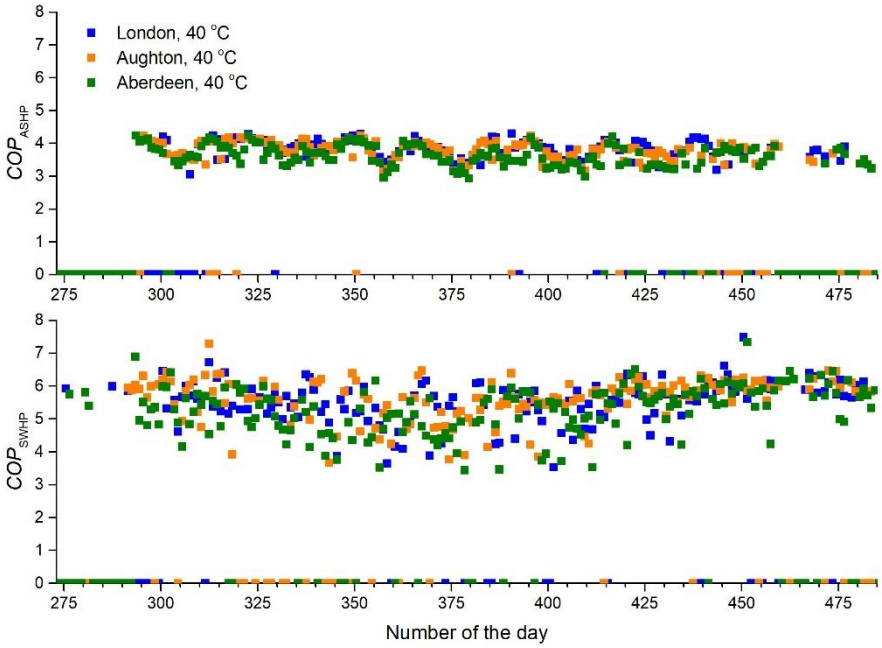

Fig. 5-13: Daily variations of averaged *COP* of the HPs over a heating season in London, Aughton and Aberdeen.

Fig. 5-14 shows the daily variations of SPF_{HP} and SPF_{sys} over the heating season in London (blue), Aughton (orange) and Aberdeen (green). In all three locations, the values of SPF_{SWHP} fall in the range of 4.0-6.5 and those of SPF_{ASHP} fall in the range of 3.5-4.5. In London, Aughton and Aberdeen, the seasonal SPF_{sys} are 4.4, 4.4 and 4.1 and the yearly SPF_{sys} are 4.9, 5.0 and 4.5. The yearly SPF_{sys} is consistent with the value of solar extractable in the three locations. In autumn and spring, the values of SPF_{sys} are seen as largely scattered and much higher due to large variations in weather conditions. In addition, the fact that the heating demand for space heating decreases results in a significant increase in the heating provided by direct SHW. Sometimes, the heating system in Aberdeen shows the highest SPF_{sys}. For example, SPF_{sys} until the 394th day in London, Aughton and Aberdeen are 3.9, 3.8 and 4.9, respectively.

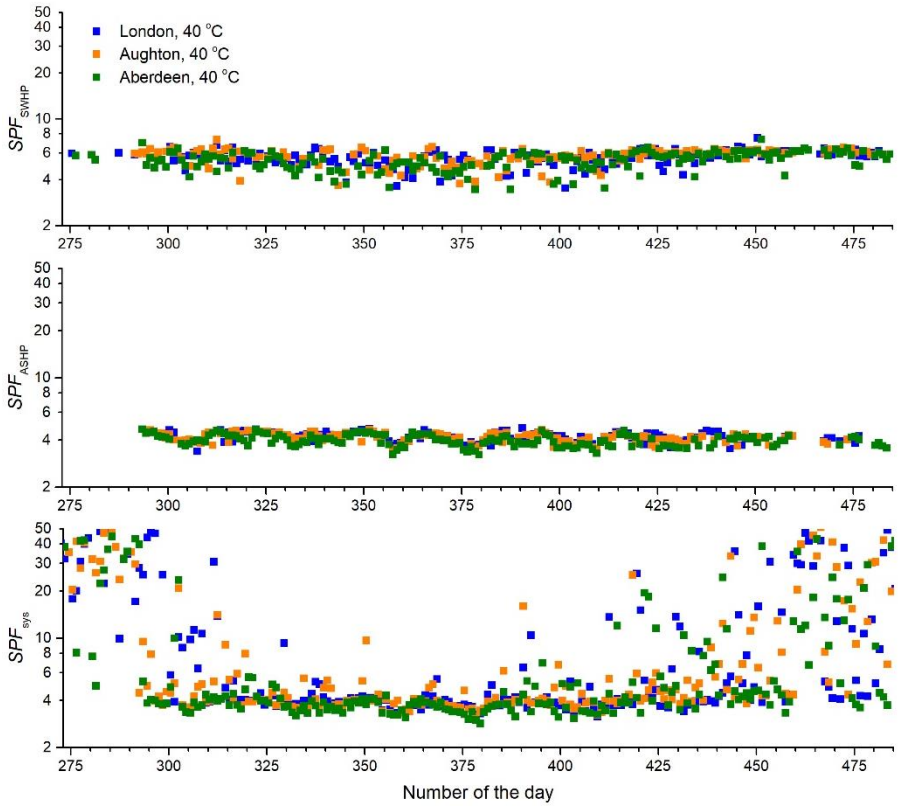

Fig. 5-14: Daily variations of SPF_{sys} and SPF_{HP} over a heating season in London, Aughton and Aberdeen

5.3 Comparison of overall heating performance

Table 5-1 lists the overall operation performances of the heating system. The heat exchange with outdoor surroundings and the stored thermal energy in the TES tanks at the beginning and ending of the simulations are considered. In all cases, the temperature for hot water and space heating is set to be the same. For each location, the heat provisions are similar because the heat demands are the same at different T_{HWS}*, but the provisions can vary slightly due to the influence of T_{HWS}*. Especially, when T_{HWS}* is 40 °C, equal to the set hot water temperature, the temperature of the hot water provided may be lower than the set hot water temperature after feed water enters TES tank 2. Therefore, heat provisions for hot water with a T_{HWS}* of 40 °C are lower than those at other T_{HWS}* in all three locations.

Table 5-1: Overall performance of the heating system operating in London, Aughton and Aberdeen

System	Period		London				Aughton				Aberdeen			
			40	45	50	55	40	45	50	55	40	45	50	55
Heat provision (kWh)	HW	Heating-season	2236.7	2237.8	2237.7	2237.7	2272	2273.0	2273.0	2272.6	2434.5	2439.9	2441.8	2440.7
		Non-heating-season	1427.0	1427.2	1427.5	1427.2	1468.8	1468.9	1469.0	1468.9	1627.9	1628.3	1628.5	1628.4
	SH		7512.0	7515.5	7527.9	7524.6	7675.4	7669.6	7676.9	7674.8	10052.4	10053.1	10053.5	10052.7
	Total		11175.7	11180.4	11193.1	11189.5	11416.2	11411.5	11419.0	11416.2	14114.8	14121.2	14123.7	14121.8
Heat provision (kWh)	SWHP		2098.2	2239.3	2289.1	2299.6	2480.4	2579.1	2607.8	2656.6	2920.6	3039.3	3123.4	3173.0
	ASHP		6565.6	6568.1	6586.6	6602.1	6362.2	6382.0	6374.9	6397.4	8560.8	8593.0	8575.1	8600.6
	Solar	Heating-season	1243.1	1195.9	1187.6	1194.1	1241.9	1171.0	1200.0	1158.5	1246.6	1217.8	1206.9	1180.4
		Non-heating-season	1487.5	1427.1	1409.4	1402.6	1553.7	1533.4	1517.5	1514.9	1605.8	1525.9	1504.2	1488.9
Electricity consumption (kWh)	SWHP		370.1	414.5	449.2	477.1	429.6	466.3	494.9	530.7	534.2	580.1	635.2	673.2
	ASHP		1574.6	1646.0	1737.7	1843.3	1539.5	1616.1	1704.5	1810.9	2175.7	2268.3	2385.1	2481.7
	Water pumps	Heating-season	276.4	284.2	295.0	307.4	277.4	285.7	295.5	308.5	357.1	367.0	372.2	391.7
		Non-heating-season	41.3	40.9	40.7	40.9	41.9	41.7	41.7	41.6	50.6	50.4	49.3	50.7
	Total		2262.4	2385.7	2522.6	2668.8	2288.3	2409.8	2536.6	2691.7	3117.6	3265.7	3441.8	3597.3
SPF_{HP}	SWHP		5.7	5.4	5.1	4.8	5.8	5.5	5.3	5	5.5	5.2	4.9	4.7
	ASHP		4.2	4.0	3.8	3.6	4.1	3.9	3.7	3.5	3.9	3.8	3.6	3.5
Heat provision period (hour)	SWHP		301.63	315.89	327.25	333.25	351.38	364.13	371.63	385.13	411.13	420.89	415.13	452.5
	ASHP		743.00	743.75	746.38	759.00	725.13	727.75	727.50	740.38	997	1000.13	899.25	1006.3
Electricity consumption per kWh heat provision (kWh)	SWHP		0.18	0.19	0.20	0.21	0.17	0.18	0.19	0.20	0.18	0.19	0.20	0.21
	ASHP		0.24	0.25	0.26	0.28	0.24	0.25	0.27	0.28	0.25	0.26	0.28	0.29
COP_{ave}	SWHP		5.6	5.3	5.0	4.8	5.6	5.4	5.2	5.0	5.4	5.1	4.8	4.7
	ASHP		3.8	3.7	3.5	3.3	3.8	3.6	3.4	3.2	3.6	3.5	3.3	3.2

Solar thermal energy (kWh)	To SWHP		1728.1	1824.8	1839.9	1822.5	2050.8	2112.7	2113.0	2125.9	2386.4	2459.3	2488.1	2499.8
	To end use	Heating-	1243.1	1195.9	1187.6	1194.1	1241.9	1171.0	1200.2	1158.5	1246.6	1217.8	1206.9	1180.4
		Non-heating-	1487.5	1427.1	1409.4	1402.6	1553.7	1533.4	1517.5	1514.9	1605.8	1525.9	1504.2	1488.9
	Total		4739.8	4720.9	4706.7	4686.0	5131.0	5095.5	5103.9	5070.2	5515.9	5471.6	5464.3	5427.6
Thermal energy from ambient air (kWh)			4991.0	4922.0	4848.9	4758.7	4822.7	4765.9	4670.4	4586.5	6385.1	6324.7	6190.0	6118.9
SF	Heating season		30.5%	31.0%	31.0%	30.9%	33.1%	33.0%	33.3%	33.0%	29.1%	29.4%	29.6%	29.5%
	Yearly		39.9%	39.8%	39.6%	39.5%	42.5%	42.2%	42.3%	42.0%	37.1%	36.8%	36.8%	36.6%
SPF_{sys}	Heating season		4.4	4.2	3.9	3.7	4.4	4.2	4.0	3.8	4.1	3.9	3.7	3.5
	Yearly		4.9	4.7	4.4	4.2	5.0	4.7	4.5	4.2	4.5	4.3	4.1	3.9

Note: Heating-: Heating season; Non-heating-: Non-heating season.

The influence of T_{HWS}* on heat provision for space heating is complex. T_{HWS} can influence the indoor air temperature and thus the heat provision period of the heating system. At a lower T_{HWS}*, the heat provision periods of both ASHP and SWHP are shorter and result in lower indoor air temperature within the temperature range for thermal comfort. Thus, the heat provision for SH is less. However, the indoor air temperature can influence the TES performance of the furniture inside the building higher indoor air temperature brings more TES and requires less heat provision. The influence on total heat provisions is a combination of both effects. Generally, for the selected three locations, a T_{HWS}* of 50 °C, the system achieves the highest heat provision for space heating.

Fig. 5-15 shows the variations of heat provision for space heating and hot water by SWHP, ASHP and direct SHW against T_{HWS}* for heating systems operating in London (black), Aughton (red) and Aberdeen (blue). The lines are a guide for the eye. It can be seen that as T_{HWS}* decreases, heat provision from HPs decreases and that from direct SHW increase. When T_{HWS}* decreases from 55 °C to 50 °C, 45 °C and 40 °C, the contribution of SWHP decrease by 0.5%, 2.6% and 8.8% in London; by 1.8%, 2.9% and 6.6% in Aughton; and by 1.6%, 4.2% and 8.0% in Aberdeen. The heat provision from ASHP shows an inapparent decreasing trend. As T_{HWS}* decreases from 55 °C to 50 °C, 45 °C and 40 °C, the contribution of ASHP decrease by 0.2%, 0.5% and 0.6% in London; by 0.4%, 0.2% and 0.6% in Aughton; and by 0.3%, 0.1% and 0.5% in Aberdeen. At the same time, the contribution of direct SHW increases by 0.01%, 1.0% and 5.2% in London; by 1.7%, 1.2% and 4.6% in Aughton; and by 1.6%, 2.8% and 6.9% in Aberdeen.

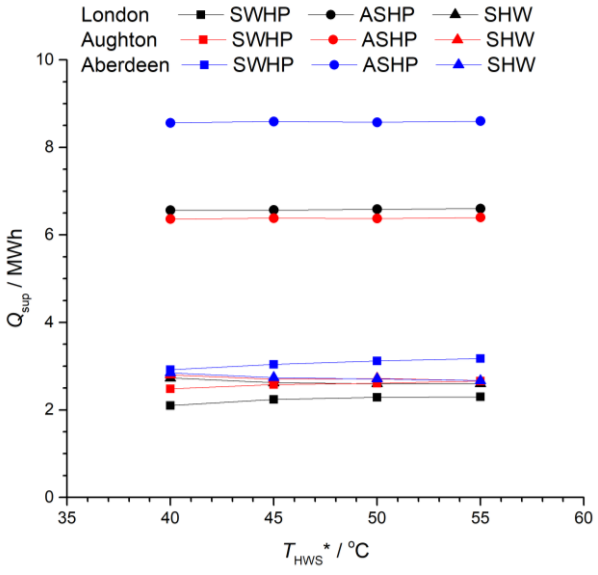

Fig. 5-15: Variations of heat for space heating and hot water by SWHP, ASHP and direct SHW against T_{HWS}* for heating systems operating in London, Aughton and Aberdeen.

Fig. 5-16 displays the variations of electricity consumed by SWHP and ASHP and the total electricity consumed by the heating system against T_{HWS}* for heating systems operating London (black), Aughton (red) and Aberdeen (blue). With the decrease of T_{HWS}* from 55 ^{o}C to 50 ^{o}C, 45 ^{o}C and 40 ^{o}C, the electricity consumed by SWHP is decreased by 5.9%, 13.1 % and 22.4% in London; by 6.8%, 12.1 % and 19.1% in Aughton; and by 5.6%, 13.8% and 20.7% in Aberdeen. The electricity consumed by ASHP is decreased by 5.7%, 10.7% and 14.6% in London; by 5.9%, 10.8 % and 15.0% in Aughton; and by 3.9%, 8.6% and 12.3% in Aberdeen.

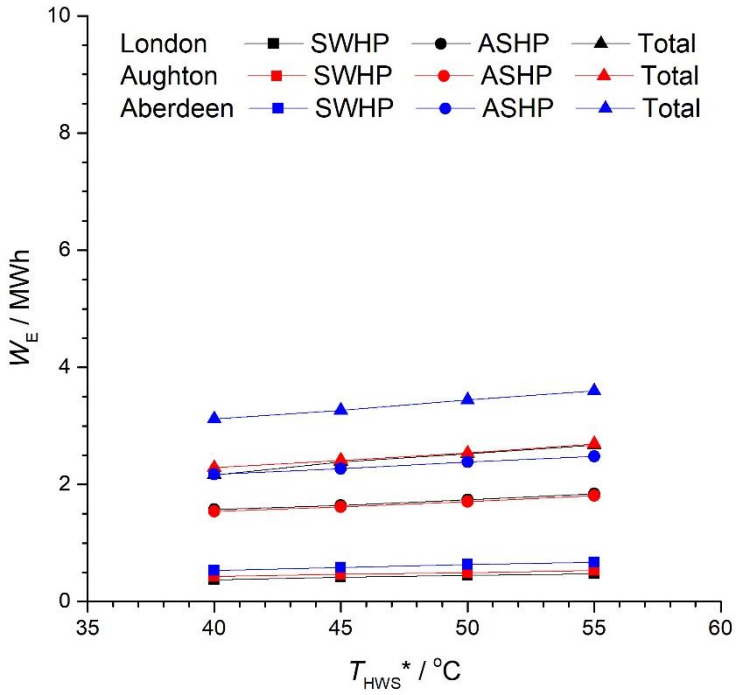

Fig. 5-16: Variations of electricity consumed by SWHP and ASHP and the total electricity consumed by the heating system against T_{HWS}* for heating systems operating London, Aughton and Aberdeen.

Fig. 5-17 shows the variation of thermal energy extracted from solar energy and ambient air against T_{HWS}* for heating systems operating in London (black), Aughton (red) and Aberdeen (blue). With the decrease of T_{HWS}* from 55 ^{o}C to 50 ^{o}C, 45 ^{o}C and 40 ^{o}C, thermal energy collections from ambient air increases by 1.9 %, 3.4% and 4.9% in London; by 1.8 %, 3.9% and 5.2% in Aughton; and by 1.2 %, 3.4% and 4.4% in Aberdeen. As T_{HWS}* decreases from 55 ^{o}C to 50 ^{o}C, 45 ^{o}C and 40 ^{o}C, thermal energy collections from solar is increased by 0.4%, 0.7% and 1.2% in London; by 0.7%, 0.5% and 1.2% in Aughton; and by 0.7%, 0.8% and 1.6% in Aberdeen.

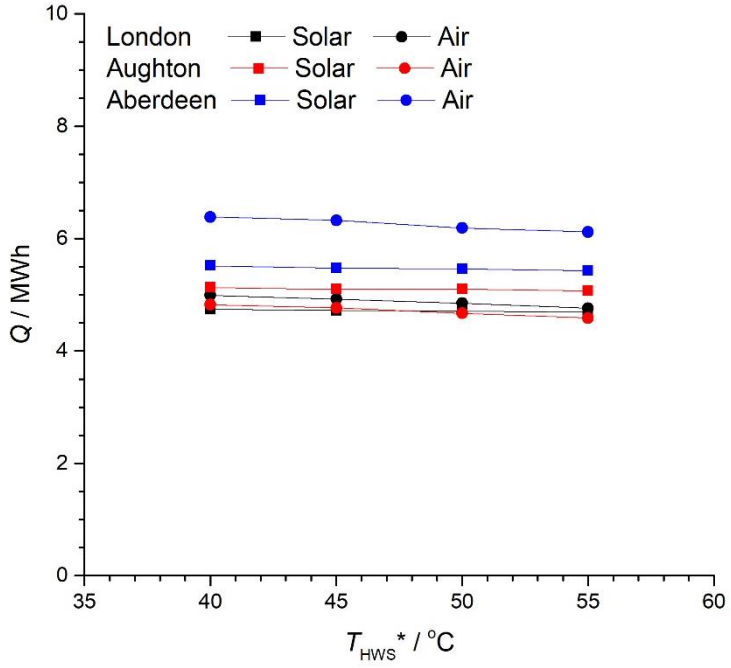

Fig. 5-17: Variation of thermal energy (Q) extracted from solar energy and ambient air against T_{HWS}* for heating systems operating in London, Aughton and Aberdeen.

Fig. 5-18 shows averaged *COP* of SWHP and ASHP with T_{HWS}* for heating systems operating in London (black), Aughton (red) and Aberdeen (blue). With the decrease of T_{HWS}* from 55 °C to 50 °C, 45 °C and 40 °C, the *COP* of SWHP increases by 4.2%, 10.4% and 16.7% in London; by 4.0%, 8.0% and 12.0% in Aughton; and by 2.1%, 8.5% and 14.9% in Aberdeen. At the same time, the *COP* of ASHP increases by 6.1%, 12.1% and 15.2% in London; by 6.3%, 12.5% and 18.8% in Aughton; and by 3.1%, 9.4% and 12.5% in Aberdeen.

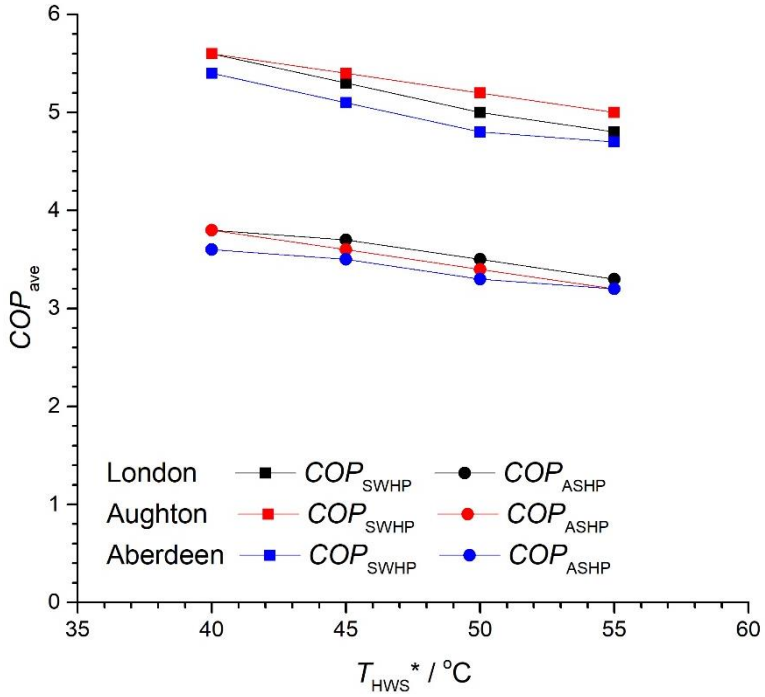

Fig. 5-18: Averaged *COP* of SWHP and ASHP with T_{HWS}* for heating systems operating in London, Aughton and Aberdeen.

Fig. 5-19 shows the variations of yearly and seasonally *SF* with T_{HWS}* for heating systems operating in London (black), Aughton (red) and Aberdeen (blue). The *SF* in the heating season shows a similar variation trend with the heat provision for space heating. For the yearly *SF*s, as T_{HWS}* decreases from 55 °C to 50 °C, 45 °C and 40 °C, it increases from 39.5% to 39.6%, 39.8% and 39.9% in London; from 42.0% to 42.3%, 42.2% and 42.5% in Aughton; and from 36.6% to 36.8%, 36.8% and 37.1% in Aberdeen.

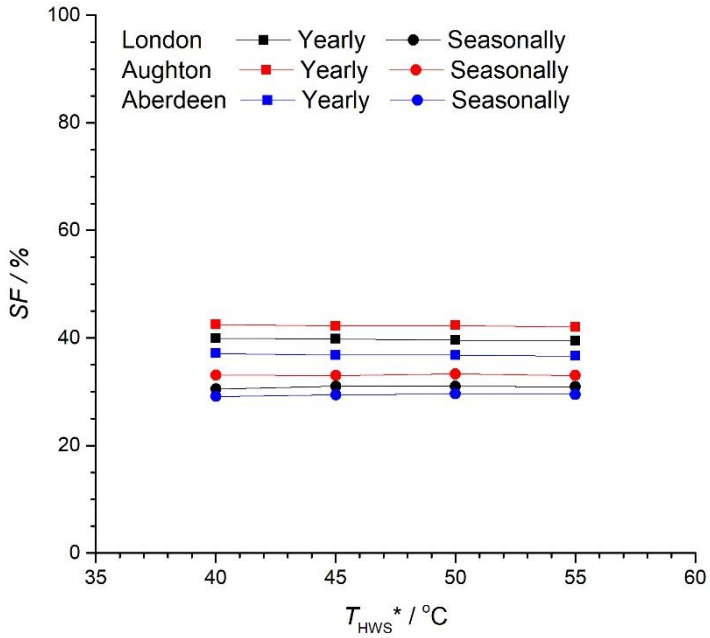

Fig. 5-19: Variations of yearly and seasonally *SF* with T_{HWS}* for heating systems operating in London, Aughton and Aberdeen.

Fig. 5-20 shows the variations of yearly and seasonally SPF_{HP} and SPF_{sys} with T_{HWS}* in London (black), Aughton (red) and Aberdeen (blue). As T_{HWS}* decreases from 55 °C to 50 °C, 45 °C and 40 °C, the *SPF* of SWHP increases by 6.3%, 12.5% and 18.8% in London; by 6.0%, 10.0% and 16.0% in Aughton; and by 4.3%, 10.6% and 17.0% in Aberdeen. At the same time, the *SPF* of ASHP increases by 5.6%, 11.1% and 16.7% in London; by 5.7%, 11.4% and 17.1% in Aughton; and by 2.9%, 8.6% and 11.4% in Aberdeen. When T_{HWS}* decreases from 55 °C to 50 °C, 45 °C and 40 °C, the yearly SPF_{sys} increases by 4.8%, 11.9% and 16.7% in London; by 7.1%, 11.9% and 19.1% in Aughton; and by 5.1%, 10.3% and 15.4% in Aberdeen. At the same time, the seasonally SPF_{sys} increases by 5.4%, 13.5% and 18.9% in London; by 5.3%, 10.5% and 15.8% in Aughton; and by 5.7%, 11.4% and 17.1% in Aberdeen.

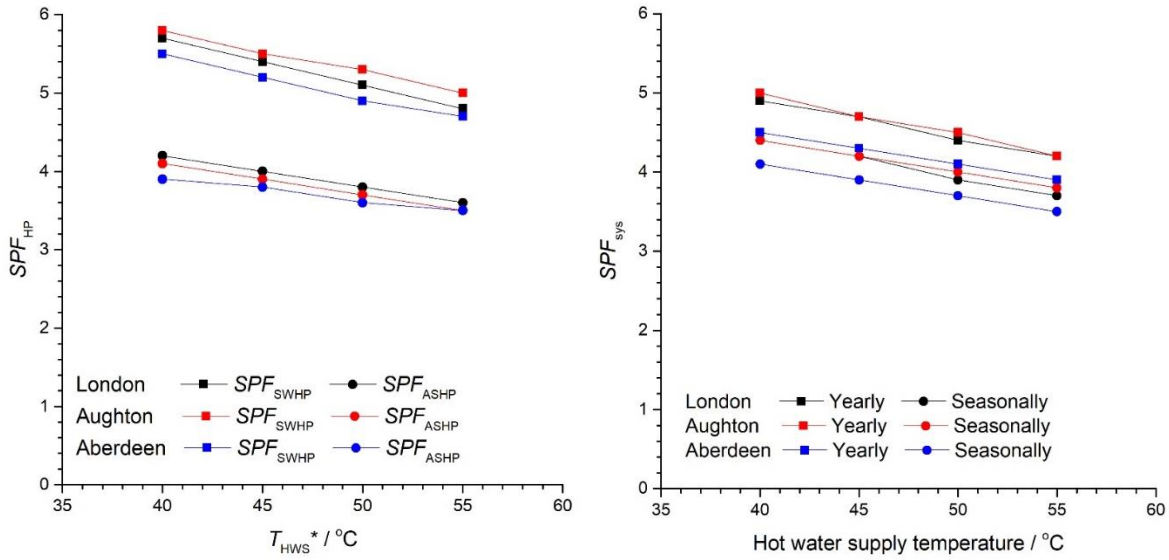

(a) (b)

Fig. 5-20: Variations of yearly and seasonally SPF_{HP} and SPF_{sys} with T_{HWS}* in London, Aughton and Aberdeen.

Low temperature heating helps to reduce electricity consumption, as shown in Fig. 5-21. For the heating system, with the decrease of T_{HWS}* from 55 °C to 50 °C, 45 °C and 40 °C, the yearly electricity consumption decreases by 5.6%, 10.5% and 19.1% in London; by 5.6%, 10.4% and 14.9% in Aughton; by 4.4%, 10.3% and 13.3% in Aberdeen. It is seen that at a higher water supply temperature, the electricity savings for the three cities are generally the same; at a lower water supply temperature, more electricity savings can be achieved in a city at lower latitude.

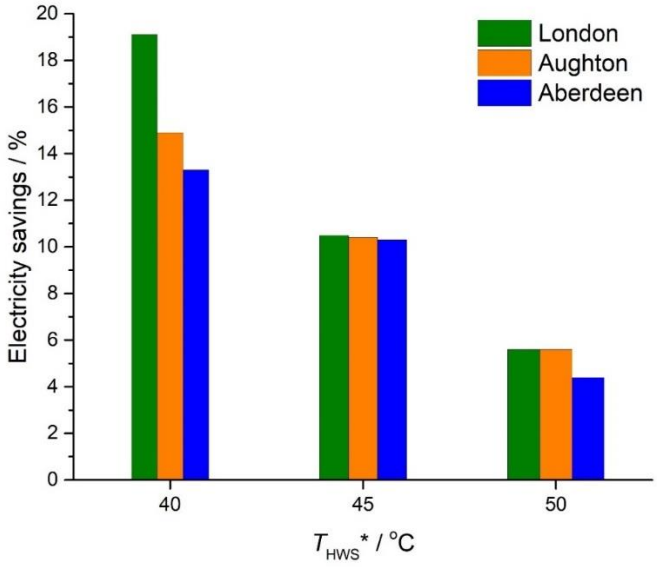

Fig. 5-21: Electricity savings at T_{HWS}* of 40 °C, 45 °C and 50 °C compared with electricity consumption at T_{HWS}* of 55 °C

5.4 Economic analyses

To understand the influence of low temperature heating on the economic performance of IX-SAASHPs, economic analyses are conducted for dual-source IX-SAASHPs of different T_{HWS}* and electric water heaters in London, Aughton and Aberdeen.

For economic analyses, the total energy consumption of the heating systems, Q_{tot}, is calculated by Eq. (5-1):

$$Q_{tot} = (Q_{sh} + Q_{hw})/\eta \quad (5\text{-}1)$$

where η is the efficiency of the electric water heater and gas boiler.

The payback period, P_{pb}, is defined based on the electric water heater by Eq. (5-2):

$$P_{pb} = C_i / C_{spy} \quad (5\text{-}2)$$

where C_i is the initial cost difference and C_{spy} is the cost saving per year calculated by Eq. (5-3) and Eq. (5-4), respectively.

$$C_i = C_{i0} - C_{ieh} \quad (5\text{-}3)$$

$$C_{spy} = C_{o0} - C_{oeh} \quad (5\text{-}4)$$

where C_{i0} and C_{o0} are the initial and operation costs of the heating system, respectively, C_{ieh} and C_{oeh} are the initial and operation costs of the electric water heater.

The efficiency of the electric water heater is taken from [161] to 0.95. The electric water heater has a TES tank of 300 L. The heat provisions of the electric water heater over the year are set to be the average value for the corresponding location. The current energy prices are taken from E.On Energy (a UK energy supplier) to be £400.2 per MWh for electricity and £ 106.8 per MWh for gas (prices in June 2022) [255]. The prices of the components of the heating systems are obtained from an online market where the flat plate solar collector price is around £30 per m^2, the water tank price is £290 per 100 L, and a pump with a head of 15 m and a capacity of 15 L/min is around £10 [256]. All the heating systems have a capacity of 8 kW. The systems are estimated to be easy to connect to the current space heating and water heater. The installation costs are assumed to be 3 hours for the SHW system and 6 hours for SAASHPs with a cost of 80 per hour [257]. The shipping fees for international shipping are not included in the current economic analysis.

Table 5-2: Results of economic analysis for the heating systems in London (2022)

		Electric water heater			**London**				**Aughton**				**Aberdeen**			
		London	Aughton	Aberdeen	40	45	50	55	40	45	50	55	40	45	50	55
Heat provision per year, MWh		11.18	11.42	14.12	11.18	11.18	11.19	11.19	11.42	11.41	11.42	11.42	14.11	14.12	14.12	14.12
Efficiency/performance		0.95	0.95	0.95	4.9	4.7	4.4	4.2	5	4.7	4.5	4.2	4.5	4.3	4.1	3.9
Electricity consumption per year, MWh		11.77	12	14.86	2.16	2.39	2.52	2.67	2.29	2.41	2.54	2.69	3.12	3.23	3.44	3.60
Initial cost, £	collector	0	0	0	540	540	540	540	540	540	540	540	540	540	540	540
	tanks	870	870	870	2320	2320	2320	2320	2320	2320	2320	2320	2320	2320	2320	2320
	Heater/HP	60	60	60	1085	1085	1085	1085	1085	1085	1085	1085	1085	1085	1085	1085
	pumps	0	0	0	30	30	30	30	30	30	30	30	30	30	30	30
	Installation	0	0	0	480	480	480	480	480	480	480	480	480	480	480	480
	total	930	930	930	4455	4455	4455	4455	4455	4455	4455	4455	4455	4455	4455	4455
Operation cost, £		4710.4	4802.4	5947.0	864.4	956.5	1008.5	1068.5	916.5	964.5	1016.5	1076.5	1248.6	1292.6	1376.7	1440.7
Cost saving per year, £		-	-	-	3845.9	3753.9	3701.9	3641.8	3885.9	3837.9	3785.9	3725.9	4698.3	4654.3	4570.3	4506.3
Payback period, year		-	-	-	0.92	0.94	0.95	0.97	0.91	0.92	0.93	0.95	0.75	0.76	0.77	0.78

The economic analysis for different T_{HWS}* for 2022 at three locations is displayed in Table 5-2. The payback periods decrease as T_{HWS}* decreases. With the decrease of T_{HWS}* from 55 ^{o}C to 50 ^{o}C, 45 ^{o}C and 40 ^{o}C, in 2022, the payback periods decrease by 2.0%, 3.0% and 5.9% in London; those decreased by 1.0%, 2.0% and 4.1 % in Aughton; the payback periods decrease by 1.2%, 2.5% and 3.7% in Aberdeen. Among the three selected locations, Aberdeen has the highest heat demand, 26.3% higher than that in London, and the lowest payback periods, around 19% lower than those in London.

5.5 Summary

TRNSYS has been used to simulate the low temperature operation performance of dual-source IX-SAASHPs under the weather conditions in London, Aughton and Aberdeen in the UK, respectively. Based on the energy and economic analyses, the conclusions below can be obtained:

(1) Low temperature heating can significantly reduce electricity consumption. For the heating system, with the decrease of the set hot-water-supply temperature from 55 ^{o}C to 40 ^{o}C, the yearly electricity consumption decreases by 19.1% in London, 14.9% in Aughton, and 13.3% in Aberdeen, respectively.

(2) Low temperature heating increases thermal energy collection from both solar energy and ambient air, and hence *COP* largely increases. With the decrease of the set hot-water-supply temperature from 55 ^{o}C to 40 ^{o}C, the *COP* of SWHP increases from 4.8 to 5.6 in London, from 5.0 to 5.6 in Aughton; and from 4.7 to 5.4 in Aberdeen, respectively, while the *COP* of ASHP increases from 3.3 to 3.8 in London; from 3.2 to 3.8 in Aughton; and from 3.2 to 3.6 in Aberdeen, respectively.

(3) Low temperature heating benefits by decreasing heat provision from ASHP and SWHP and increasing the heat provision from direct SHW, resulting in much better system efficiency. When the set hot-water-supply temperature decreases from 55 ^{o}C to 40 ^{o}C, the yearly SPF_{sys} increases from 4.2 to 4.9 in London; from 4.2 to 5.0 in Aughton; and from 3.9 to 4.5 in Aberdeen, respectively.

(4) At the set hot-water-supply temperature of 40 ^{o}C, the heat provided by ASHP is about three times that by SWHP and about six times that by direct SHW, and the electricity consumed by ASHP is about four times that by SWHP and about five times that by pumps in the three locations.

(5) *SF* appears to be negligibly influenced by latitude and set hot-water-supply-temperature. For different set hot-water-supply-temperature, *SF* is 40% in London, 42% in Aughton, and 37% in Aberdeen.

(6) The payback periods slightly decrease as the set hot-water-supply temperature decreases. With the decrease of the set hot-water-supply-temperature from 55 ºC to 40 ºC, for the electricity price in April 2022, the payback periods decrease from 1.01 years to 0.95 years in London, from 0.98 years to 0.94 years in Aughton, and from 0.81 years to 0.78 years in Aberdeen.

6. Operation performance of the system using compound parabolic concentrator-capillary tube solar collector

Solar assisted air source heat pump heating systems are capable of achieving green heating. High thermal performance and low cost of such heating systems are essentially required and solar collectors play an important role in achieving such targets. This chapter reports numerical simulations of solar assisted air source heat pump heating systems, by integrating compound parabolic concentrator-capillary tube solar collectors which have high collector efficiency at high temperatures, benefitting to work with sensible TES methods. The heating system is used to provide both space heating and hot water for a single-family house in London, UK. The operation of the heating system is simulated by TRNSYS. The system using CPC-CSC achieves an *SPF* of 4.7 in London weather conditions. Particularly, for almost the same seasonal performance factor, the area required for the concentrated solar collector is 12 m^2 while the area required for the flat plate solar collector is 18 m^2, leading to one third collector size reduction and hence significant cost reduction and convenient installation. According to both system performance and economic analysis, CPC-CSC with an area of around 9 m^2 is recommended. Considering further improvements in system design and operation, the heating system using smaller size CPC-CSC e.g. 6 m^2 can potentially achieve a higher SPF_{sys}. Since solar collectors with a smaller size can be much more easily adopted for domestic use, using CPC-CSC benefits the wide rollout of SAASHP heating systems for domestic heating.

6.1 Compound parabolic concentrator-capillary solar collector

The CPC-CSC consists of CPCs, capillary tubes, a glass cover, an insulation layer and a baseplate (see Fig. 6-1(a)) [108]. Each CPC unit has an aperture width of 53 mm, a groove depth of 52.5 mm and a concentration ratio of 4.22. The capillary tubes with an outer diameter of 4 mm and an inner diameter of 2 mm are placed and fixed at the circle for involute of the CPC. To reflect all the solar radiation to the absorber surface, the diameter of the circle for the involute of the CPC concentrator is set to be the outer diameter of the capillary tubes. The reflective surface is coated with an aluminium foil layer with a thickness of 0.1 mm and a reflectivity of 0.85. Two copper tubes with an outer diameter of 12 mm and an inner diameter of 10 mm work as the inlet and outlet headers connecting the capillary tubes. The single-layer high-transparent glass cover has a thickness of 4 mm. The four sides and the baseplate of the

solar collector are insulated to reduce heat loss. Water is used as the working fluid. The CPC-CSC has high collector efficiency at high temperatures, benefitting to work with sensible TES methods.

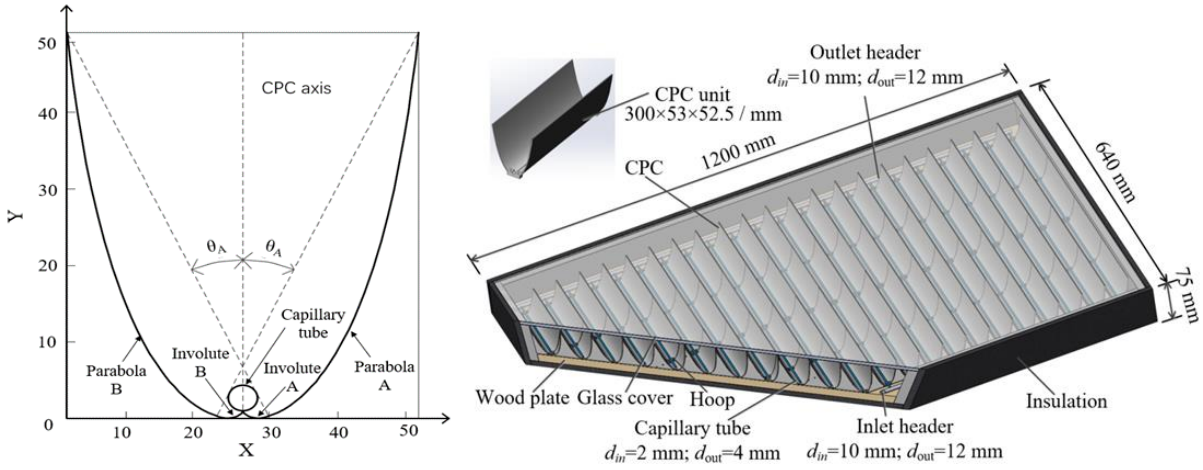

(a) (b)

Fig. 6-1: Structure of CPC-CSC: (a) geometry (b) schematic [108]

As shown in Fig. 6-1(b), the CPC concentrator consists of two pairs of symmetrical curves (circle for involute of the CPC and parabola line) with compound rotation. The circle for involute of the CPC is defined by Eq. (6-1) for $0 \leq \varphi \leq 90° + \theta_A$:

$$X = \frac{d}{2}(\sin\varphi - \varphi\cos\varphi)$$

$$Y = -\frac{d}{2}(\varphi\sin\varphi + \cos\varphi) \quad (6\text{-}1)$$

where φ is the angle between the incident ray and the X-axis. The parabola line is defined by Eq. (6-2) for $90° + \theta_A \leq \varphi \leq 270° + \theta_A$:

$$X = \frac{d}{2}(\sin\varphi - A^*\cos\varphi)$$

$$Y = -\frac{d}{2}(A^*\sin\varphi + \cos\varphi) \quad (6\text{-}2)$$

where

$$A^* = \frac{\frac{\pi}{2} + \theta_A + \varphi - \cos(\varphi - \theta_A)}{1 + \sin(\varphi - \theta_A)} \quad (6\text{-}3)$$

θ_A is the aperture angle of the CPC defined by Eq. (6-4):

$$\theta_A = \sin^{-1}\left(\frac{1}{CR}\right) \quad (6\text{-}4)$$

where CR is the concentration ratio, given by Eq. (6-5):

$$CR = \frac{D}{\pi \times d} \tag{6-5}$$

where D is the aperture width and d is the outer diameter of the capillary tube absorber. The average heat flux of the evaporation section of the absorber can be calculated by Eq. (6-6):

$$q = \frac{D \times I}{\pi \times d} = CR \times I \tag{6-6}$$

where I is the solar irradiation intensity measured by a pyranometer.

6.1.1 Numerical simulation and verification

Numerical simulations are conducted using Ansys-Fluent for three-dimensional heat transfer of CPC-CSC. One of the CPC units is selected for computation. The geometry of the unit is 600 mm x 53 mm x 75 mm. The parameters specifying the CPC model are listed in Table 6-1 where the working fluid is set to be water.

The solar collection process combines conduction, convection, and radiation heat transfer. Convective heat transfer occurs between the outer wall of the capillary tubes and the air layer. The water flow inside the tubes is regarded as a 3D, steady, constant-property, laminar flow. Considering the heat transfer process, governing equations are the following [108]:

Conservation of mass:

$$div(\boldsymbol{U}) = 0 \tag{6-7}$$

Conservation of momentum:

$$div(u\vec{U}) = div(vgradu) - \frac{1}{\rho}\frac{\partial p}{\partial x} \tag{6-8}$$

$$div(v\vec{U}) = div(vgradv) - \frac{1}{\rho}\frac{\partial p}{\partial y} \tag{6-9}$$

$$div(w\vec{U}) = div(vgradw) - \frac{1}{\rho}\frac{\partial p}{\partial z} \tag{6-10}$$

Conservation of energy for heat transfer of air and water flow:

$$div(\vec{U}T) = div(\frac{\lambda}{\rho c_p} gradT) \tag{6-11}$$

Conservation of energy for heat transfer in solid:

$$\frac{\partial T^2}{\partial x^2} + \frac{\partial T^2}{\partial y^2} + \frac{\partial T^2}{\partial z^2} = 0 \tag{6-12}$$

For the convection of air inside the collector, the Boussinesq assumption is taken to calculate the density.

$$\left(\rho_{\mathrm{a}}-\rho_{\mathrm{amb}}\right)g=-\rho_{\mathrm{amb}}\beta_{\mathrm{a}}\left(T-T_{\mathrm{amb}}\right)g \tag{6-13}$$

where ρ_a is the air density, ρ_{amb} is the density of ambient air at its temperature T_{amb} and β_a is the thermal expansion coefficient of air.

The boundary conditions for the domain are:

Upper and lower surfaces at *x*-*z* plane y=0, H_{D}: the convection boundary condition with air temperature given;

Front and back end surfaces at *x*-*y* planes *z*=0, L_{D}: adiabatic condition;

Left and right surfaces at *y*-*z* planes *x*=0, W_{D}: symmetrical boundary condition.

The air inside the collector: The non-slip boundary conditions are applied to all solid-air interfaces.

Water flow in capillary tubes: At the inlet: velocities $u=u_{\mathrm{in}}$, $v=0$, $w=0$; temperature $T=T_{\mathrm{in}}$; at the outlet: partial unidirectional condition; The non-slip boundary condition is applied to the solid-water interface.

Since the diameter of the copper capillary tubes is small compared with the size of CPCs and hence are regarded as a homogeneous body heat source. All the surface temperatures of solid components are obtained from the coupled numerical simulations of air convection inside the collector, water flowing inside the capillary tubes and heat conduction in the solids.

To verify the model and numerical simulation, a set of experiments was conducted in Beijing, China. The working conditions of the experiments are listed in Table 6-2. The measurements were conducted, and the experimental data were processed according to Chinese standards for the test methods of solar collectors GB/T 4271-2007. The experimental results show good agreement with simulation results [108]. Therefore, the simulated results are used to establish the module in TRNSYS.

6.1.2 Empirical formula and module in TRNSYS

The CPC-CSC works to concentrate solar incidence to the capillary tube and transfer solar energy into thermal energy. The thermal energy obtained by CPC-CSC, Q_{SC}, can be expressed as Eq. (6-14):

$$Q_{\mathrm{SC}} = IA - Q_{\mathrm{loss,sc}} = cm(T_{\mathrm{out}} - T_{\mathrm{in}}) \tag{6-14}$$

where I is the global solar irradiance on the tilted surface, A is the collector area, m is the mass flow rate, c is the specific heat of the working fluid, T_{in} and T_{out} are the temperatures of the working fluid at the inlet and outlet of CPC-CSC. $Q_{\mathrm{loss,sc}}$ is the heat loss from the solar collector

to ambient air. Following Dickes et al. [258], the heat loss from the CPC-CSC per meter (along the length), Q_{loss}, is calculated by Eq. (6-15):

$$Q_{loss} = c_0 + c_1(T_{sc} - T_{amb}) + c_2(T_{sc} - T_{amb})^2 + c_3T_{sc}^3 + I(c_4\sqrt{v_a} + c_5T_{sc}^2) + v_a[c_6 + c_7(T_{sc} - T_{amb})] + \sqrt{v_a}[c_8 + c_9(T_{sc} - T_{amb})] \quad (6\text{-}15)$$

where T_{amb} is the temperature of ambient air, and v_a is the wind speed. T_{sc} is the surface temperature of CPC-CSC, calculated by Eq. (6-16):

$$T_{SC} = (T_{in} + T_{out})/2 \quad (6\text{-}16)$$

According to the standards of system control, the inlet water temperature of CPC-CSC ranges from -5 to 80 ^oC. Therefore, the parameters given in Table 6-3 are selected for numerical simulation. The mass flow rate of water is set at 0.23 kg/h, i.e. 7.23 kg/h-m^2.

The simulated results are divided into a training group (75%) and a test group (25%) to train the empirical formula and avoid overfitting. The formula obtained from the training group is Eq. (6-17):

$$Q_{loss} = 0.1458(T_{sc} - T_{amb}) + 2.3843\times10^{-4}(T_{sc} - T_{amb})^2 - 5.8303\times10^{-6}T_{sc}^3 + I(0.0013\sqrt{v_a} + 8.1302\times10^{-7}T_{sc}^2) + v_a[-0.088 + 5.2377\times10^{-4}(T_{sc} - T_{amb})] + \sqrt{v_a}[0.422 - 0.0104(T_{sc} - T_{amb})] \quad (6\text{-}17)$$

Table 6-1: Parameters for the CPC-CSC model [108]

Material	Thickness (mm)	Thermal conductivity (W/m-K)	Density (kg/m^3)	Specific heat (J/kg-K)	Thermal expansion coefficient (/K)	Viscosity (kg/m-s)
Glass	4	0.76	2500	790	-	-
Air	-	0.0267	1.225	1005	0.0033	0.00001 7894
Water	-	0.6	998.2	4182	-	0.00100 3
CPC material (ABS plastic)	1	0.25	1050	1591	-	-
Thermal insulation material	10	0.034	54	1500	-	-
Capillary tube material (copper)	1	387.6	8978	381	-	-

Table 6-2: Environmental conditions of the experiments [108]

	Solar radiation intensity (W/m^2)	Ambient temperature (K)	Air velocity (m/s)	Date of experiments
Set 1	290-1000	288-291	1-2	10. Oct. 2016-20 Nov. 2016
Set 2	920-1000	289-293	1-2	5 Apr. 2016-10 May 2017

Table 6-3: Weather parameters for numerical simulation

Parameters	Values
Solar irradiance on the tilted surface, W/m^2	100, 400, 700, 1000
Air velocity, m/s	0, 3, 6, 9, 12, 15, 18, 21, 24
Inlet water temperature of solar collector, ^oC	0, 25, 50, 75
Ambient air temperature, ^oC	0, 10, 20

The R^2 of the training group is 0.9903 and that of the test group is 0.9915. This suggests the reliability of the empirical correlation. Based on Eqs. (13) and (16), the CPC-CSC module is established in TRNSYS and is named Type 219. The flow chart for the operation of the CPC-CSC module is shown in Fig. 6-2.

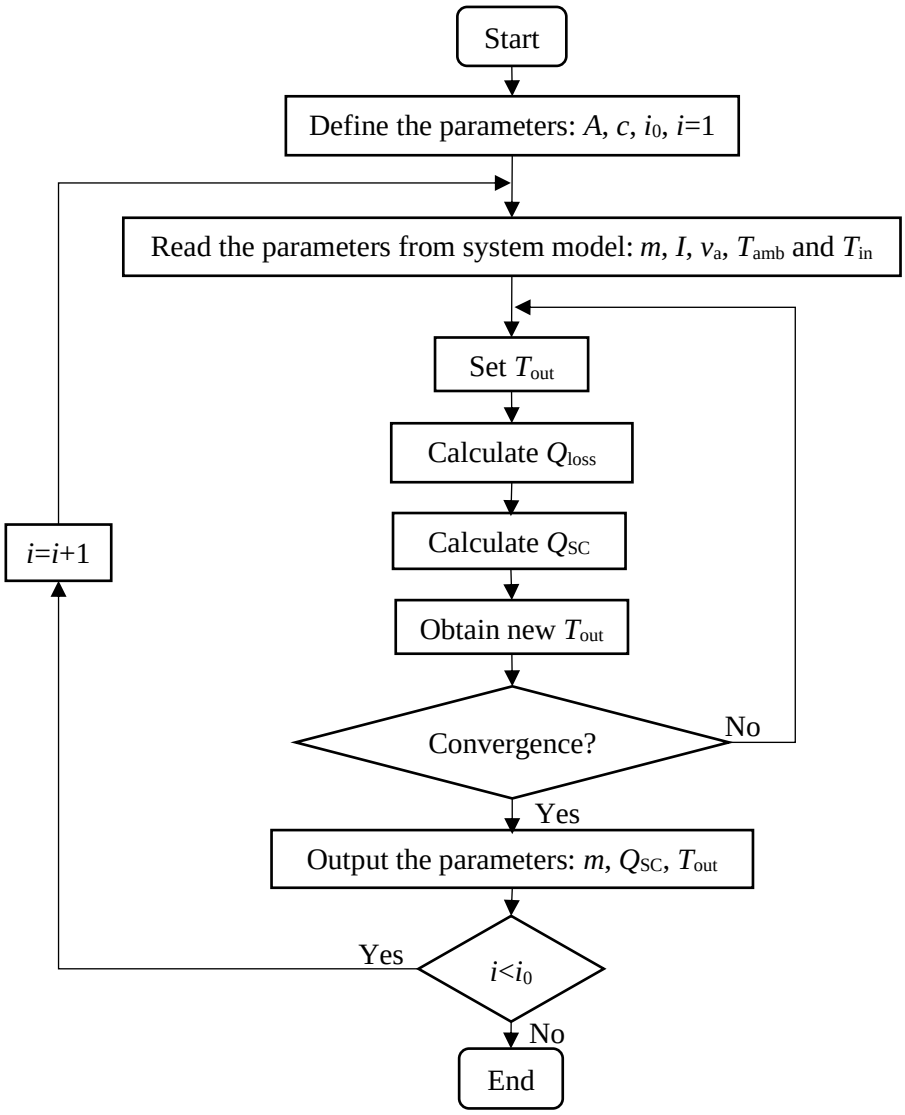

Fig. 6-2: Flow chart for the operation of the CPC-CSC module

6.2 Results and discussion

Numerical simulations for SAASHP using CPC-CSC have been conducted. The obtained results are compared with those of the SAASHP using FPC to understand the advantages of CPC-CSC. The effects of the collector area of CPC-CSC on system performance are analysed.

6.2.1 Comparison of systems using different collectors

In this section, the performance of a system using a CPC-CSC of 18 m^2 is compared with that of a system using an FPC of 18 m^2. Fig. 6-3 shows the variation of indoor air temperature

and hot water supply temperature of systems using different solar collectors in the heating season. CPC-CSC can realise high temperature and collector efficiency since the capillary tube reduces the surface area for heat transfer and thus the heat loss from the surface. In addition, horizontal CPC separates the air layer which reduces the convective heat transfer caused by gravity. In non-heating periods, it is more often for the system using CPC-CSC to obtain a higher T_{HWS} since CPC-CSC can have a better collection efficiency at higher water temperatures. In heating periods, the T_{HWS} of the system using CPC-CSC shows less variation than that of the system using FPC. This suggests that the high collector efficiency of CPC-CSC benefits the response speed of the SAASHP to water draw.

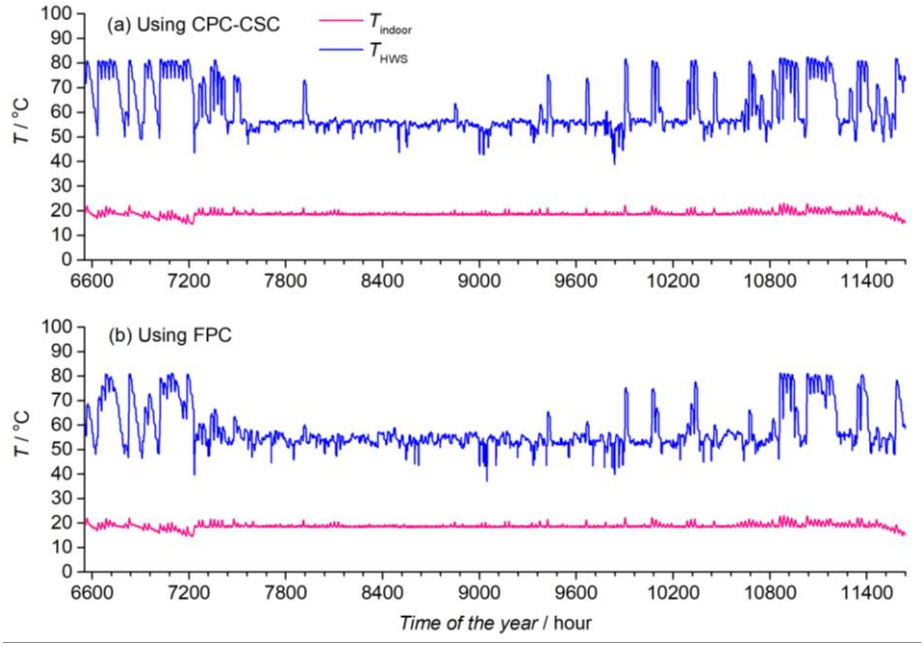

Fig. 6-3: Variations of room air temperature and hot water temperature at the outlet of TES tank 2 over a heating season.

Fig. 6-4 shows the daily variation of heat provision for HW and SH over a heating season. The columns are stacked to represent total heat provision. Since the systems work shares the same working conditions, the heat provision is generally similar. Sometimes, for example, on the 304th day, the Q_{SH} of the system using CPC-CSC can be much smaller. This situation results from the TES of the building structure and the high T_{HWS}.

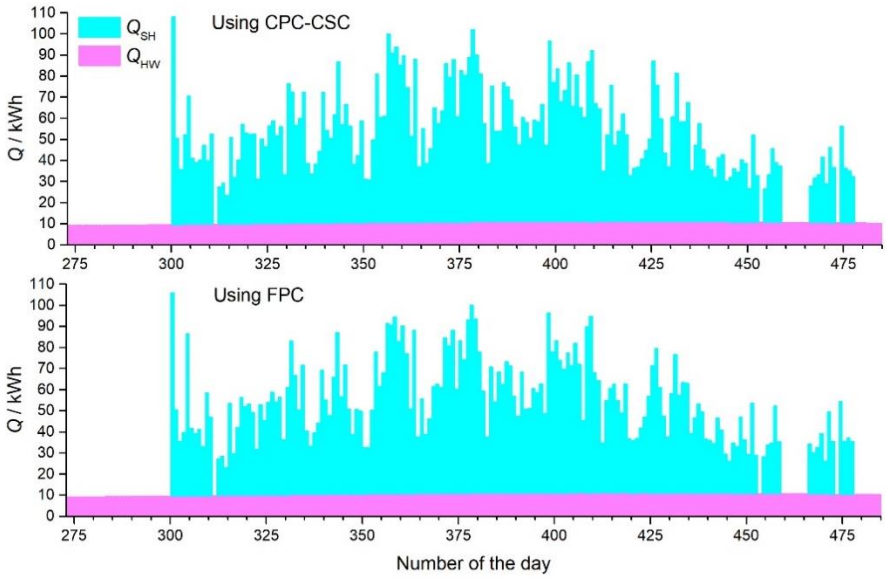

Fig. 6-4: Daily variations of heat for space heating and hot water over a heating season

Fig. 6-5 shows the heat provision from ASHP, SWHP and direct solar hot water (SHW) over a heating season. The columns are stacked to represent the total daily heat provision. Using CPC-CSC, heat provision by ASHP, SWHP and direct SHW is 6.4 MWh, 1.9 MWh and 1.7 MWh; that for the system using FPC is 6.6 MWh, 2.3 MWh, and 1.2 MWh. The results are also summarised in Table 6-4. Compared with the system using FPC, the heat provision from SWHP is significantly reduced by 17.4% using CPC-CSC and the heat provision by ASHP is slightly reduced by 3.0%. Since CPC-CSC can help to obtain higher water storage temperature, more stored hot water in TES tank 1 can be directly used for end use. Using CPC-CSC can increase heat provision by direct SHW by 41.7%.

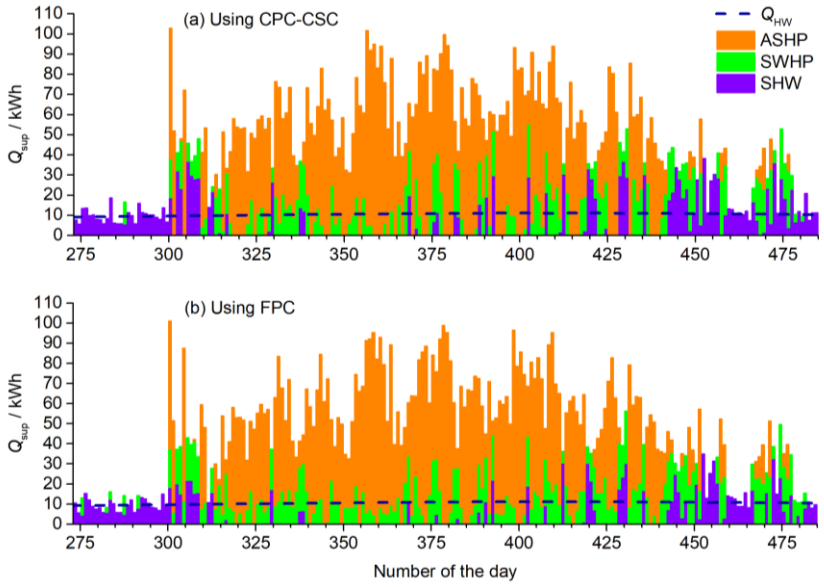

Fig. 6-5: Daily variations of heat for space heating and hot water by direct SHW, ASHP and SWHP over a heating season

Fig. 6-6 shows the daily electricity consumption of ASHP, SWHP and pumps. The columns are stacked to represent the total daily electricity consumption. The electricity consumptions by ASHP, SWHP and pumps in the system using CPC-CSC are 1.69 MWh, 0.37 MWh and 0.28 MWh; those for the system using FPC are 1.74 MWh, 0.45 MWh and 0.30 MWh. The results are also summarised in Table 6-4. Using CPC-CSC can reduce electricity consumption from all three terms. Since the requirements of pumps to assist SWHP is reduced, though heat provision by SHW is increased, electricity consumption from pumps is reduced in the system using CPC-CSC. Overall, compared with the heating system using FPC, the heating system using CPC-CSC can save electricity consumption by 6.1% per year.

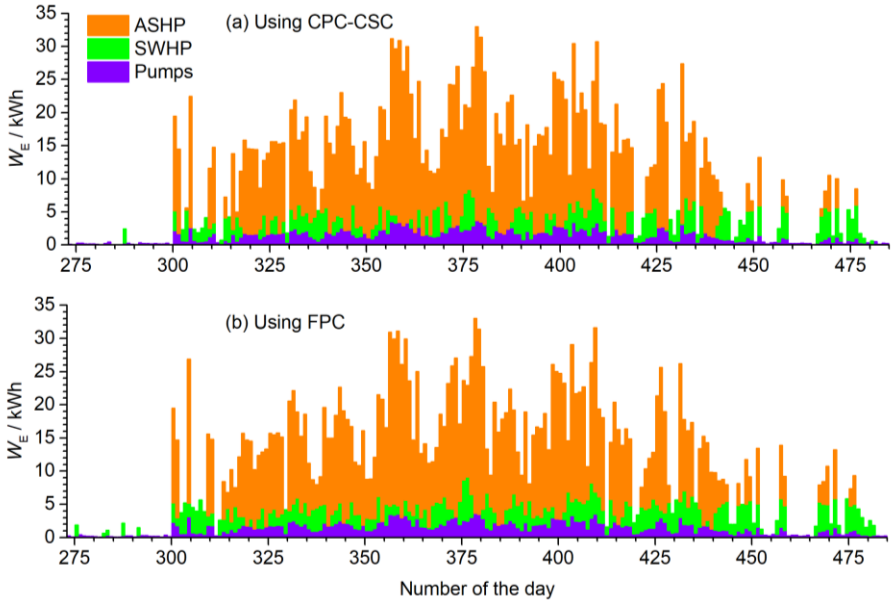

Fig. 6-6: Daily variations of electricity consumed by ASHP, SWHP and SHW over a heating season

Fig. 6-7 shows the daily variations of solar energy used. Systems using CPC-CSC can make use of more solar energy than the system using FPC. In detail, more solar energy is used by SHW. Since CPC-CSC can help to obtain higher water storage temperature, more stored hot water in TES tank 1 can be directly used for end use. The yearly solar energy used by the system using CPC-CSC is 6.5% higher than that of the system using FPC.

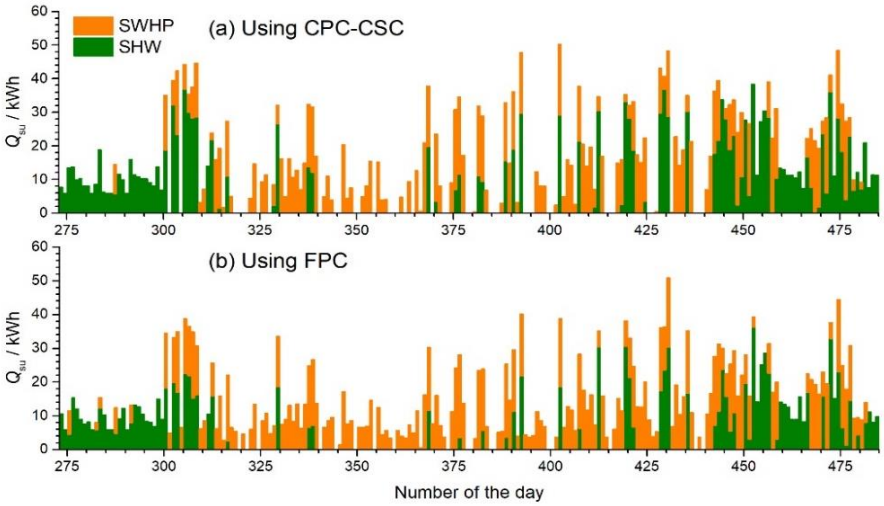

Fig. 6-7: Daily variations of thermal energy extracted from solar energy either used as the heat source for SWHP or directly for hot water (SHW) over a heating season

Fig. 6-8 shows the daily variation of thermal energy charged (positive) and discharged (negative) in TES tank 2 over a heating season. It can be observed that the heating system using CPC-CSC has a larger capacity of Q_{TES} charged in and discharged from TES tank 2. Furthermore, the higher charge and discharge capacities of the TES tank 2 in the system using CPC-CSC reduce the variation frequency of Q_{TES}.

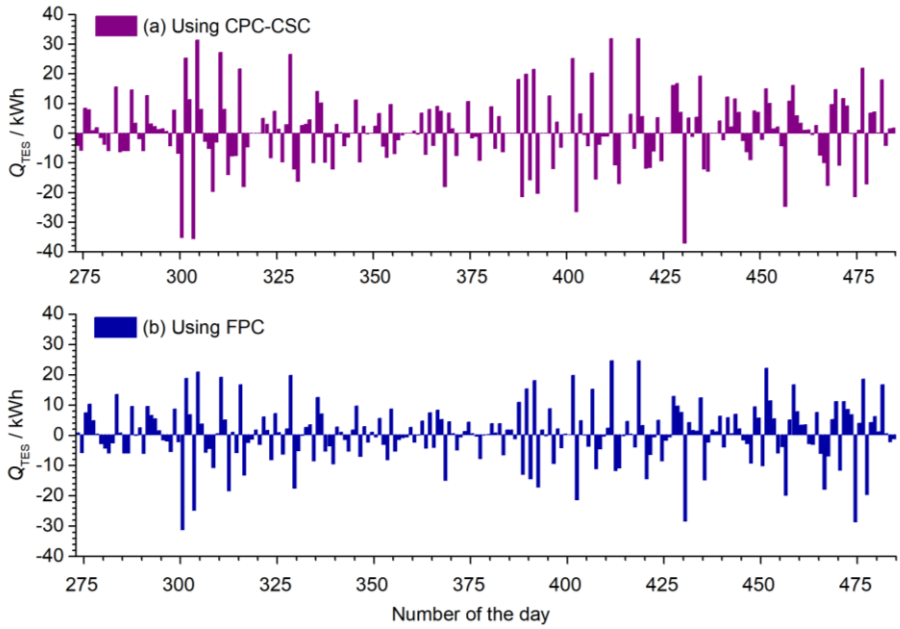

Fig. 6-8: Daily variations of Q_{TES} charged (positive) and discharged (negative) over a heating season

Fig. 6-9 shows the variations of COP_{ASHP} and COP_{SWHP} over a heating season. The average COP_{ASHP} and COP_{SWHP} are 3.5 and 5.1 in the system using CPC-CSC and those in the system using FPC are 3.5 and 5.0. Using CPC-CSC leads to high water storage temperature in TES tank 1 and thus ASHP only needs to work at higher T_{amb}. However, the system using CPC-CSC is easy to have a higher condensing temperature for ASHP and thus average COP_{ASHP}s are the same for both systems. At higher water storage temperature in TES tank 1, thermal energy is provided by SHW directly. Operation of SWHP at higher efficiency is avoided in the system using CPC-CSC. Thus, for both systems, COP_{SWHP} shows a similar range.

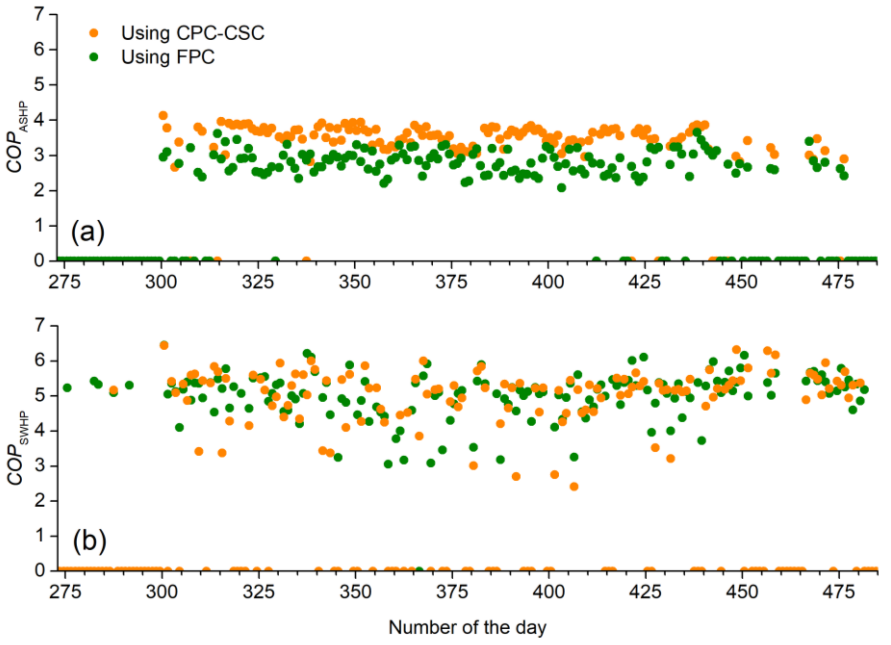

Fig. 6-9: Variations of daily averaged *COP* of the HPs over a heating season

Fig. 6-10 shows the variations of *SPF* over a heating season. The SPF_{ASHP} and SPF_{SWHP} are 3.8 and 5.2 in the system using CPC-CSC and those in the system using FPC are 3.8 and 5.1. In most cases, the heating system using CPC-CSC has higher SPF_{ASHP} and SPF_{SWHP} than the heating system using FPC. Sometimes, the system using CPC-CSC has a lower value, such as on the 316th day (for SPF_{ASHP}) and 383rd day (for SPF_{SWHP}). In the case of low SPF_{SWHP} for the system using CPC-CSC, the water storage temperature in TES tank 1 still meet the operation requirement while that in the system using FPC is low for SWHP operation and ASHP works. Therefore, even though the system using CPC-CSC has a low SPF_{SWHP}, the operation of ASHP is avoided. The overall system efficiency is improved. The heating system using CPC-CSC has a yearly SPF_{sys} of 4.7 while the heating system using FPC has a yearly

SPF_{sys} of just 4.4. In heating periods, the SPF_{sys} of the heating system using CPC-CSC is more even than that of the heating system using FPC since the system using CPC-CSC relies more on stored solar energy in a stable range.

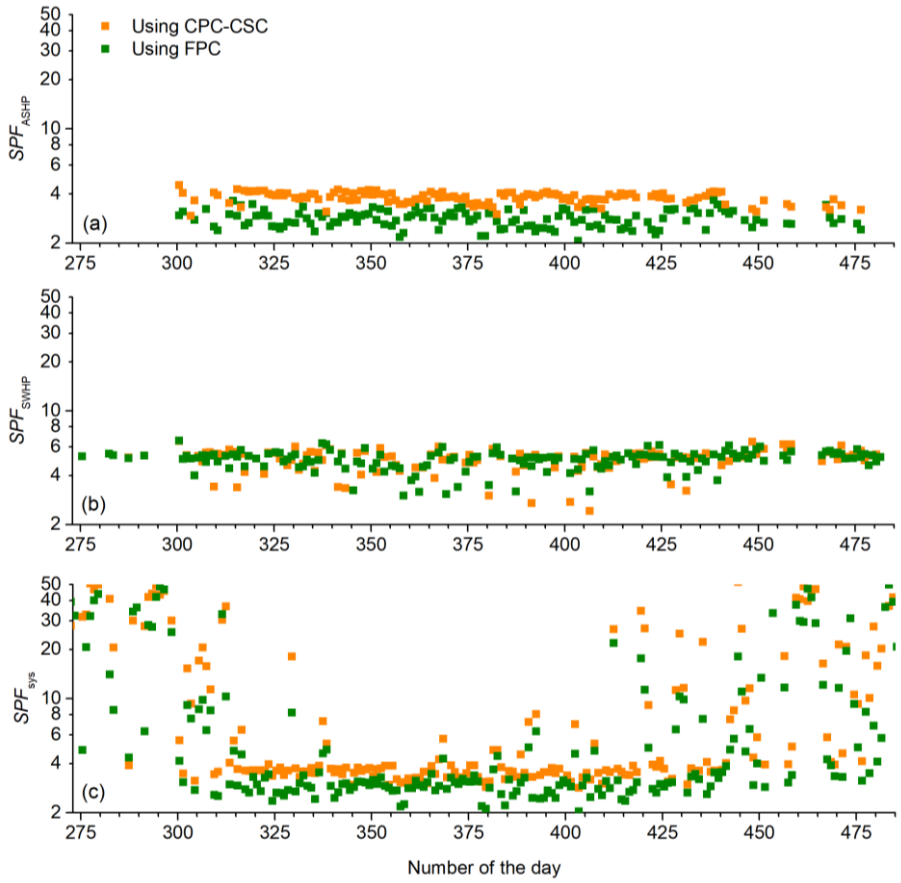

Fig. 6-10: Daily variations of SPF_{sys} and SPF_{HP} over a heating season

6.2.2 Comparison of systems using concentrators of different areas

The operation performance of the system using CPC-CSC of different areas is compared over a heating season. Fig. 6-11 shows the variations of heat provision for space heating and hot water. It can be seen that heat provision for end use is merely influenced by the collector area since the working conditions are the same and the ASHP can work to compensate for the shortage of solar collection.

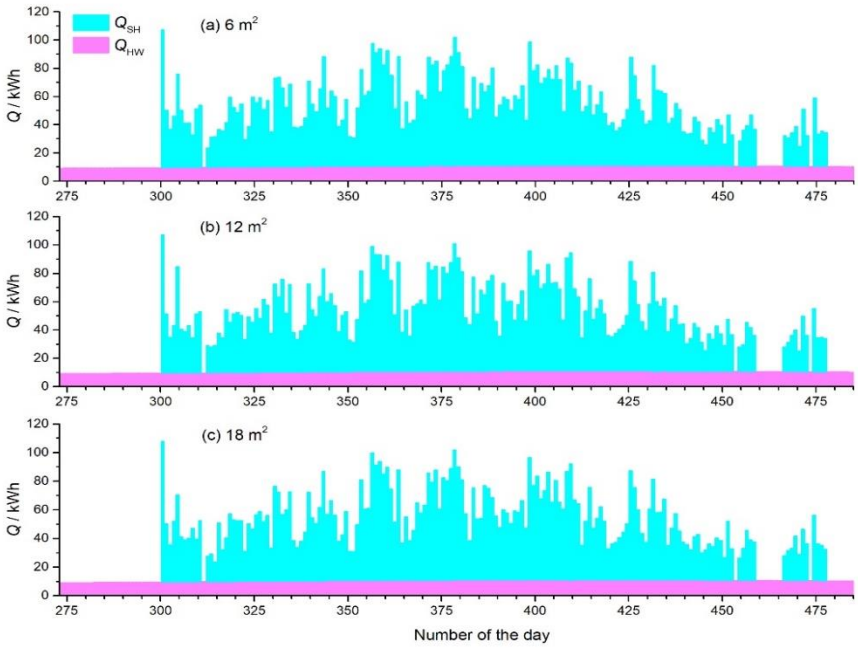

Fig. 6-11: Daily variations of heat for space heating and hot water over a heating season

Fig. 6-12 shows the variations of heat provision from ASHP, SWHP and direct SHW. The columns are stacked to represent the total daily heat provision. The heat provisions from ASHP, SWHP and direct SHW are 7.9 MWh, 1.8 MWh and 0.4 MWh when the collector area is 6 m^2; 7.0 MWh, 1.9 MWh and 1.1 MWh when the collector area is 12 m^2; and 6.4MWh, 1.9 MWh and 1.6 MWh when collector area is 18 m^2. The results are also summarised in Table 6-4. As the collector area decreases from 18 m^2 to 6 m^2, the heat provision by ASHP increases by 23.7% and that by SHW decreases by 46%. At the same time, the heat provision from SWHP slightly decreases by 5.3%. During the non-heating periods, using a collector area of 6 m^2 requires SWHP, even ASHP, for HW while a collector area of 12 m^2 seems sufficient to ensure direct SHW to provide the majority of heat provision.

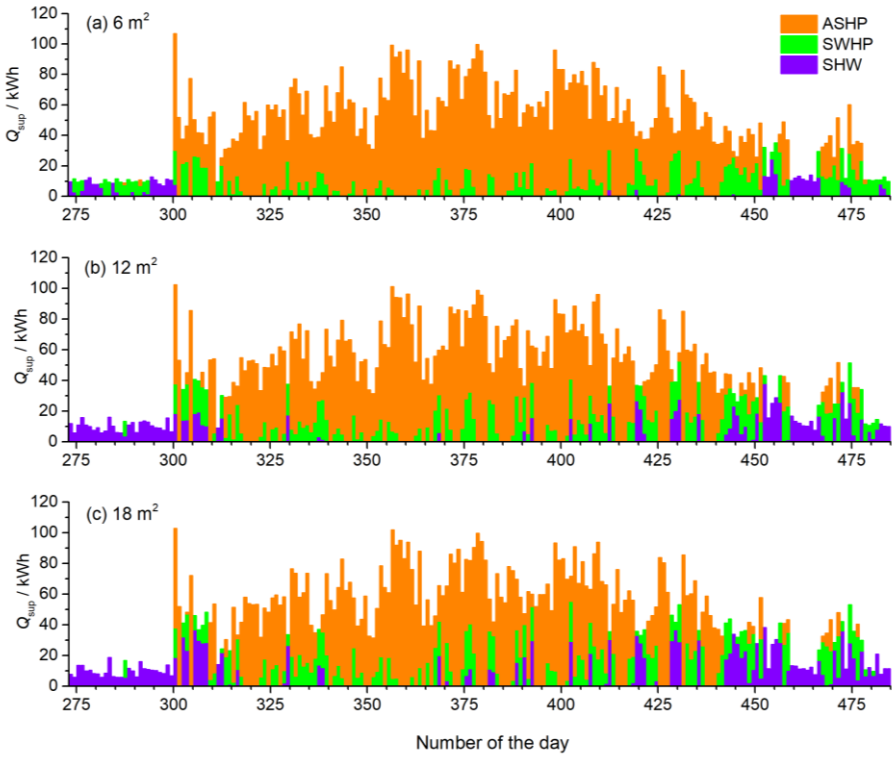

Fig. 6-12: Daily variations of heat for space heating and hot water by direct SHW, ASHP and SWHP over a heating season

Fig. 6-13 shows the variations of electricity consumption by ASHP, SWHP and pumps. The columns are stacked to represent the total daily electricity consumption. The electricity consumed by ASHP, SWHP and pumps are 2.08 MWh, 0.37 MWh and 0.30 MWh when the collector area is 6 m^2; 1.84 MWh, 0.37 MWh and 0.29 MWh when the collector area is 12 m^2; and 1.69 MWh, 0.37 MWh and 0.28 MWh when collector area is 18 m^2. The results are also summarised in Table 6-4. It can be seen that the collector area has a mere influence on electricity consumption by SWHP. In terms of ASHP and pumps, a decrease in collector area brings more electricity consumption. As collector area decreases, though heat provision from direct SHW decreases, pumps need more frequent for solar collection and thus consume more electricity.

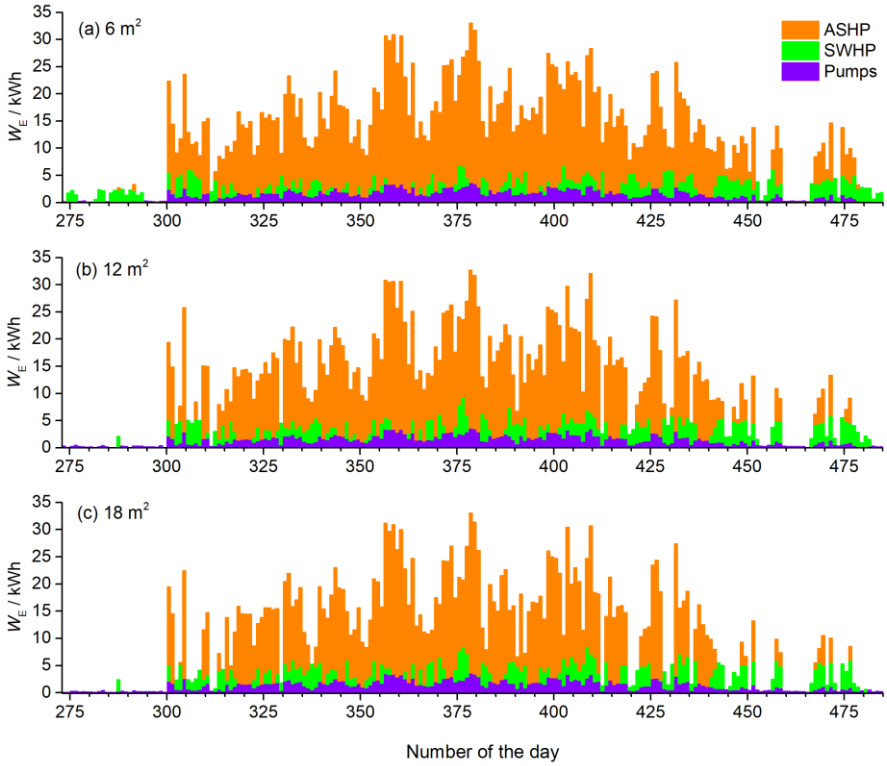

Fig. 6-13: Daily variations of electricity consumed by ASHP, SWHP and pumps over a heating season

Fig. 6-14 shows the variations of thermal energy absorbed from solar energy. A larger collector area brings more total thermal energy absorbed from solar energy and more solar energy used by SHW. In non-heating periods, a system with a smaller collector area has fewer variations of total absorbed solar energy.

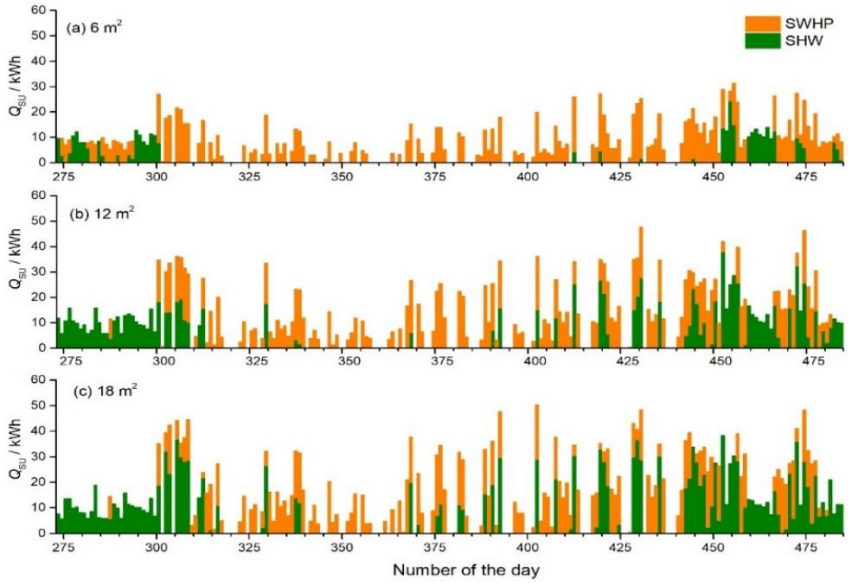

Fig. 6-14: Daily variations of thermal energy extracted from solar energy either used as the heat source for SWHP or directly for hot water (SHW) over a heating season

Fig. 6-15 shows the variations of Q_{TES} charged (positive) and discharged (negative) of TES tank 2 over a heating season. A smaller collector area leads to less solar energy collection and thus less thermal energy stored in TES tank 1. Therefore, the capacity of Q_{TES} charged in and discharged from TES tank 2 decreases relatively as the collector area decreases.

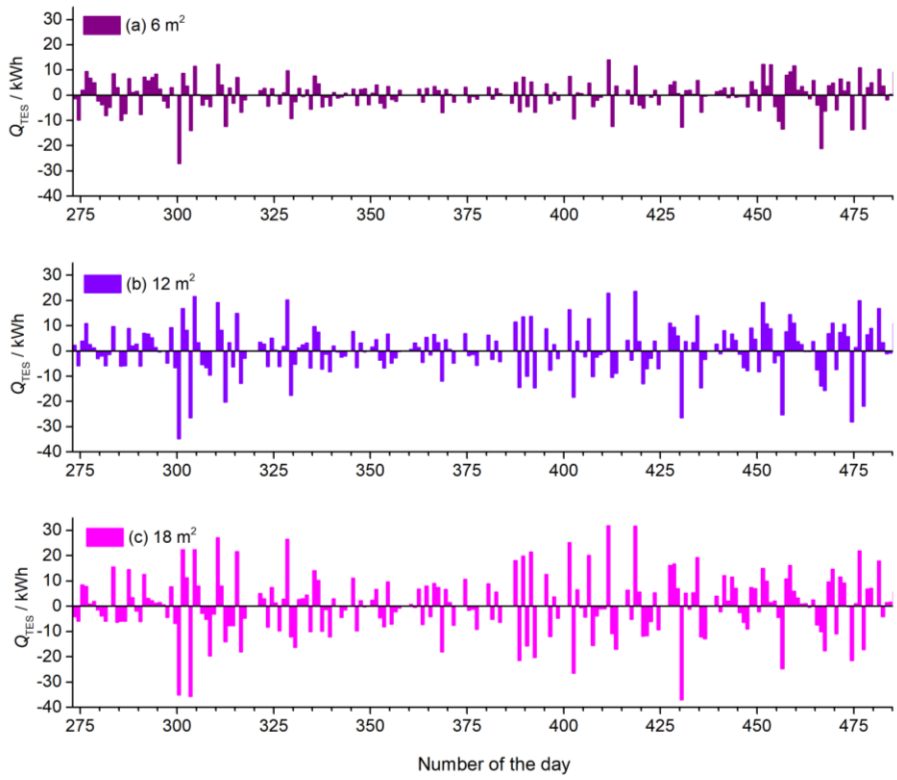

Fig. 6-15: Daily variations of Q_{TES} charged (positive) and discharged (negative) over a heating season

Fig. 6-16 shows the variations of daily COP_{ASHP} and COP_{SWHP} over a heating season. The average daily COP_{ASHP} is 3.5 for different collector areas while the average daily COP_{SWHP} is 4.8, 5.0 and 5.1 for collector areas of 6 m^2, 12 m^2 and 18 m^2. Most time, the COP_{ASHP} is almost the same for different collector areas; in late heating periods, the COP_{ASHP} increases as the collector area decreases. This is because for a larger collector area, the water temperature in TES tank 1 is higher and ASHP only needs to work at a higher ambient temperature while the condensing temperature is also higher, limiting the efficiency of ASHP, especially in late heating periods. COP_{SWHP} generally increases as the collector area increases due to a large increase in the temperature of the heat source. For a system using CPC-CSC of 6 m^2, both ASHP and SWHP are more frequently used, even in non-heating periods.

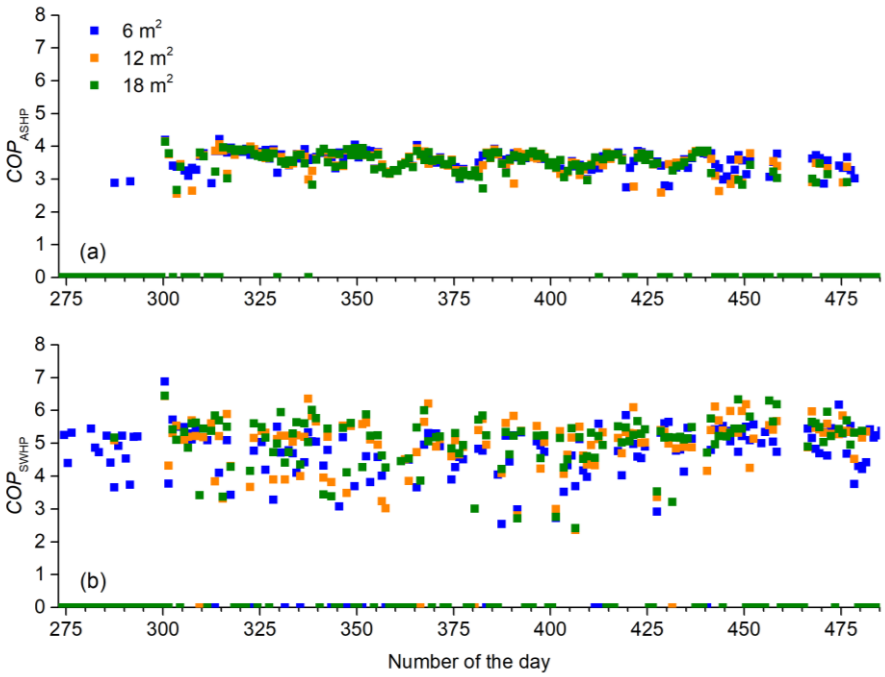

Fig. 6-16: Daily variations of averaged *COP* of the HPs over a heating season

Fig. 6-17 shows the variation of *SPF* of the heating system using CPC-CSC of different areas over a heating season. The SPF_{ASHP} is 3.8 for different collector areas while the SPF_{SWHP} is 4.9, 5.2 and 5.2 for collector areas of 6, 12 and 18 m^2. The seasonal SPF_{sys} are 3.6, 3.9 and 4.2 for collector areas of 6, 12 and 18 m^2. It can be seen that most time, the SPF_{sys} for the system using different collector areas are generally the same. In the late heating period (since the 412th day), the SPF_{sys} show an apparent difference in that the system with CPC-CSC of the larger area has a larger SPF_{sys}. This is because as solar availability increases, for larger collector areas, more heating is provided by direct SHW and SWHP and the efficiency of SWHP increases as well.

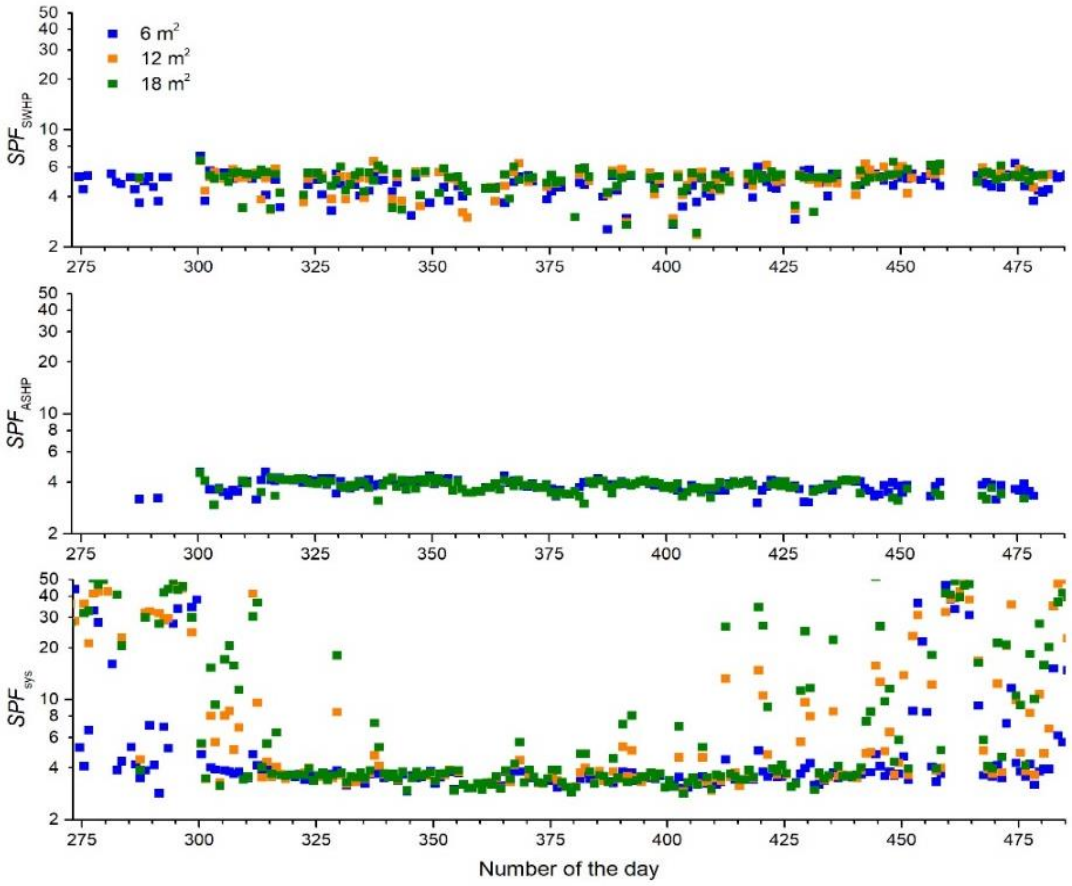

Fig. 6-17: Daily variations of SPF_{sys} and SPF_{HP} over a heating season

6.2.3 Influences of collector areas on operation performances

The effect of collector area on the yearly operation performance of the heating system is analysed for collector areas of 6, 9, 12, 15 and 18 m^2. Fig. 6-18 shows the variation of yearly heat provision by ASHP, SWHP and SHW of the heating system using CPC-CSC. As the collector area decreases, the heat provision by SWHP is merely changed while that by ASHP increases and that by SHW decreases. As the collector area decreases from 18 m^2 to 6 m^2, the heat provision by ASHP is increased by 23.7% and that by SHW is decreased by 46.0%.

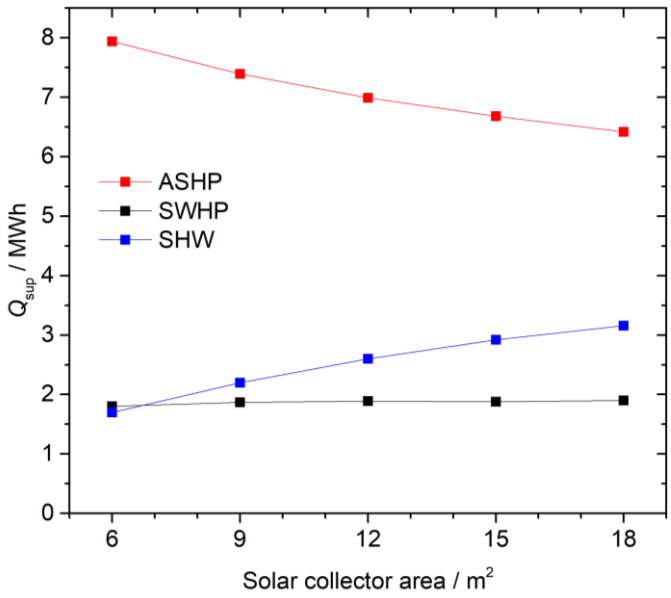

Fig. 6-18: Variations of heat for space heating and hot water by SWHP, ASHP and direct SHW

Fig. 6-19 shows the variations in electricity consumption by ASHP, SWHP and pumps. As the collector area decreases from 18 m^2 to 6 m^2, electricity consumed by ASHP is increased, by 23.0 %. Electricity consumption by pumps is slightly increased, by 8.1% because pumps need to work more frequently to compensate for the low collection capacity of small solar collectors. Electricity consumed by SWHP is merely changed.

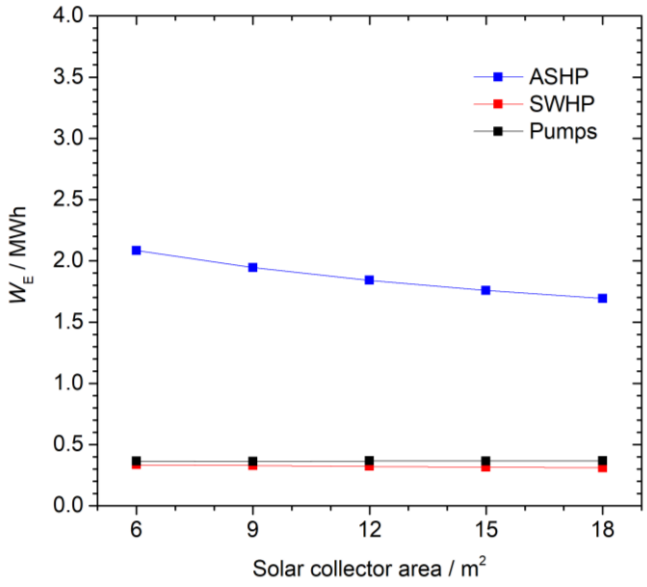

Fig. 6-19: Variations of electricity consumed by SWHP and ASHP and the total electricity consumed by the heating system

Fig. 6-20 shows the variations of thermal energy collected from solar energy and ambient air. As the collector area decreases from 18 m^2 to 6 m^2, thermal energy obtained from the air is increased by 23.9%. At the same time, thermal energy obtained from solar energy is decreased by 33.8%. The total thermal energy obtained from clean energy is reduced by 5.8%. Both curves change quickly at low collector areas and then slowly at high collector areas. This suggests that the influence of collector area on system performance tends to be insignificant at large collector areas.

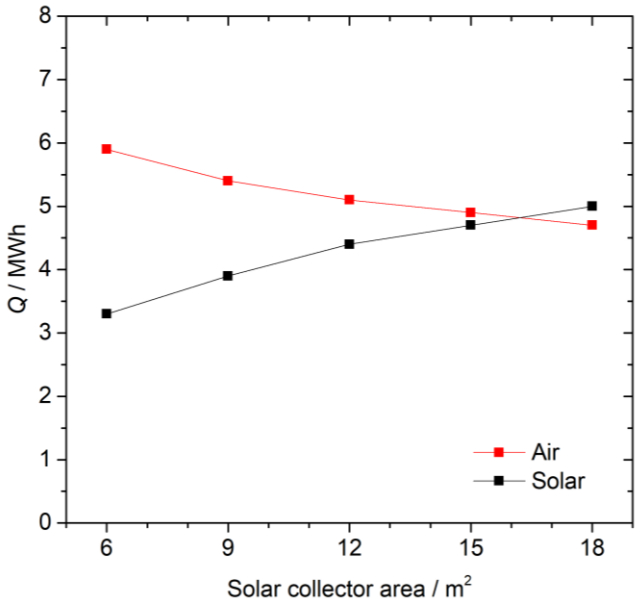

Fig. 6-20: Variation of thermal energy (*Q*) extracted from solar energy and ambient air

Fig. 6-21 shows the variations of solar fraction over a year and over a heating season. With the decrease of collector area from 18 m^2 to 6 m^2, seasonal *SF* decreases from 32.7% to 18.9%; yearly *SF* decreases from 42% to 28.1%. The decrease in *SF* is more significant as the collector area decreases from 9 m^2 to 6 m^2, from 23.5% to 18.9% and 33.3% to 28.1% for seasonal and yearly *SF*, respectively.

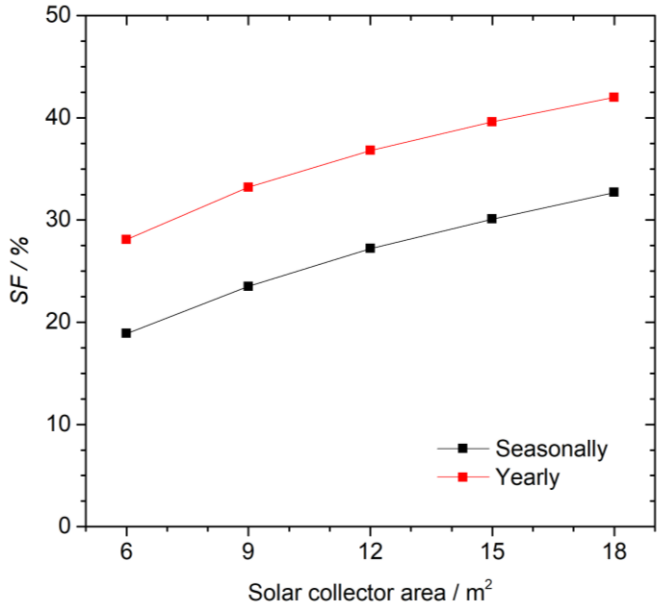

Fig. 6-21: Variations of yearly and seasonally *SF*

Fig. 6-22 shows the variation of yearly averaged COP_{ASHP} and COP_{SWHP} of the heating system using CPC-CSC. The COP_{ASHP} is almost the same for different collector areas, at around 3.5. COP_{SWHP} is generally around 5.0 but shows a slightly decreasing trend as the collector area decreases. Especially, as the collector area decreases from 9 m^2 to 6 m^2, COP_{SWHP} is decreased by 4.0% while as the collector area decreases from 18 m^2 to 6 m^2, COP_{SWHP} is decreased by 5.9%.

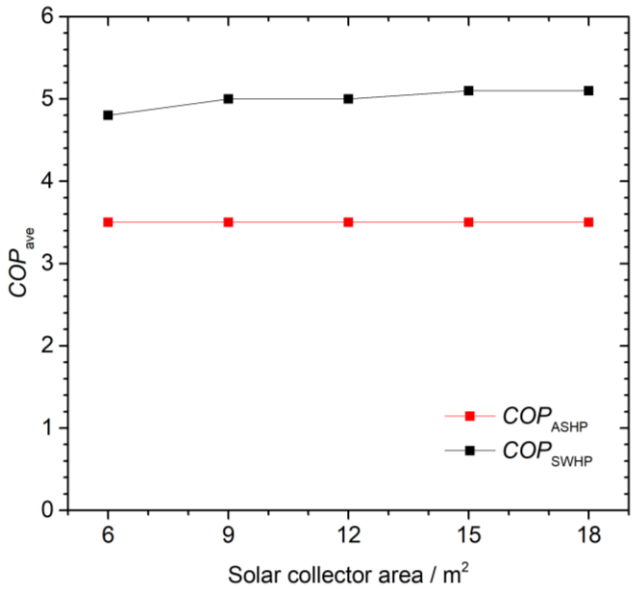

Fig. 6-22: Averaged *COP* of SWHP and ASHP

Fig. 6-23 shows the variations of *SPF* of the heating system using CPC-CSC. SPF_{ASHP} remains consistent for different collector areas, at around 3.8. SPF_{SWHP} keeps even at collector area no smaller than 9 m^2, at around 5.2. As the collector area decreases from 9 m^2 to 6 m^2, SPF_{SWHP} decreases by 5.8%. As the collector area decreases from 18 m^2 to 6 m^2, seasonal and yearly SPF_{sys} decrease by 14.3% and 14.9%.

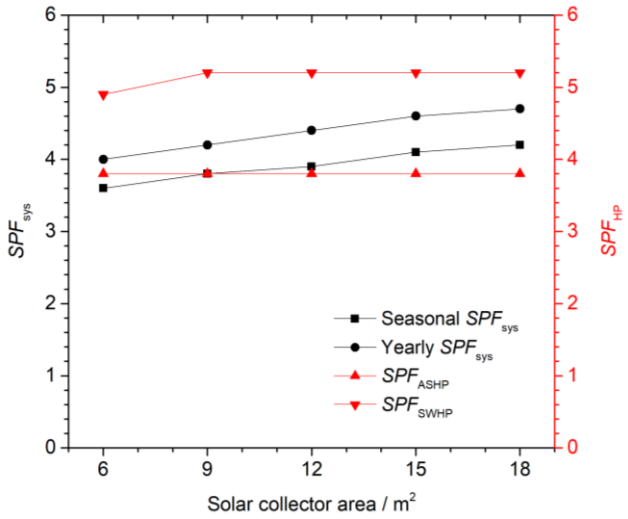

Fig. 6-23: Variations of yearly and seasonally SPF_{HP} and SPF_{sys}

Details for the operation performance of the SAASHP using CPC-CSC of different areas are listed in Table 6-4. For comparison, the performance of SAASHP using an FPC of 18 m^2 is also included. It can be seen that, at the same collector area, the yearly solar energy used by the system using CPC-CSC is 6.5% higher than that of the system using FPC. For almost the same SPF_{sys}, the area of the CPC-CSC required is 12 m^2 while the area required for the FPC is 18 m^2, reduced by one third. These benefits reduce the scale of SAASHP and promote its popularity.

Table 6-4: Overall operation performance of the IX-SAASHPs using CPC-CSC

System		Period	Using CPC-CSC					Using FPC
			6	9	12	15	18	18
Heat provision (kWh)	HW	Heating season	2238.7	2238.1	2238.0	2237.9	2237.9	2237.7
		Non-heating season	1427.6	1427.5	1427.3	1427.2	1427.2	1427.5
	SH		7523.9	7522.9	7524.5	7521.6	7520.3	7527.9
	Total		11190.1	11188.5	11189.8	11186.7	11185.4	11193.1
Heat provision (kWh)	SWHP		1802.8	1874.3	1886.7	1881.5	1903.8	2289.1
	ASHP		7942.8	7393.4	6990.3	6679.9	6419.6	6586.6
	Solar	Heating season	403.9	781.9	1134.2	1423.2	1649.7	1187.6
		Non-heating season	1299.2	1415.2	1464.9	1494.8	1511.1	1409.4
Electricity consumption (kWh)	SWHP		365.1	362.4	365.5	364.7	366.2	449.2
	ASHP		2083.5	1944.6	1841.3	1757.8	1692.3	1737.7
	Water pumps	Heating season	300.8	293.0	286.7	280.3	275.7	295.0
		Non-heating season	34.1	35.8	35.5	34.3	34.0	40.7
	Total		2783.4	2635.8	2529.0	2437.0	2368.1	2522.6
SPF_{HP}	SWHP		4.9	5.2	5.2	5.2	5.2	5.1
	ASHP		3.8	3.8	3.8	3.8	3.8	3.8
COP_{ave}	SWHP		4.8	5.0	5.0	5.1	5.1	5.0
	ASHP		3.5	3.5	3.5	3.5	3.5	3.5
Solar thermal energy (kWh)	To SWHP		1437.7	1512.0	1521.1	1516.9	1537.6	1839.9
	To end use	Heating season	403.9	781.9	1134.2	1423.2	1649.7	1187.6
		Non-heating season	1299.2	1415.2	1464.9	1494.8	1511.1	1409.4
	Total		3317.8	3939.4	4376.8	4719.4	5013.5	4706.7
Thermal energy from ambient air (kWh)			5859.3	5448.8	5149.0	4922.1	4727.3	4848.9
SF	Heating season		18.9%	23.5%	27.2%	30.1%	32.7%	31.0%
	Yearly		28.1%	33.2%	36.8%	39.6%	42.0%	39.6%
SPF_{sys}	Heating season		3.6	3.8	3.9	4.1	4.2	3.9
	Yearly		4.0	4.2	4.4	4.6	4.7	4.4

6.3 Economic Analyses

To evaluate and compare the economic performance of IX-SAASHPs, economic analyses are conducted for IX-SAASHPs using CPC-CSC of different areas and FPC, electric water heater and gas boiler, as well as electric heater and gas boiler boosted SHW systems.

For economic analyses, the total energy consumption of the heating systems, Q_{tot}, is calculated by Eq. (6-18):

$$Q_{tot} = (Q_{sh} + Q_{hw} - Q_{ce})/\eta \quad (6\text{-}18)$$

where Q_{ce} is the clean energy (extracted from solar and ambient air sources) used by the heating system and η is the efficiency of the electric water heater and gas boiler.

The payback period, P_{pb}, is defined based on the electric water heater by Eq. (6-19):

$$P_{pb} = C_i / C_{spy} \quad (6\text{-}19)$$

where C_i is the initial cost difference and C_{spy} is the cost saving per year calculated by Eq. (6-20) and Eq. (6-21), respectively.

$$C_i = C_{i0} - C_{ieh} \quad (6\text{-}20)$$

$$C_{spy} = C_{o0} - C_{oeh} \quad (6\text{-}21)$$

where C_{i0} and C_{o0} are the initial and operation costs of the heating system, respectively, C_{ieh} and C_{oeh} are the initial and operation costs of the electric water heater.

The efficiencies of the electric water heater and gas boiler are taken from [161] to be 0.95 and 0.85, respectively. The electric water heater and gas boiler have a TES tank of 300 L. For the SHW systems, the sizes of the solar collector and outdoor TES tank are taken to be the same as those of the dual-source IX-SAASHP and therefore both systems have the same amount of solar thermal energy collected i.e. ca. 4.71 MWh. The heat provisions of the three heating systems for SH and HW over the year is ca. 11.19 MWh.

The current energy prices are taken from E.On Energy (a UK energy supplier) to be £400.2 per MWh for electricity and £ 106.8 per MWh for gas (prices in June 2022) [255]. The prices of the components of the heating systems are obtained from an online market where the flat plate solar collector price is around £30 per m^2, the water tank price is £290 per 100 L, and a pump with a head of 15 m and a capacity of 15 L/min is around £10 [256]. Since CPC-CSC is a novel collector in research and development status, the price of ETC is adopted to assume CPC-CSC price after commercialisation, £40 per m^2. All the heating systems have a capacity of 8 kW. . The systems are estimated to be easy to connect to the current space heating and water heater. The installation costs are assumed to be 3 hours for the SHW system and 6 hours

for SAASHPs with a cost of 80 per hour [257]. The shipping fees for international shipping are not included in the current economic analysis.

The economic analyses for different CPC-CSC areas in 2022 are displayed in Table 6-5. It can be seen that, though the unit price of FPC is assumed to be 25% cheaper than that of CPC-CSC, at the current electricity price, the SAASHP heating system using CPC-CSC can have a 1.1 % shorter payback period than the SAASHP heating system using FPC of the same SPF_{sys}. For CPC-CSC of different areas, SPF_{sys} and the payback period decrease as the collector area decrease. As the collector area decreases from 18 m^2 to 6 m^2, the payback period decreases by 6.3%. According to both system performance and economic analyses, for domestic heating of an SFH 45 building in London, it is the potential to reduce the required size of CPC-CSC to 9 m^2 or even less. Since solar collectors with a smaller size can much more easily be adapted for domestic use, using CPC-CSC benefits the wide rollout of SAASHP heating systems for domestic heating.

Table 6-5: Economic analysis for electric heater, direct SHW and SAASHP heating systems based on the energy prices in June, 2022

		Electric water heater	**Gas boiler**	**Electric heater boosted SHW**	**Gas boiler boosted SHW**	**SAASHP (FPC)**	**SAASHP (CPC-CSC)**				
Collector area		-	-	18	18	18	6	9	12	15	18
Heat provision per year, MWh		11.19	11.19	11.19	11.19	11.19	11.19	11.19	11.19	11.19	11.19
Efficiency/performance		0.95	0.85	0.95	0.85	*SPF*=4.4	*SPF*=4.0	*SPF*=4.2	*SPF*=4.4	*SPF*=4.6	*SPF*=4.7
Energy consumption per year, MWh		11.8	13.2	7.2	8.0	2.2	2.5	2.4	2.2	2.1	2.1
Initial cost, £	collector	0	0	540	540	540	240	360	480	600	720
	tanks	870	870	2320	2320	2320	2320	2320	2320	2320	2320
	Heater/HP	60	15	60	15	1085	1085	1085	1085	1085	1085
	pumps	0	0	20	20	30	30	30	30	30	30
	Installation	0	0	240	240	480	480	480	480	480	480
	total	930	885	3180	3135	4455	4155	4275	4395	4515	4635
Operation cost, £		4714.3	1406.5	2881.7	854.7	897.8	999.6	946.3	897.8	853.5	832.8
Cost saving per year, £		-	3307.8	1832.6	3859.6	3816.5	3714.7	3768.0	3816.5	3860.8	3881.5
Payback period, year		-	-	1.23	0.57	0.92	0.87	0.89	0.91	0.93	0.95

6.4 Summary

In this chapter, the solar assisted air source heat pump heating system integrating compound parabolic concentrator-capillary tube solar collector has been modelled and numerically simulated. The operation performance of this heating system is compared with that of the heating system using a flat plate collector. The effect of the solar collector size on the operation performance and economics of the heating system has been analysed. The following conclusions can be drawn:

1. For the same SPF_{sys}, the size of the CPC-CSC required is 12 m^2 whereas the size of the FPC required is 18 m^2, leading to one third reduction in solar collector size.
2. For the heating systems using the same size solar collector of 18 m^2, the CPC-CSC increases the utilisation of solar energy by 6.5%, reduces the electricity consumption by 6.1% and hence increases SPF_{sys} by 6.8%, compared with the FPC. The system using CPC-CSC achieves an *SPF* of 4.7 in London weather conditions.
3. As collector size decreases, both SPF_{sys} and the payback period decreases. As the collector area decreases from 18 m^2 to 6 m^2, seasonal and yearly SPF_{sys} decrease by 14.3% and 14.9% while the payback period decreases by 6.3%. Considering both thermal and economic performances, the size of the concentrated solar collector could potentially be reduced to 9 m^2 or less.
4. As the collector area decreases from 18 m^2 to 6 m^2, the heat provision by ASHP increases by 23.7% and that by SHW decreases by 46%, and the electricity consumed by ASHP and the pumps increases by 23 % and 8.1%. For SWHP, the heat provision slightly decreases by 5.3% and the electricity consumption is merely influenced.

7. Conclusions and future work

In this study, simulation models of serial, parallel and dual-source solar assisted air source heat pumps are established in TRNSYS. The SAASHP systems are adopted to provide space heating and hot water for SFH 45 building. Operation performances and economic efficiencies are investigated to evaluate the potential to utilise SAASHP in the UK. The influence of the heating temperatures is numerically investigated. A compound parabolic concentrator-capillary tube solar collector is used to enhance the solar collection and thus the operation efficiency of the SAASHP systems. The outcomes of this study are concluded below.

7.1 Conclusion

According to the simulation results, the application performances of SAASHP in the UK can be summarised as:

1. All three IX-SAASHPs can achieve a yearly SPF_{sys} higher than 4.4, suggesting their potential to be applied for domestic heating under weather conditions in high latitude regions.
2. The heat provision of the serial IX-SAASHP is limited by the availability of solar irradiance. Since solar energy is the sole heat source of the serial system, it requires large sizes of solar collectors and TES tanks, resulting in high installation costs and a longer payback period.
3. The parallel IX-SAASHP has the simplest pipe connection and control function. It shows the highest SPF_{sys} and the most stable operation performance, as well as the lowest payback period, 0.72 years.
4. The dual-source IX-SAASHP shows a much lower cost than the serial system and similar operation performance to the parallel system. the dual-source IX-SAASHP has a payback period of 0.92 years. It is also an attractive alternative to gas boilers and gas boosted SHW systems.
5. Low temperature heating can significantly reduce electricity consumption. For the heating system, with the decrease of the set hot-water-supply temperature from 55 ^{o}C to 40 ^{o}C, the yearly electricity consumption decreases by 19.1% in London, 14.9% in Aughton, and 13.3% in Aberdeen, respectively.
6. Low temperature heating increases thermal energy collection from both solar energy and ambient air, and hence *COP* largely increases. With the decrease of the set hot-water-supply temperature from 55 ^{o}C to 40 ^{o}C, the *COP* of SWHP increases from 4.8 to 5.6 in London,

from 5.0 to 5.6 in Aughton; and from 4.7 to 5.4 in Aberdeen, respectively, while the *COP* of ASHP increases from 3.3 to 3.8 in London; from 3.2 to 3.8 in Aughton; and from 3.2 to 3.6 in Aberdeen, respectively.

7. Low temperature heating benefits by decreasing heat provision from ASHP and SWHP and increasing the heat provision from direct SHW, resulting in much better system efficiency. When the set hot-water-supply temperature decreases from 55 ^{o}C to 40 ^{o}C, the yearly SPF_{sys} increases from 4.2 to 4.9 in London; from 4.2 to 5.0 in Aughton; and from 3.9 to 4.5 in Aberdeen, respectively.
8. At the set hot-water-supply temperature of 40 ^{o}C, the heat provided by ASHP is about three times that by SWHP and about six times that by direct SHW, and the electricity consumed by ASHP is about four times that by SWHP and about five times that by pumps in the three locations.
9. *SF* appears to be negligibly influenced by latitude and set hot-water-supply-temperature. For different set hot-water-supply-temperature, *SF* is 40% in London, 42% in Aughton, and 37% in Aberdeen.
10. The payback periods slightly decrease as the set hot-water-supply temperature decreases. With the decrease of the set hot-water-supply-temperature from 55 ^{o}C to 40 ^{o}C, for the electricity price in April 2022, the payback periods decrease from 1.01 years to 0.95 years in London, from 0.98 years to 0.94 years in Aughton, and from 0.81 years to 0.78 years in Aberdeen.
11. For the same SPF_{sys}, the size of the CPC-CSC required is 12 m^2 whereas the size of the FPC required is 18 m^2, leading to one third reduction in solar collector size.
12. For the heating systems using the same size solar collector of 18 m^2, the CPC-CSC increases the utilisation of solar energy by 6.5%, reduces the electricity consumption by 6.1% and hence increases SPF_{sys} by 6.8%, compared with the FPC.
13. As collector size decreases, both SPF_{sys} and the payback period decreases. As the collector area decreases from 18 m^2 to 6 m^2, seasonal and yearly SPF_{sys} decrease by 14.3% and 14.9% while the payback period decreases by 6.3%. Considering both thermal and economic performances, the size of the concentrated solar collector could potentially be reduced to 9 m^2 or less.
14. As the collector area decreases from 18 m^2 to 6 m^2, the heat provision by ASHP increases by 23.7% and that by SHW decreases by 46%, and the electricity consumed by ASHP and the pumps increases by 23 % and 8.1%. For SWHP, the heat provision slightly decreases by 5.3% and the electricity consumption is merely influenced.

7.2 Future work

1. Due to the lockdown for COVID-19, a corresponding experimental investigation was not conducted. In the future, the test rig of the IX-SAASHP using CPC-CSC with low hot water supply temperature will be designed and established for domestic heating in London.
2. The building model of the simulation will be improved from a model for typical reference buildings to a model for a real building whose parameters can be monitored. Then the experimental results obtained will be compared with the simulation results.
3. The current economic analysis adopts quotations from the international market and the shipment fees are ignored. In the future, the economic analysis will be more accurate considering the domestic component market or the international shipping fees.

References

[1] Department for Business, Energy & Industrial Strategy. 2050 Pathways Analysis. 2010. https://assets.publishing.service.gov.uk/government/uploads/system/uploads/attachment_data/file/68816/216-2050-pathways-analysis-report.pdf. [accessed 11 September 2020]

[2] EDF energy, UK Gas Boiler Ban – Everything You Need to Know, https://www.edfenergy.com/heating/advice/uk-boiler-ban, [accessed on May 20th, 2021]

[3] Department of Energy and Climate Change Statistics. Special feature -- estimates of heat use in the UK. 2014. https://assets.publishing.service.gov.uk/government/uploads/system/uploads/attachment_data/file/386858/Estimates_of_heat_use.pdf. [accesses 11 September 2020]

[4] Department for Business, Energy & Industrial Strategy, Energy consumption in the UK, 2018

[5] International Energy Agency. https://www.iea.org/reports/heat-pumps. [accessed 10 September 2020]

[6] Demir H, Mobedi M, Ülkü S. A review on adsorption heat pump: problems and solutions. Renew Sustain Energy Rev 2008;12:2381-2403.

[7] Kara O, Ulgen K, Hepbasli A. Exergetic assessment of direct-expansion solar-assisted heat pump systems: review and modeling. Renew Sustain Energy Rev 2008;12:1383–1401.

[8] Omojaro P, Breitkopf C. Direct expansion solar assisted heat pumps: a review of applications and recent research. Renew Sustain Energy Rev 2013;22:33–45.

[9] Shi GH, Aye L, Li D, Du XJ. Recent advances in direct expansion solar assisted heat pump systems: a review. Renew Sustain Energy Rev 2019;109:349-366.

[10] Facao J, Carvalho MJ. New test methodologies to analyse direct expansion solar assisted heat pumps for domestic hot water. Solar Energy 2014;100:66–75.

[11] Amin ZM, Hawlader MNA. A review on solar assisted heat pump systems in Singapore. Renew Sustain Energy Rev. 2013;26:286–293.

[12] Abou-Ziyan HZ, Ahmed MF, Metwally MN, El-Hameed HM Abd. Solar-assisted R22 and R134a heat pump systems for low-temperature applications. Appl Therm Eng 1997;17:455-469.

[13] Karagiorgas M, Galatis K, Tsagouri M, Tsoutsos T, Botzios-Valaskakis A. Solar assisted heat pump on air collectors: a simulation tool. Solar Energy 2010;84:66–78.

[14] Asaee SR, Ugursal VI, Beausoleil-Morrison I. Techno-economic assessment of solar assisted heat pump system retrofit in the Canadian housing stock. Appl Energy 2017;190:439–452.

[15] International Energy Agency. Technology road map - solar heating and cooling. 2012. http://www.iea-shc.org/data/sites/1/publications/2012_SolarHeatingCooling_Roadmap.pdf. [accessed 10 September 2020]

[16] Carbonell D, Haller MY, Frank E. Potential benefit of combining heat pumps with solar thermal for heating and domestic hot water preparation. Energy Procedia 2014;57:2656–2665.

[17] Wang ZY, Guo P, Zhang HJ, Yang WS, Mei S. Comprehensive review on the development of SAHP for domestic hot water. Renew Sustain Energy Rev 2017;72:871–881.

[18] Ozgener O, Hepbasli A. A review on the energy and exergy analysis of solar assisted heat pump systems. Renew Sustain Energy Rev 2007;11:482–496.

[19] Haller MY, Bertram E, Dott R, Afjei T, Ochs F, Hadorn JC. Review of component models for the simulation of combined solar and heat pump heating systems. Energy Procedia 2012;30:611–622.

[20] Buker MS, Riffat SB. Solar assisted heat pump systems for low temperature water heating applications: a systematic review. Renew Sustain Energy Rev 2016;55:399-413.

[21] Wang XR, Xia L, Bales C, Zhang XX, Copertaro B, Pan S, Wu JS. A systematic review of recent air source heat pump (ASHP) systems assisted by solar thermal, photovoltaic and photovoltaic/thermal sources. Renew Energy 2020;146:2472-2487.

[22] Poppi S, Sommerfeldt N, Bales C, Madani H, Lundqvist P. Techno-economic review of solar heat pump systems for residential heating applications. Renew Sustain Energy Rev 2018;81:22–32.

[23] Mohanraj M, Belyayev Ye, Jayaraj S, Kaltayev A. Research and developments on solar assisted compression heat pump systems – A comprehensive review (Part A: modeling and modifications). Renew Sustain Energy Rev 2018;83:90-123.

[24] Mohanraj M, Belyayev Ye, Jayaraj S, Kaltayev A. Research and developments on solar assisted compression heat pump systems – a comprehensive review (Part-B: applications). Renew Sustain Energy Rev 2018;83:124-155.

[25] Ruschenburg J, Herkel S. A review of market-available solar thermal heat pump systems: a technical

report of subtask A'. 2013. http://task44.iea-shc.org/data/sites/1/publications/T44A38-SubA-Report1-1305031.pdf. [accessed 11 September 2020]
[26] Ruschenburg J, Herkel S, Henning HM. A statistical analysis on market-available solar thermal heat pump systems. Solar Energy. 2013;95:79–89.
[27] Frank E, Haller M, Herkel S, Ruschenburg J. System classification of combined solar thermal and heat pump systems. Proceedings of the EuroSun 2010 Conf. Graz, Austria.
[28] Sezen K, Tuncer AD, Akyuz AO, Gungor A. Effects of ambient conditions on solar assisted heat pump systems: a review. Sci Total Environ 2021;778:146362.
[29] Cai JY, Li ZH, Ji J, Zhou F. Performance analysis of a novel air source hybrid solar assisted heat pump. Renew Energy 2019;139:1133-1145.
[30] Hesaraki A, Holmberg S, Haghighat F. Seasonal thermal energy storage with heat pumps and low temperatures in building projects - a comparative review. Renew Sustain Energy Rev 2015;43:1199-1213.
[31] Kaygusuz K. Investigation of a combined solar-heat pump system for residential heating. Part 2: simulation results. Int J Energy Res 1999;23:1225-1237.
[32] Chow TT, Pei G, Fong KF, Lin Z, Chan ALS, He M. Modelling and application of direct-expansion solar-assisted heat pump for water heating in subtropical Hong Kong. Appl Energy 2010;87:643–649.
[33] Chaturvedi SK, Shen JY. Thermal performance of a direct expansion solar-assisted heat pump. Solar Energy 1984;33:155-162.
[34] Deng W, Yu J. Simulation analysis on dynamic performance of a combined solar/air dual source heat pump water heater. Energy Convers Manage 2016;120:378-387.
[35] Huang BJ, Lee JP, Chyng JP. Heat-pipe enhanced solar-assisted heat pump water heater. Solar Energy 2005;78:375–381.
[36] Chaturvedi SK, Abdel-Salam TM, Sreedharan SS, Gorozabel FB. Two-stage direct expansion solar-assisted heat pump for high temperature applications. Appl Therm Eng 2005;29:2093–2099.
[37] Kuang YH, Wang RZ. Performance of a multi-functional direct-expansion solar assisted heat pump system. Solar Energy 2006;80:795-803.
[38] Zhu L, Yu JL, Zhou ML, Wang X. Performance analysis of a novel dual-nozzle ejector enhanced cycle for solar assisted air-source heat pump systems. Renew Energy 2014;63:735-740.
[39] Yan G, Bai T, Yu J. Energy and exergy efficiency analysis of solar driven ejector—compressor heat pump cycle. Solar Energy 2016;125:243-255.
[40] Chen J, Yu J, Theoretical analysis on a new direct expansion solar assisted ejector-compression heat pump cycle for water heater, Solar Energy, 2017;142:299-307.
[41] Bakirci K, Yuksel B. Experimental thermal performance of a solar source heat-pump system for residential heating in cold climate region. Appl Therm Eng 2011;31:1508-1518.
[42] Yumrutas R, Kaska O. Experimental investigation of thermal performance of a solar assisted heat pump system with an energy storage. Int J Energy Res 2004;28:163–175.
[43] Li H, Yang HX. Study on performance of solar assisted air source heat pump systems for hot water production in Hong Kong. Appl Energy 2010;87:2818–2825.
[44] Cai JY, Ji J, Wang YY, Huang WZ. Numerical simulation and experimental validation of indirect expansion solar-assisted multi-functional heat pump. Renew Energy 2016;93:280-290.
[45] Air-Conditioning, Heating, and Refrigeration Institute. 2008 standard for performance rating of unitary air-conditioning & air-source heat pump equipment. 2012. http://www.ahrinet.org/App_Content/ahri/files/standards%20pdfs/ANSI%20standards%20pdfs/ANSI.AHRI%20Standard%20210.240%20with%20Addenda%201%20and%202.pdf. [accessed 11 September 2020]
[46] Lerch W, Heinz A, Heimrath R. Direct use of solar energy as heat source for a heat pump in comparison to a conventional parallel solar air heat pump system. Energy Buildings 2015;100:34–42.
[47] Kaygusuz K. Experimental and theoretical investigation of a solar heating system with heat pump. Renew Energy 2000;21:79-102.
[48] Kaygusuz K. Investigation of a combined solar-heat pump system for residential heating. Part 1: experimental results. Int J Energy Res 1999;23:1213-1223.
[49] Dikici A, Akbulut A. Exergetic performance evaluation of heat pump systems having various heat sources. Int J Energy Res 2008;32:1279-1296.
[50] Liu Y, Ma J, Zhou GH, Zhang C, Wan WL. Performance of a solar air composite heat source heat pump system. Renew Energy 2016;87:1053-1058.
[51] Yerdesh Y, Abdulina Z, Aliuly A, Belyayev Y, Mohanraj M, Kaltayev A. Numerical simulation on

solar collector and cascade heat pump combi water heating systems in Kazakhstan climates. Renew Energy 2020;145:1222-1234.
[52] Lv XL, Yan G, Yu JL. Solar-assisted auto-cascade heat pump cycle with zeotropic mixture R32/R290 for small water heaters. Renew Energy 2015;76:167-172.
[53] Sterling SJ. Feasibility analysis of two indirect heat pump assisted solar domestic hot water systems. M.S. thesis, University of Waterloo, Canada. 2011.
[54] Sterling SJ, Collins MR. Feasibility analysis of an indirect heat pump assisted solar domestic hot water system. Appl Energy 2012;93:11–17.
[55] Deng S, Dai YJ, Wang RZ. Performance study on hybrid solar-assisted CO2 heat pump system based on the energy balance of net zero energy apartment. Energy Buildings 2012;54:337–349.
[56] Faria RN, Nunes RO, Koury RNN, Machado L, Dynamic modeling study for a solar evaporator with expansion valve assembly of a transcritical CO_2 heat pump. Int J Refrig 2016;64:203–213.
[57] Deng S, Dai YJ, Wang RZ. Performance optimization and analysis of solar combi-system with carbon dioxide heat pump. Solar Energy 2013;98:212–225.
[58] Chen JF, Dai YJ, Wang RZ. Experimental and theoretical study on a solar assisted CO_2 heat pump for space heating. Renew Energy 2016;89:295-304.
[59] Ziemelis I, Kancevica L, Jesko Z, Putans H. Calculation of energy produced by solar collectors. In: Proceedings of Engineering for Rural Development: Jelgava, Latvia; 2009.
[60] Sun XL, Dai YJ, Novakovic V, Wu J, Wang RZ. Performance comparison of direct expansion solar-assisted heat pump and conventional air source heat pump for domestic hot water. Energy Procedia 2015;70:394-401.
[61] Scarpa F, Tagliafico LA. Exploitation of humid air latent heat by means of solar assisted heat pumps operating below the dew point. Appl Therm Eng 2016;100:820–828.
[62] Trinkl C, Zörner W, Hanby V. Simulation study on a domestic solar/heat pump heating system incorporating latent and stratified thermal storage. J Solar Energy Eng 2009;131:041008.
[63] Freeman TL, Mitchell JW, Audit TE. Performance of combined solar-heat pump systems. Solar Energy 1979;22:125-135.
[64] Kaygusuz K, Comakli O, Ayhan T. Solar-assisted heat pump systems and energy storage. Solar Energy 1991;47:383-391.
[65] Chyng JP, Lee CP, Huang BJ. Performance analysis of a solar-assisted heat pump water heater. Solar Energy 2003;74:33–44.
[66] Kaygusuz K. Calculation of required collector area of a solar-assisted series heat pump for domestic heating. Energy Sources 2000;22:247-256.
[67] Kuang YH, Wang RZ, Yu LQ. Experimental study on solar assisted heat pump system for heat supply. Energy Convers Manage 2003;44:1089–1098.
[68] Yumrutas R, Unsal M. Analysis of solar aided heat pump systems with seasonal thermal energy storage in surface tanks. Energy 2000;25:1231–1243.
[69] Yumrutas R, Kunduz M, Ayhan T, Investigation of thermal performance of a ground coupled heat pump system with a cylindrical energy storage tank. Int J Energy Res 2003;27:1051–1066.
[70] Kuang YH, Sumathy K, Wang RZ. Study on a direct-expansion solar-assisted heat pump water heating system. Int J Energy Res 2003;27:531–548.
[71] Xu GY, Zhang XS, Deng SM. A simulation study on the operating performance of a solar–air source heat pump water heater. Appl Therm Eng 2006;26:1257-1265.
[72] Li YW, Wang RZ, Wu JY, Xu YX. Experimental performance analysis and optimization of a direct expansion solar-assisted heat pump water heater. Energy 2007;32:1361–1374.
[73] Kong XQ, Zhang D, Li Y, Yang QM. Thermal performance analysis of a direct-expansion solar-assisted heat pump water heater. Energy 2011;36:6830-6838.
[74] Li YW, Wang RZ, Wu JY, Xu YX. Experimental performance analysis on a direct-expansion solar-assisted heat pump water heater. Appl Therm Eng 2007;27:2858–2868.
[75] Dikici A, Akbulut A. Performance characteristics and energy–exergy analysis of solar-assisted heat pump system. Building Environ 2008;43:1961–1972.
[76] Ito S, Miura N, Wang K. Performance of a heat pump using direct expansion solar collectors. Solar Energy 1999;65:189–196.
[77] Dong X, Tian Q, Li Z. Energy and exergy analysis of solar integrated air source heat pump for radiant floor heating without water. Energy Buildings 2017;142:128–138.
[78] Caglar A, Yamalı C. Performance analysis of a solar-assisted heat pump with an evacuated tubular collector for domestic heating. Energy Buildings 2012;54:22–28.

[79] Liang CH, Zhang XS, Li XW, Zhu X. Study on the performance of a solar assisted air source heat pump system for building heating. Energy Buildings 2011;43:2188–2196.
[80] Qu SL, Ma F, Ji R, Wang DX, Yang LX. System design and energy performance of a solar heat pump heating system with dual-tank latent heat storage. Energy Buildings 2015;105:294–301.
[81] Youssef W, Ge YT, Tassou SA. Effects of latent heat storage and controls on stability and performance of a solar assisted heat pump system for domestic hot water production. Solar Energy 2017;150:394–407.
[82] Carbonell D, Haller MY, Philippen D, Frank E. Simulations of combined solar thermal and heat pump systems for domestic hot water and space heating. Energy Procedia 2014;48:524-534.
[83] Ortiz-Rivera EI, Feliciano-Cruz LI. Performance evaluation and simulation of a solar thermal power plant. In: Proceedings of the IEEE energy conversion congress and exposition. San Jose, California, USA. 2009.
[84] Eslami-nejad P, Bernier M. Coupling of geothermal heat pumps with thermal solar collectors using double U-tube boreholes with two independent circuits. Appl Therm Eng 2011;31:3066-3077.
[85] Wang QK, Huang Q. Research on integrated solar and geothermal energy engineering design in hot summer and cold winter area. Procedia Eng 2011;21:648-655.
[86] Cristofari C, Notton G, Poggi P, Louche A. Influence of the flow rate and the tank stratification degree on the performances of a solar flat-plate collector. Int J Therm Sci 2003;42:455–469.
[87] Han YM, Wang RZ, Dai YJ. Thermal stratification within the water tank. Renew Sustain Energy Rev 2009;13:1014–1026.
[88] Ghaddar NK. Stratified storage tank influence on performance of solar water heating system tested in Beirut. Renew Energy 1994;4:911-925.
[89] Huang HL, Ge XS, Su YH. Theoretical thermal performance analysis of two solar-assisted heat-pump systems. Int J Energy Res 1999;23:1-6.
[90] Carbonell D, Philippen D, Granzotto M, Haller MY, Frank E. Simulation of combined solar thermal, heat pump, ice storage and waste water heat recovery systems. Design Criteria and Parametric Studies. Proceedings of EuroSun ISES, Aixlse Bains, France. 2014
[91] Han ZW, Zheng MY, Kong FH, Wang F, Li ZJ, Bai T. Numerical simulation of solar assisted ground-source heat pump heating system with latent heat energy storage in severely cold area. Appl Therm Eng 2008;28:1427-1436.
[92] Zivkovic, B, Fujii, I. An analysis of isothermal phase change of phase change material within rectangular and cylindrical containers. Solar Energy 2001;70:51–61.
[93] Niu FX, Ni L, Qu ML, Yao Y, Deng SM. A novel triple-sleeve energy storage exchanger and its application in an environmental control system. Appl Therm Eng 2013;54:1-6.
[94] Ni L, Qv DH, Yao Y, Niu FX, Hu WJ. An experimental study on performance enhancement of a PCM based solar-assisted air source heat pump system under cooling modes. Appl Therm Eng 2016;100:434-452.
[95] Qv DH, Ni L, Yao Y, Hu WJ. Reliability verification of a solar-air source heat pump system with PCM energy storage in operating strategy transition. Renew Energy 2015;84:46-55.
[96] Kaygusuz K. Utilization of solar energy and waste heat. Energy Sources 1999;21:595-610.
[97] Tamasauskas J, Poirier M, Zmeureanu R, Kegel M, Sunye R. Development and validation of a solar-assisted heat pump using ice slurry as a latent storage material. Sci Tech Built Environ 2015;21:837-846.
[98] Carbonell D, Philippen D, Haller MY, Frank E. Development and validation of a mathematical model for ice storages with heat exchangers that can be de-iced. Energy Procedia 2014;57:2342-2351.
[99] Carbonell D, Philippen D, Haller MY, Frank E. Modeling of an ice storage based on a de-icing concept for solar heating applications. Solar Energy 2015;121:2–16.
[100] Carbonell D, Philippen D, Haller MY, Brunold S. Modeling of an ice storage buried in the ground for solar heating applications. Validations with one year of monitored data from a pilot plant. Solar Energy 2016;125:398-414.
[101] Esen M. Thermal performance of a solar-aided latent heat store used for space heating by heat pump. Solar Energy 2000;69:15-25.
[102] Schmidt T, Mangold D, Muller-Steinhagen H. Central solar heating plants with seasonal storage in Germany. Solar Energy 2004;76:165–174.
[103] Gao LH, Zhao J, Tang ZP. A review on borehole seasonal solar thermal energy storage. Energy Procedia 2015;70:209–218.
[104] Reuss M, Beuth W, Schmidt M, Schoelkopf W. Solar district heating with seasonal storage in

Attenkirchen. In: Proceedings of the IEA Conf ECOSTOCK. New Jersey, USA. 2006.
[105] Hasnain SM. Review on sustainable thermal energy storage technologies, part i: heat storage materials and techniques. Energy Convers Manage 1998;39:1127-1138.
[106] Shah SK, Aye L, Rismanchi B. Seasonal thermal energy storage system for cold climate zones: a review of recent developments. Renew Sustain Energy Rev 2018;97:38-49.
[107] Gari HN, Loehrke RI. A controlled buoyant jet for enhancing stratification in a liquid storage tank. J Fluids Eng 1982;104:475-481.
[108] Xu RJ, Zhao YQ, Chen H, Wu Q, Yang LW, Wang HS. Numerical and experimental investigation of a compound parabolic concentrator-capillary tube solar collector. Energy Convers Manage 2020;204:112218.
[109] Qi Q, Deng SM, Jiang YQ. A simulation study on a solar heat pump heating system with seasonal latent heat storage. Solar Energy 2008;82:669–675.
[110] Yao Y, Jiang YQ, Deng SM, Ma ZL. A study on the performance of the airside heat exchanger under frosting in an air source heat pump water heater/chiller unit. Int J Heat Mass Transfer 2004;47:3745–3756.
[111] Kondepudi S, O'Neal DL. Frosting performance of tube fin heat exchangers with wavy and corrugated fins. Exp Therm Fluid Sci 1991;4:613-618.
[112] Sheng W, Liu PP, Dang CB, Liu GX. Review of restraint frost method on cold surface. Renew Sustain Energy Rev 2017;79:806–813.
[113] Kim MH, Kim H, Lee KS, Kim DR. Frosting characteristics on hydrophobic and superhydrophobic surfaces: a review. Energy Convers Manage 2017;138:1–11.
[114] Song MJ, Deng SM, Dang CB, Mao N, Wang ZH. Review on improvement for air source heat pump units during frosting and defrosting. Appl Energy 2018;211:1150-1170.
[115] Byun JS, Jeon CD, Jung JH, Lee JH. The application of photo-coupler for frost detecting in an air-source heat pump. Int J Refrig 2006;29:191–198.
[116] Jang JY, Bae HH, Lee SJ, Ha MY. Continuous heating of an air-source heat pump during defrosting and improvement of energy efficiency. Appl Energy 2013;110:9–16.
[117] Tang JC, Gong GC, Su H, Wu FH, Herman C. Performance evaluation of a novel method of frost prevention and retardation for air source heat pumps using the orthogonal experiment design method. Appl Energy 2016;169:696–708.
[118] Jiang YQ, Fu HY, Yao Y, Yan L, Gao Q. Experimental study on concentration change of spray solution used for a novel non-frosting air source heat pump system. Energy Buildings 2014;68:707–712.
[119] Wu XM, Webb RL. Investigation of the possibility of frost release from a cold surface. Exp Therm Fluid Sci 2001;24:151-156.
[120] Shen JB, Qian ZJ, Xing ZW, Yu Y, Ge MC. A review of the defrosting methods of air source heat pumps using heat exchanger with phase change material. Energy Procedia 2019;160:491–498.
[121] Qu ML, Xia L, Deng SM, Jiang YQ. Improved indoor thermal comfort during defrost with a novel reverse-cycle defrosting method for air source heat pumps. Building Environ 2010;45:2354-2361.
[122] Hu WJ, Jiang YQ, Qu ML, Ni L, Yao Y, Deng SM. An experimental study on the operating performance of a novel reverse-cycle hot gas defrosting method for air source heat pumps. Appl Therm Eng 2011;31:363-369.
[123] Zhang L, Dong J, Jiang YQ, Yao Y. A novel defrosting method using heat energy dissipated by the compressor of an air source heat pump. Appl Energy 2014;133:101–111.
[124] Wang ZH, Zheng YX, Wang FH, Wang XK, Lin Z, Li JC, Huan C. Experimental analysis on a novel frost-free air-source heat pump water heater system. Appl Therm Eng 2014;70:808-816.
[125] Wang FH, Wang ZH, Zheng YX, Lin Z, Hao PF, Huan Ch, Wang T. Performance investigation of a novel frost-free air-source heat pump water heater combined with energy storage and dehumidification. Appl Energy 2015;139:212–219.
[126] Mohamed E, Riffat S, Omer S. Low-temperature solar-plate-assisted heat pump: A developed design for domestic applications in cold climate. Int J Refrig 2017;81:134-150.
[127] Kong XQ, Li JY, Wang BG, Li Y. Numerical study of a direct-expansion solar-assisted heat pump water heater under frosting conditions based on experiments. Solar Energy 2020;196:10-2
[128] Huang WZ, Ji J, Xu N, Li GQ. Frosting characteristics and heating performance of a direct-expansion solar-assisted heat pump for space heating under frosting conditions. Appl Energy 2016;171:656–666.
[129] James A, Mohanraj M, Srinivas M, Jayaraj S. Thermal analysis of heat pump systems using photovoltaic-thermal collectors: a review. Journal of Thermal Analysis and Calorimetry. 2021;144:1-39

[130] Breidenich C, Magraw D, Rowley A, Rubin J. The Kyoto protocol to the United Nations framework convention on climate change. American J Int Law 1998;92:315-331.
[131] Heath E. Amendment to the Montreal protocol on substances that deplete the ozone layer (Kigali Amendment). Int Legal Materials 2017;56:193-205.
[132] United Nations Environment Programme. The Montreal protocol on substances that deplete the ozone layer. 1987. https://unep.ch/ozone/pdf/Montreal-Protocol2000.pdf. [accessed 10 September 2020]
[133] International Electrotechnical Commission. https://webstore.iec.ch/publication/62243. [accessed 25 October 2020]
[134] Chaturvedi SK, Chen DT, Kheireddine A. Thermal performance of a variable capacity direct expansion solar-assisted heat pump. Energy Convers Manage 1998;39:181-191.
[135] Paradeshia L, Srinivasb M, Jayaraj S. Parametric studies of a simple direct expansion solar assisted heat pump operating in a hot and humid environment. Energy Procedia 2016;90:635-644.
[136] Molinaroli L, Joppolo CM, De Antonellis S. Numerical analysis of the use of R-407C in direct expansion solar assisted heat pump. Energy Procedia 2014;48:938–945.
[137] Huang BJ, Chyng JP. Performance characteristics of integral type solar-assisted heat pump. Solar Energy 2001;71:403–414.
[138] Anderson TN, Morrison GL. Effect of load pattern on solar-boosted heat pump water heater performance. Solar Energy 2007;81:1386–1395.
[139] Mohanraj M, Jayaraj S, Muraleedharan C. Modeling of a direct expansion solar assisted heat pump using artificial neural networks. Int J Green Energy 2008;5:520-532.
[140] Axaopoulos P, Panagakis P, Kyritsis S. Experimental comparison of a solar-assisted heat pump vs. a conventional thermosyphon solar system. Int J Energy Res 1998;22:1107-1120.
[141] Huang BJ, Lee CP. Long-term performance of solar-assisted heat pump water heater. Renew Energy 2003;29:633–639.
[142] Huang BJ, Lee CP. Performance evaluation method of solar-assisted heat pump water heater. Appl Therm Eng 2007;27:568–575.
[143] Moreno-Rodríguez A, González-Gil A, Izquierdo M, Garcia-Hernando N. Theoretical model and experimental validation of a direct-expansion solar assisted heat pump for domestic hot water applications. Energy 2012;45:704-715.
[144] Moreno-Rodríguez A, Garcia-Hernando N, González-Gil A, Izquierdo M. Experimental validation of a theoretical model for a direct-expansion solar-assisted heat pump applied to heating. Energy 2013;60:242-253.
[145] Mohanraj M, Jayaraj S, Muraleedharan C. Performance prediction of a direct expansion solar assisted heat pump using artificial neural networks. Appl Energy 2009;86:1442–1449.
[146] Ito S, Miura N, Takano Y. Studies of heat pumps using direct expansion type solar collectors. J Solar Energy Eng 2005;127:60-64.
[147] Mohanraj M, Jayaraj S, Muraleedharan C. Exergy analysis of direct expansion solar-assisted heat pumps using artificial neural networks. Int J Energy Res 2009;33:1005–1020.
[148] Huang BJ, Chyng JP. Integral-type solar-assisted heat pump water heater. Renew Energy 1999;16:731-734.
[149] Sun XL, Wu JY, Dai YJ, Wang RZ. Experimental study on roll-bond collector/evaporator with optimized channel used in direct expansion solar assisted heat pump water heating system. Appl Therm Eng 2014;66:571-579.
[150] Fernández-Seara J, Piñeiro C, Alberto DJ, Fernandes F, Sousa PXB. Experimental analysis of a direct expansion solar assisted heat pump with integral storage tank for domestic water heating under zero solar radiation conditions. Energy Convers Manage 2012;59:1–8.
[151] Gorozabel CFB, Chaturvedi SK, Almogbel A. Analysis of a direct expansion solar assisted heat pump using different refrigerants. Energy Convers Manage 2005;46:2614–2624.
[152] Aziz W, Chaturvedi SK, Kheireddine A. Thermodynamic analysis of two-component, two-phase flow in solar collectors with application to a direct-expansion solar-assisted heat pump. Energy 1999;24:247–259.
[153] Chaturvedi SK, Gagrani VD, Abdel-Salam TM. Solar-assisted heat pump -- A sustainable system for low-temperature water heating applications. Energy Convers Manage 2014;77:550–557.
[154] Zhang D, Wu QB, Li JP, Kong XQ. Effects of refrigerant charge and structural parameters on the performance of a direct-expansion solar-assisted heat pump system. Appl Therm Eng 2014;73:522-528.
[155] Scarpa F, Tagliafico LA, Tagliafico G. Integrated solar-assisted heat pumps for water heating coupled

to gas burners; control criteria for dynamic operation. Appl Therm Eng 2011;31:59-68.
[156] Tagliafico LA, Scarpa F, Valsuani F. Direct expansion solar assisted heat pumps: a clean steady state approach for overall performance analysis. Appl Therm Eng 2014;66:216-226.
[157] Kong XQ, Li Y, Lin L, Yang YG. Modeling evaluation of a direct-expansion solar assisted heat pump water heater using R410A. Int J Refrig 2017;76:136–146.
[158] Scarpa F, Tagliafico LA., Bianco V. A novel steady-state approach for the analysis of gas-burner supplemented direct expansion solar assisted heat pumps. Solar Energy 2013;96:227–238.
[159] Chaturvedi SK, Mohieldin TO, Chen DT. Second-law analysis of solar-assisted heat pumps. Energy 1991;16:941-949.
[160] Aye L, Charters WWS, Chaichana C. Solar heat pump systems for domestic hot water. Solar Energy 2002;73:169–175.
[161] Li H, Yang HX. Potential application of solar thermal systems for hot water production in Hong Kong. Appl Energy 2009;86:175–180.
[162] Torres-Reyes E, Cervantes JG. Optimal performance of an irreversible solar-assisted heat pump. Exergy, an Int J 2001;1:107–111.
[163] Torres-Reyes E, Picon-Nunez M, Cervantes JG. Exergy analysis and optimization of a solar-assisted heat pump. Energy 1998;23:337–344.
[164] Cervantes JG, Torres-Reyes E. Experiments on a solar-assisted heat pump and an exergy analysis of the system. Appl Therm Eng 2002;22:1289–1297.
[165] Chow TT, Bai Y, Fong KF, Lin Z. Analysis of a solar assisted heat pump system for indoor swimming pool water and space heating. Appl Energy 2012;100:309–317.
[166] Chaichana C, Kiatsiriroat T, Nuntaphan A. Comparison of conventional flat-plate solar collector and solar boosted heat pump using unglazed collector for hot water production in small slaughterhouse. Heat Transfer Eng 2010;31:419-429.
[167] Fraga C, Mermoud F, Hollmuller P, Pampaloni E, Lachal B. Large solar driven heat pump system for a multifamily building: long term in-situ monitoring. Solar Energy 2015;114:427–439.
[168] Nuntaphan A, Chansena C, Kiatsiriroat T. Performance analysis of solar water heater combined with heat pump using refrigerant mixture. Appl Energy 2009;86:748–756.
[169] Banister CJ, Collins MR. Development and performance of a dual tank solar-assisted heat pump system. Appl Energy 2015;149:125–132.
[170] He W, Hong XQ, Zhao XD, Zhang XX, Shen JC, Ji J. Operational performance of a novel heat pump assisted solar façade loop-heat-pipe water heating system. Appl Energy 2015;146:371–382.
[171] Wang Q, Ren B, Zeng ZY, He W, Liu YQ, Xu XG, Chen GM. Development of a novel indirect-expansion solar-assisted multifunctional heat pump with four heat exchangers. Building Services Eng Res Tech 2015;36:469–481.
[172] Wang Q, Liu YQ, Liang GF, Li JR, Sun SF, Chen GM. Development and experimental validation of a novel indirect-expansion solar-assisted multifunctional heat pump. Energy Buildings 2011;43:300–304.
[173] Winteler C, Dott R, Afjei T, Hafner B. Seasonal performance of a combined solar, heat pump and latent heat storage system. Energy Procedia 2014;48:689-700.
[174] Tamasauskas J, Poirier M, Zmeureanu R, Sunye R. Modeling and optimization of a solar assisted heat pump using ice slurry as a latent storage material. Solar Energy 2012;86:3316– 3325.
[175] Li H, Sun LL, Zhang YG. Performance investigation of a combined solar thermal heat pump heating system. Appl Therm Eng 2014;71:460-468.
[176] Bellos E, Tzivanidis C. Energetic and financial sustainability of solar assisted heat pump heating systems in Europe. Sustain Cities Society 2017;33:70-84.
[177] He W, Hong XQ, Zhao XD, Zhang XX, Shen JC, Ji J. Theoretical investigation of the thermal performance of a novel solar loop-heat-pipe facade-based heat pump water heating system. Energy Buildings 2014;77:180–191.
[178] Tagliafico LA, Scarpa F, Tagliafico G, Valsuani F. An approach to energy saving assessment of solar assisted heat pumps for swimming pool water heating. Energy Buildings 2012;55:833–840.
[179] Li QY, Chen Q, Zhang X. Performance analysis of a rooftop wind solar hybrid heat pump system for buildings. Energy Buildings 2013;65:75–83.
[180] Panaras G, Mathioulakis E, Belessiotis V. Investigation of the performance of a combined solar thermal heat pump hot water system. Solar Energy 2013;93:169–182.
[181] Shan M, Yu T, Yang X. Assessment of an integrated active solar and air-source heat pump water heating system operated within a passive house in a cold climate zone. Renew Energy 2016;87:1059-

1066.
[182] Li YH, Kao WC. Performance analysis and economic assessment of solar thermal and heat pump combisystems for subtropical and tropical region. Solar Energy 2017;153:301–316.
[183] Panaras G, Mathioulakis E, Belessiotis V. A method for the dynamic testing and evaluation of the performance of combined solar thermal heat pump hot water systems. Appl Energy 2014;114:124–134.
[184] Poppi S, Bales C, Haller MY, Heinz A. Influence of boundary conditions and component size on electricity demand in solar thermal and heat pump combisystems. Appl Energy 2016;162:1062–1073.
[185] Poppi S, Bales C, Heinz A, Hengel F, Chèze D, Mojic I, Cialani C. Analysis of system improvements in solar thermal and air source heat pump combi systems. Appl Energy 2016;173:606–623.
[186] Ji J, Cai JY, Huang WZ, Feng Y. Experimental study on the performance of solar-assisted multi-functional heat pump based on enthalpy difference lab with solar simulator. Renew Energy 2015;75:381-388.
[187] Ni L, Qv DH, Shang RX, Yao Y, Niu FX, Hu WJ. Experimental study on performance of a solar-air source heat pump system in severe external conditions and switchover of different functions. Sustain Energy Tech Assess 2016;16:162–173.
[188] Xu RJ, Hu WJ, Wu QP, Wang RX, Wang HS, Hu J. Liquid flow control method for heating plant and thermal energy collector. ZL201610792318.7. Issued date 18th June 2019.
[189] International Energy Agency. Solar heat worldwide--global market development and trends in 2019 & detailed market data 2018. https://www.iea-shc.org/solar-heat-worldwide-2020. [accessed 10 September 2020]
[190] Li YH. Variable frequency drive applications in HVAC systems. New Applications of Electric Drives. Miroslav Chomat. IntechOpen. 2015.
[191] Lerch W, Heinz A, Heimrath R. Evaluation of combined solar thermal heat pump systems using dynamic system simulations. Energy Procedia 2014;48:598–607.
[192] Hawlader MNA, Chou SK, Ullah MZ. The performance of a solar assisted heat pump water heating system. Appl Therm Eng 2001;21:1049-1065.
[193] Kong XQ, Sun PL, Jiang KL, Dong SD, Li Y, Li JB. A variable frequency control method and experiments of a direct-expansion solar-assisted heat pump system. Solar Energy 2018;176: 572-580.
[194] Kong XQ, Wang BG, Shang YP, Li JY, Li Y. Influence of different regulation modes of compressor speed on the performance of direct-expansion solar-assisted heat pump water heater. Appl Therm Eng 2020;169:115007.
[195] Kong XQ, Zhang MY, Yang YM, Li Y, Wang DC. Comparative experimental analysis of direct-expansion solar-assisted heat pump water heaters using R134a and R290. Solar Energy 2020;203:187-196.
[196] Kong XQ, Sun PL, Dong SD, Jiang KL, Li Y. Experimental performance analysis of a direct-expansion solar-assisted heat pump water heater with R134a in summer. Int J Refrig 2018;91:12-19.
[197] Kong XQ, Yang YM, Zhang MY, Li Y, Li JB. Experimental investigation on a direct-expansion solar-assisted heat pump water heater using R290 with micro-channel heat transfer technology during the winter period. Int J Refrig 2020;113:38-48.
[198] Kong XQ, Jiang KL, Dong SD, Li Y, Li JB. Control strategy and experimental analysis of a direct-expansion solar-assisted heat pump water heater with R134a. Energy 2018;145:17-24.
[199] Kong XQ, Sun PL, Li Y, Jiang KL, Dong SD. Experimental studies of a variable capacity direct-expansion solar-assisted heat pump water heater in autumn and winter conditions. Solar Energy 2018;170:352-357.
[200] Dong X, Tian Q, Li Z. Experimental investigation on heating performance of solar integrated air source heat pump. Appl Therm Eng 2017;123:1013-1020.
[201] Xian T, Wu JH, Zhang X. Study on the operating characteristics of a solar heat pump water heater based on data fusion. Solar Energy 2020;212:113-124.
[202] Wu JH, Xian T, Liu X. All-weather characteristic studies of a direct expansion solar integrated air source heat pump system based on PCMs. Solar Energy 2019;191:34-45.
[203] Kutlu C, Zhang YN, Elmer T, Su YH, Riffat S. A simulation study on performance improvement of solar assisted heat pump hot water system by novel controllable crystallization of supercooled PCMs. Renew Energy 2020;152:601-612.
[204] Buker SM, Riffat SB. Build-up and performance test of a novel solar thermal roof for heat pump operation. Int J Ambient Energy 2017;38:365-379.
[205] Huan C, Wang FH, Li ST, Zhao YJ, Liu L, Wang ZH, Ji CF. A performance comparison of serial and

parallel solar-assisted heat pump heating systems in Xi'an, China. Energy Sci Eng 2019;7:1379-1393.
[206] Liu FZ, Wang L, Wang Q, Wang HF. Experiment study on heating performance of solar-air source heat pump unit. Procedia Eng 2017;205:3873–3878.
[207] Ran SY, Lyu WH, Li XT, Xu W, Wang BL. A solar-air source heat pump with thermosiphon to efficiently utilize solar energy. J Building Eng 2020;31:101330.
[208] Liu ZJ, Liu YW, Wu D, Jin GY, Yu HC, Ma WS. Performance and feasibility study of solar-air source pump systems for low-energy residential buildings in Alpine regions. Journal of Cleaner Production 2020;256:120735.
[209] Kim T, Choi BI, Han YS, Do KH. A comparative investigation of solar-assisted heat pumps with solar thermal collectors for a hot water supply system. Energy Convers Manage 2018;172:472-484.
[210] Qiu GD, Wei XH, Xu ZF, Cai WH. A novel integrated heating system of solar energy and air source heat pumps and its optimal working condition range in cold regions. Energy Convers Manage 2018;174:922-931.
[211] Long JB, Xia KM, Zhong HH, Lu HL, A YG. Study on energy-saving operation of a combined heating system of solar hot water and air source heat pump. Energy Convers Manage 2021;220:113624.
[212] Chargui R, Awani S. Determining of the optimal design of a closed loop solar dual source heat pump system coupled with a residential building application. Energy Convers Manage 2017;147:40-54.
[213] Huang WZ, Zhang T, Ji J, Xu N. Numerical study and experimental validation of a direct-expansion solar-assisted heat pump for space heating under frosting conditions. Energy Building 2019;185:224-238.
[214] Cai JY, Ji J, Wang YY, Huang WZ. Operation characteristics of a novel dual source multi-functional heat pump system under various working modes. Appl Energy 2017;194:236-246.
[215] Cai JY, Zhang F, Ji J. Comparative analysis of solar-air dual source heat pump system with different heat source configurations. Renew Energy 2020;150:191-203.
[216] Zhang F, Cai JY, Ji J, Han KD, Ke W. Experimental investigation on the heating and cooling performance of a solar air composite heat source heat pump. Renew Energy 2020;161:221-229.
[217] Ji WA, Cai JY, Ji J, Huang WZ. Experimental study of a direct expansion solar-assisted heat pump (DX-SAHP) with finned-tube evaporator and comparison with conventional DX-SAHP. Energy Buildings 2020;207:109632.
[218] Rabelo SN, Paulino TF, Duarte WM, Sawalha W, Machado L. Experimental analysis of the influence of water mass flow rate on the performance of a CO_2 direct-expansion solar assisted heat pump. Int Scho Sci Res Innov 2018;12:327-331.
[219] Treichel C, Cruickshank CA. Energy analysis of heat pump water heaters coupled with air-based solar thermal collectors in Canada and the United States. Energy 2021;221:119801.
[220] Treichel C, Cruickshank CA. Greenhouse gas emissions analysis of heat pump water heaters coupled with air-based solar thermal collectors in Canada and the United States. Energy Buildings 2021;231:110594.
[221] Treichel C, Cruickshank CA. Analysis of a coupled air-based solar collector and heat pump water heater in Canada and the United States. IEA SHC Int Conf on Solar Heating and Cooling for Buildings and Industry 2019.
[222] Li YL, Li BG, Liu CY, Su SQ, Xiao HH, Zhu CH. Design and experimental investigation of a phase change energy storage air-type solar heat pump heating system. Appl Therm Eng 2020;179:115506.
[223] Aktas M, Kosan M, Arslan E, Tuncer AD. Designing a novel solar-assisted heat pump system with modification of a thermal energy storage unit. J Power Energy 2019;233:588–603.
[224] Kaygusuz K. Performance of solar assisted parallel and series heat pump systems with energy storage for building heating. J Eng Res Appl Sci 2018;7:759-764.
[225] Stritih U, Zavrl E, Paksoy HO. Energy analysis and carbon saving potential of a complex heating system with solar assisted heat pump and phase change material (PCM) thermal storage in different climatic conditions. Euro J Sustain Develop Res 2019;3:em0067.
[226] Fan CC, Yan G, Yu JL. Thermodynamic analysis of a modified solar assisted ejector-compression heat pump cycle with zeotropic mixture R290/R600a. Appl Therm Eng 2019;150:42-49.
[227] Chen JH, Yu JL. Energy and exergy analysis of a new direct-expansion solar assisted vapor injection heat pump cycle with subcooler for water heater. Solar Energy 2018;171:613-620.
[228] Chen JH, Yu JL, Qian SX. Subcooling control method for the adjustable ejector in the direct expansion solar assisted ejector-compression heat pump water heater. Appl Therm Eng 2019;148:662-673.
[229] Fraga C, Hollmuller P, Mermoud F, Lachal B. Solar assisted heat pump system for multifamily buildings: Towards a seasonal performance factor of 5? Numerical sensitivity analysis based on a

monitored case study. Solar Energy 2017;146:543-564.
[230] Duarte WM, Paulino TF, Pabon JJG, Sawalha S, Machado L. Refrigerants selection for a direct expansion solar assisted heat pump for domestic hot water. Solar Energy 2019;184:527-538.
[231] Ran SY, Li XT, Xu W, Wang BL. A solar-air hybrid source heat pump for space heating and domestic hot water. Solar Energy 2020;199:347-359.
[232] Paulino TF, Oliveira RN, Maia AAT, Palm B, Machado L. Modeling and experimental analysis of the solar radiation in a CO2 direct-expansion solar-assisted heat pump. Appl Therm Eng 2019;148:160-172.
[233] Wang YQ, Rao ZH, Liu JX, Liao SM. An optimized control strategy for integrated solar and air-source heat pump water heating system with cascade storage tanks. Energy Buildings 2020;210:109766.
[234] Paradeshi L, Srinivas M, Jayaraj S. Performance studies of R433A in a direct expansion solar-assisted heat pump. Int J Ambient Energy 2020;41:262-273.
[235] Li FL, Chang Z, Li XC, Tian Q. Energy and exergy analyses of a solar-driven ejector-cascade heat pump cycle. Energy 2018;165:419-431.
[236] Lee SJ, Shon BH, Jung CW, Kang YT. A novel type solar assisted heat pump using a low GWP refrigerant (R1233zd(E)) with the flexible solar collector. Energy 2018;149:386-396.
[237] Cao Y, Mihardjob LWW, Parikhanic T. Thermal performance, parametric analysis, and multi-objective optimization of a direct-expansion solar-assisted heat pump water heater using NSGA-II and decision makings. Appl Therm Eng 2020;181:115892.
[238] Liu M, He YE, Zhang HF, Su H, Zhang ZW. The feasibility of solar thermal-air source heat pump water heaters in renewable energy shortage regions. Energy 2020;197:117189.
[239] Han ZW, Bai CG, Ma X, Li B, Hu HH. Study on the performance of solar-assisted transcritical CO2 heat pump system with phase change energy storage suitable for rural houses. Solar Energy 2018;174:45-54.
[240] Li YH, Kao WC. Taguchi optimization of solar thermal and heat pump combi systems under five distinct climatic conditions. Appl Therm Eng 2018;133:283-297.
[241] Vega J, Cuevas C. Parallel vs series configurations in combined solar and heat pump systems: a control system analysis. Appl Therm Eng 2020;166:114650.
[242] Rabelo SN, Paulino TF, Machado L, Duarte WM. Economic analysis and design optimization of a direct expansion solar assisted heat pump. Solar Energy 2019;188:164-174.
[243] Liu ZJ, Wang QM, Wu D, Zhang YL, Yin H, Yu HC, Jin GY, Zhao XD. Operating performance of a solar/air-dual source heat pump system under various refrigerant flow rates and distributions. Appl Therm Eng 2020;178:115631.
[244] Youssef W, Ge YT, Tassou SA. Indirect expansion solar assisted heat pump system for hot water production with latent heat storage and applicable control strategy. Energy Procedia 2017;123:180–187.
[245] Ma JL, Fung AS, Brands M, Juan N, Moyeed OMA. Performance analysis of indirect-expansion solar assisted heat pump using CO2 as refrigerant for space heating in cold climate. Solar Energy 2020;208:195-205.
[246] Rabelo SN, Paulino TF, Duarte WM, Maia AAT, Machado L. Experimental analysis of the influence of the expansion valve opening on the performance of the small size CO2 solar assisted heat pump. Solar Energy 2019;190:255-263.
[247] Wei B, Wang YZ, Liu ZJ, Liu BX. Optimization study on a solar-assisted air source heat pump system with energy storage based on the economics method. Int J Energy Res 2020;44:2023–2036.
[248] De León-Ruiz JE. Carvajal-Mariscal I. Mathematical thermal modelling of a direct-expansion solar-assisted heat pump using multi-objective optimization based on the energy demand. Energies 2018;11:1773.
[249] Lu J, He GQ, Mao F. Solar seasonal thermal energy storage for space heating in residential buildings: Optimization and comparison with an air-source heat pump. Energy Sources, Part B: Economics, Planning, and Policy 2020;15:279-296.
[250] Dott R, Haller MY., Ruschenburg Jörn, Ochs Fabian, Bony Jacques, The Reference Framework for System Simulations of the IEA SHC Task 44 / HPP Annex 38—Part B: Buildings and Space Heat Load, A technical report of subtask C—Report C1 Part B, International Energy Agency, 2013, http://task44.iea-shc.org/Data/Sites/1/publications/T44A38_Rep_C1_B_ReferenceBuildingDescription_Final_Revised_130906.pdf
[251] Met Office, UK maps of monthly data, https://www.metoffice.gov.uk/research/climate/maps-and-

data/summaries/index
[252] World Health Organization, LEGIONELLA and the prevention of legionellosis, 2007.
[253] Charted Institute of Plumbing and Heating Engineering, https://www.ciphe.org.uk/consumer/safe-water-campaign/hot-water-scalds/, [accessed on January 22nd, 2022].
[254] Volume 4—Mathematical Reference, TRNSYS 17
[255] E.ON Energy, https://www.eonenergy.com/for-your-home/products-and-services/best-deal-for-you/quote, [accessed on January 22nd, 2022].
[256] https://www.made-in-china.com, [accessed on January 22nd, 2022].
[257] Plumber Costs: 2021 Call Out Charges & Hourly Prices UK, https://tradesmencosts.co.uk/plumbers/, [accessed on January 22nd, 2022].
[258] Dickes R, Lemort V, Quoilin S, Semi-empirical correlation to model heat losses along solar parabolic trough collectors Proceedings of ECOS 2015-28th International Conference on Efficiency, Cost, Optimization, Simulation and Environmental Impact of Energy Systems. Pau, France: ECOS, 2015.